Multiplex detection of DNA damage

by

Sindhu G. Nair

A thesis submitted in partial fulfillment of the requirements for the degree of

Doctor of Philosophy

Department of Chemistry
University of Alberta

Spring, 2015

Abstract

A large number of exogenous and endogenous agents can result in DNA damage leading to mutagenesis and cell death. A thorough knowledge and understanding about the effects of these agents on different sequences of DNA is important for elucidating the fundamental chemical mechanisms of DNA damage. Therefore, developing a rapid and inexpensive technique for the detection of damage in multiple samples is of great importance. Numerous DNA detection techniques, involving polymerase chain reaction and gel electrophoresis, have been developed. However, most of these techniques are cumbersome and/or expensive. In this thesis, we develop a simple, sensitive, inexpensive, mix-and-read assay to detect DNA damage with higher throughput and better ease-of-use. The goal of this work is to design simple hybridization assays for DNA damage detection of multiple sequences in single and double stranded DNA on a 96-well microplate platform.

We first replaced the conventional cuvette method with the well plate method in order to study UVC-induced ssDNA damage on four sequences simultaneously. In this study, we measured the change in fluorescence intensity of a series of sequence-specific smart probes (SPs) for quantifying the extent of damage. The results show that this method has similar reproducibility as the cuvette method, but designing SPs complementary to each sequence makes the method tedious and expensive.

In the second approach we developed a microplate assay coupled with EvaGreen (EG), an intercalating dye to quantify both ssDNA and dsDNA damage in an inexpensive way. This gives maximum sensitivity for detecting damage since the dye gives zero/minimum fluorescence with ssDNA and a maximum fluorescence with dsDNA. This dye gave good sensitivity and selectivity for quantification of dsDNA damaged by both UVC and a Ru *cis*-platin analog. The calibration

curve for the EG probe shows good linearity ($R^2 = 0.99$) with a limit of detection of 2.3 nM for dsDNA. Confirmation that EG can detect damage was done by melting curve and matrix-assisted laser desorption/ ionization time-of-fight mass spectroscopy (MALDI-TOF-MS). We also used our method to study the effect of the number and position of mismatches on the stability of dsDNA with another intercalating dye, Hoechst 33258 (H258). Results show that the sensitivity of the dsDNA detection is determined more by the position of mismatches than by the number of mismatches. We also compared the UVC-induced DNA damage kinetics of ssDNA and dsDNA. Our results are in agreement with *in vitro* and *in vivo* studies, which show ssDNA to be more vulnerable to damage than dsDNA. The H258 dye was much cheaper than the EG dye, but its use is limited because of its high selectivity for A-T rich regions of dsDNA.

Finally, we explored the ability of our method to detect DNA damage in multiple samples of K-*Ras* and N-*Ras* proto-oncogenes. Results show that the K-*Ras* sequences are more mutagenic than the N-*Ras* sequences. This result is in excellent agreement with past biological studies performed on K-*Ras* and N-*Ras* genes. Thus, our method proves as a simple, inexpensive, mix-and-read assay for the reproducible quantification of DNA damaged induced by different etiological agents.

Preface

This thesis is based on my research work done at University of Alberta during my PhD studies. Chapter 2 of this thesis has been published as S.G. Nair and G.R. Loppnow, Multiplexed, UVC-Induced, Sequence-Dependent DNA Damage Detection *Photochem. Photobiol*. 89 (2013) 884-890. I was responsible for designing and performing various experiments involved in this project. I wrote the manuscript and Professor G.R. Loppnow was the supervisory author who was involved in the concept formation and manuscript edits.

Chapter 3 and a part of Chapter 4 of this thesis are ready for submission. I was responsible for designing and performing the various experiments involved in these projects. I wrote the draft of the manuscripts. Professor G. R. Loppnow supervised the project and did manuscript edits.

Dedicated to

my dear parents, my affectionate parents-in-law, my beloved husband Renjith and adorable daughter Neharika.

Acknowledgement

First and foremost, I would like to express my deepest appreciation to my supervisor, Prof. Glen R. Loppnow for his thorough supervision, guidance and valuable suggestions throughout my PhD research work. He continually and convincingly provided endless advices and supported my good ideas, but discouraged my poorer one gently. Without his persistent help my research would not have been completed. I would also like to thank my committee members Prof. James Harynuk, Prof. Christopher W. Cairo, Prof. X. Chris Le and Prof. Dipanker Sen for their acceptance to take charge as examiners. I also express my sincere gratitude to Prof. Robert E. Campbell for letting me use his lab facilities for my research work

My special thanks to past and present members of Dr Loppnow's group, especially Dr. Swaroop Sasidharanpillai, Dr. Sulayman Adeyemi Oladepo and Dr. Amira F. EL-Yazbi for helping and guiding me during the initial stages of my work. I also would like to thank Faranak Teimoory and Zahra Shire for their support and concern.

My sincere thanks to all people in mass spectrometry, analytical services, microarray facility, glass shop, electrical shop and machine shop for providing me the necessary help and instrumental assistance. I am also indebted to Tyler Peterson who has been an invaluable help in solving any issues related to my computer system

At this juncture, I would like to extend my gratitude to my friends Krishna Ramachandran, Javix Thomas, Bindu Pillai and Jerry Alfred Fereiro for their unforgettable help and suggestions. My appreciation also goes to all my other friends who showed concern during my PhD program.

Above all I owe to my parents, my in laws, my sister and my brother in law for their inseparable support and prayers. Words fail me to express my thanks to my dearest husband Renjith Pillai, for his love, encouragement, patience and persistent confidence in me. Above all I would like to express my appreciation to my little daughter, Neharika, for being the most wonderful kid. Her smile and childish talk would help me relax after long busy days in the lab.

Finally, I admit that this research would have not been completed without the financial support provided by the Department of Chemistry, the Faculty of Graduate Studies and Research, the Natural Sciences and Engineering Research Council of Canada (NSERC) and the Canadian Foundation of Innovation (CFI) and express my gratitude to these agencies.

Table of Contents

Chapter 1 : General Introduction

Chapter 2 : Multiplexed, UVC-Induced, Sequence-Dependent DNA Damage Detection

Chapter 3 : Sequence-specific DNA Damage Induced by a Ruthenium Anti-cancer Drug Detected in a Multi-sample Platform

List of Table

List of Figures

List of Abbreviations

2AP	2-aminopurine
A	adenine
bpy	bipyridine
C	cytosine
CPD	cyclobutyl pyrimidine dimers
DNA	deoxyribonucleic acid
EG	EvaGreen
EDTA	ethylenediaminetetraacetic acid
ELISA	enzyme-linked immunosorbent assay
FAM	6-carboxyfluorescein
FISH	fluorescence in-situ hybridization
FRET	Förster or fluorescence resonance energy transfer
H 258	Hoechst 33258 dye
HPLC	high performance liquid chromatography
HTS	high-throughput screening
G	guanine
GC	gas chromatography
ISB	immuno-slot-blot
LNA-MB	locked nucleic acid molecular beacon
LOD	limit of detection
LOQ	limit of quantification
MB	molecular beacon

MS	mass spectrometry
PCR	polymerase chain reaction
PET	photoelectron transfer
PNA	peptide nucleic acid
QF	quencher free
RIA	radioimmunoassay
ROS	reactive oxygen species
RNA	ribonucleic acid
SNP	single nucleotide polymorphism
SP	smart probe
T	thymine
T_m	melting temperature
U	uracil
UV	ultraviolet
UVA	ultraviolet A (315-400 nm)
UVB	ultraviolet B (280-315 nm)
UVC	ultraviolet C (200-280 nm)

1
General Introduction

1.1 The structure and function of nucleic acids

Nucleic acids are large organic polymers found in all living organisms [1]. They are divided into two types: deoxyribonucleic acid (DNA) and ribonucleic acid (RNA). Both of these nucleic acids consist of nucleotides which serves as their monomer units. Each nucleotide is composed of a pentose sugar, an organic base and an inorganic phosphate group (Figure 1.1). Sugar linked *via* phosphate bond forms a constant backbone but differ in the bases from one monomer unit to other. The primary nucleobases are adenine (A) guanine (G), cytosine (C) thymine (T) and uracil (U). Their structures are shown in Figure 1.2. DNA differs from RNA by the presence of thymine instead of a uracil nucleobase. They also differ in the structure of the sugar in their nucleotides. DNA contains deoxyribose sugar while RNA contains a ribose sugar [1,2].

DNA is formed of two chains that winds together into double-helix structure due to base-pairing interactions. The double helical structure of DNA is formed when guanine pairs with cytosine and adenine pairs with thymine nucleobase among the two strands. These base pairs are held together by intermolecular hydrogen bonding. Thus, separation of the double helix into two single-strands would act as a template for the synthesis of new double-stranded DNA (dsDNA) [3,4].

1.2 DNA damage

Maintaining the stability of the human genome is crucial for cell growth and development. The stability of the genome is constantly undermined by DNA damage which generates potentially harmful mutations that can alter the genetic information's stored in the DNA. As a result, damage can hinder replication of DNA, leading to mutation and/or cell death [4]. DNA damage can occur through different mechanisms leading to the formation of various types of lesions. First, the DNA

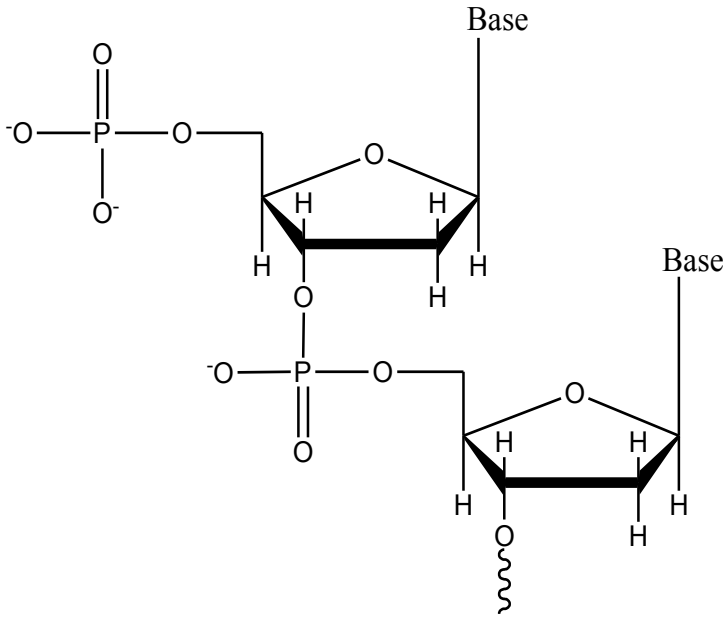

Figure 1.1 Organization of repeating units of polynucleotides

Pyrimidines

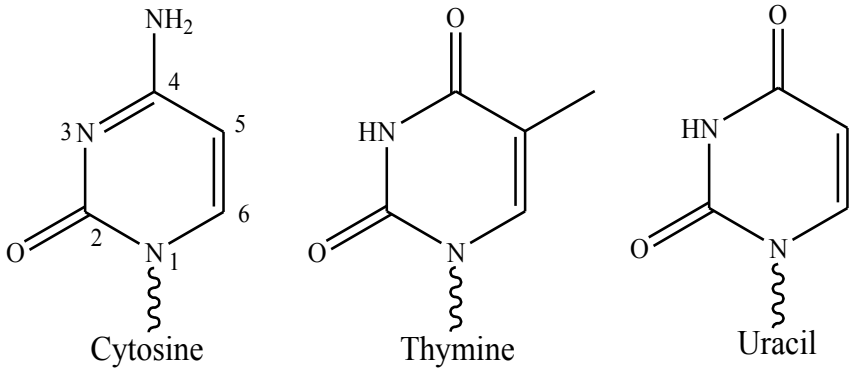

Purines

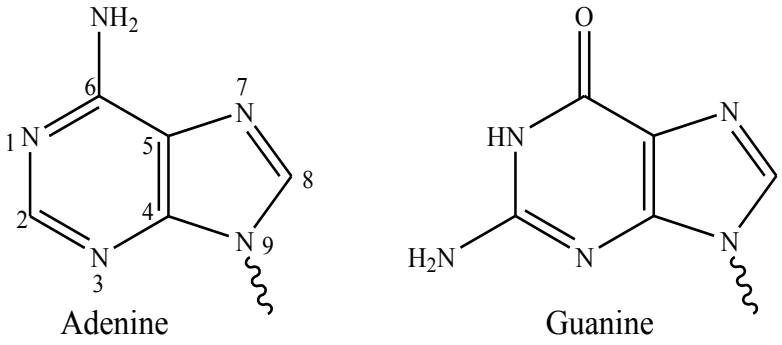

Figure 1.2 Structures of the five nucleobases. The atomic numbering scheme for the ring atoms is shown on the first member of each group

molecule can break down through hydrolysis of the nucleosides creating abasic sites and deamination products under physiological conditions. Secondly, metabolic processes can produce highly reactive species which creates different types of DNA damage such as strand breaks and base modifications [5]. Thirdly, replication error may cause transversion, insertion or deletion of DNA bases [6]. Lastly, exogenous agents such as ultraviolet (UV) radiation, ionizing radiation, industrial chemicals, drugs and food contaminates may damage DNA [5,7-10].

The amount of damage that occurs naturally due to various cellular and metabolic functions introduces 10^5 lesions per cell per day. But these are less harmful, since the repair mechanism inside our body identify and repair most of these damages. However, exposure to external sources such as UV radiation is one of the main causes for genomic instability. The amount of UV radiation that we are exposed can itself cause 10^5 lesions per day. In addition to UV, ionizing radiation causes a majority of single and double strand breaks which can ultimately end up in cell arrest, chromosomal rearrangement and other deleterious mutations in the DNA [11].

1.2.1 UV-induced DNA damage and DNA photoproducts

UV light is one of the most harmful components of solar radiation that can induce mutations in human genome. UV radiation constitutes just a minor portion of the total solar radiation but its biological impact is immense. UV radiation is divided into three regions which extend from 200-400 nm [12]. UVA radiation (315-400 nm) has a poor efficiency in inducing DNA damage because it is weakly absorbed by DNA and proteins. However, UVA radiation can damage the DNA *via* indirect photosensitizing reactions by producing singlet oxygen ($^1O_2$). These reactive oxygen species (ROS) are similar to those produced by ionizing radiation and induces the formation of 8-oxo-7,8-dihydro-2'-deoxyguanosine (8-oxoGua), oxidized pyrimidines, strand breaks and DNA-protein crosslinks [5,13]. UVB radiation (280-315 nm) makes up less than 1% of the total solar

radiation. Under normal condition of solar exposure, it is the most energetic component of solar radiation that reaches the Earth's surface. DNA bases can directly absorb incident UVB radiation leading to DNA damage. This damage is mainly responsible for sunburn, cataract and skin cancer [12].

UVC radiation (200-280 nm) is absorbed by ozone layer in the atmosphere and normally does not reach the Earth surface. However, continuous use of certain chemicals such as chlorofluorocarbons destroys the ozone layer leading to its depletion. As a consequence, high level of UVC radiation can reach the Earth's surface [14]. Exposure to high amounts of UVC radiation can have a serious effect on the DNA because DNA has a strong absorption maximum in the UVC range. Thus, the shorter-wavelength and higher-energy associated with UVC radiation makes it the most dangerous radiation [15].

When DNA is exposed to UVB or UVC radiation, the pyrimidine nucleobases thymine and cytosine undergo photochemical reactions, forming different photoproducts (Figure 1.3 and 1.4). The best known photoproducts are cyclobutane pyrimidine dimers (CPDs), 6-4 pyrimidine-pyrimidinone dimers (6-4 PPs) and photohydrate lesions [16,17]. These photoproducts can introduce bends or kinks in DNA strands which can interfere with the mechanism of DNA polymerase. This leads to DNA transcription and replication errors, causing mutation, genomic instability and carcinogenesis.

1.2.2 CPDs

The mechanism by which CPD photoproducts are formed from UV light is [2π + 2π] cycloaddition reaction between carbon 5 and 6 of the two adjacent pyrimidine bases on the same strand. The most commonly formed CPD photoproduct is the thymine-thymine dimer. Four

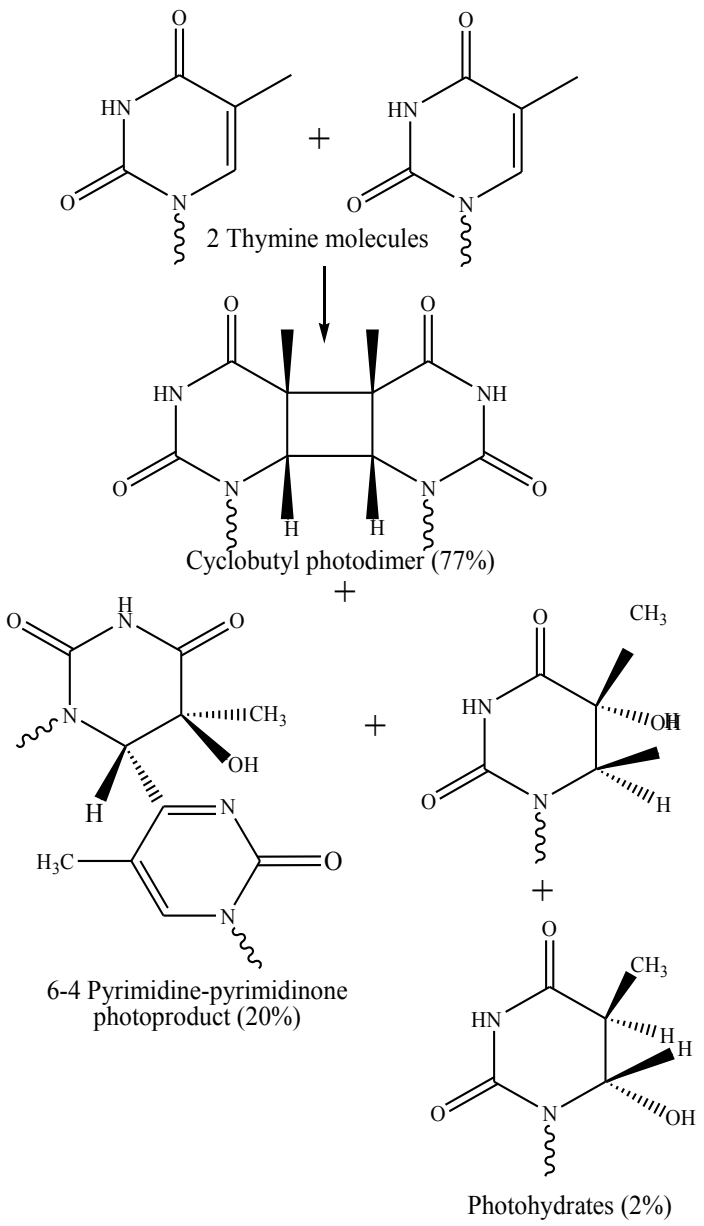

Figure 1.3 Chemical structure of photoproduct formed by thymine. The percentage yield of each photoproduct is indicated.

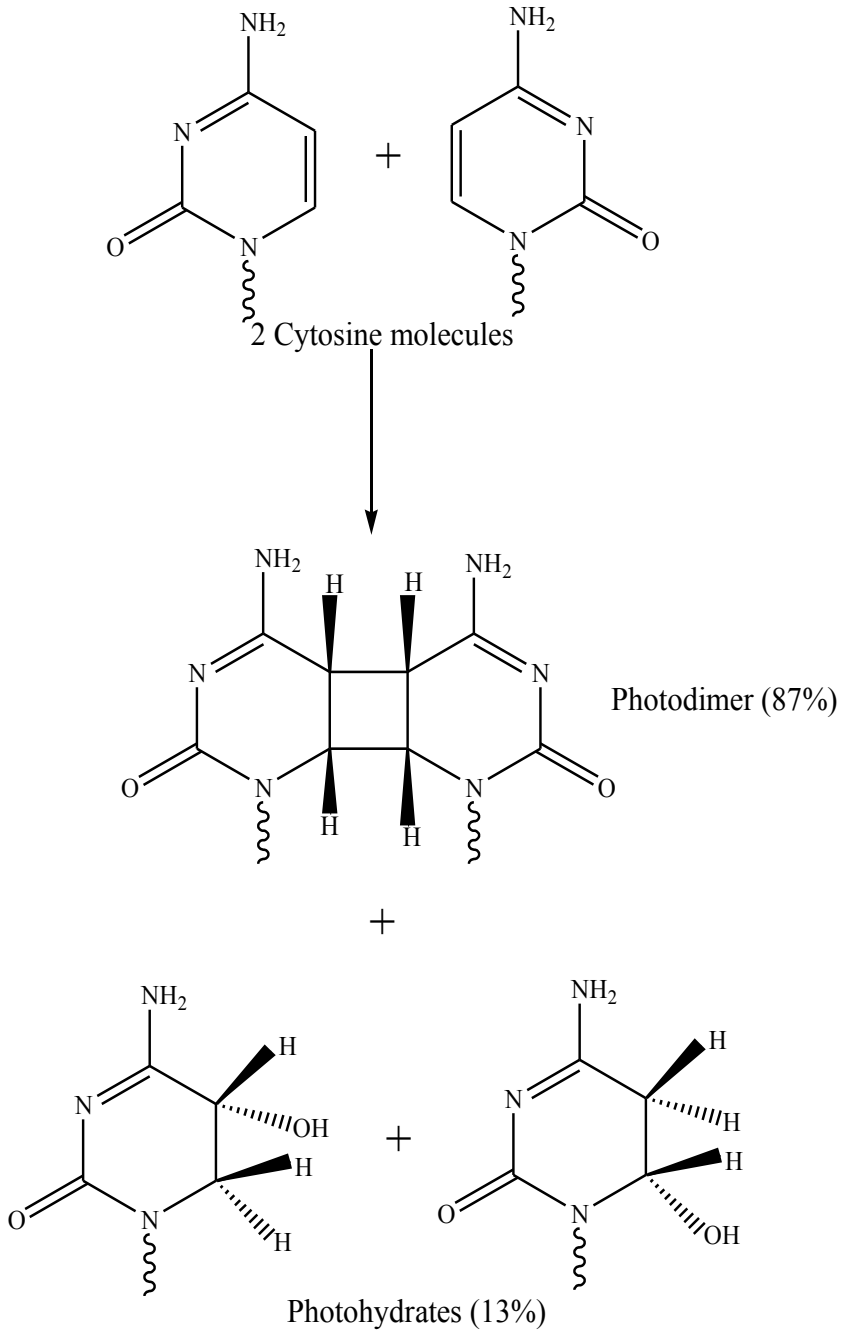

Figure 1.4 Chemical structure of photoproduct formed by cytosine. The percentage yield of each photoproduct is indicated.

diastereomers may be generated for thymine dimer according to the position of the two thymine moieties with respect to the cyclobutane ring (cis/trans) and on the relative orientation of the C5-C6 bonds (syn/anti) [16]. Due to steric constraints between the two thymine molecules only syn isomers can be generated within DNA. The cis-syn isomer predominates in the dsDNA whereas formation of minor amounts of tran-syn isomer has been seen in ssDNA [17].

Other dipyrimidines forming CPD photoproducts include thymine-cytosine, cytosine-thymine and cytosine-cytosine [18]. An investigation on the major hot spots of CPD formation revealed that these photoproducts are influenced by sequence context [17].The presence of 5′ methylcytosine was found to be an ideal hot spot for CPD formation upon irradiation with natural sunlight [17]. The rate of CPD formation was also found to be wavelength dependent. With longer wavelength UVB light, an increase in mainly cytosine-cytosine dimer formation was observed. In contrast thymine-thymine dimer was formed at shorter wavelength UVC light [19]. Here it is worth mentioning that the study of action spectrum of lethality for CPD photoproducts reveals that UVB radiation is more lethal than the UVC radiation. UVC radiation was found to be more mutagenic but not cell killing [20]. This is because some mutations cause changes in the DNA conformation that can be easily detected and fixed by the repair enzymes [21]. On the contrary, when the mutations are not detected by the enzymes they remain unrepaired, causing errors in the DNA. Misreading of these genetic codes could have serious implication such as ageing and cell death [22].

1.2.3 6-4 PPs

Like CPDs, 6-4 PPs are also formed by the [2π + 2π] cycloaddition reaction between the C5=C6 double bond of the 5′ pyrimidine base and the C4=O carbonyl group of the 3′ pyrimidine base *via* an oxetane or azetidine intermediate [23]. These intermediates are unstable and spontaneously

rearrange to a pyrimidine pyrimidinone adduct with a stable covalent bond formed between C4 and C6 of the two adjacent pyrimidines. The 6-4 PPs further undergo photo-isomerization on irradiation with UVB radiation and form their corresponding Dewar valence structures [24,25]. Studies [26] have shown that a greater unwinding of the DNA helix occurs for (6-4) PPs and Dewar PPs when compared to CPDs. However, greater helical distortion has been seen in (6-4) PPs than Dewar PPs [26]. Thus, (6-4) PPs lesions can be easily identified by the repair enzymes and replaced or corrected rapidly. The (6-4) PP can be formed at all the four dipyrimidine sites but its highest quantum yield is at 5′ TC and 5′ CC sites. Negligible amount of (6-4) PP formation occurs at 5′ TT, 5′ CT and the 5′ methylcytosine sites [24].

1.2.4 Purine photoproducts

Purine photoproducts have not been studied as extensively as pyrimidine lesions [24]. It is supposed that one of the purine base adenine is photochemically inert since no photoproducts derived from adenine have been isolated from UV irradiated DNA. However, Pörschke in 1973 found that the poly(dA) sequences undergo photodimerization between adjacent adenine bases upon irradiation at 254 nm with high quantum yield of 2.5×10^{-3} [27]. Later, he also found that 8,8-adenine dehydrodimers were formed upon irradiation at 313 nm [28]. The kinetics of formation for these photoproducts were found to depend on the composition and conformation of the DNA strands with poly (dA) residues. Investigation of the photodimers of adenine shows two distinct photoproducts. One of these corresponds to A=A and the other photoproduct is AA* (Figure 1.5) [29]. These photoproducts are estimated to comprise of only 1% of the total UV photoproducts formed after irradiation [24]. The biological effect of these photoproducts is not well explored.

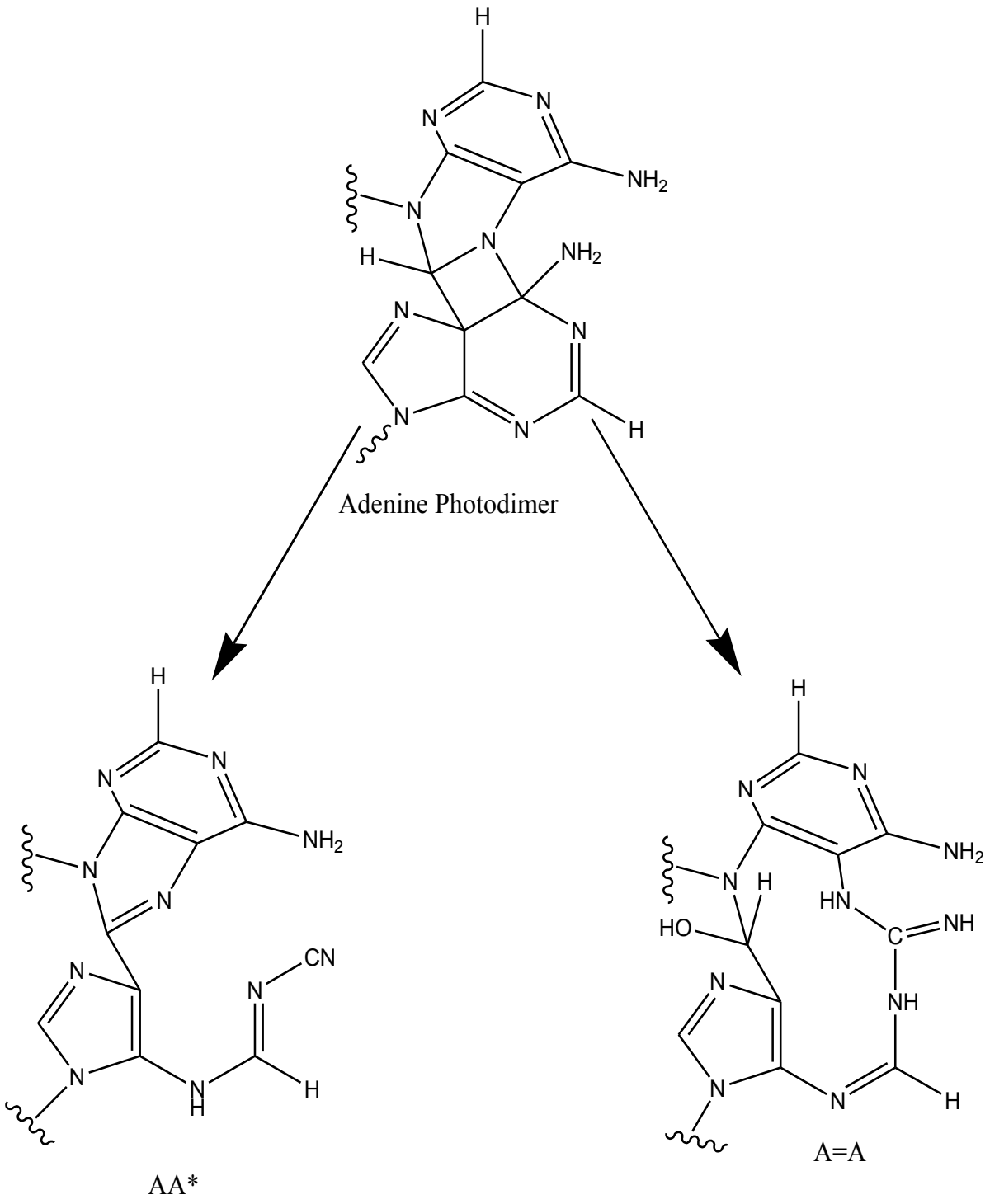

Figure 1.5 Chemical structures of photoproducts formed by adenine.

Another purine photoproduct is the 8-oxoGua (Figure 1.6). This ubiquitous oxidative product is formed in DNA of UVA and UVB irradiated cells by hole migration from initially photo-ionized pyrimidine and adenine bases or singlet oxygen oxidation [30,31]. Guanine, that has the lowest ionization potential among the DNA bases, is the preferential target for most of the one- electron oxidation induced by chemical and physical agents. Oxidation of guanine leads to the formation of 8-oxoGuo, that is used as a biomarker for exposure to oxidative agents [32].

1.2.5 Chemically-induced DNA damage

Exposures to certain chemicals are known to be associated with the induction of human cancer These include insecticides, food additives, preservatives, antibiotics and anticancer drugs [15]. Chemical carcinogens mainly induces DNA damage by the formation of DNA adducts, oxidative damage, DNA-strand crosslinks, DNA strand breaks, chromosomal rearrangement and deletion [33-35]. The type of DNA damage determines the fate of the cell by either causing cell death or by introducing mutations that could be identified and repaired. Mutation in proto-oncogenes, tumour suppression genes or the genes that control the cell cycle can lead to the uncontrolled growth of the cells resulting in increased rate of cell proliferation. Generally, cytotoxic agents which can induce high levels of DNA damage are used as antitumor drugs to kill cancerous cells, but the damage to healthy cells is unavoidable.

The classification of these cytotoxic agents is based on their mechanism of action and the type of DNA damage induced by them. The first chemotherapeutic drug used as a DNA damage agent was nitrogen mustard and nitrosourea [33]. These are alkylating agents that covalently transfer alkyl group onto the DNA bases and form interstrand crosslinks between guanine-guanine and

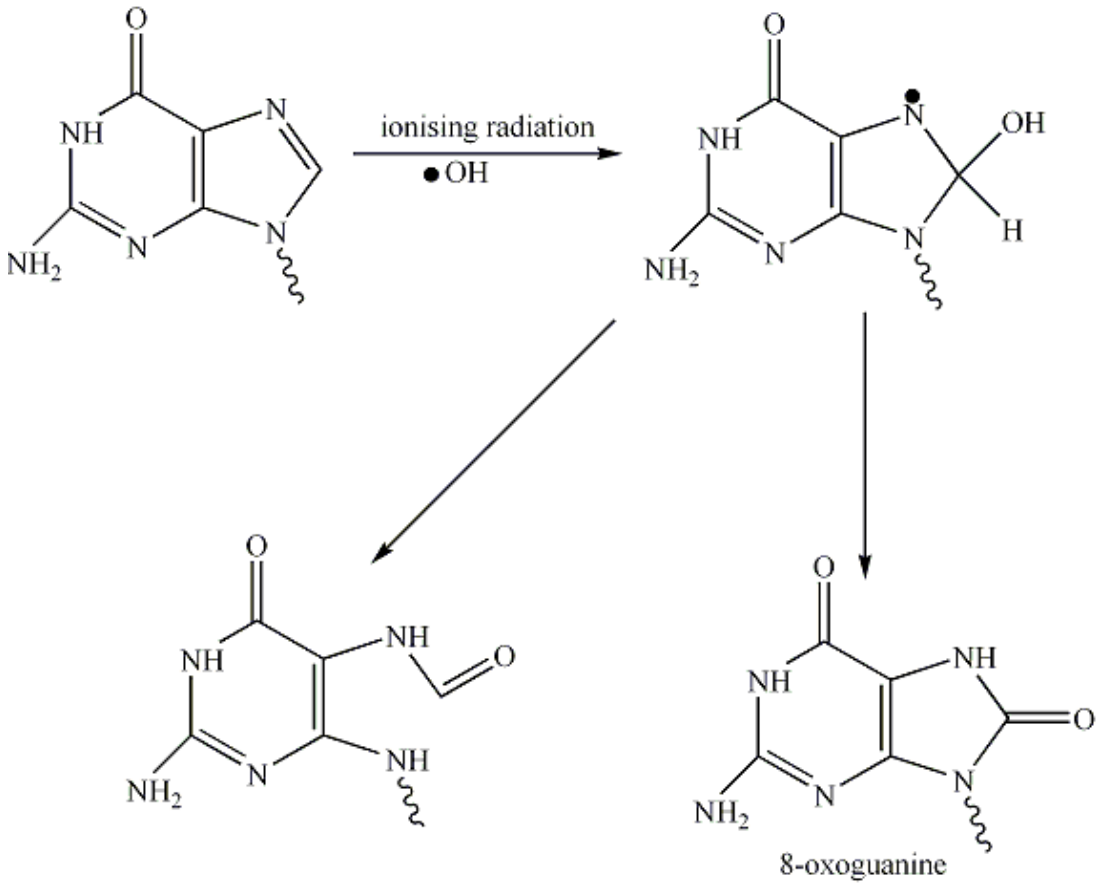

Figure 1.6 Chemical structure and mechanism of photoproduct formed by guanine

guanine-adenine. Other effectively used chemotherapeutic drugs are antimetabolite drugs. They are low molecular weight compounds having structures similar to various metabolites used in nucleic acid synthesis. However, the structures differ enough to interfere with normal cell activities inducing cell death.

Cis-platin (*cis*-diamminedichloroplatinum(II)), and related Pt(II) compounds are antitumor drugs and have been in use for the past three decades. Their mechanism of action is similar to that of the alkylating agents (Figure 1.7). These compounds covalently bind to N7 position of guanine and adenine bases making either monofunctional adducts or inter- and intra- strand crosslinks. The continuous use of these Pt drugs are hindered by their acquired cellular resistance and toxicity towards the healthy cells. Efforts to mitigate these pitfalls lead to the discovery of a variety of analogues of cisplatin which could selectively target the cancerous cells. Metal complexes used for targeted therapy includes complexes of ruthenium [36-38], rhodium [39], cadmium [40], cobalt [41] and nickel [42].

1.3 DNA damage detection

Detection and quantification of the damage caused by different damaging agents such as UV and chemical agents are very important in order to study the overall cytotoxic and mutagenic effects. Thus, several methods have been used for the sensitive and precise measurements of DNA damage.

1.3.1 High-Performance Liquid Chromatography-Electrospray Ionization-Mass Spectrometry (HPLC-ESI-MS)

HPLC coupled to ESI-MS, is a powerful tool for the determination of DNA damage [43]. It has become one of the viable methods for the quantification of DNA adducts formed after exposure to endogenous and exogenous damage agents [44]. In this method, DNA is first enzymatically digested followed by its separation into individual monomer units by running through a HPLC

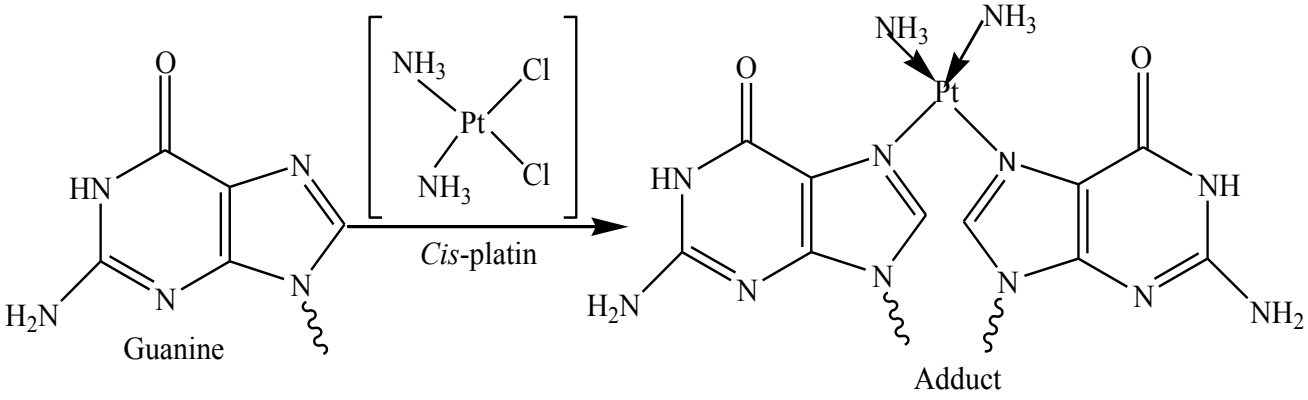

Figure 1.7 Formation of intrastrand adduct between *cis*-platin and guanine nucleobases.

column. Further, the samples were analyzed by direct coupling of the HPLC with MS through ESI source. The process of ESI occurs at atmospheric pressure where the HPLC eluent is converted to a gas phase ion through soft ionization techniques, with negligible dissociation of the molecular ion into fragment ions. The analysis of these molecular ion peaks of the DNA adduct is generally done by a triple quadrupole analyzer. This system comprises of three quadrupoles, where first and third quadrupole serves as a mass analyzer and the second quadrupole serve as a collision cell. The molecular ion of interest is selected by the first quadrupole, followed by collision in the second quadrupole to form specific product ions. Finally the product mass is determined by the third quadrupole. Thus, HPLC-ESI-MS/MS can be used for sensitive and quantitative analysis of DNA adducts. It has been successfully used for measuring all the twelve photoproducts of TT, CT, TC and CC dimers located within isolated and cellular DNA exposed to low level of UVB and UVC radiations [45]. Further, the use of internal standards can provide highly accurate and reproducible results. The detection limit for adducted bases was 0.2-2.0 adduct per 10^8 unmodified DNA bases [44]. Currently, technological advancements are on-going and these efforts have led to the development of chip/LC-MS [46].

1.3.2 Gel Electrophoresis

Gel electrophoresis is an essential tool in molecular biology and is very often used for analysis of DNA damage. This technique separates the DNA exploiting the difference in mobility with size. Thus, it is very sensitive to strand breaks, particularly for single-stranded DNA (ssDNA). Strand breaks could be directly introduced in DNA by the UV and ionizing radiation. Ahmed and Setlow [47] quantified the CPD sites in DNA by investigating the single strand breaks produced at the photoproduct sites by the use of targeted enzymes such as CPD-specific T4 phage endonuclease V. This enzyme cleaves the DNA at 5′ position of CPD photoproducts and subsequently breaks

the phosphodiester backbone *via* abasic cleavage [48]. The migration profile of the DNA relative to molecular weight standards, were used to estimate the number of strand breaks or the number of CPDs/kb. However, the use of this method was limited due to the need of calibration for each run. Overcoming this limitation advanced methods such as phosphorimage analysis has been developed [47]. The sensitivity of gel electrophoresis is influenced by DNA purification and enzyme treatment, since they can introduce additional lesions.

1.3.3 Polymerase Chain reaction (PCR)

PCR is one of the most accurate techniques for detecting DNA damage since the amplification stops at the site of damage. Ligation-mediated PCR (LMPCR) has been widely used for mapping dimeric pyrimidine photoproducts particularly CPD photoproducts in mammalian cells and basal layer of skin [32]. Quantification of CPDs is achieved by the nicking activity of T4 endonuclease V followed by photoreactivation with CPD photolyase to convert the breaks into ligatable 5′ termini. This method achieves high selectivity for CPD amplification. However, its use is limited for mapping (6-4) PPs due to the high background introduced by lesions produced during chemical treatment. Terminal transferase-dependent PCR (TDPCR) is other technique used for mapping of (6-4) PPs [49]. PCR also shows a drastic decrease in amplification rate in the presence of other DNA damage sites such as 8-oxogaunine, 8-oxoadenine and abasic sites [50]

PCR has also been effectively used for the study of DNA damage resulting from drug-DNA interactions. It is assumed that the polymerase progression in PCR is blocked by the presence of even a single lesion, thus making it a great method to quantitate and measure the fraction of undamaged DNA. This method is highly reproducible and used for the detection of damage in both ss and dsDNA [51].

1.3.4 Immunoassa

Immunoassays, which involve the binding of antibodies to DNA molecule is considered to be the most sensitive method in biochemistry [52]. This assay involves the detection of various DNA adducts by their specifically designed antibodies. Several monoclonal and polyclonal antibodies have been synthesized against common DNA damage adducts such as pyrimidine photoproducts [45], oxidative products and DNA carcinogen adducts. The major advantages of immunoassays are their high specificity and sensitivity. But a limitation associated with this method is the lack of calibration curve which prevents the accurate quantification of the DNA adducts. In addition, problems with cross-reactivity do not allow differentiation between the four possible bipyrimidine lesions, providing only semi-quantitative results [45]. Different immunoassays used for DNA adduct quantification are discussed below.

ELISA is one of the method, which has been commonly used for the quantification of CPDs. In this assay, the antigen, antibody and a secondary antibody conjugated to an enzyme are immobilized on an ELISA plate. Upon addition of the substrate for the enzyme, chromogenic reaction products with intense absorption are formed that enables the quantification of the bound antigens [53].

Anti-carcinogen adducts and carcinogen-modified DNA antibodies coupled to radioactive isotopes have been used in radioimmunoassays (RIA). This method is also effectively used for the detection of very low quantity of CPDs and (6-4) PPs formed by low dose of UVB radiation [54].

Immuno-slot-blot (ISB) assay is a highly sensitive assay used for the detection and quantification of DNA adducts produced by carcinogens, mutagens or chemotherapeutic agents [55]. The standard protocol of this assay involves the fragmentation of DNA containing the modified bases by sonication or denaturation at alkaline pH. These fragments are then immobilized on nitrocellulose membrane along with the primary antibody against the DNA adduct under

investigation. Eventually, the detection and quantification of the DNA adduct is accomplished after the secondary antibody binds to the alkaline phosphatase enzyme which produces chemiluminescence signals. The ISB assay is used to detect very low level of adducts in small amounts of DNA [32,56,57]. The method is highly sensitive, reproducible and not limited by the issue of cross reactivity. Thus, ISB assays have been effectively used for the detection and quantification of pyrimidine dimers formed by UVC radiation and carcinogen DNA adducts [57,58].

1.3.5 Comet assay

Comet assay (single-cell gel electrophoresis) is a very sensitive, rapid and reliable method to measure DNA damage such as strand breaks, alkali-liable sites and cross-links. The comet assays are generally performed on two protocols. First, the protocol was given by Singh et al. (1988) who performed the assay at highly alkaline pH. This method was used to measure the low level strand breaks with great sensitivity [59]. Secondly, Olive et al. (1989) used less alkaline pH to study the sensitivity of cells towards drugs and radiation [60]. The simple protocol of the comet assay involves the following steps [61,62]. The cells are embedded in agarose on a glass slide followed by the treatment with cell lysis solution to unwind the DNA. The DNA is then subjected to alkaline electrophoresis and the cellular DNA is visualized using fluorescence microscopy after staining with dyes such as cyber green, ethidium bromide or propidium bromide. The tail has an appearance of a comet which increases in length and size with increasingdamage [63,64]. Comet assays have been successfully used to detect DNA damage in occupational exposure situations or after anticancer drug treatments.

Lesion-specific enzyme treatment extends the usefulness of this method to investigate different kinds of damages. Instant recognition of 8oxoGua is done by formamidopyrimidine-DNA

glycosylase (FPG) enzyme, cytosine hydrate by endonuclease III and CPD by T4 endonuclease V [62]. Modified comet assays have been also used to measure DNA repair activity by treating cells with repair enzymes and monitoring the breaks induced at the damage sites [65]. When comet assay is coupled with fluorescence in situ hybridization (FISH), the assay could be then used for detection of DNA damage and repair at the single gene level [66].

Comet assay is found to be a sensitive method for the detection of low level DNA damage. It requires only small number of cells per sample and the assay is performed in short time. In addition the assay can also be used for the measurement of DNA repair rates in wide range of tumor cells by making certain modification in the experimental protocols [67].

1.3.6 Fluorescent probes

Fluorescence methods have become an essential tool to detect biological molecules with exquisite sensitivity and selectivity. A number of fluorescent probes have been proposed to study DNA damage. These probes are discussed below.

1.3.6.1 Molecular Beacons (MBs)

MBs are hairpin probes that fluoresce upon hybridization with its target [68,69]. They have a stem-loop structure containing fluorescent dye on one end and the quencher on the other end (Figure 1.8): The loop portion of the probe is designed complementary to the target molecule and the stem portion is constructed of annealed complementary arm sequence with 5 to 7 nucleotides The 5′ end of the stem comprises of the fluorescent reporter group and the 3′ end has the quenching group In the absence of the target DNA the stem keeps the fluorophore and quencher in close proximity to each other, causing the fluorescence of the fluorophore to be quenched by Förster resonance energy transfer (FRET). However, in the presence of the complementary target sequence, the MB hybridizes with the target, resulting in an increase in fluorescence. Therefore,

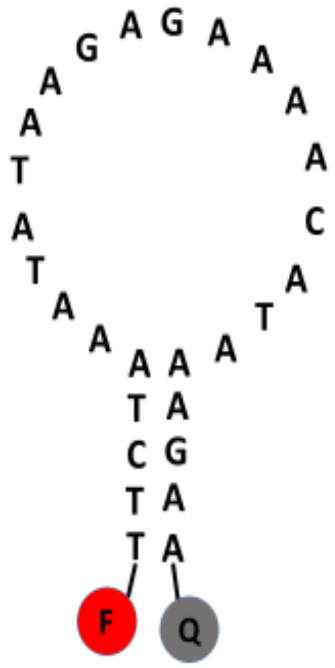

Figure 1.8. Schematic diagram of the stem-loop structure of the molecular beacon. Here "F" denotes fluorophore and "Q" denotes quencher.

the MBs servers as a molecular photo-switch, which turns 'off' in the absence of target due to the closed hairpin form whereas on recognizing its complementary target will immediately switch the fluorescence 'on' [70-72]. When a target sequence is damaged or consists of mismatches, the hybrid formed between the MB and damaged DNA is less stable. This condition results in lower fluorescence from damaged target-hybrid and, consequently, a maximum discrimination of damaged *versus* undamaged target. These inherent properties make MBs a highly sensitive and selective probe for DNA damage studies. Thus, MBs have been used for wide variety of application including qPCR, mutation detection, assaying for nucleic acid cleavage and cancer cell detection [73-75] .

Despite the exquisite sensitivity and wide application of MBs, they suffer from a few limitations [76]. First of all, they require labelling on both 5′ and 3′ end of the hairpin with a fluorophore and a quencher. This patented method of synthesis involves complicated steps that makes the MB probe synthesis tedious and expensive [74]. Secondly, these hairpin probes could not be used for any further modification such as attaching them to a solid support, since both the hairpin terminal are already occupied by a donor and an acceptor. Thirdly, if the MB is not purified properly, there is possibility of MBs with only fluorophore or quencher to be present, which would result in a high background noise or low signal. To overcome these problems some modified hairpin probes were developed, which lack these pitfalls of MBs.

1.3.6.2 Modified Hairpin probes

Development in hybridization assay with fluorescent hairpin probes lead to the extension of MB probes without the quencher moiety. These are called "quencher-free molecular beacons (QF-MBs) [77,78]. Based on the design the QF-MBs can be classified into two categories (a) QF-MBs

with fluorophore at the end of the sequence and (b) QF-MBs with fluorophore in the middle of the sequence.

The QF-MB containing fluorophore at the strand end is known as the “smart probes” (SPs), designed by Sauer and coworkers [79]. In SPs the fluorophore such as 6-carboxyfluorescein (FAM) or rhodamine (R6G) is attached at the 5′-end and the fluorescence is quenched by the neighboring guanine residue chain linked at 3′-end. The quenching occurs due to the effective photoelectron transfer (PET) between the guanine nucleobases and the fluorophore.

SPs (Figure 1.9 (A)), similar to MBs, exists in a stem-loop structure in the absence of complementary target sequences and exhibit a minimum fluorescence intensity due to the quenching of the fluorophore by the guanine residues. However, in the presence of complementary target sequences, the stem unwinds forcing the fluorophore and the guanosine residues far apart, thereby giving a maximum fluorescence intensity. Thus, these probes detect DNA damage and single base mismatches in a similar way as the MB probe [76]. In contrast to MBs, SPs are less expensive and easy to synthesize. The use of SPs, is limited due to the high fluorescence background which results in an increase in analytical parameters such as limit of detection (LOD) and limit of quantification (LOQ).

The QF-MBs containing fluorophore in the center of the sequence is quenched by the adjacent guanines. In hairpin form the guanine effectively quenches the fluorescence of the fluorophore and upon hybridization with the complementary fully matched target sequence a rapid fluorescence enhancement is observed. These probes have also been used for detecting single base mismatches. However, the attachment of a fluorophore in the center of the sequences makes these probes expensive. A much cost effective alternative is the introduction of 2-aminopurine (2AP) group at the center of the hairpin probe (Figure 1.9 (B)). 2AP is a fluorescent base analog of adenine and

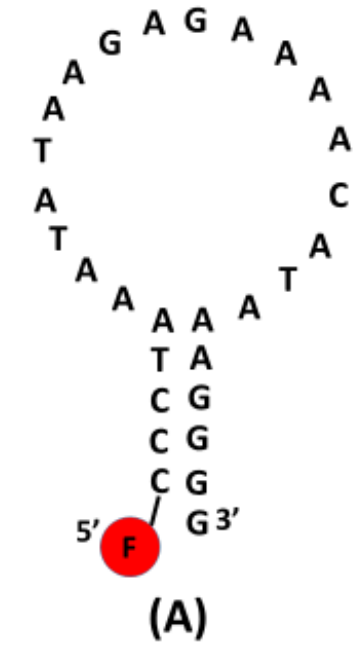

(A)

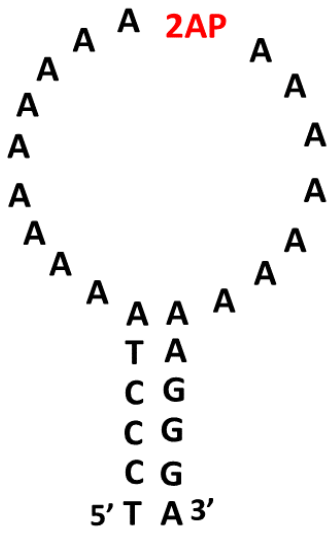

(B)

Figure 1.9. Schematic diagram of the stem-loop structure of (A) smart probe and (B) 2-aminopurine. Here "F" denotes fluorophore and "2AP" denotes 2-aminopurine.

has two useful features. Unlike natural nucleobases, 2AP is fluorescent and its fluorescence intensity depends on the local environment. The 2AP is highly fluorescent when free in solution, but its fluorescence is somewhat quenched in ssDNA and highly quenched in ds DNA due to base stacking interactions [80]. Another advantage of this probe is the ease of its synthesis since being an adenine base analogue they can be easily incorporated into DNA sequences. Moreover they can pair with thymine, similar to adenine and cause minimal disruption of DNA structure.

Although, all above mentioned hairpin probes can be effectively used for DNA damage and single base mismatch studies, these probes need to be designed complementary to the target sequence under study. Thus, for multiple sample analysis different probe sequences has to be designed which makes the method a cumbersome process.

1.4 Multiplex technologies

Multiplex techniques provide a powerful platform to develop valuable tools for high-throughput quantification assays. These types of assays can simultaneously measure multiple samples in one single run. These techniques have the potential to produce considerable saving in time, cost and effort involved within the laboratory without compromising on the accuracy and precision of the experiments.

Microarray multiplex techniques have potential applications in disease diagnostics and drug discovery [81-83]. DNA microarray are slides made of glass, plastic or silicon supports with 10-100 μm reaction zones [84]. They provide an unprecedented opportunity for comprehensive concurrent analysis of thousands of gene expressions in one single run. In this method the DNA target are attached on the slide surface, exposed to DNA damage agent and then damage is quantified by hybridization of the DNA target sequences with their complementary probes (discussed in section 1.5.6.1). Depending on the application, various DNA targets or DNA probes

such as MBs, hairpin probes and peptide nucleic acids (PNA) can be immobilized on the surface of microarray slides [84-86]. The reproducibility of the microarray technique is governed by the efficacy of the immobilization method.

Microarray technology is being extensively used for the study of gene expression and the changes in gene expression profiles in different cell states for a large population of genes simultaneously. Thus, the method is being exploited in pharmaceutical and drug industries to study the effect of drugs, its target and its mechanism. Moreover, it has been used as a diagnostic tool in identification of diseases such as cancer at an early stage [87].

Along with different advantages, various pitfalls are associated with every emerging technology. The major pitfalls of microarray techniques are the issues of reproducibility, repeatability and compatibility across platforms and laboratories [84]. This is because of different parameters involved in the reproducibility of microarray experiments [82]. These include balance between the internal controls and the samples, reproducibility with the microarray scanning parameters and limitations associated with each immobilization technique.

1.5 Aim of the thesis.

The brief discussion presented in the preceding sections illustrates that significant efforts have been focused on detecting DNA damage caused by different mutagenic agents. However, most of the proposed methods mainly focus on the analysis of single sample in a single run. Moreover, developing assays for multiple samples with the above mentioned methods turns out to be a challenging task. Microarray technique (section 1.4.) provided advancement in multiple sample analysis on solid support. Studies have already reported that the conformational dynamics of DNA in solution and solid support are entirely different [88]. Therefore, to understand the damage mechanism of DNA and relate it to human genome, we need to perform our experiments at

physiological conditions. Hence, the major motivation of my work outlined in this thesis is to develop methods for DNA damage detection in multiple samples simultaneously, at physiological conditions.

Chapter 2 describes the use of a 96-well plate coupled with a novel automated sample mover for quantifying UVC-induced DNA damage in multiple samples. To validate our method we compared the damage constant obtained for four different sequences by well-plate method to the cuvette method. Even though well plate method could study the damage kinetics of multiple samples in one single run however, the use of SPs to quantitate the DNA damage makes the method cumbersome. To overcome this limitation we extended our work by using an intercalating dye EvaGreen (EG), to quantify chemically induced-DNA damage. Chapter 3 of this thesis describes in detail the standardization of the experimental parameters done to develop a simple, sensitive, mix-and-read assay to detect DNA damage in multiple samples using EG dye. This dye shows maximum fluorescence for undamaged DNA and a minimum fluorescence for damaged DNA. This change in fluorescence upon damage is used to quantitate Ru-induced DNA damage in multiple ssDNA. Efforts have been made to establish a relation between the damage observed and the Ru-DNA adduct formed. Results show monoadduct formation with Gs and diaaduct formation with GG and GA sites.

Chapter 2 and 3 focus on the development of an analytical technique that could study both the kinetics of DNA damage and determine the harmful dose level of DNA damaging agents. The experimental outline to perform these experiments is shown in Figure 1.10 and 1.11. In chapters 4 and 5, the multiplex method is used to investigate the damage of multiple sequences of dsDNA and ssDNA. In Chapter 4, a comparative study of UVC-induced ssDNA and dsDNA is presented. This study supports the fact that ssDNA are damaged at a much faster rate than dsDNA.

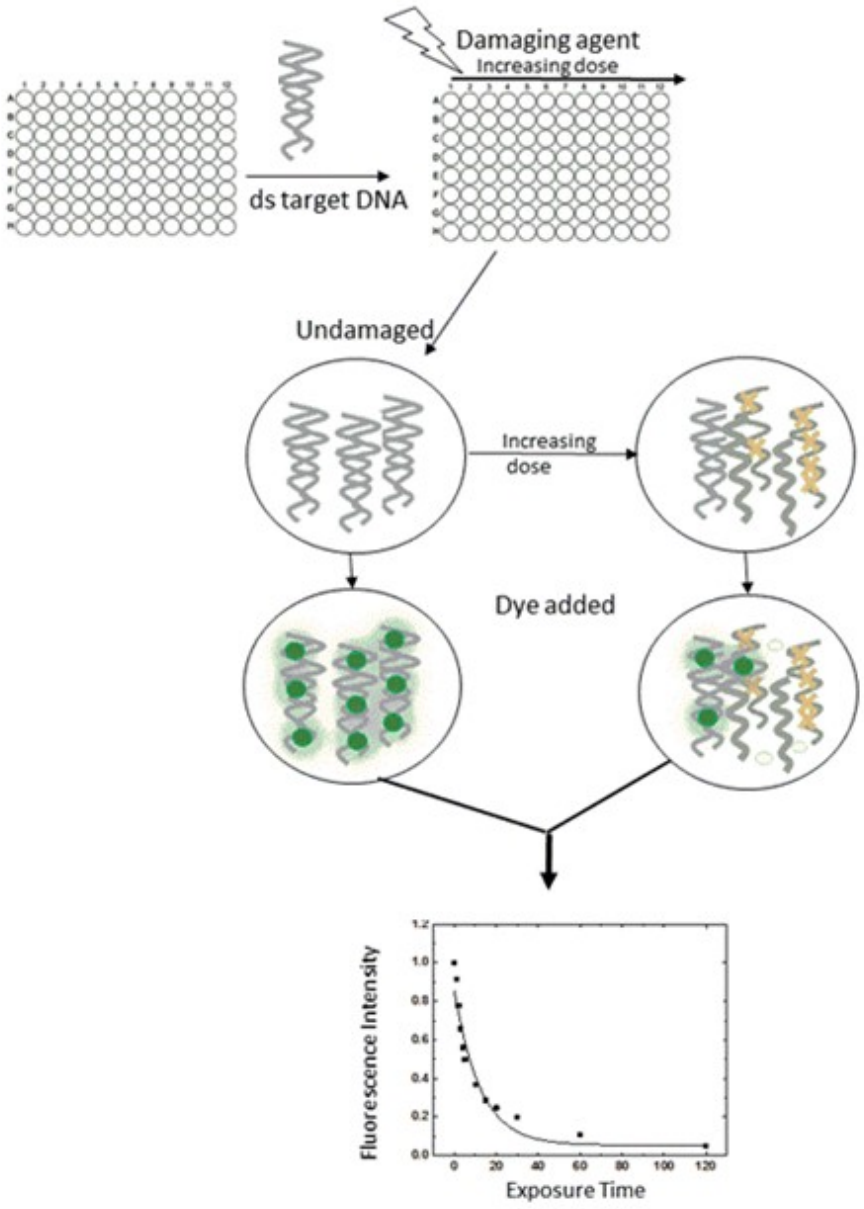

Figure 1.10 Schematic diagram of the experimental outline of DNA damage kinetic study.

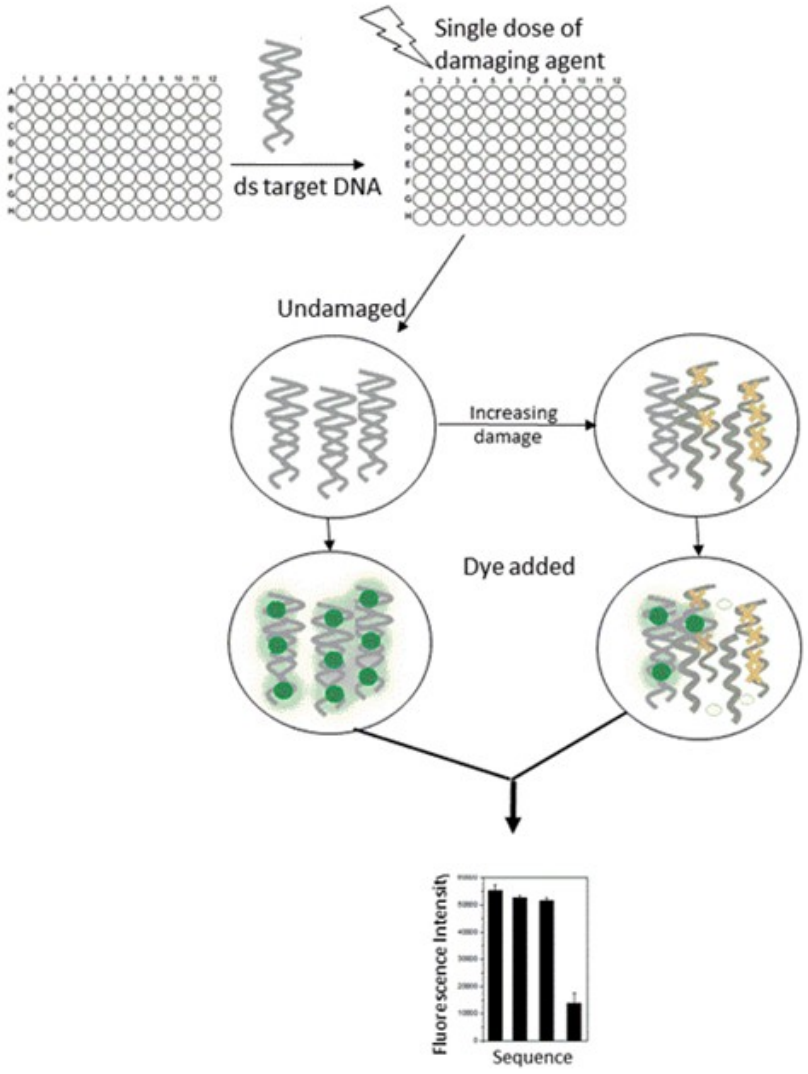

Figure 1.11 Schematic diagram of the experimental outline of exposure study. All the samples were subjected to a single dose of damage agent.

Furthermore, we studied mismatches in dsDNA at varying positions and numbers. We found that the positions of mismatch greatly influences the conformation of the B-DNA helix. Results demonstrate that mismatches at certain positions greatly affects the conformation of the dsDNA rather than the hydrogen bonding as predicted by the melting temperature studies. In Chapter 5, we applied our multiplex method to understand the fundamental chemical mechanism of DNA damage induced by various etiological agents on different sequences of *Ras* genes. With our earlier understanding about the effect of UVC and Ru-induced DNA damage, we set forward the following hypothesis: (1) an increase in UVC-induced DNA damage should be observed with increasing number of Ts and (2) an increase in Ru-induced DNA damage should be observed with increasing number of Gs in the *Ras* sequences. To check this hypothesis we selected few sequences of K-*Ras* and N-*Ras* proto-oncogenes based on either higher number of Gs or Ts in the sequences. Further, we studied the effect of UVC and *cis* Ru-platin analogue on these selected sequences. Surprisingly, we found a good correlation of UVC damage with the number of TT and Ru damage with the number of Gs in the sequences. To understand the damage in detail, we also tried to study the effect of neighboring groups of TT and G sites to the extent of UVC and Ru damage, respectively. In conclusion, the investigations conducted in this thesis open up a new route for a fast, inexpensive mix-and-read assay for multiple sample detection.

Reference List

[1] C.F.A. Bryce and D. Pacini, The Biochemical Society, (1998) pp 6-14, Holbrooks press, UK.

[2] J.M. Berg, J.T. Tymoczko and L. Stryer, Biochemistry, (2002) pp 117-128 Macmillan press, NY.

[3] J.D. Watson and F.H. Crick, Molecular structure of nucleic acids, Nature. **171** (1953) 737-738.

[4] T. Lindahl, Instability and decay of the primary structure of DNA, Nature. **362** (1993) 709-715.

[5] M.S. Cooke, M.D. Evans, M. Dizdaroglu and J. Lunec, Oxidative DNA damage: mechanisms, mutation and disease, FASEB J. **17** (2003) 1195-1214.

[6] S.P. Jackson and J. Bartek, The DNA-damage response in human biology and disease, Nature. **461** (2009) 1071-1078.

[7] B.N. Ames and L.S. Gold, Endogenous mutagens and the causes of aging and cancer, Mutat. Res-Fund Mol M. **250** (1991) 3-16.

[8] A.I. Haza and P. Morales, Spanish honeys protect against food mutagen-induced DNA damage, J. Sci. Food Agric. **93** (2013) 2995-3000.

[9] L.J. Marnett and J.P. Plastaras, Endogenous DNA damage and mutation, Trends Genet.**17** (2001) 214-221.

[10] H.A. Yousef, A. Afify, H.M. Hasan and A.A. Meguid, DNA damage in hemocytes of Schistocerca gregaria (Orthoptera: Acrididae) exposed to contaminated food with cadmium and lead, Nat. Sci. **2** (2010) 292.

[11] J.H. Hoeijmakers, DNA damage, aging and cancer, N. Engl. J. Med. **361** (2009) 1475-1485.

[12] M. Peak, J. Peak, M. Moehring and R. Webs, Ultraviolet action spectra for DNA dimer induction, lethality, and mutagenesis in Escherichia coli with emphasis on the UVB region, Photochem. Photobiol. **40** (1984) 613-620.

[13] R.P. Rastogi, Richa, A. Kumar, M.B Tyagi and R.P. Sinha, Molecular mechanisms of ultraviolet radiation-induced DNA damage and repair, J. Nucleic Acids. **2010** (2010) 592980-593012.

[14] R.P. Sinha and D. Häder, UV-induced DNA damage and repair: a review, Photochem. Photobiol. Sci. **1** (2002) 225-236.

[15] M. Ichihashi, M. Ueda, A. Budiyanto, T. Bito, M. Oka, M. Fukunaga, K. Tsuru and T. Horikawa, UV-induced skin damage, Toxicology. **189** (2003) 21-39.

[16] L. Francesco and W. Horspool, CRC handbook of Organic Photochemistry and Photobiology, (2003) pp.140.1-140.8. CRC Press, USA.

[17] J.L. Ravanat, T. Douki and J. Cadet, Direct and indirect effects of UV radiation on DNA and its components, J. Photochem. Photobiol. B. **63** (2001) 88-102.

[18] A.G. Zavala, R.T. Morris, J.J. Wyrick and M.J. Smerdon, High-resolution characterization of CPD hotspot formation in human, Nucleic Acid Res. **42** (2014) 893-905.

[19] Y.K. Law, J. Azadi, C.E. Crespo-Hernández, E. Olmon and B. Kohler, Predicting thymine dimerization yields from molecular dynamics simulations, Biophys. J. **94** (2008) 3590-3600.

[20] S.I. Tsilimigaki, N. Messini-Nikolaki, M. Kanariou and S.M. Piperakis, A study on the effects of seasonal solar radiation on exposed populations, Mutagenesis. **18** (2003) 139-143.

[21] K. Lin and A.Wang, UV mutagenesis in Escherichia coli K-12: Cell survival and mutation frequency of the chromosomal genes lacZ, rpoB, ompF, and ampA, J. Exp. Microbiol. Immunol. **1** (2001) 32-46.

[22] D.L. Mitchell, J. Jen and J.E. Cleaver, Sequence specificity of cyclobutane pyrimidine dimers in DNA treated with solar (ultraviolet B) radiation, Nucleic Acids Res. **20** (1992) 225-229.

[23] J. Li, Z. Liu, C. Tan, X. Guo, L. Wang, A. Sancar and D. Zhong, Dynamics and mechanism of repair of ultraviolet-induced (6-4) photoproduct by photolyase, Nature. **466** (2010) 887-890.

[24] G.P. Pfeifer, Formation and processing of UV photoproducts: effects of DNA sequence and chromatin environment, Photochem. Photobiol. **65** (1997) 270-283.

[25] P.J. Rochette, N. Bastien, T. Todo and R. Drouin, Pyrimidine (6–4) pyrimidone photoproduct mapping after sublethal UVC doses: nucleotide resolution using terminal transferase-dependent PCR, Photochem. Photobiol. **82** (2006) 1370-1376.

[26] A. Besaratinia, S.I. Kim and G.P. Pfeifer, Rapid repair of UVA-induced oxidized purines and persistence of UVB-induced dipyrimidine lesions determine the mutagenicity of sunlight in mouse cells, FASEB J. **22** (2008) 2379-2392.

[27] S. Kumar, P.C. Joshi, N.D. Sharma, S.N. Bose, R. Jeremy, H. Davies, N. Takeda and J.A. McCloskey, Adenine photodimerization in deoxyadenylate sequences: elucidation of the mechanism through structural studies of a major d(ApA) photoproduct, Nucleic Acids Res. **19** (1991) 2841-2847.

[28] F.P. Gasparro and J.R. Fresco, Ultraviolet-induced 8,8-adenine dehydrodimers in oligo- and polynucleotides, Nucleic Acids Res. **14** (1986) 4239-4251.

[29] R.O. Rahn, Search for an adenine photoproduct in DNA, Nucleic Acids Res. **3** (1976) 879-890.

[30] J. Cadet, S. Courdavault, J. Ravanat and T. Douki, UVB and UVA radiation-mediated damage to isolated and cellular DNA, Pure Appl. Chem. **77** (2005) 947-961.

[31] T. Douki, D. Perdiz, P. Grof, Z. Kuluncsics, E. Moustacchi, J. Cadet and E. Sage, Oxidation of guanine in cellular DNA by solar UV radiation: biological role, Photochem. Photobiol. **70** (1999) 184-190.

[32] J. Cadet, E. Sage and T. Douki, Ultraviolet radiation-mediated damage to cellular DNA, Mutat. Res-Fund Mol M. **571** (2005) 3-17.

[33] L.H. Swift and R.M. Golsteyn, Genotoxic anti-cancer agents and their relationship to DNA damage, mitosis and checkpoint adaptation in proliferating cancer cells, Int. J. Mol. Sci. **15** (2014) 3403-3431.

[34] I. Casorelli, C. Bossa and M. Bignami, DNA damage and repair in human cancer: molecular mechanisms and contribution to therapy-related leukemias, Int. J. Environ. Res. Public Health. **9** (2012) 2636-2657.

[35] M.C. Poirier, Chemical-induced DNA damage and human cancer risk, Nat. Rev. Cancer. **4** (2004) 630-637.

[36] C.S. Allardyce and P.J. Dyson, Ruthenium in medicine: current clinical uses and future prospects, Platin. Met. Rev. **45** (2001) 62-69

[37] M. Groessl, Y.O. Tsybin, C.G. Hartinger, B.K. Keppler and P.J. Dyson, Ruthenium versus platinum: interactions of anticancer metallodrugs with duplex oligonucleotides characterized by electrospray ionization mass spectrometry, J. Biol. Inorg. Chem. **15** (2010) 677-688.

[38] S. Page and R. Wheeler, Ruthenium compounds as anticancer agents, Educ. Chem. **49** (2012) 26-29.

[39] B. Peña, R. Barhoumi, R.C. Burghardt, C. Turro and K.R. Dunbar, Confocal fluorescence microscopy studies of a fluorophore-labeled dirhodium compound: visualizing metal–metal bonded molecules in lung cancer (A549) Cells, J. Am. Chem. Soc. **136** (2014) 7861-7864.

[40] M. Zec, T. Srdic-Rajic, A. Konic-Ristic, T. Todorovic, K. Andjelkovic, I. Filipovic-Ljeskovic and S. Radulovic, Anti-metastatic and anti-angiogenic properties of potential new anti-cancer drugs based on metal complexes of selenosemicarbazones, Anti-Cancer Agents in Med. Chem.**12** (2012) 1071-1080.

[41] S. Chattopadhyay, S. Chakraborty, D. Laha, R. Baral, P. Pramanik and S. Roy, Surface-modified cobalt oxide nanoparticles: new opportunities for anti-cancer drug development, Cancer Nanotechnology. **3** (2012) 13-23.

[42] A.S. Abu-Surrah and M. Kettunen, Platinum group antitumor chemistry: design and development of new anticancer drugs complementary to cisplatin, Curr. Med. Chem. **13** (2006) 1337-1357.

[43] Y. Esaka, S. Inagaki and M. Goto, Separation procedures capable of revealing DNA adducts, J. Chrom. B. **797** (2003) 321-329.

[44] R. Singh and P.B. Farmer, Liquid chromatography-electrospray ionization-mass spectrometry: the future of DNA adduct detection, Carcinogenesis. **27** (2006) 178-196.

[45] T. Douki and J. Cadet, Individual determination of the yield of the main UV-induced dimeric pyrimidine photoproducts in DNA suggests a high mutagenicity of CC photolesions, Biochemistry. **40** (2001) 2495-2501.

[46] D.P. Wasalathanthri, S. Malla, I. Bist, C.K. Tang, R.C. Faria and J.F. Rusling, High-throughput metabolic genotoxicity screening with a fluidic microwell chip and electrochemiluminescence, Lab Chip. **13** (2013) 4554-4562.

[47] V.A. Bespalov, A. Conconi, X. Zhang, D. Fahy and M.J. Smerdon, Improved method for measuring the ensemble average of strand breaks in genomic DNA, Environ. Mol. Mutagen. **38** (2001) 166-174.

[48] D.B. Yarosh, S. Boumakis, A.B. Brown, M.T. Canning, J.W. Galvin, D.M. Both, E. Kraus, A. O. Connor and D.A. Brown, Measurement of UVB-induced DNA damage and its consequences in models of immunosuppression, Methods. **28** (2002) 55-62.

[49] J. Komura and A.D. Riggs, Terminal transferase-dependent PCR: a versatile and sensitive method for in vivo footprinting and detection of DNA adducts, Nucleic Acids Res. **26** (1998) 1807-1811.

[50] J.A. Sikorsky, D.A. Primerano, T.W. Fenger and J. Denvir, Effect of DNA damage on PCR amplification efficiency with the relative threshold cycle method, Biochem. Biophys. Res. Commun. **323** (2004) 823-830.

[51] K.A. Grimaldi, C.J. McGurk, P.J. McHugh and J.A. Hartley, PCR-based methods for detecting DNA damage and its repair at the sub-gene and single nucleotide levels in cells, Mol. Biotechnol. **20** (2002) 181-196.

[52] H. Waller, E. Friess and J. Kiefer, On the immunological detection of X-ray induced DNA damage, Radiat. Environ. Biophys. **19** (1981) 259-264.

[53] J. Peccia and M. Hernandez, Rapid immunoassays for detection of UV-induced cyclobutane pyrimidine dimers in whole bacterial cells, Appl. Environ. Microbiol. **68** (2002) 2542-2549.

[54] M.C. Poirier, S.H. Yuspa, I.B. Weinstein and S. Blobstein, Detection of carcinogen–DNA adducts by radioimmunoassay, Nature **270** (1977) 186-188.

[55] M.C. Poirier, The use of carcinogen-DNA adduct antisera for quantitation and localization of genomic damage in animal models and the human population, Environ. Mutagen. **6** (1984) 879-887.

[56] M. Karbaschi, N.J. Brady, M.D. Evans and M.S. Cooke, DNA repair protocols, (2012) 163-175, Springer, Humuna Press, NJ.

[57] S. Kumari, R.P. Rastogi, K.L. Singh, S.P. Singh and R.P. Sinha, DNA damage: detection strategies, EXCLI J. **7** (2008) 44-62.

[58] A.A. Wani, S.M. D.Ambrosio and N.K. Alvi, Quantification of pyrimidine of pyrimidine dimers by immunoslot blot following sublethal UV-Irradiation of human cells, Photochem. Photobiol. **46** (1987) 477-482.

[59] N.P. Singh, M.T. McCoy, R.R. Tice and E.L. Schneider, A simple technique for quantitation of low levels of DNA damage in individual cells, Exp. Cell Res. **175** (1988) 184-191.

[60] D. Anderson, T.W. Yu and D.B. McGregor, Comet assay responses as indicators of carcinogen exposure, Mutagenesis. **13** (1998) 539-555.

[61] D.W. Fairbairn, P.L. Olive and K.L. O'Neill, The comet assay: a comprehensive review, Mut. Res-Rev Gen. Toxicol. **339** (1995) 37-59.

[62] P. Moller, L.E. Knudsen, S. Loft and H. Wallin, The comet assay as a rapid test in biomonitoring occupational exposure to DNA-damaging agents and effect of confounding factors, Cancer Epidemiol. Biomarkers Prev. **9** (2000) 1005-1015.

[63] M. Lemay and K.A. Wood, Detection of DNA damage and identification of UV-induced photoproducts using the CometAssay™ kit, BioTechniques. **27** (1999) 846-851.

[64] L. Marrot, J. Belaidi, F. Lejeune, J. Meunier, D. Asselineau and F. Bernerd, Photostability of sunscreen products influences the efficiency of protection with regard to UV-induced genotoxic or photoageing-related endpoints, Br. J. Dermatol. **151** (2004) 1234-1244.

[65] A. Azqueta, J. Slyskova, S. Langie, I. Gaivão and A.R. Collins, Comet assay to measure DNA repair: approach and applications, Front. Genet. **5** (2014) 1-19.

[66] M. Glei and W. Schlörmann, Functional analysis of DNA and chromatin, (2014) pp 39-48, Springer,Humuna Press, NJ.

[67] G. Speit and A. Rothfuss, DNA repair protocols, 2012, pp. 79-90, Springer, Humuna Press, NJ.

[68] A. Maksimenko, A.A. Ishchenko, G. Sanz, J. Laval, R.H. Elder and M.K. Saparbaev, A molecular beacon assay for measuring base excision repair activities, Biochem. Biophys. Res. Commun. **319** (2004) 240-246.

[69] W. Tan, K. Wang and T.J. Drake, Molecular beacons, Curr. Opin. Chem. Biol. **8** (2004) 547-553.

[70] L.C. Riches, A.M. Lynch and N.J. Gooderham, A molecular beacon approach to detecting RAD52 expression in response to DNA damage in human cells, Toxicology in Vitro. **24** (2010) 652-660.

[71] Z.J. Shire and G.R. Loppnow, Molecular beacon probes for the detection of cisplatin-induced DNA damage, Anal. Bioanal. Chem. **88** (2012) 1-6.

[72] S. Tyagi and F.R. Kramer, Molecular beacons: probes that fluoresce upon hybridization, Nat. Biotechnol. **14** (1996) 303-308.

[73] X.H. Peng, Z.H. Cao, J.T. Xia, G.W. Carlson, M.M. Lewis, W.C. Wood and L. Yang, Real-time detection of gene expression in cancer cells using molecular beacon imaging: new strategies for cancer research, Cancer Res. **65** (2005) 1909-1917.

[74] Y.L. Jiang, C.A. McGoldrick, D. Yin, J. Zhao, V. Patel, M.F. Brannon, J.W. Lightner, K. Krishnan and W.L. Stone, A specific molecular beacon probe for the detection of human prostate cancer cells, Bioorg. Med. Chem. Lett. **22** (2012) 3632-3638.

[75] D. Klein, Quantification using real-time PCR technology: applications and limitations, Trends Mol. Med. **8** (2002) 257-260.

[76] S.A. Oladepo and G.R. Loppnow, Self-quenching smart probes as a platform for the detection of sequence-specific UV-induced DNA photodamage, Anal. Bioanal. Chem. **397** (2010) 2949-2957.

[77] K.T. Kim, R.N. Veedu, Y.J. Seo and B.H. Kim, Quencher-free molecular beacons as probes for oligonucleotides containing CAG repeat sequences, Chem. Commun. **50** (2014) 1561-1563.

[78] N. Kim, S and Jinks-Robertson, Transcription as a source of genome instability, Nature Rev. Genet. **13** (2012) 204-214.

[79] J.P. Knemeyer, N. Marme and M. Sauer, Probes for detection of specific DNA sequences at the single-molecule level, Anal. Chem. **72** (2000) 3717-3724.

[80] A.F. El-Yazbi and G.R. Loppnow, 2-Aminopurine hairpin probes for the detection of ultraviolet-induced DNA damage, Anal. Chim. Acta. **726** (2012) 44-49.

[81] S. Chakravarty, W. Lai, K. Moncivais, X. Wang, C. Lin, Z.J. Zhang and R.T. Chen, Photonic crystal microarray nanoplatform for high throughput detection of biomolecules, **8034** (2011)m 1-6.

[82] R. Wang, A. Biales, D. Bencic, D. Lattier, M. Kostich, D. Villeneuve, G.T. Ankley, J. Lazorchak and G.Toth, DNA microarray application in ecotoxicology: experimental design,

microarray scanning, and factors affecting transcriptional profiles in a small fish species, Environ. Toxicol. Chem. **27** (2008) 652-663.

[83] H. Wei, P.F. Kuan, S. Tian, C. Yang, J. Nie, S. Sengupta, V. Ruotti, G.A. Jonsdottir, S. Keles, J.A. Thomson and R. Stewart, A study of the relationships between oligonucleotide properties and hybridization signal intensities from NimbleGen microarray datasets, Nucleic Acids Res. **36** (2008) 2926-2938.

[84] A. Sassolas, B.D. Leca-Bouvier and L.J. Blum, DNA biosensors and microarrays, Chem. Rev. **108** (2008) 109-139.

[85] O. Brandt and J.D. Hoheisel, Peptide nucleic acids on microarrays and other biosensors, Trends Biotechnol. **22** (2004) 617-622.

[86] O. Brandt, J. Feldner, A. Stephan, M. Schroder, M. Schnolzer, H.F. Arlinghaus, J.D. Hoheisel and A. Jacob, PNA microarrays for hybridisation of unlabelled DNA samples, Nucleic Acids Res. **31** (2003) 119.

[87] J. Powell, M. Bennett, R. Waters and S. Reed, A novel global genome method to measure and map DNA damage: application for chemotherapy treatment stratification, The Lancet. **383** (2014) 46-49.

[88] J. Yoo and A. Aksimentiev, In situ structure and dynamics of DNA origami determined through molecular dynamics simulations, PNAS. **110** (2013) 20099-20104.

Chapter 2

Multiplexed, UVC-Induced, Sequence-Dependent DNA Damage Detection

(A version of this chapter has been published: S.G. Nair and G.R. Loppnow, Photochem. Photobiol. 89 (2013) 884-890.)

2.1 Introduction

DNA damage leads to cancer, aging and other inheritable diseases [1]. The major sources of DNA damage are ionizing radiation, UV radiation and chemicals. High levels of DNA damage [1] occur from exposure to UV radiation which extends from the UVA band (315-400 nm) through the UVB band (280-315 nm) and to the UVC band (190-280 nm). The primary products of DNA damage due to UV radiation are the pyrimidine dimers such as cyclobutane pyrimidine dimers (CPDs) and [6-4] pyrimidine pyrimidinone photoproducts ([6-4] PPs), as well as uracil and thymine photohydrates[2-4]. In addition, oxidative damage may lead to the formation of 8-oxo-7, 8-dihydro-2′-deoxyguanosine (8-oxodGuo) [5] and other products, such as oxidized pyrimidine bases and DNA-protein crosslinks.

Studies show that tumor genes contain multiple hotspots of damage that are sequence specific [6-8]. Various computational [7] and statistical approaches [9] have been introduced to study the hot spots of mutation in human genome. Recently, a permutation-based study of the melanoma exome to look at mutations caused by UV light exposure led to the discovery of six novel melanoma genes [10]. Also mapping of the hot spots of DNA damage in human P53 gene [11-12] has been studied extensively, but the method involved is long and tedious. Thus there is a need for simple methods that can detect the hot spots of DNA damage in human genome.

A number of techniques have been used to detect DNA damage, including the polymerasechain reaction (PCR) [13,14], HPLC/MS-MS [15-17], GC-MS [18], gel electrophoresis [19], ^{32}P-

postlabeling-HPLC assays [20] and various immunoassays [21]. Though all the methods mentioned above have their advantages, they all involve the isolation and pre-purification of the damaged DNA. This separation is time consuming, expensive and may introduce additional lesions.

The development of fluorescence-based methods, such as molecular beacons [22], has introduced a new class of nucleic acid probes for DNA and DNA damage. Molecular beacons (MBs) are dual-labelled DNA hairpins with a fluorescent dye at one end and a fluorescence quencher at the opposite end. The MB is designed such that in the absence of target, the 3′ and 5′ ends self-hybridize, forcing the beacon to adopt a stem-loop structure and bringing the fluorophore and quencher into close proximity. This arrangement quenches the fluorescence and no signal is observed. Upon hybridization of the MB loop to the complementary DNA target, however, the stem unwinds, forcing the fluorophore and quencher far apart and restoring the fluorescence [23-30]. MBs have rapidly found applications in single-base pair mismatch measurements because of their high sensitivity and selectivity.

Increased knowledge about DNA damage and its direct link to cancer drives an urgent need for an analytical technique which is not only selective and sensitive but can detect damage in a large number of sequences simultaneously. But to study UV irradiation of ssDNA in vitro followed by its detection using MB, a typical experiment involves the irradiation of each sample under study in a cuvette [22, 31-33]. Major limitations of this latter assay are that only a few samples can be simultaneously tested and it is an elaborate assay.

In this study, DNA damage susceptibility in four sequences is measured simultaneously with the high throughput of a 96-well plate. To assay the DNA damage quantitatively, analogues of MBs called smart probes are used. These smart probes (SPs) use multiple guanines as the

fluorescence quencher [33-36]. Also, an automated remote well-plate mover is used to control the damage dose received by each sample. Thus our method can be used to construct a library of hot spots of DNA damage in different genomic sequence. The results obtained showed that this platform for inducing and detecting ssDNA damage compares favourably and quantitatively with cuvette based methods.

2.2 Experimental

2.2.1 Materials. The SPs, MB and single-stranded oligonucleotide targets were obtained from Integrated DNA Technologies Inc. (Coralville, IA, USA). The sequences of the SPs, MB and target oligonucleotides used for this study are listed in Table 2.1. The target oligonucleotides were purified by standard desalting whereas the SPs and MB were purified by HPLC. Tris was obtained from ICN biomedicals (Aurora, OH, USA) and ethylenediaminetetraacetic acid (EDTA) was obtained from BDH Inc. (Toronto, ON, Canada). All chemicals were used as received. Nanopure water (Barnsted Nanopure, Boston, MA, USA) was used to prepare all solutions.

2.2.2 UV Irradiation. Oligonucleotides were dissolved in nanopure water and the SPs and MB were dissolved in Tris buffer (10 mM Tris, 1 mM EDTA, pH ~7.4). All samples were kept frozen at -20^{o}C until needed. Upon thawing, the oligonucleotides are diluted to the required concentration in nanopure water. The MB and SPs were diluted in Tris buffer and annealed each time they are diluted. 100 μL of 1.6 μM nitrogen-purged samples of all four target sequences were placed in a 96-well plate (Corning Special Optics, NY, USA). UV light from UVC lamps emitting at 254 nm was chosen for the irradiation. The UVC light was turned on for 20 min prior to the experiment to ensure a stabilized light source. The photoreactor was purged continuously with nitrogen to remove oxygen and minimize ozone generation from the lamps. Finally, the 96- well plate was placed inside the remote plate mover (RPM) and positioned inside the Luzchem (Ottawa,

Table 2.1 Oligonucleotides and probes used in this study.

Name	Sequences
TarC	5′-AAA AAA CCA AAA AAA AAA-3′
TarG	5′-AAA AAA AAG GAA AAA AAA-3′
TarT	5′-AAA AAA AAT TAA AAA AAA-3′
dT_{17}	5′-TTT TTT TTT TTT TTT TT-3′
SP_{TarC}	5′-(6-FAM)-CCC CTT TTT TTT TTG GTT TTT TAA GGG G-3′
SP_{TarG}	5′-(6-FAM)-CCC CTA ATT TTT TTT CCT TTT TTT TAG GGG-3′
SP_{TarT}	5′-(6-FAM)-CCA CAA TTT TTT TTA ATT TTT TTT GTG G-3′
SP_{dT17}	5′-(6-FAM)-CCC AAA AAA AAA AAA AAA AAT TGG G-3′
MB_{dT17}	5′-(6-FAM)-CAC TTT AAA AAA AAA AAA AAA AAG TG-(3DAB)-3′

Oligonucleotide target sequences and probe sequences used in this study. 5′-Fluorescein (6-FAM) is the fluorophore attached at the 5′-end for both MB and SPs, and 3′dabcyl (3DAB) is the dark fluorescence quencher attached to the 3′-end of the MB only. The underlined bases in the sequence of MB and SPs are the bases that form the stem, and the underlined bases in the targets are the nominal site of damage.

ON, Canada) DEV photoreactor. Each well was exposed to UVC light for a specified time. Control samples were handled under identical condition, but were not exposed to UVC light.

The RPM is a device designed specifically for multiplexed irradiation experiments and can hold a maximum of two 96-well plates. The electronic control panel has 10 different time regulators, each of which can regulate time between 0.5 - 256 min. After the sample plates were positioned in the RPM, each row of the 96-well plate was set to a different exposure time. After irradiation, the 96-well plates were taken out of the RPM and the respective SPs were added to each well. The final concentration of the targets and SPs were made to 0.53 μM and 0.18 μM, respectively, by adding buffer (10 mM Tris, 1 mM EDTA, 5 mM $MgCl_2$, and 20 mM NaCl, pH ~7.4). The well plates were then incubated for 20 h in the dark at room temperature. For sensitivity measurements, 13.3 μL aliquots of dT_{17} sample were taken from 8 μM of irradiated solution in a cuvette at different time intervals and mixed with the appropriate amount of the probe and buffer to give a final concentration of 0.53 μM target and 0.18 μM complementary SP. These solutions were incubated in the dark for 20 h at room temperature and fluorescence spectra were recorded as described below.

2.2.3 Chemical Actinometer. Potassium iodide-iodate actinometer was used for measuring the amount of photon absorbed by the triiodide sample in case of cuvette and well plate method. The standard solution, consisting of 0.1 M KIO_3, 0.6 M KI and 0.01 M borate buffer at pH 9.25 was prepared as described by Rahn [37].The samples were placed in the photoreactor and irradiated with UVC light in both well plate and cuvette, simultaneously. For cuvette experiment 3 mL of the iodide-iodate solution was irradiated in sealed, 1cm path length UV-transparent cuvette and for well plate experiment 100 μL of the solution was taken in the 96-well plate. The samples were exposed to radiation from four UVC lamp held at vertical position. The absorbance measurements

before and after irradiation were made using Hewlett-Packard (Sunnyvale, California) 8452A diode array spectrophotometer. All measurements were made against water as blank.

2.2.4 Fluorescence and absorbance measurements. Room-temperature fluorescence intensities were measured using the Safire fluorescence plate reader (Tecan, Mannendorf, Switzerland) for 300 μL of the hybridization mixture in the 96-well plate, containing 0.53 μM target and either 0.18 μM SP or MB in buffer. Fluorescence emission spectra were recorded using an excitation wavelength of 480 nm and an emission wavelength of 520 nm. The bandwidth for excitation and emission were 10 and 12 nm, respectively.

The SPs were characterized by their melting curve, in which temperature-dependent fluorescence measurements were carried out on buffered solutions of SPs incubated in the presence and absence of their complementary targets. These melting curves were also measured on solutions of SPs with irradiated target. The temperature was varied from 20 ^{o}C to 80 ^{o}C in increments of 4 ^{o}C, a heating rate of 1 ^{o}C/min and a 5 min settling time. Fluorescence spectra were measured using a Photon Technologies International (Birmingham, New Jersey) fluorescence system. The excitation wavelength was fixed at 480 nm and the emission was recorded from 490 to 700 nm (Figure A 1). The bandwidth for both excitation and emission were set at 4 nm. A 10 mm path length Suprasil quartz fluorescence cuvette was used for these measurements. Both melting and cooling curves were measured for all four SPs and their complementary targets, with SP concentrations of 0.18 μM and target concentration of 0.53 μM. Absorbance measurements were performed on a Hewlett-Packard (Sunnyvale, California) 8452A diode array spectrophotometer.

2.3 Results and Discussion

In this chapter, a method for simultaneously assaying the damage to a large number of single-stranded oligonucleotide samples was devised using a 96-well plate. All four oligonucleotide

targets were irradiated in a 96-well plate and the resulting damage was measured by fluorescence. The damage constants obtained were compared with those obtained by the cuvette method.

2.3.1 Characterization of the Smart Probes. All the SPs used in this study were designed carefully to get the maximum performance as sensitive probes for DNA damage. A maximum discrimination between the SP and the SP-target hybrid for all the different sequences is obtained for a buffer with 10 mM Tris, 1 mM EDTA, 5 mM $MgCl_2$ and 20 mM NaCl, pH~7.4 (Figure A 4) and for an optimum working ratio between the SP and the target of 1:3 (Figure A 3). All the SPs used in this study were carefully designed to optimize their performance in selectively discriminating damage in the target oligonucleotides. The melting curves for all the SPs, in the absence and presence of complementary target oligonucleotide, are shown in Figure 2.1. It can be seen from the figure that the SPs exist in the hairpin form at low temperature and exhibit minimal fluorescence intensity. At these temperatures, the guanine residues at the 3′ end are in close proximity to the dye, quenching its fluorescence. As the temperature increases, the stem begins to melt, forcing the quenching guanosine residues farther from the fluorophore and resulting in higher fluorescence intensity (33). Finally at temperature higher than 60 ^{o}C, we see a decrease in fluorescence with increasing temperature since the intensity of the dye FAM, decreases at higher temperature (Figure A 5).

In the presence of the perfectly complementary oligonucleotide target, a different pattern is seen for the melting curve. The hybrid melting curve started with high fluorescence intensity due to the open form of the SPs, and gradually the fluorescence decreased until the target completely

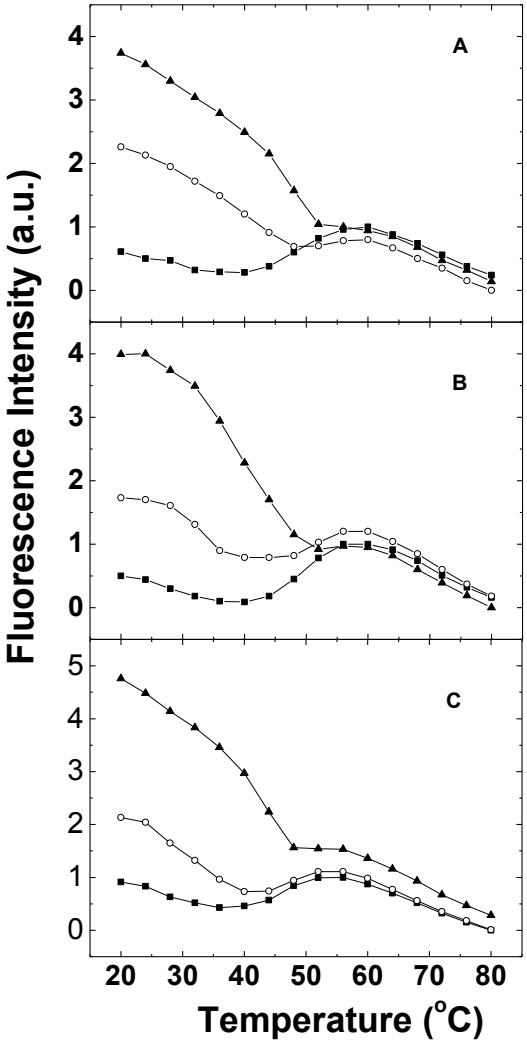

Figure 2.1 Melting curve of 0.18 μM SP alone (filled squares), 0.18 μM SP in the presence of a 3-fold excess of perfectly complementary undamaged oligonucleotide target (filled triangles) and 0.18 μM SP in the presence of a 3-fold excess of complementary damaged oligonucleotide target (open circles). The different panels represent the melting curves for (A) SP_{TarC}, (B) SP_{TarG}, and (C) SP_{TarT}. Fluorescence curves have each been scaled to the SP alone.

melted away from the hairpin probe. The hairpin probe reformed its stem-loop structure exhibiting low fluorescence intensity and, with the further increase in the temperature, gave the intermediate, high temperature fluorescence intensity of the SP-alone melting curve.

Similar patterns to the hybrid melting curves are obtained when the melting curves are plotted for the damaged oligonucleotide target-SP hybrids (Figure 2.1). As expected, the binding for the hybrid should be destabilized upon damaging the target sequence. For all the melting curves between the SPs and the damaged oligonucleotide targets in Figure 2.1, the hybrid had a lower fluorescence signal at low temperatures than the hybrid with the undamaged oligonucleotide. Also, the apparent melting temperature (T_m) of the damaged oligonucleotide target-SP hybrid is lower than that of the undamaged oligonucleotide target-SP hybrid. From Figure 2.1(B) if we compare the melting temperatures between TarG-SP_{TarG} damaged and undamaged hybrids, we found that the melting temperature decreased from 40 ^oC to 32 ^oC upon 88 min damage.

This hybrid stability in the presence and absence of damage can be correlated to the amount of damage. Figure 2.2 shows the melting curve for the SP_{dT17} alone and in the presence of irradiated dT_{17} at different time intervals. With the increase in the exposure time, the fluorescence melting curve is lower, indicating increasing damage. In addition, the T_m of the damaged target-SP hybrid also decreased with increasing irradiation time. This result showed that the SP is able to discriminate between different amounts of damage caused by UVC radiation. Similar results were obtained for the other targets.

2.3.2 DNA damage. The selectivity of SP to detect UVC-induced damage in oligonucleotide target dT_{17} was compared with that of the MB by the well plate method. The sequence of the MB used in this study is listed in Table 2.1. Similar to the SP, the MB has a fluorescein (FAM) fluorophore at the 5′ end but the guanine quencher is replaced by a dabcyl (DAB) quencher at its

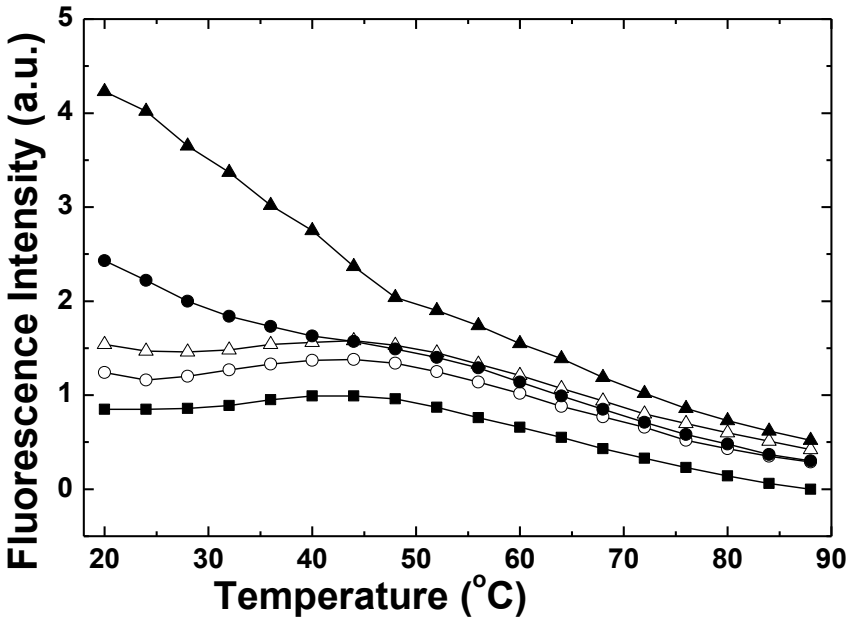

Figure 2.2 Melting curve of 0.53 μM SP_{dT17} alone (filled squares), 0.18 μM SP_{dT17} in the presence of a 3-fold excess of perfectly complementary oligonucleotide target (filled triangles) and 0.18 μM SP_{dT17} in the presence of a 3-fold excess of complementary oligonucleotide damaged for 9 min (filled circles), 25 min (open triangles) and 57 min (open circles). Fluorescence curves have each been scaled to the SP_{dT17} alone.

3′ end. The decrease in the MB and SP fluorescence intensity for dT_{17} target with increasing irradiation is shown in Figure 2.3. The damage constant obtained for the SP was 1.6 fold higher than the MB probe. The higher value of the damage constant the lower the selectivity of the probe to detect damage. Thus, we can conclude that the selectivity of SP toward detecting UV damage is slightly less than that of the MB. This may be due to inefficient quenching of fluorescence by the guanosine residues [32] as depicted by its higher residual fluorescence.

To study the sensitivity of the SP for UVC-induced photoproducts, a dT_{17} target was chosen because of its well-known photochemistry. The primary photoproducts of this target are thymine CPDs along with lower yields of [6-4] PPs and the Dewar isomer, in the ratio of 77:20:0.8 [2]. To quantify the amount of photoproduct formed in this experiment, the absorbance of dT_{17} at 260 nm was measured as a function of irradiation time by the cuvette method (Figure A 2). This absorbance band gradually bleaches with increasing irradiation time due to the loss of C_5=C_6 bond during the formation of thymine photoproducts. To confirm that the bleaching is only due to thymine photoproduct formation, the absorbance at 260 nm of the unirradiated control was also taken. Thus, the absorbance peak measured at 260 nm at different irradiation times is the weighted average of all three photoproducts formed [38]. Figure 2.4 shows the calibration curve obtained by plotting the SP fluorescence as a function of calculated total concentration of photoproducts obtained from the absorbance measurements. At a zero concentration of photoproduct, the target is a perfect complement to the SP and gives maximum fluorescence intensity. As the amount of photoproduct increases up to 10×10^{-7} M, there is no considerable change in the fluorescence intensity, indicating that the SP has a threshold for the detection of DNA damage. Since the target concentration is 5.4×10^{-7} M and the threshold is 10×10^{-7} M, taking the ratio of the threshold concentration of DNA photoproduct to the target concentration yields a value of ~ 2. Thus the presence of 2-3 lesion sites

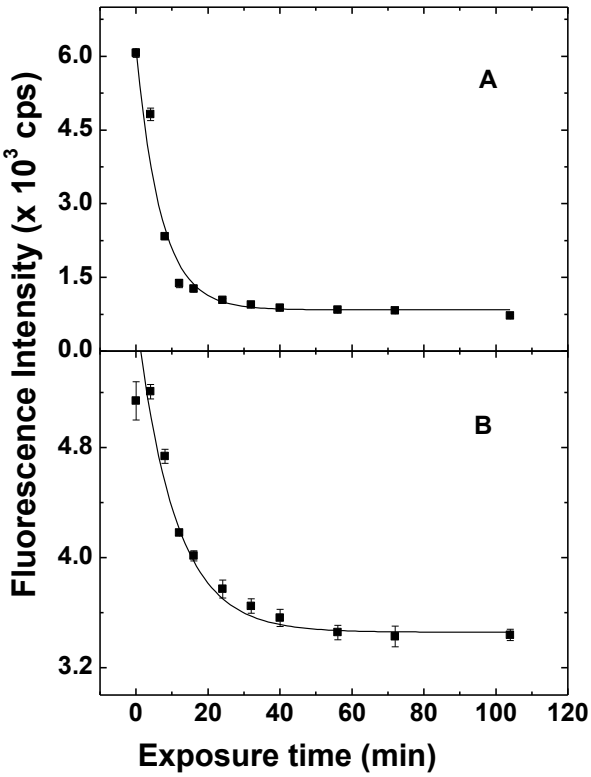

Figure 2.3 Fluorescence decay curves for (A) MB and (B) SP detection of damage in dT_{17}. The curve were obtained by exciting the hybridization mixture of 0.53 μM target and 0.18 μM complementary SP_{dT17} or MB_{dT17} in buffer (5 mM $MgCl_2$, 20 mM NaCl, 10 mM Tris and 1 mM EDTA, pH 7.4) at 480 nm and emission recorded at 520 nm. The solid lines through the points are single exponential $I_F = I_o + Ae^{-t/\tau}$ fits. The fluorescence parameters obtained from the fit for dT_{17} with MB probe are $I_o = 0.84 \pm 0.02 \times 10^3$ cps, $A = 5.32 \pm 0.37 \times 10^3$ cps and $\tau_1 = 6.90 \pm 0.70$ min. The fluorescence parameters obtained from the fit for dT_{17} with SP probe are $I_o = 3.46 \pm 0.07 \times 10^3$ cps, $A = 2.31 \pm 0.21 \times 10^3$ cps and $\tau_1 = 10.72 \pm 1.28$ min.

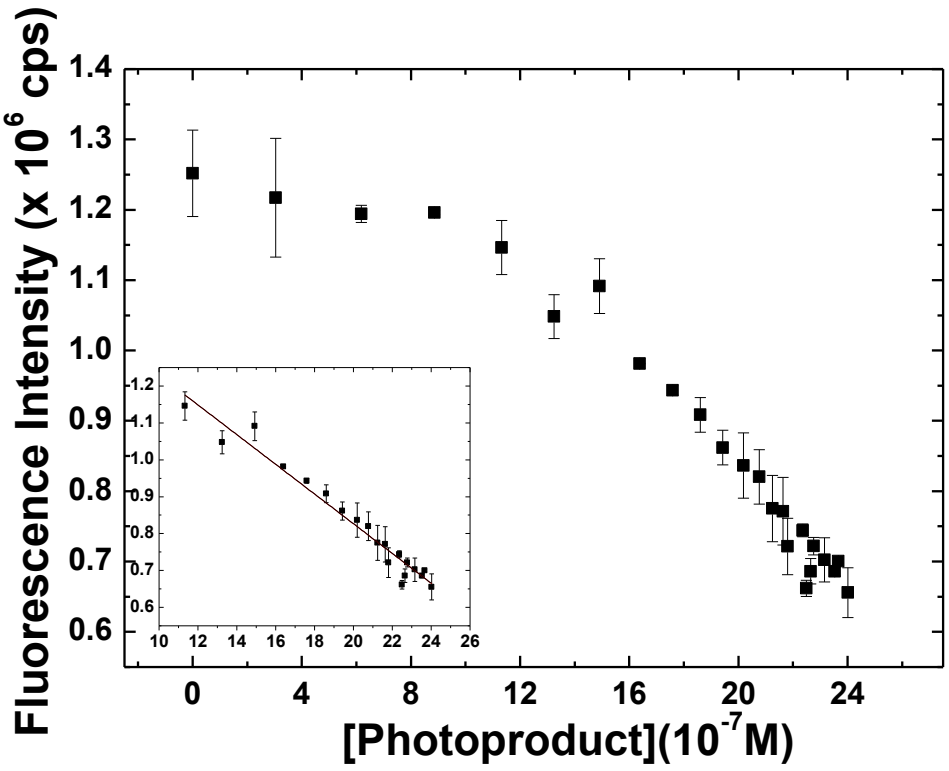

Figure 2.4 SP_{dT17}-target hybrid fluorescence intensity at 520 nm as a function of calculated photoproduct formation in a 0.18 μM solution of dT_{17}. Inset shows the linear portion of the graph with $R^2 = 0.96$. The sensitivity (slope of the calibration curve) is 4.0×10^{11} M^{-1}. LOD and LOQ values are 55 nM and 183 nM, respectively.

on each target strand are necessary before the SP-target hybrid is destabilized enough to show a fluorescence decrease. This compares favourably to the 3-4 lesion necessary for the MBs [22].

With a further increase in concentration of photoproduct, the fluorescence intensity decreases rapidly, showing the sensitivity of the SP toward DNA damage (Figure 2.4). The linear drop of fluorescence with increasing amount of photoproduct formation is shown more clearly in the inset of Figure 2.4. The calibration curve in this region showed good linearity with a linear regression coefficient of 0.96 and sensitivity (slope of the calibration curve) of 4.0×10^{11} M^{-1}. The resulting limit of detection (LOD) and limit of quantification (LOQ) values are therefore 55 nM and 183 nM of damaged ssDNA, respectively. The standard deviation of the background used for the above calculation was obtained by measuring the fluorescence intensity of unhybridized SP samples (Table A 1).

2.3.3 Detection of UV-induced DNA photodamage in 96-well plate. Oligonucleotide solutions of all four sequences from Table 2.1 were irradiated in a 96-well plate at constant temperature and the damage constants for each sequence were obtained (Figure 2.5).The maximum irradiation time was set to 248 min, when all the four target oligonucleotide were completely damaged and gave the fluorescence similar to their SP alone values. The damage constants along with their standard deviations are listed in Table 2.2. The damage constants obtained in this study for TarC and TarT are 130± 40 min and 90.1 ± 10 min, respectively. Previous studies had shown that exposure of DNA containing adjacent pyrimidines, to UVC irradiation gives the CPD as the main photoproduct, with [6-4] PP and the Dewar isomers as the minor products [2]. But the quantum yield for formation of photoproducts between adjacent thymines is larger than that for adjacent cytosines [39]. The results obtained in this study clearly supported the fact that thymine nucleobases are a preferential target for UVC-induced damage compared to cytosine.

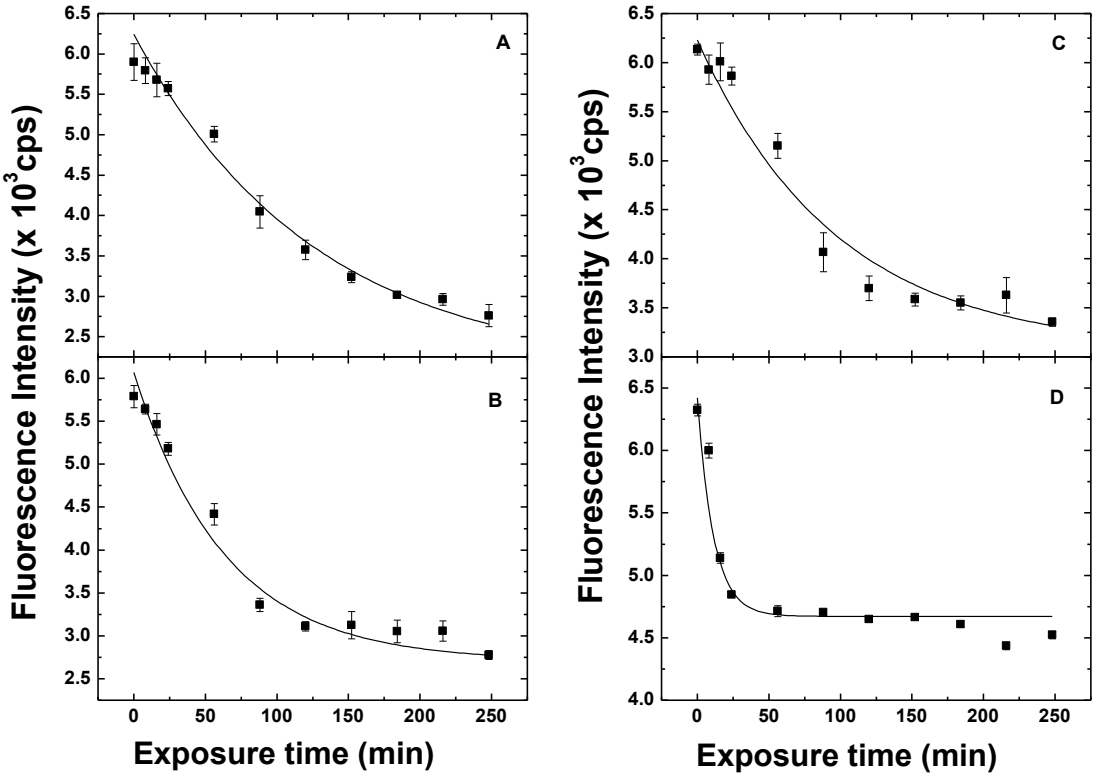

Figure 2.5 Fluorescence damage curve for (A) TarC, (B) TarG, (C) TarT and (D) dT_{17}. Graphs were obtained by exciting the hybridization mixture of 0.53 μM target and 0.18 μM SP_{TarC} in Tris buffer at 480 nm and recording the emission at 520 nm. The solid lines through the points are single exponential $I_F = I_o + Ae^{-t/\tau}$ fits. The fluorescence parameters obtained from the fit for TarC are I_o = 2.08 ± 0.39 x 10^3 cps, A = 4.2 ± 0.31 x 10^3 cps and τ_1 = 125.75 ± 28.23 min. The fluorescence parameter obtained for sequences TarG are I_o = 2707.35 ± 120.13 x 10^3 cps, A = 3362.59 ± 140.09 x 10^3 cps and τ_1 = 63.67 ± 8.90 min. The fluorescence parameter obtained for sequences TarT are I_o = 2661.31 ± 65.59 x 10^3 cps, A = 3061.42 ± 64.84 x 10^3 cps and τ_1 = 84.93 ± 5.87 min. The fluorescence parameters obtained for sequences dT_{17} are I_o = 4693.78 ± 10.38 x 10^3 cps, A = 1704.22 ± 31.12 x 10^3 cps and τ_1 = 12.90 ± 0.58 min.

The damage constants obtained for dT_{17} and TarT are 12 ± 0.7 min and 90 ± 10 min respectively. As discussed above CPD is one of the major photoproduct formed between adjacent thymine, therefore the ratio of formation of photoproduct between dT_{17} and Tar T is 8: 1. Thus we expect the damage constant for Tar T would be 8 times higher than dT_{17}. The results obtained for these sequences were found to be consistent with the theoretical explanation.

The damage constant obtained for TarG in this study is 60 ± 10 min, which is surprisingly lower than that of TarT. The major photoproduct of guanine in DNA is the formation of 8-oxodGuo, which has a very low photoproduct formation rate [40]. In both TarG and TarT sequences, the 'GG' and 'TT' nucleobases had adenine as their neighbouring groups. Thus, there is a possibility of forming various photoproducts. Previous studies [41,42] have shown that UVC irradiation of DNA strand containing 'AATTAA' would produce the AA and TA photoproducts, along with the CPD and [6-4] PP. The yield of formation of the [6-4] PP was found to have a sequence-dependent photochemistry. However, in the case of guanine, UVC excitation may produce guanine radical cations followed by 8-oxodGuo formation [43]. Thus, the selectivity of SP to detect damage will depend on the change in the conformation of nucleobases upon photoproduct formation, and the 8-oxo-dG photoproduct may be more disruptive to SP hybridization.

This discrepancy in the decay rates of TarT and TarG may also be attributed to the difference in damage kinetics of the sequences due to the neighbouring nucleobases. In a previous experiment [44] designed to study the reactivity of a TT dinucleotide embedded in different sequences, it was shown that the rate of formation of thymine photoproduct is surprisingly reduced when the neighbouring groups are changed from cytosines to adenines. It was assumed that the thymine nucleobases could be locked between the neighbouring adenine residues, hindering the CPD photoproduct formation [44]. Not much work has been done to study the neighbouring group effect

Table 2.2 UVC damage constants obtained for the 4 different DNA target sequences.

Name	96 well plate experiment τ (min)		Average τ (min)	Cuvette Experiment τ (min)
	1	2		
TarC	130 ± 20	130 ± 30	130 ± 40	30 ± 2.0
TarG	60 ± 10	60 ± 9.0	60 ± 10	8 ± 1
TarT	100 ± 10	85 ± 6	90 ± 10	15 ± 3.0
dT_{17}	11 ± 0.4	13 ± 0.6	12 ± 0.7	3.8 ± 0.1

Damage constants obtained for the four oligonucleotide sequences used in this work. The values were obtained from the fluorescence damage curves which were fit to a single exponential function.

adenine nucleobases due to its large size, and thus become more UVC-vulnerable.

of the adenine nucleobases on the stability of guanine radical cation. We assume that in such sequence the oxidation of C-8 carbon atom of guanine nucleobases are not hindered by the adjacent However, despite of the advantages of SP of being a general and inexpensive probe to detect DNA damage. SPs have the disadvantage of not being a very selective probe for different type of photoproduct formed during the DNA damage. Thus it may respond differently to different damage product. Moreover due to the inefficient quenching by the guanosine residues constant background fluorescence is observed. Thus probes with better sensitivity and selectivity are to be studied [38].

Also a comparative study of the damage constant obtained by the 96-well plate experiment was done with that of the cuvette experiments. Both methods gave the highest damage constant value for TarC and the lowest value for dT_{17}. Thus supporting the fact that oligonucleotide dT_{17} has much faster rate of photoproduct formation when compared to the other three targets. However, the actual damage constants obtained in the cuvette experiments are lower than the 96-well plate experiments as shown in Table 2.2. This change is due to the difference in the experimental conditions. When the experiments are performed in the cuvette, the samples are constantly stirred and subjected to a power of 223.6 mW from the UVC lamp. But for the 96-well plate experiments the power received by the unstirred samples in the wells drop down to 2.64 mW. Similar results were obtained when iodide- iodate chemical actinometry was performed using both cuvette and well plate method. The formation of triiodide was calculated by studying the change in absorbance at 352 nm with increasing irradiation time. A calibration curve is obtained by plotting the moles of triiodide formed at six different exposure times as a function of exposure time (Figure A 6). The rate of formation of triiodide is given by the slope of the calibration curve [45]. On comparing

the rate of triiodide formation by cuvette method to that of well plate method, we found that the cuvette method is 33 times faster than the well plate method. This supports our results that the sample irradiated in the cuvette receives more photons than the samples in the well plate, thus giving faster decay kinetics. Since the rate of irradiation in the cuvette experiment was much faster than the well plate, the concentration of iodide-iodate sample for cuvette experiment was chosen to be half the concentration for well plate. No formation of triiodide was observed for unirradiated sample in both cases.

However, on comparing the statistical ratio between the damage constants obtained for the four oligonucleotide targets by these two methods, they are found to be different. TarC and dT_{17} showed a 4-fold increase in the damage constants whereas TarG and TarT showed a 7-fold increase in the value of their damage constants on switching from the cuvette experiment to the well plate experiment. This difference in the ratio of damage constants can be explained by lower UVC intensity in the well plate experiment and that the 96-well plate samples are unstirred. Thus, there is the possibility of secondary photoproduct formation which affects the quantum yield and absorption cross-sections, changing the kinetics of photochemical decay. However, the results show that both methods are consistent, and gave a similar pattern of damage constants for all the oligonucleotides.

2.4 Conclusion.

We have designed a novel analytical technique to detect DNA damage in a 96-well plate coupled with an automated sample mover. This method has the advantage of irradiating multiple samples in a 96-well plate followed by a fluorescence measurement in a simple mix-and-read assay using smart probes. Thus, we have developed a methodology to examine different damage susceptibilities across multiple oligonucleotide sequences rapidly and efficiently. It is possible to

apply this method to construct a library of hot spots which can help in the study of mutagenic mechanism. Although used here for UVC-induced damage, this platform can be used for any environmental or chemical damage agent. The application of this method can be further extended by the use of different probes and well plate of higher density. Thus, this method can be widely used to determine hot spots for DNA damage.

Reference List

(1) L. Marrot and J. R. Meunier, Skin DNA photodamage and its biological consequences. J. Am. Acad. Dermatol. **58,** (2008) S139-S148.

(2) L. Francesco and W. Horspool (Eds) (2003) CRC handbook of Organic Photochemistry and Photobiology . pp.140.1-140.8. CRC Press, USA.

(3) A. J. Varghese and S. Y. Wang, Thymine-thymine adduct as a photoproduct of thymine. Science. **160**, (1968) 186-187.

(4) J. L. Ravanat, T. Douki and J. Cadet, Direct and indirect effects of UV radiation on DNA and its components. J. Photochem. Photobiol. B: Biol. **63**, (2001) 88-102.

(5) T. Douki, D. Perdiz, P. Grof, Z. Kuluncsics, E. Moustacchi, J. Cadet, and E. Sage, Oxidation of guanine in cellular DNA by solar UV radiation: biological role. Photochem. Photobiol. **70**, (1999) 184-190.

(6) P. Schuchert, M. Langsford, E. Kaslin and J. Kohli, A specific DNA sequence is required for high frequency of recombination in the *ade6* gene of fission yeast. EMBO J. **10**, (1991) 2157-2163.

(7) W.P. Wahls and M. K. Davidson, DNA sequence-mediated, evolutionarily rapid redistribution of meiotic recombination hotspots. Genetics. **189**, (2011) 685-694.

(8) N. Galtier, D. Enard, Y. Radondy, E. Bazin and K. Belkhir, Mutation hot spots in mammalian mitochondrial DNA. Genome Res. **16**, (2006) 215-222.

(9) I. B. Rogozin and Y. I. Pavlov, Theoretical analysis of mutation hotspots and their DNA sequence context specificity. Mutat. Res. **544**, (2003) 65-85.

(10) E. Hodis, I. R. Watson, G. V. Kryukov, S. Arold, M. Imielinski, J. Theurillat, E. Nickerson, D. Auclair, L. Li, C. Place, D. DiCara, A. H. Ramos, Lawrence, M. S. K. Cibulskis, A. Sivachenko, D. Voet, G. Saksena, N. Stransky, R. C. Onofrio, W. Winckler, K. Ardlie, N. Wagle, J. Wargo, K. Chong, D. L. Morton, K. S. Hale, G. Chen, M. Noble, M. Meyerson, J. E. Ladbury, M. A. Davies, J. E. Gershenwald, S. N. Wagner, D. S. B. Hoon, D. Schadendorf, E. S. Lander, S. B. Gabriel, G. Getz, L. A. Garraway and L. A. Chin, Landscape of driver mutation in melanoma. Cell. **150**, (2012) 251-263.

(11) L.E. Smith, M.F. Denissenko, W.P. Bennett, H. Li, S. Amin, M.S. Tang and G.P. Pfeifer, Targeting of lung cancer mutational hotspots by polycyclic aromatic hydrocarbans. J. Natl.Cancer Inst. **92**, (2000) 803-811.

(12) M.F. Denissenko, J.X. Chen, M.S.Tang and G.P. Pfeifer, Cytosine methylation determines hot spots of DNA damage in the human P53 gene. Proc. Natl. Acad. Sci. **94**, (1997) 3893-3898.

(13) A. Kumar, M.B. Tyagi and P.N. Jha, Evidences showing ultraviolet-B radiation-induced damage of DNA in cyanobacteria and its detection by PCR assay. Biochem. Biophys. Res. Commun. **318**, (2004) 1025-1030.

(14) P.J. Rochette, N. Bastien, T. Todo and R. Drouin, Pyrimidine (6–4) Pyrimidone photoproduct mapping after sublethal UVC doses: nucleotide resolution using terminal transferase-dependent PCR. Photochem. Photobiol. **82**, (2006) 1370-1376.

(15) T. Douki, S. Sauvaigo, F. Odin and J. Cadet, Formation of the main UV-induced thymine dimeric lesions within isolated and cellular DNA as measured by high performance liquid chromatography-tandem mass spectrometry. J. Biol. Chem. **275**, (2000) 11678-11685.

(16) S. Mouret, C. Baudouin, M. Charveron, A. Favier, J. Cadet and T. Douki, Cyclobutane pyrimidine dimers are predominant DNA lesions in whole human skin exposed to UVA radiation. Proc. Natl. Acad. Sci. **103**, (2006) 13765-13770.

(17) S. Frelon, T. Douki and J. Cadet, Radical oxidation of the adenine moiety of nucleoside and DNA: 2-hydroxy-2'-deoxyadenosine is a minor decomposition product. Free Radic. Res. **36**, (2002) 499-508.

(18) M. Dizdaroglu, The use of capillary gas chromatography-mass spectrometry for identification of radiation-induced DNA base damage and DNA base-amino acid cross-links. J. Chromatogr. A. **295**, (1984) 103-121.

(19) T.A. Slieman and W.L. Nicholson, Artificial and solar UV radiation induces strand breaks and cyclobutane pyrimidine dimers in Bacillus subtilis spore DNA. Appl. Environ. Microbiol. **66**, (2000) 199-205.

(20) M. Weinfeld and K.J.M. Soderlind, Phosphorus-32-postlabeling detection of radiation-induced DNA damage: identification and estimation of thymine glycols and phosphoglycolate termini. Biochemistry. **30**, (1991) 1091-1097.

(21) A.G. Kriste, B.S. Martincigh and L. F. Salter, A sensitive immunoassay technique for thymine dimer quantitation in UV-irradiated DNA. J. Photochem. Photobiol. A. **93**, (1996) 185-192.

(22) S. Yarasi, C. McConachie and G. R. Loppnow, Molecular beacon probes of photodamage in thymine and uracil oligonucleotides. Photochem. Photobiol. **81**, (2005) 467-473.

(23) S. Tyagi and F.R. Kramer, Molecular beacons: probes that fluoresce upon hybridization. Nat. Biotechnol. **14**, (1996) 303-308.

(24) A. Maksimenko, A.A. Ishchenko, G. Sanz, J. Laval, R.H. Elder and M.K. Saparbaev, A molecular beacon assay for measuring base excision repair activities. Biochem. Biophys. Res. Commun. **319**, (2004) 240-246.

(25) L.C. Riches, A.M. Lynch and N.J. Gooderham, A molecular beacon approach to detecting RAD52 expression in response to DNA damage in human cells. Toxicol. In Vitro. **24**, (2010) 652-660.

(26) N.E. Broude, Stem-loop oligonucleotides: a robust tool for molecular biology and biotechnology. Trends Biotechnol. **20**, (2002) 249-256.

(27) A. Misra, P. Kumar and K. Gupta, Design and synthesis of hairpin probe for specific mis-match discrimination. Nucleic Acids Symp. Ser. **51**, (2007) 311-312.

(28) A. Tsourkas, M.A. Behlke and G. Bao, Structure–function relationships of shared-stem and conventional molecular beacons. Nucleic Acids Res. **30**, (2002) 4208-4215.

(29) A. Tsourkas, M.A. Behlke, S.D. Rose and G. Bao, Hybridization kinetics and thermodynamics of molecular beacons. Nucleic Acids Res. **31**, (2003) 1319-1330.

(30) W. Tan, K. Wang and T.J. Drake, Molecular beacons. Curr. Opin. Chem. Biol. **8**, (2004) 547-553.

(31) A.F. El-Yazbi and G.R. Loppnow, Locked nucleic acid hairpin detection of UV-induced DNA damage. Can. J. Chem. **89**, (2011) 402-408.

(32) S.A. Oladepo and G.R. Loppnow, The Effect of Tryptophan on UV-induced DNA Photodamage. Photochem. Photobiol. **86**, (2010) 844-851.

(33) S.A. Oladepo and G.R. Loppnow, Self-quenching smart probes as a platform for the detection of sequence-specific UV-induced DNA photodamage. Anal. Bioanal. Chem. **397**, (2010) 2949-2957.

(34) K. Stohr, B. Hafner, O. Nolte, J. Wolfrum, M. Sauer and D.P. Herten, Species-specific identification of mycobacterial 16S rRNA PCR amplicons using smart probes. Anal. Chem. **77**, (2005) 7195-7203.

(35) T. Maruyama, T. Shinohara, T. Hosogi, H. Ichinose, N. Kamiya and M. Goto, Masking oligonucleotides improve sensitivity of mutation detection based on guanine quenching. Anal. Biochem. **354**, (2006) 8-14.

(36) J.P. Knemeyer, M. Sauer and N. Marme, Probes for detection of specific DNA sequences at the single-molecule level. Anal. Chem. **72**, (2000) 3717-3724.

(37) O.R. Rahn, Potassium iodide as a chemical actinometer for 254 nm radiation: use of iodate as an electron scavenger. Photochem. Photobiol. **66**, (1997) 450-455.

(38) A.F. El-Yazbi and G.R. Loppnow, 2-amino purine hairpin probes for the detection of UV-Induced DNA damage. Anal. Chim. Acta. **726**, (2012) 44-49.

(39) T. Douki and J. Cadet, Individual determination of the yield of the main UV-induced dimeric pyrimidine photoproducts in DNA suggests a high mutagenicity of CC photolesions. Biochemistry. **40**, (2001) 2495-2501.

(40) X. Zhang, B. S. Rosenstein, Y. Wang, M. Lebwohl, D.M. Mitchell and H. Wei, Induction of 8-Oxo-7, 8-Dihydro-2'-Deoxyguanosine by Ultraviolet Radiation in Calf Thymus DNA and HeLa Cells. Photochem. Photobiol. **65**, (1997) 119-124.

(41) C.A. Smith and J. Taylor, Preparation and characterization of a set of deoxyoligonucleotide 49-mers containing site-specific cis-syn, trans-syn-I, 96-40, and dewar photoproducts of thymidyly (3′-5′)-thymidine. J. Biol. Chem. **15**, (1993) 11143-11151.

(42) S.A. Oladepo and G.R. Loppnow, Initial excited-state structural dynamics of 9-methyladenine from UV resonance raman spectroscopy. J. Phys. Chem. *B*. **115**, (2011) 6149-6156.

(43) Y. Kurosaki, H. Abe, H. Morioka, J. Hirayama, K. Ikebuchi, N. Kamo, O. Nikaido, H. Azuma and H. Ikeda, Pyrimidine dimer formation and oxidative damage in M13 bacteriophage inactivation by Ultraviolet C irradiation. Photochem. Photobiol. **78**, (2003) 349-354.

(44) L.M. Kundu, U. Linne, M. Marahiel and T. Carell, RNA is more UV resistant than DNA: The formation of UV-induced DNA lesions is strongly sequence and conformation dependent. Chem. Eur. J. **10**, (2004) 5697-5705.

(45) O.R. Rahn, I. M. Stefan, R.J. Bolton, E. Goren, S.P. Shaw and R.K. Lykke, Quantum yeild of the iodide-iodate chemical actinometer: dependence on wavelength and concentration. Photochem. Photobiol. (2003) **78**, 146-152.

-

Chapter 3
Sequence-specific DNA Damage Induced by a Ruthenium Anti-cancer Drug Detected in a Multi-sample Platform

(A version of this chapter is ready for submission)

3.1 Introduction

DNA damage may lead to cancer [1]. Such damage can be caused by physical or chemical factors such as high temperature, ultraviolet (UV) radiation, ionizing radiation, reactive oxygen species (ROS), heavy metal ions, drugs and pesticides and their metabolites [1]. *Cis*-platin (*cis*-diamminedichloroplatinum(II)), and related Pt(II) compounds are used as antitumor drugs for the treatment of testicular and ovarian cancer [2]. A major drawback of these complexes is their nonspecific action on both healthy and cancerous cells due to thermal activation, leading to a large number of adverse side-effects [3,4]. These drawbacks have catalyzed a search for other metal-based anti-tumor agents which could be used for the treatment of various cancers in a safer and more effective way. Thus, a new family of Ru complexes were introduced that offers lower toxicity than the Pt (II) complexes [5].

The main property that makes Ru compounds better candidate than Pt compounds is their ability to mimic iron in binding to certain biological molecules, exploiting mechanisms the body has developed for the non-toxic transport of iron [6,7]. They also have a range of accessible oxidation states. In addition to these properties, Ru compounds are non-toxic until activated upon irradiation with near-UV light. These properties broaden the possible uses of Ru compounds in cancer, such as the treatment of Pt-resistant tumour cells [8] and in photodynamic theory [3]. Therefore, the anticancer activity of a series of Ru complexes with ligands such as amine, imine, polyaminopolycarboxylate, and many more have been studied extensively [9,10].

The sensitive and accurate determination of DNA damage induced by Ru compounds are

essential for understanding the strength and specificity of binding, and the efficiency of DNA cleavage. Several techniques have been used to detect DNA damage including mass spectrometry [11], gel electrophoresis [8,12], capillary electrophoresis [13] and immunological assays [14]. While these techniques are able to measure damage, they are destructive, time-consuming and may introduce additional lesions. To overcome these limitations, hybridization assays have been developed [15-18].

Many hybridization assays for DNA and DNA damage detection use fluorescently-labelled hairpin probes. These probes include molecular beacons (MBs)[18,19], modified MBs [15,17] and smart probes (SPs) [20,21]. These hairpin probes are labelled with a fluorophore at one end and a quencher at the opposite end. In closed form, they exhibit minimum fluorescence intensity due to the proximity of the quencher and fluorophore. However, in the presence of the complementary target sequence, the hairpin opens and hybridizes to the target. In this form, maximum fluorescence is observed, since the fluorophore and quencher are separated. Thus, in the presence of a mixture of damaged and undamaged DNA sequences, the thermodynamic balance between the closed form and the hybridized forms is what gives these probes their high selectivity. 2-Aminopurine [15] and locked nucleic acids (LNA) [17] are modified MBs that have been explored for greater selectivity and/or sensitivity in detecting DNA damage. However, despite the wide application of these hairpin probes, their use is limited due to the complexity associated with their synthesis and high cost.

The use of intercalating dyes as a fluorescent probe is also based on a hybridization approach. Unlike hairpin probes, intercalating dyes are small molecules that insert between the stacked bases of dsDNA [22]. Possessing very low intrinsic fluorescence in aqueous solution, the intercalating dyes fluoresce significantly more upon binding to dsDNA. Some of the most commonly used DNA

intercalating dyes are ethidium bromide [23], PicoGreen [24], Thiazole Orange [25] and SYBR Green [26]. Some of these dyes are mutagenic or their general use is limited by their preferential selectivity to certain nucleobases. A novel DNA intercalating dye named EvaGreen (EG) (Figure 3.1) [27,28] has been recently introduced to overcome these limitations. This dye is stable, noncytotoxic, non-mutagenic and is completely impermeable to the cell membrane, which makes it an environmentally safe dye. EG binding to dsDNA is found to be much more sensitive than other intercalating dyes. Thus, the dye has also been extensively used for dsDNA quantification assays [29].

In this work, we report a novel multiplexed solution-phase hybridization assay for the selective determination of DNA damage induced by *cis*-$[Ru(bpy)_2(CH_3CN)_2]Cl_2$. The assay is performed in a 96-well microplate, which offers several advantages over the conventional single sample fluorescence assay [17]. To study the preferential DNA binding sites of *cis*-$[Ru(bpy)_2(CH_3CN)_2]Cl_2$, we have designed sequences with all possible sites of DNA damage induced by this Ru compound. The results obtained correlate the amount of DNA damage with the number and position of guanines in a sequence, supporting the hypothesis that guanines are the most vulnerable site of DNA damage induced by this Ru compound. These results were further confirmed using MALDI-TOF-MS and melting curve measurements.

3.2 Experimental.

3.2.1 Materials. The single-stranded oligonucleotide targets were obtained from Integrated DNA Technologies Inc. (Coralville, IA, USA). The sequences of the target oligonucleotides used for this study are listed in Table 3.1. Oligonucleotides were dissolved in nanopure water. All samples were kept frozen at -20 ^oC until needed. Upon thawing, the oligonucleotides are diluted to the required concentration in Tris buffer (10 mM Tris, 1 mM EDTA, 10 mM NaCl, pH ~7.4).

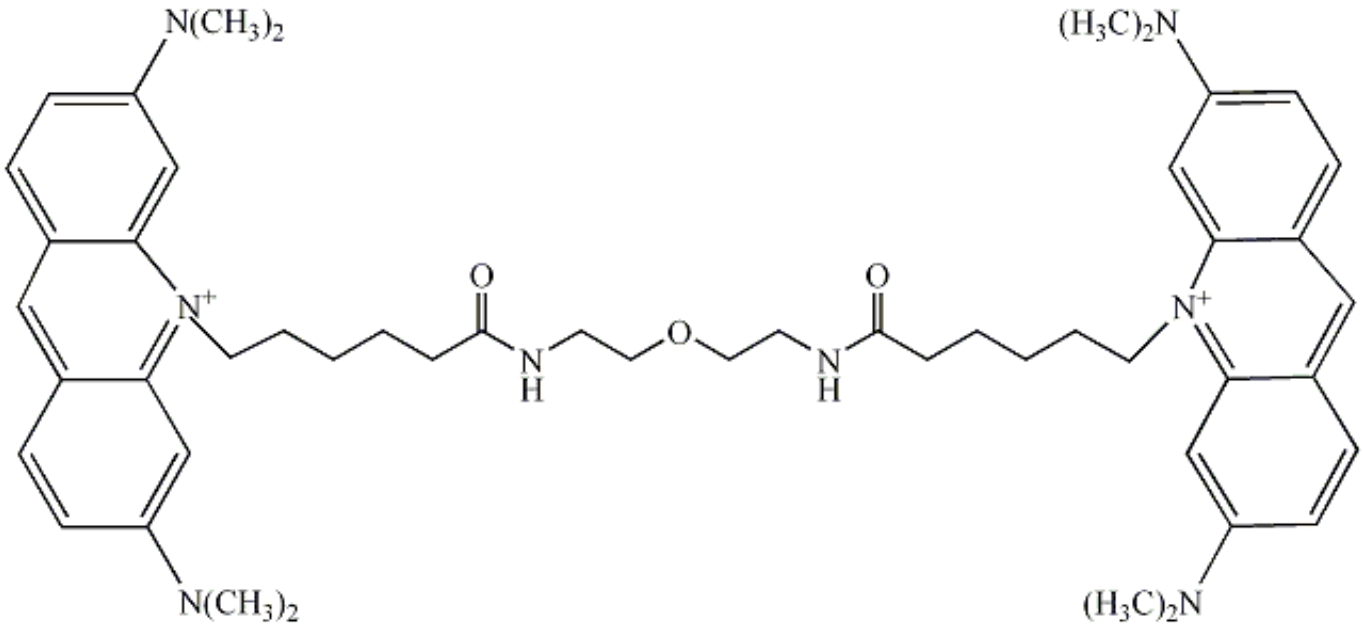

Figure 3.1 Structure of EvaGreen dye

Table 3.1 Oligonucleotides used in this study.

Name	Sequence	Type of damage site	Monoadduct sites	Diadduct sites
T_{17}	5′ TTT TTT TTT TTT TTT TT 3′	None	0	0
T_{2g} (T_{gg})	5′ TTT TTT TGG TTT TTT TT 3′	G	2	1
T_{3g}	5′ TTT TTT TGG GTT TTT TT 3′	G	3	2
T_{4g}	5′ TTT TTT GGG GTT TTT TT 3′	G	4	3
T_{ga}	5′ TTT TTT TGA TTT TTT TT 3′	GA	1	1
T_{gc}	5′ TTT TTT TGC TTT TTT TT 3′	GC	1	0
T_{gt}	5′ TTT TTT TGT TTT TTT TT 3′	GT	1	0
T_{2ga}	5′ TTT TTT GAG ATT TTT TT 3′	GA	2	2
T_{2gc}	5′ TTT TTT GCG CTT TTT TT 3′	GC	2	0
T_{2gt}	5′ TTT TTT GTG TTT TTT TT 3′	GT	2	0
T_{tc}	5′ TTT TTT TTC TTT TTT TT 3′	TC	0	0
T_{ta}	5′ TTT TTT TTA TTT TTT TT 3′	TA	0	0
T_{ca}	5′ TTT TTT TCA TTT TTT TT 3′	CA	0	0
T_{cc}	5′ TTT TTT TCC TTT TTT TT 3′	CC	0	0
T_{aa}	5′ TTT TTT TAA TTT TTT TT 3′	AA	0	0
T_{2gg}	5′ TTT GGT TTT TTT GGT TT 3′	GG	4	2
$T_{2gg,15}$	5′ TTT GGT TTT TGG TTT 3′	GG	4	2

Oligonucleotide sequences were designed to have different *cis*-$[Ru(bpy)_2(CH_3CN)_2]^{2+}$ binding sites (underlined bases). The subscripts in the name of the sequences represent the expected binding site and the number of such sites in the sequences

The sodium hydroxide and magnesium chloride were obtained from EMD Chemical Inc. (Gibbstown, NJ, USA), hydrochloric acid was obtained from Anachemia (Montreal, QC, Canada), sodium chloride was obtained from ACP Chemical Inc. (Montreal, Quebec), Tris was obtained from ICN biomedicals (Aurora, OH, USA) and ethylenediaminetetraacetic acid (EDTA) was obtained from BDH Inc. (Toronto, ON, Canada). All chemicals were used as received. Nanopure water (Barnsted Nanopure, Boston, MA,USA) was used to prepare all solutions.

3.2.2. Fluorescence measurement of DNA damage induced by *cis*-[Ru(bpy)$_2$(CH$_3$CN)$_2$]Cl$_2$. The photolysis of *cis*-[Ru(bpy)$_2$(CH$_3$CN)$_2$]Cl$_2$ was carried out by irradiating 25 μM aqueous Ru complex in a UV-transparent 1 cm path length cuvette for 10 min in a Luzchem (Ottawa, Ontario) DEV photoreactor chamber with UVA from lamps emitting in the wavelength range of 320-400 nm. Absorbance spectra were taken on Hewlett-Packard 8452 A diode array spectrophotometer (Sunnyvale, CA) before and after irradiation. The formation of the peak at 490 nm confirms the photolysis of the Ru complex into the *cis*-[Ru(bpy)$_2$(H$_2$O)]$_2$Cl$_2$ active form (Figure 3.2) [30].

For fluorescence measurements, a solution of 10 μM ssDNA and 10 or 20 μM activated Ru complex was prepared in Tris buffer (10 mM Tris, 1 mM EDTA, 10 mM NaCl, pH ~7.4). Solutions of all the ssDNA (Table 3.1) target and the Ru complex were placed on the magnetic stirrer under constant stirring throughout the DNA damage experiment. Aliquots from each solution were pipetted out after reaction times of 0, 5, 48 and 96 hr. These samples were then hybridized with their complementary target and were further diluted with Tris buffer to give a final concentration of 1 μM double-stranded DNA (dsDNA) in each well of the 96-well microplate. The sample mixtures were then incubated in the dark for 1 hr. Room-temperature fluorescence intensities were

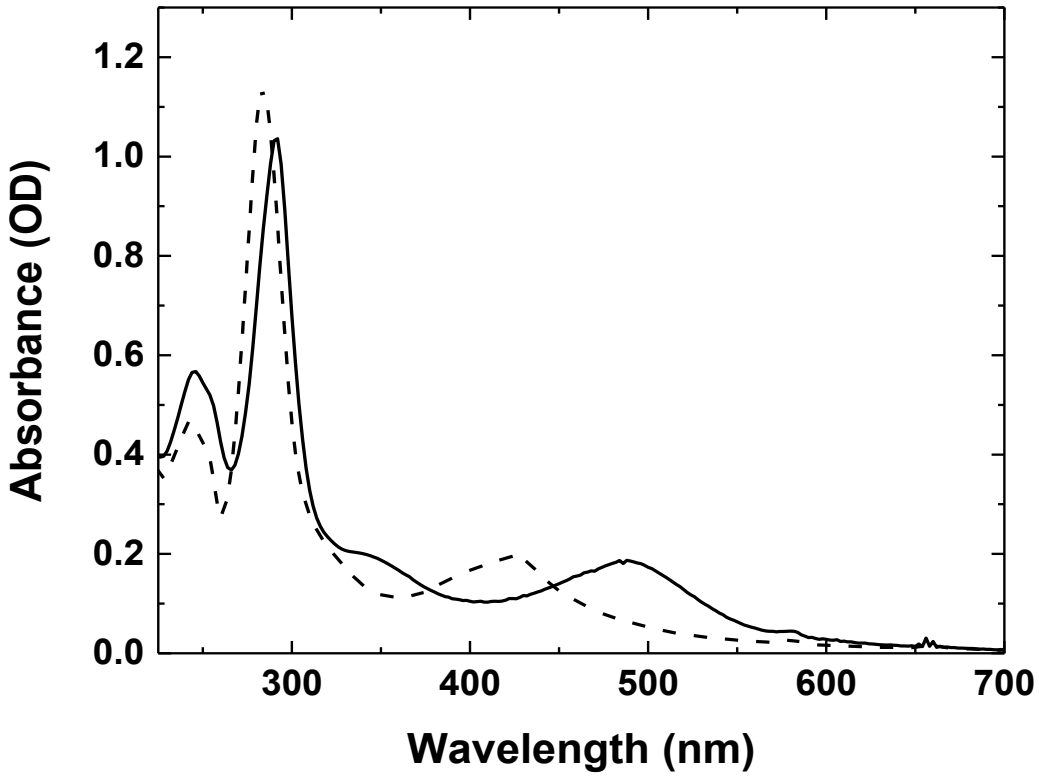

Figure 3.2 The absorption spectrum of *cis*-$[Ru(bpy)_2(CH_3CN)_2]Cl_2$ (dashed line) as it converts to *cis*-$[Ru(bpy)_2(H_2O)_2]Cl_2$ (solid line) during photolysis (λ_{irr} > 320 nm for 10 min) in water. The absorption band at 490 nm in *cis*-$[Ru(bpy)_2(H_2O)_2]Cl_2$ was diagnostic for the active form of the Ru complex.

measured using the Safire fluorescence plate reader (Tecan, Mannendorf, Switzerland) after the addition of EG dye followed by incubation at 37 ^{o}C for 20 min in the dark. The dsDNA: EG concentration ratios were fixed at 1:1.33. Fluorescence emission spectra were recorded using an excitation wavelength of 490 nm and an emission wavelength of 530 nm. Here it is worth mentioning that fluorescence spectra of the Ru complex and/or dsDNA gave a minimum or zero background at 530 nm emission wavelength. (Figure A 7)

3.2.3. MALDI-TOF mass spectrometry. Solution of 10 μM *cis*-$[Ru(bpy)_2(H_2O)]_2Cl_2$ and 10 μM ssDNA targets, $T_{gg,}$ $T_{ga,}$ $T_{2gg,15}$ and T_{17} (Table 3.1), were measured by negative ion MALDI-TOF-Mass spec-Elite Voyager (Lancashire, United Kingdom) equipped with a nitrogen laser for ionization and desorption. The nitrogen laser operated at 337 nm with 3 ns pulses delivered to the sample at 20 Hz. Each sample was repeatedly washed with 1M triethanolammonium acetate (TEAA) and 50 % acetonitrile/50 % water, and loaded onto the sample plate of the mass spectrometer along with the matrix (2,4,6 trihydroxyacetopheno -ne:diammonium citrate). Control samples of pure oligonucleotide targets were also prepared and analyzed as discussed above.

3.3 Results and Discussion

As shown in Reaction 1, irradiation of *cis*-$[Ru(bpy)_2(CH_3CN)_2]^{2+}$ in water with λ_{irr}> 320 nm

$$cis\text{-}[Ru(bpy)_2(CH_3CN)_2]^{2+} \xrightarrow{h\upsilon} \underset{\text{Activated form}}{cis\text{-}[Ru(bpy)_2(H_2O)_2]^{2+}} \rightarrow cis\text{-}[Ru(bpy)_2(H_2O)(ssDNA)]^{2+} \quad (1)$$

results in the substitution of two CH_3CN groups to form the activated bis-aqua *cis*-$[Ru(bpy)_2(H_2O)_2]^{2+}$.The quantum yield of CH_3CN photoaquation is related to energy difference between the low energy metal-ligand charge transfer (MLCT) and d-d orbital transitions [30]. This

adduct, on continuous treatment with ssDNA, covalently binds to adjacent purines in ssDNA and replaces one of the H_2O groups to form the *cis*-$[Ru(bpy)_2(H_2O)(ssDNA)]^{2+}$ adduct [30].

3.3.1 DNA quantification using EG dye. Figure 3.3 shows a plot of EG fluorescence as a function of the concentration of ssDNA and dsDNA. Upon addition of dsDNA, the fluorescence of EG increases significantly and continues to increase linearly with increasing concentration. A strong linear relationship is observed when the concentration of dsDNA is less than 1 μM at an [EG] = 1.33 μM. Saturation in the intensity of fluorescence is observed at dsDNA concentration higher than ~7 μM. The calibration curve in this region shows a regression coefficient of 0.99 and sensitivity (slope of the calibration curve) of 3.4 x 10^{10} cps M^{-1}. The resulting limit of detection (LOD) and limit of quantification (LOQ) values for quantifying dsDNA are 2.3 nM and 7.7 nM, respectively, with a noise level standard deviation of 0.26 x 10^2 cps. The noise was obtained from the fluorescence signal of a solution of EG alone in water.

For ssDNA a much slower increase in fluorescence signal is seen with increasing concent ration for both single-stranded poly-dA_{17} and poly-dT_{17}. Both of the control ssDNA solution shows very low fluorescence and do not have any remarkable enhancement with increasing concentration. It is noteworthy that the fluorescence intensity of the EG-dsDNA and EG-ssDNA solution remained constant up to 48 hr; no significant change in EG fluorescence was observed over this time period

3.3.2. Effect of ionic strength of the medium. In order to optimize the ability of the EG dye to discriminate between damaged and undamaged DNA, we investigated the effect of Mg^{2+} and Na^+ ions on EG fluorescence intensity of ds T_{17}•A_{17} target. Figure 3.4A shows the fluorescence of EG-dsDNA as a function of increasing Na^+ concentration alone. The results show that the fluorescence intensity of EG attains a maximum at a Na^+ concentration of 10 mM and decreases with any increase in $[Na^+]$. Similarly, the EG fluorescence intensity decreases with any increase

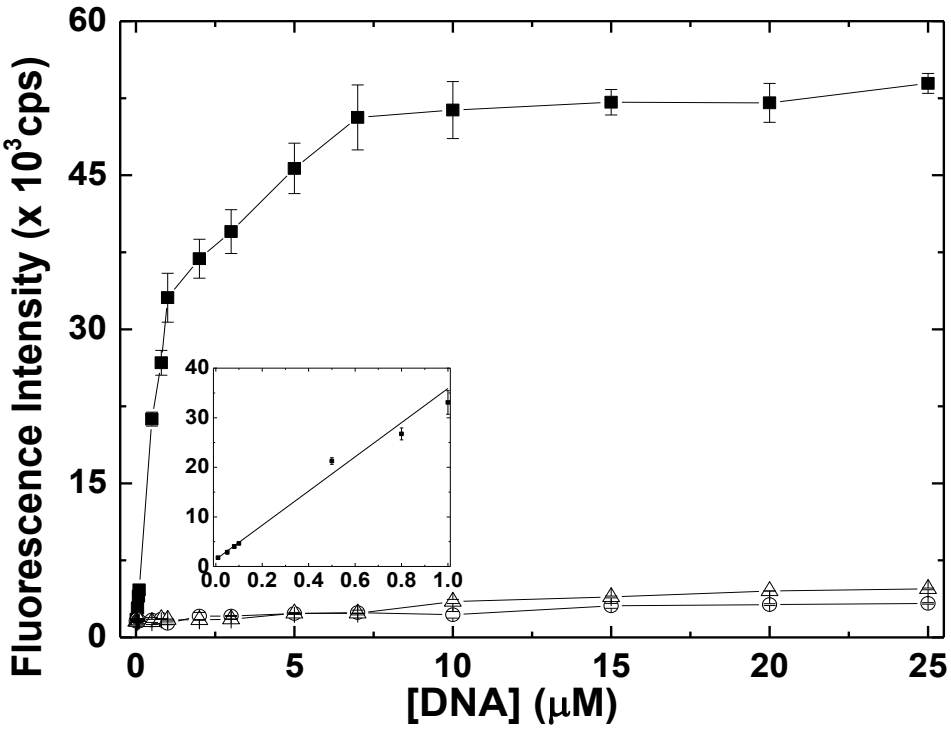

Figure 3.3 Fluorescence of 1.33 μM EG as a function of the concentration of oligonucleotide poly-dT_{17}. Filled squares represent dsDNA and open circles and triangle represents single stranded poly-dT_{17} and poly-dA_{17}, respectively. The linear region of Figure 3.3 is expanded in the inset of Figure 3.3. Inset shows the linear portion of the calibration curve with $R^2 = 0.99$ the sensitivity (slope of the calibration curve) is 3.4×10^{10} cps M^{-1}, the limit of detection (LOD) is 2.3 nM and the limit of quantification (LOQ) is 7.7 nM. The noise level standard deviation for EG dye is 0.26×10^2 cps.

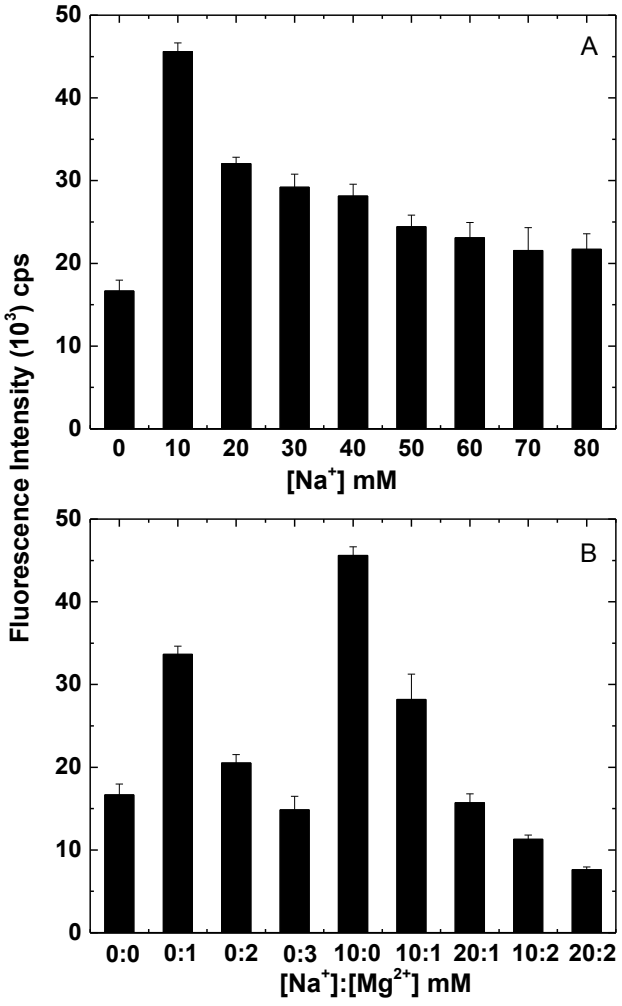

Figure 3.4 Effect of (A) Na^+ concentration and (B) Na^+:Mg^{2+} concentration ratios on the fluorescence intensity at 530 nm of the EG complex with ds T_{17}•A_{17}.

in either [Mg^{2+}] alone or both [Mg^{2+}] and [Na^{+}] simultaneously (Figure 3.4B). The results clearly show that the optimum condition for dsDNA detection is low [Na^{+}]. Also, the results show that the fluorescence intensity of EG is lower in the absence of both ions. Thus 10 mM NaCl was used for all experiments to yield the maximum EG fluorescence intensity with dsDNA. No remarkable change in the fluorescence intensity of EG was observed upon binding to ssDNA at different concentrations of Mg^{2+} and Na^{+} (data not shown).

3.3.3 MALDI-TOF-MS analysis of DNA adducts formed by Ru complex. Products of the binding of active *cis*-[$Ru(bpy)_2(H_2O)_2$]$^{2+}$ to single-stranded oligonucleotides for the T_{gg}, T_{ga}, $T_{2gg,15}$, and T_{17} sequences listed in Table 3.1 were detected by MALDI-TOF-MS to identify possible conjugates. Figure 3.5 shows the mass spectrum of these oligonucleotides in the absence and presence of *cis*-[$Ru(bpy)_2(H_2O)_2$]$^{2+}$. The results show that in the absence of *cis* [$Ru(bpy)_2(H_2O)_2$]$^{2+}$, only the ssDNA parent peak is seen at m/z values of 4601, 5159, 5144 and 5108 respectively, for $T_{2gg,15}$, T_{gg}, T_{ga} and T_{17}. The binding of one molecule of *cis*-[$Ru(bpy)_2$] is observed at the peak labeled ′B′ for $T_{2gg,15}$, T_{gg}, and T_{ga} in the 96 hr mass spectra. The binding of two molecule of *cis*-[$Ru(bpy)_2$] is observed at the peak labeled ′C′ for T_{2gg} in the 96 hr mass spectrum. This latter result is expected, because $T_{2gg,15}$ is the only sequence that contains two guanine-guanine binding sites. Note that the spectrum of T_{17} shows only the presence of the parent molecular ion, confirming that the *cis*-[$Ru(bpy)_2$] fragment does not bind to T_{17}, making it a good control for our experiment. Smaller peaks in all the spectra are due to one or more noncovalently complexed sodium ions.

3.3.4. Melting curves of EG-dsDNA. To examine the selectivity of this method for the detection of DNA damage induced by Ru complex, we measured the melting curve profile for sequences $T_{2gg,15}$, T_{gg}, T_{ga} and T_{17}. Here it is worth mentioning that the sequence $T_{2gg,15}$, was

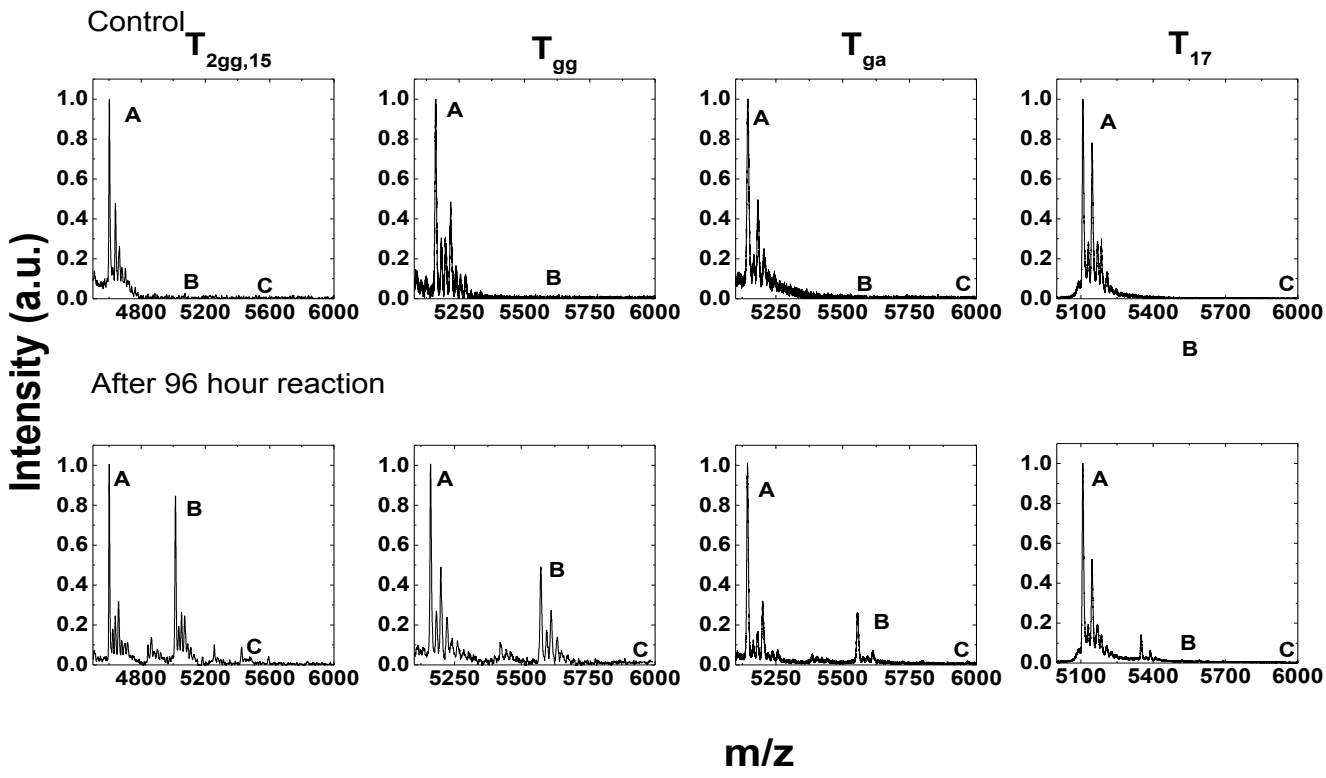

Figure 3.5 MALDI mass spectrometry of oligonucleotides in the absence (top row) and presence (bottom row) of Ru complex for sequences $T_{2gg,15}$ (column 1), T_{gg} (column 2), T_{ga} (column 3) and T_{17} (column 4). In each panel, the peak labelled ′A′ represents the parent ion peak, peak ′B′ represents the binding of one $Ru(bpy)_2$ moiety to the sequence and peak ′C′ represents the binding of two $Ru(bpy)_2$ moieties to the sequence. The control spectra were obtained in the absence of Ru complex and the 96 hr spectra were obtained after 96 hr of reaction with *cis*-$[Ru(bpy)_2(CH_3CN)_2]^{2+}$ (10 mM Tris, 10 mM NaCl, 1mM EDTA, pH ~7.4) for all sequences.

designed with only 15 nucleobases instead of 17 nucleobases to attain similar melting temperature as other sequences and T_{2gg} was designed with 17 nucleobases so that it has same sequence length as others. Thus we could overlook any discrepancy, which may occur due to difference in melting temperature as well as length of sequence. The melting curves were plotted by measuring the fluorescence of EG at 530 nm as a function of temperature after hybridization with their respective complementary strand. We also measured the resulting melting curves after the respective ssDNA hybrids were exposed to the active *cis*-$[Ru(bpy)_2(H_2O)_2]^{2+}$ complex for 11 and 96 hr followed by hybridization with their complementary strands. Figure 3.6 shows the melting curves of these sequences incubated with EG post hybridization via the "release on demand" mechanism [31]. The EG dye is constructed of two monomeric units joined through a flexible linker. This dimeric dye is inactive in the absence of dsDNA and assumes a closed looped conformation with the two chromophores in close proximity to one another. In this conformation, the fluorescence is quenched. When dsDNA is present, the looped conformation of EG opens upon binding, separating the two chromophores, and EG exhibits a maximum fluorescence. In the melting curves, at low temperature, the dsDNA is perfectly hybridized and the EG dye binds in its open conformation to emit maximum fluorescence. As the temperature increases, the hybrid begins to melt, forcing the EG dye to detach from the DNA groove, form the closed conformation and exhibit minimal fluorescence emission. Thus we see a decrease in the fluorescence intensity with increasing temperature. This pattern is observed in Figure 3.6 for all the sequences. Upon exposure to activated Ru complex, a decrease in the fluorescence signal at low temperature and a decrease in the melting point is observed for the $T_{2gg,15,}$ T_{gg} and T_{ga} sequences. No such change is observed for the T_{17} control. This result is expected, because T_{17} lacks any damage sites, as observed in the MALDI-TOF-MS. Further, the binding for damaged dsDNA is destabilized. From Figure 3.6B

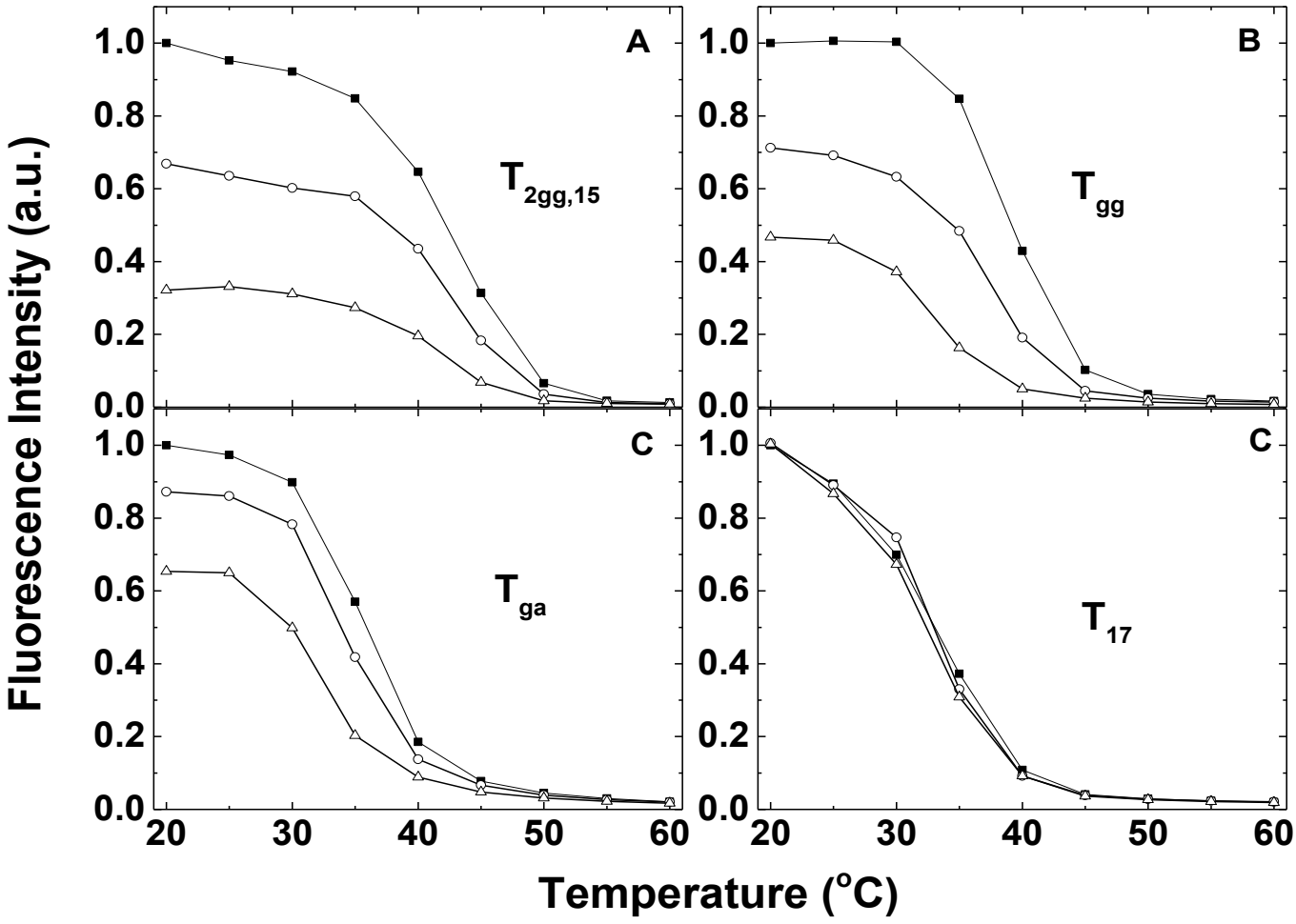

Figure 3.6 Melting curves for 1 μM dsDNA exposed to active *cis*-$[Ru(bpy)_2(H_2O)_2]^{2+}$ and 1.33 μM of EG in Tris buffer after 0 hr (filled squares), 11 hr (open circles) and 96 hr (open triangles). The different panels represent the melting curves for (A) $T_{2gg,15}$, (B) T_{gg}, (C) T_{ga} and (D) T_{17}. The fluorescence intensity has been normalized to the fluorescence intensity at 0 hr, 20 °C for each sequence.

(T_{gg}), if we compare the melting temperatures between the damaged and undamaged hybrids, we find that the melting temperature decreases from 40 ^{o}C to 37 ^{o}C upon 11 hr damage and further to 34 ^{o}C upon 96 hr damage. Similar, but smaller, decreases in melting temperature upon damage are observed for the $T_{2gg,15}$ and T_{ga} sequences. This decrease in melting temperature can be correlated to adduct formation. A drop in melting temperature indicates an increase in the number of adducts formed.

As shown in Figure 3.6, there is good discrimination in the fluorescence intensity between the undamaged and damaged target. This difference in hybrid stability can be correlated to the amount of damage and the number of damage sites. With the increase in damage time, a lower fluorescence intensity is observed at 20 ^{o}C. A comparison of the fluorescence intensities between damaged and undamaged target for the sequences $T_{2gg,15,}$ $T_{gg,}$ T_{ga} and T_{17} shows that there was no decrease in fluorescence intensity for target T_{17} with increasing damage time with Ru complex. T_{gg} and T_{ga} are expected to show a similar response to one another, because they both have one site of diadduct formation. But on comparing their melting curves, we see a large decrease in fluorescence intensity for T_{gg} upon 11 hr of damage and gradually the drop in fluorescence for both the sequences becomes almost similar on increasing the damage time from 11 to 96 hr. This could be due to more affinity of *cis*-$[Ru(bpy)_2(H_2O)_2]^{2+}$ towards GG sites than GA sites. $T_{2gg,15}$ exhibits a rapid drop in fluorescence intensity with increasing damage time, indicating that it has been subjected to the maximum amount of damage when incubated with *cis*-$[Ru(bpy)_2(H_2O)_2]^{2+}$. This result is also expected because $T_{2gg,15}$ has two possible sites of diadduct formation. Furthermore, if we compare the melting curve for $T_{2gg,15}$ and T_{gg} for the first 11 hr of damage time, we see a similar drop in the fluorescence intensity, which may be due to the addition of one *cis*-$[Ru(bpy)_2(H_2O)_2]^{2+}$ to the target sequences, but on further increasing the damage time, the drop in florescence intensity for

$T_{2gg,15}$ occurs at a faster rate than for T_{gg} . This is attributed to the addition of a second *cis*-$[Ru(bpy)_2(H_2O)_2]^{2+}$. From these results, we can conclude that the EG dye is efficient enough to detect chemically-induced DNA damage.

3.3.5 DNA damage from active *cis*-$[Ru(bpy)_2(H_2O)_2]^{2+}$ complex. Figure 3.7 shows the comparison of damage for the sequences T_{gg}, $T_{2gg,15}$, T_{ga} and T_{17} as a function of time at two different Ru complex concentration. No decrease in fluorescence signal was observed when dsDNA was immediately mixed with EG and *cis*-$[Ru(bpy)_2(H_2O)_2]^{2+}$, or when no *cis*-$[Ru(bpy)_2(H_2O)_2]^{2+}$ was added (Figure A 8), indicating that the Ru complex must damage DNA over time, consistent with the mass spectra as a function of exposure time. This result was obtained at both concentrations of the Ru complex.

To get an insight into the preferred DNA binding sites for *cis*-$[Ru(bpy)_2(CH_3CN)_2]^{2+}$ complex, the rate of damage was studied by incubating oligonucleotides with the Ru complex for 0, 5, 48 and 96 hr. Of the four sequences measured, the T_{17} sequence showed a very small change in fluorescence with increasing incubation time with Ru complex. This sequence also showed no correlation between amount of damage and Ru complex concentration. This result is expected, because T_{17} lacks a putative Ru complex binding site. For all the other sequences, we observe a two-fold increase in the damage rate with a two-fold increase in concentration of the Ru complex. On comparing T_{gg} and T_{ga}, which possess only one site of diadduct formation, the results show a higher damage rate for T_{gg} than T_{ga} at all exposure times. Thus, similar to *cis*-platin [18], *cis*-$[Ru(bpy)_2(CH_3CN)_2]^{2+}$ complex also prefers to bind to GG sites than to GA sites. Indeed, the highest rate of damage of all the sequences was observed in the $T_{2gg,15}$ sequence containing multiple guanines. As discussed before, $T_{2gg,15}$ has two possible sites for divalent binding. These results are in accordance with the mass spectroscopy and melting curve results mentioned above.

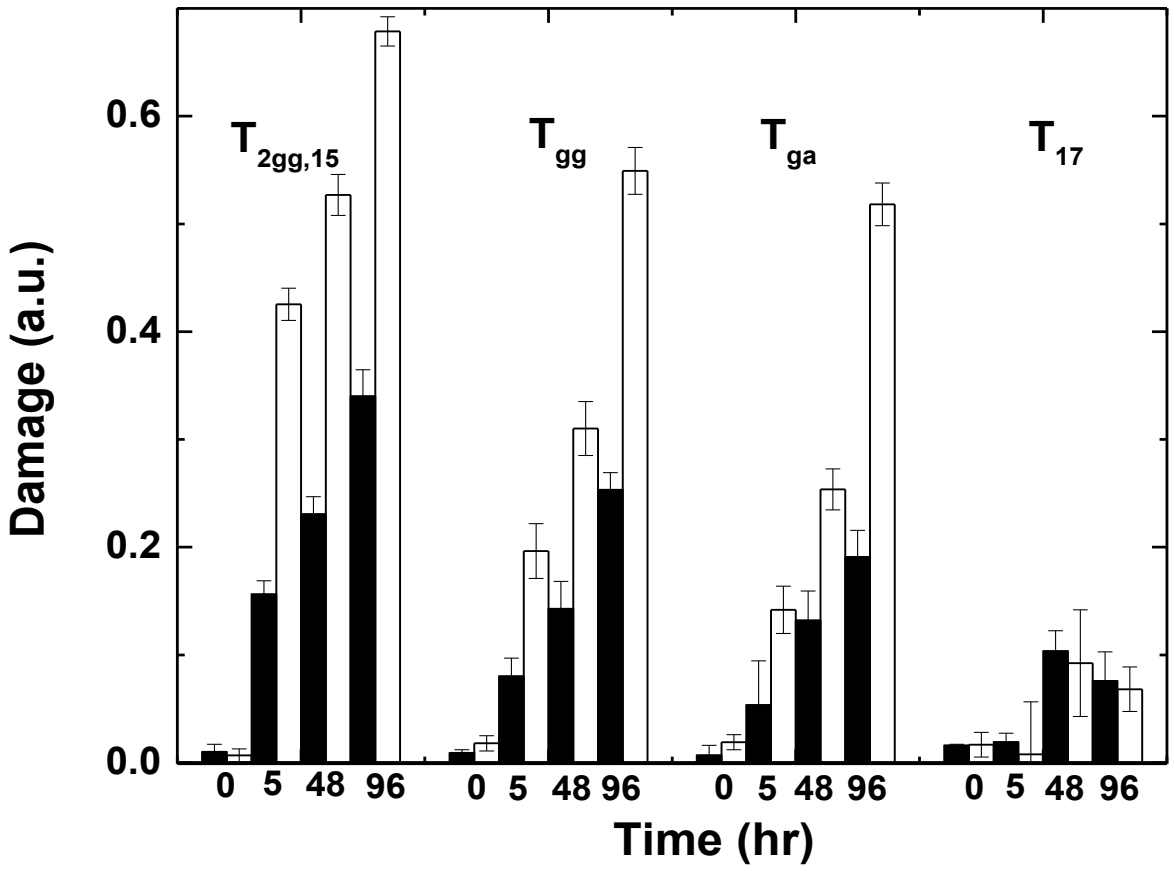

Figure 3.7 Comparison between damage of 10 μM ssDNA hybridized to its complementary target after incubation with 10 μM Ru (filled bar) and with 20 μM Ru (open bar) as a function of exposure time to activated Ru complex. The values on the y-axis are 1-F, where $F = F_{i,min}/F_{0,min}$, $F_{i,min}$ is the fluorescence intensity of EG-dsDNA-Ru complex at 'i' min of exposure time and $F_{0,min}$ is the fluorescence intensity at 0 min exposure time.

To further investigate the preferential binding sites of *cis*-$[Ru(bpy)_2(CH_3CN)_2]^+$, this EG assay was performed on all sequences in Table 3.1. The sequences were designed to study both the number and type of possible damage sites. Figure 3.8 shows the results of damage induced by *cis*-$[Ru(bpy)_2(H_2O)_2]^{2+}$ on all the sequences in Table 3.1. The results show that CC, TC, TA, CA and AA sites are only minimally damaged by *cis*-$[Ru(bpy)_2(CH_3CN)_2]^{2+}$ complex, if at all. However, a considerable amount of damage was found for sequences with GC, GT, GA and GG sites. Figure 3.8 shows that T_{gc}, T_{ga}, T_{gt} and T_{gg} sequences incubated with *cis*-$[Ru(bpy)_2(H_2O)_2]^{2+}$ exhibit differential sensitivity to binding, with greater damage seen in T_{gg} and T_{ga}, while T_{gc} showed lower damage. This result is expected, since *cis*-$[Ru(bpy)_2(CH_3CN)_2]^{2+}$ is considered to be a photochemical analog of cis-platin [30], and thus is expected to have a similar diadduct formation chemistry. Thus the N7 position of guanine and the N7 position of adenine are both preferable binding site for Ru complexes [32]. This result suggests there is a possibility of diadduct formation for T_{ga} and T_{gg} whereas only monoadduct formation can occur for T_{gc} and T_{gt} (Figure 3.9). Also similar to cis-platin, T_{gg} shows faster rate of damage when compared with T_{ga}.. We also see an increase in damage rate with increasing number of guanines in a sequence (Figure 3.8). For example, T_{4g} with four sequential guanines is damaged more than T_{3g} with three sequential guanines which in turn is more damaged than T_{gg} with two sequential guanines. This is attributed to the increase in the number of possible sites for crosslinking. Similarly the extent of damage increases with the increasing number of GC, GA and GT sites from single to double in a given sequence. But, surprisingly we found that a minimal increase was observed for two GA sites

formed for T_{gc} and T_{gt}, but a different adduct may form for T_{ga}, or that the kinetics of adduct formation may be very different in T_{ga} compared to T_{gc} or T_{gt}. Also, earlier studies with *cis*-platin

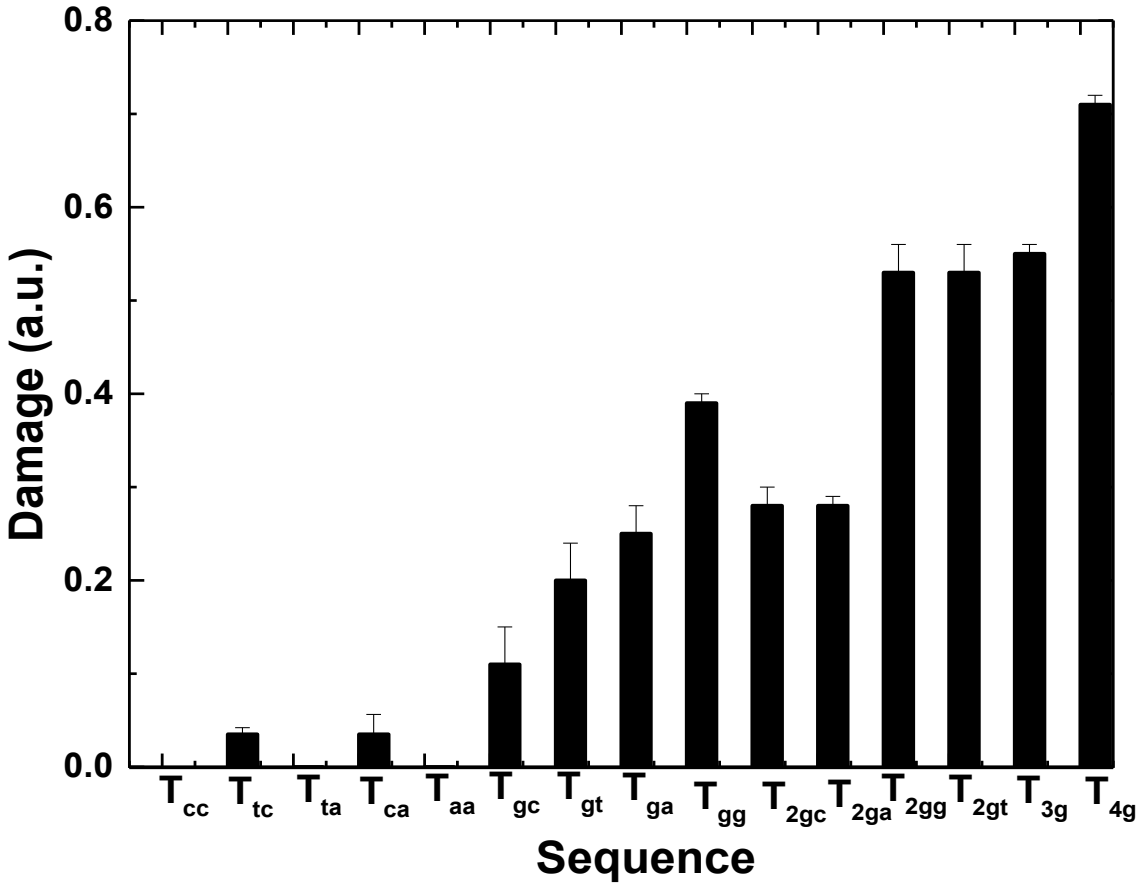

Figure 3.8 Comparison of the fluorescence intensities obtained of all sequences (10 μM) in Table 3.1 after exposure to activated 20 μM Ru complex for 96 hr. The values on the y-axis are 1-F, where $F = F_{i,min}/F_{0,min}$, $F_{i,min}$ is the fluorescence intensity of EG-dsDNA-Ru complex at 'i' min of exposure time and $F_{0,min}$ is the fluorescence intensity at 0 min exposure time.

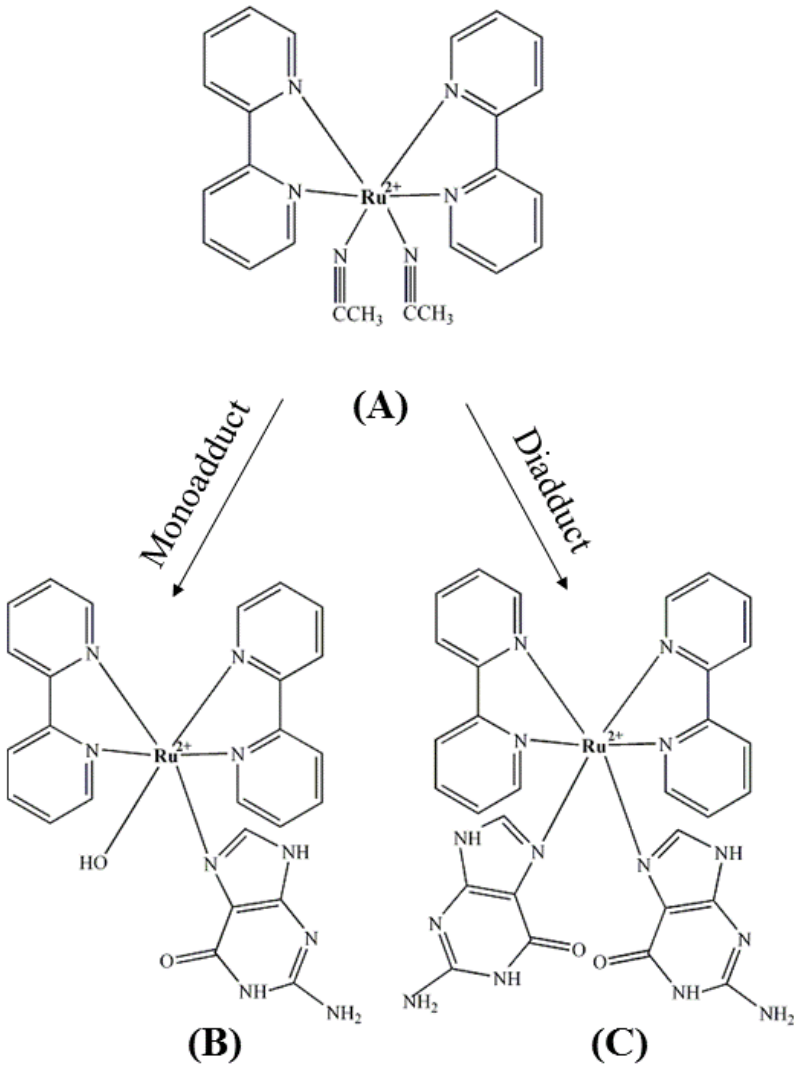

Figure 3.9 Structure of (A) *cis*-$[Ru(bpy)_2(CH_3CN)_2]^{2+}$ complex c (B) monoadduct formed with guanine (C) diadduct formed with two adjacent guanine

compared to one, whereas a ~60 % increase in damage rate was observed on going to two GC or GT sites for T_{gc} and $T_{gt,}$ respectively. This result indicates that similar types of adducts would have have shown that a GG diadduct formation can occur in single-stranded oligonucleotides containing the sequence d(GXG) (X being adenine, cytosine and thymine residue) and the conformational dynamics of GG adduct depend on the sequence context [33,34]. This leads to a change in the dsDNA groove conformation, which in turn could affects the strength of intercalation. The results show a possible formation of GG diadduct for T_{gc} and T_{gt} sequences whereas a GA diadduct formation for T_{ga} sequence. Thus, further investigation is required to confirm if the discrepancy in the result is due to faster damage kinetics or the strength of intercalation of EG to the dsDNA or some other factor.

Surprisingly, on comparing the sequences T_{2gg} and T_{4g}, we saw a higher damage rate for T_{4g} than T_{2gg} even though both sequence have four guanines. This result can be explained by the position of the guanine in the given sequence. In $T_{4g,}$ the Gs are located continuously at the center of the sequence, giving a possibility of forming three GG diadducts. In T_{2gg} the guanine pairs are separated by a stretch of nucleobases, giving a possibility of forming just two GG diadducts. This is similar to $T_{3g,}$ which has the possibility of forming two GG diadducts. Thus, we saw a similar damage rate for both of T_{2gg} and $T_{3g.}$

3.4 Conclusion

To summarize, we have designed an assay to detect DNA damage induced by *cis*-$Ru(bpy)_2(CH_3CN)_2]^+$ in a 96-well microplate. This method has the advantage of assaying multiple samples in a well plate in a simple mix-and-read assay using EvaGreen dye to detect undamaged dsDNA. The decrease in fluorescence intensity with increasing damage sites and low LOD and

LOQ shows that the EG dye has superior selectively and sensitivity to DNA damage induced by Ru complex. Our results indicate that the observed decrease in fluorescence signal is indeed due to the DNA damage induced by *cis*-$[Ru(bpy)_2(CH_3CN)_2]^{2+}$, and the decrease in EG fluorescence intensity correlates to both exposure of the drug and the number of Ru damage sites in the target strand. We have also conclusively shown that GG is the major and GA the minor diadduct formation sites for *cis*-$[Ru(bpy)_2(CH_3CN)_2]^{2+}$ complex.

Reference List

[1] L. Marrot and J. Meunier, Skin DNA photodamage and its biological consequences, J. Am. Acad. Dermatol. **58** (2008) S139-S148.

[2] L. Kelland, The resurgence of platinum-based cancer chemotherapy, Nat. Rev. Cancer. **7** (2007) 573-584.

[3] R.N. Garner, L.E. Joyce and C. Turro, Effect of electronic structure on the photoinduced ligand exchange of Ru (II) polypyridine complexes, Inorg. Chem. **50** (2011) 4384-4391.

[4] R.B. Sears, L. Joyce, M. Ojaimi, J. Gallucci, R. Thummel and C. Turro, Photoinduced ligand exchange and DNA binding of *cis*-[Ru (phpy)(phen)$(CH_3CN)_2]^+$ with long wavelength visible light, J. Inorg. Biochem. **121** (2012) 77-87.

[5] S. Page and R. Wheeler, Ruthenium compounds as anticancer agents, Educ. Chem. **49** (2012) 26-29.

[6] V. Brabec and O. Nováková, DNA binding mode of ruthenium complexes and relationship to tumor cell toxicity, Drug Resist. Updates. **9** (2006) 111-122.

[7] C.S. Allardyce and P.J. Dyson, Ruthenium in medicine: current clinical uses and future prospects, Platin. Met. Rev. **45** (2001) 62-69.

[8] S. Fruhauf and W.J. Zeller, New platinum, titanium, and ruthenium complexes with different patterns of DNA damage in rat ovarian tumor cells, Cancer Res. **51** (1991) 2943-2948.

[9] S. Kapitza, M.A. Jakupec, M. Uhl, B.K. Keppler and B. Marian, The heterocyclic ruthenium (III) complex KP1019 (FFC14A) causes DNA damage and oxidative stress in colorectal tumor cells, Cancer Lett. **226** (2005) 115-121.

[10] J.M. Kelly, A.B. Tossi, D.J. McConnell and C. OhUigin, A study of the interactions of some polypyridylruthenium (II) complexes with DNA using fluorescence spectroscopy, topoisomerisation and thermal denaturation, Nucleic Acids Res. **13** (1985) 6017-6034.

[11] M. Groessl, Y.O. Tsybin, C.G. Hartinger, B.K. Keppler and P.J. Dyson, Ruthenium versus platinum: interactions of anticancer metallodrugs with duplex oligonucleotides characterized by electrospray ionization mass spectrometry, J. Biol. Inorg. Chem. **15** (2010) 677-688.

[12] Y. Liu, N. Wang, W. Mei, F. Chen, L. He, L. Jian, R. Wang and F. Wu, Photoinduced cleavage and DNA-binding of the ruthenium (II) polypyridyl complex [Ru $(phen)_2$ (ipbd)]$(ClO_4)_2$, Transit. Met. Chem. **32** (2007) 332-337.

[13] F. Sang and J. Ren, Capillary electrophoresis of double-stranded DNA fragments using a new fluorescence intercalating dye EvaGreen, J. Sep. Sci. **29** (2006) 1275-1280.

[14] R.M. Santella, Immunological methods for detection of carcinogen-DNA damage in humans, Cancer Epidemiol. Biomarkers Prev. **8** (1999) 733-739.

[15] A.F. El-Yazbi and G.R. Loppnow, 2-Aminopurine hairpin probes for the detection of ultraviolet-induced DNA damage, Anal. Chim. Acta. **726** (2012) 44-49.

[16] A.F. El-Yazbi and G.R. Loppnow, Terbium fluorescence as a sensitive, inexpensive probe for UV-induced damage in nucleic acids, Anal. Chim. Acta. **786** (2013) 116-123.

[17] A.F. El-Yazbi and G.R. Loppnow, Locked nucleic acid hairpin detection of UV-induced DNA damage, Can. J. Chem. **89** (2011) 402-408.

[18] Z.J. Shire and G.R. Loppnow, Molecular beacon probes for the detection of cisplatin-induced DNA damage, Anal. Bioanal. Chem. **88** (2012) 1-6.

[19] L.C. Riches, A.M. Lynch and N.J. Gooderham, A molecular beacon approach to detecting RAD52 expression in response to DNA damage in human cells, Toxicol. in Vitro. **24** (2010) 652-660.

[20] S.A. Oladepo and G.R. Loppnow, Self-quenching smart probes as a platform for the detection of sequence-specific UV-induced DNA photodamage, Anal. Bioanal. Chem. **397** (2010) 2949-2957.

[21] S.G. Nair and G.R. Loppnow, Multiplexed, UVC-induced, sequence-dependent DNA damage detection, Photochem. Photobiol. **89** (2013) 884-890.

[22] G. Cosa, K. Focsaneanu, J. McLean, J. McNamee and J. Scaiano, Photophysical properties of fluorescent DNA-dyes bound to single-and double-stranded DNA in aqueous buffered solution, Photochem. Photobiol. **73** (2001) 585-599.

[23] J. Olmsted J and D.R. Kearns, Mechanism of ethidium bromide fluorescence enhancement on binding to nucleic acids, Biochem. **16** (1977) 3647-3654.

[24] S.J. Ahn, J. Costa and J.R. Emanuel, PicoGreen quantitation of DNA: effective evaluation of samples pre- or post-PCR, Nucleic Acids Res. **24** (1996) 2623-2625.

[25] T.G. Deligeorgiev, S. Kaloyanova and J.J. Vaquero, Intercalating cyanine dyes for nucleic acid detection, Recent Pat Mater Sci. **2** (2009) 1-26.

[26] X. Yan, W.K. Grace, T.M. Yoshida, R.C. Habbersett, N. Velappan, J.H. Jett, R.A. Keller and B.L. Marrone, Characteristics of different nucleic acid staining dyes for DNA fragment sizing by flow cytometry, Anal. Chem. **71** (1999) 5470-5480.

[27] Y. Li, Z. Chu, X. Liu, H. Jing, Y. Liu and D. Hao, A Cost-effective high-resolution melting approach using the EvaGreen dye for DNA polymorphism detection and genotyping in plants, J. Integr. Plant Biol. **52** (2010) 1036-1042.

[28] P. Zhang, Y. Liu, M. Alsarakibi, J. Li, T. Liu, Y. Li and G. Li, Application of HRM assays with EvaGreen dye for genotyping Giardia duodenalis zoonotic assemblages, Parasitol. Res. **111** (2012) 2157-2163.

[29] W. Wang, K. Chen and C. Xu, DNA quantification using EvaGreen and a real-time PCR instrument, Anal. Biochem. **356** (2006) 303-305.

[30] T.N. Singh and C. Turro, Photoinitiated DNA binding by *cis*-$[Ru(bpy)_2(NH_3)_2]_2$, Inorg. Chem. **43** (2004) 7260-7262.

[31] M. Safdar, Y. Junejo, K. Arman and M. Abasiyanik, Rapid bovine and Caprine species identification in ruminant feeds by duplex real-time PCR melting curve analysis using EvaGreen fluorescence dye, Mol. Biotechnol. **56** (2014) 770-776.

[32] A. Robertazzi and J.A. Platts, Hydrogen bonding and covalent effects in binding of cisplatin to purine bases: ab initio and atoms in molecules studies, Inorg. Chem. **44** (2005) 267-274.

[33] M. Boudvillain, R. Dalbies, C. Aussourd and M. Leng, Intrastrand cross-links are not formed in the reaction between transplatin and native DNA: relation with the clinical inefficiency of transplatin, Nucleic Acids Res. **23** (1995) 2381-2388.

[34] S. Ramachandran, B.R. Temple, S.G. Chaney and N.V. Dokholyan, Structural basis for the sequence-dependent effects of platinum-DNA adducts, Nucleic Acids Res. **37** (2009) 2434-2448.

Chapter 4
Sequence-specific Recognition of Mismatches and Damage in Double-stranded DNA.

4.1 Introduction

The genetic information of the human genome consists of about 6 billion base pairs. Defects in these genomes may lead to genomic instability causing cancer [1]. Mutations can be introduced from either endogenous or exogenous sources. One of the exogenous sources is exposure to ultraviolet (UV) radiation, which is considered the primary etiological agent in human skin cancer [2]. Short wavelength UVC light is strongly absorbed by DNA, producing direct damage products such as cyclobutane pyrimidine dimers (CPD), (6-4) pyrimidine-pyrimidinone (6-4 PP) photoproducts and Dewar pyrimidinones [2,3]. These photoproducts are repaired by nucleotide excision repair (NER) [4]; failure to do so can lead to interference in the DNA replication process by these lesions. Potentially crucial genes for cancer are the proto-oncogenes and tumour suppression genes, which play an important role in carcinogenesis, aging and cell death [5].

Human chromosomes consist of dsDNA. However, regions of single-stranded DNA (ssDNA) are formed during processes such as replication, transcription and recombination [6]. Thus, the cells, when subjected to DNA damaging agents, can undergo both ss- and double-stranded DNA (dsDNA) damage, depending on the rate of these process. It has long been reported that dsDNA is less prone to damage due to its double helical structure, which can protect it from chemical attack. On the contrary, ssDNA is more susceptible to DNA damage and undergoes chemical modifications such as depurination, depyrimidination, deamination and alkylation at a much faster rate than dsDNA [7]. Moreover, certain repair mechanism such as base-excision repair

(BER) and NER are specific to dsDNA damage, subjecting the ssDNA to a greater risk of DNA damage [8]. However, the effect of other damage agents differentially on dsDNA and ssDNA still needs to be investigated to further understand their overall genomic stability [9].

The effect of DNA damage on the molecular origin of mutagenesis and carcinogenesis has been studied by many techniques. These include the most commonly used chromatographic technique such as high performance liquid chromatography (HPLC) coupled with mass spectrometry (MS) [10] to attain high sensitivity and selectivity. Gel electrophoresis [11] is another commonly used method, which is selective to the size and length of damaged and mismatched DNA. While these techniques are able to assess damage effectively, they require complex and time-consuming procedures such as DNA digestion, pre-filtration and enzymatic cleavage, which introduce additional lesions and increase experimental error. To reduce these limitations, hybridization methods have been developed.

Hybridization assays rely on the simple concept that target oligonucleotide sequences hybridize with their perfect complementary DNA strand, while non-complementary strands do not. These complementary probes are usually combined with fluorescent probes to enhance sensitivity. These probes include molecular beacons (MBs) [12] and modified MBs such as locked nucleic acids (LNAs) [13], smart probes (SPs) [14] and 2-aminopurine MBs (2-AP MBs) [15]. Despite the wide application of these probes, their use is limited to quantification of ssDNA damage only. Also, they need to be designed to be complementary to every sequence studied.

Peptide nucleic acids (PNAs) for dsDNA damage detection has been popularly used due to strong binding of PNA in the major grooves of the DNA double helix via Hoogsteen bonds [16]. The binding efficiency of PNA to dsDNA to form a DNA-PNA-DNA triplex is extremely stable

and irreversible. Likewise, the binding of PNA to a dsDNA target is sequence specific, and is destabilized with a single base mismatch in the sequence [17,18]. Thus, PNA probes have several attractive advantages, such as higher binding affinity for dsDNA and increased specificity for single base mismatch. However, there are some disadvantages associated with the neutral backbone of PNA, which can cause self-aggregation. Also, the use of these probes are limited to the study of few sequences since they need to be designed to be complementary to each dsDNA target under study. Thus, the probe design and synthesis for multiple samples is an elaborate and expensive process.

The use of intercalating dyes as fluorescent probes overcomes the limitations of MB and PNA probes. These dyes are small molecules that can insert between the stacked bases of dsDNA producing a large increase in fluorescence intensity. The most commonly used intercalating dyes are Thiazole orange [19], PicoGreen [20], EvaGreen (EG) [21], the SYTO dyes and the SYBR dyes [22]. Although, these dyes display a ca. 1000-fold increase in fluorescence upon binding to dsDNA, they are devoid of DNA selectivity towards dsDNA and bind equally to both dsDNA and ssDNA. Another potential disadvantage of these dyes is that they unwind and extend the DNA helix upon binding to DNA [23]. However, certain structural modifications to these dyes, such as extending the known intercalating dyes with benzothiazole or benzoxazole moieties will shift the binding mode from intercalation to minor groove binding [23,24]. An attractive feature of these minor groove binders are their high selectivity towards dsDNA when compared to ssDNA. These dyes become fluorescent upon interaction with dsDNA but exhibit zero or reduced fluorescence in absence of dsDNA or in the presence of ssDNA. Thus these dyes can be used *in vivo* to quantitatively assay DNA even in the presence of RNA. Moreover, the minor groove binders do not unwind the DNA and thus have no effect on the DNA conformation. The most commonly

studied minor groove binders are Hoechst dye [23,25,26] and DAPI [23], which bind preferentially to AT-rich regions of B-DNA.

In this paper, we examine the relative rates of damage in ssDNA and dsDNA, in both synthetic and naturally occurring DNA. Previous studies have shown that the hotspots of DNA damage might be related to DNA double strand breaks (DSB) with the possibility of forming clusters of multiple simultaneous mutations in regions of ssDNA formed at DSBs, replication fork and uncapped telomeres [8,27]. Here, we explore the detection of mismatches in varying quantities and locations of dsDNA. A Hoechst minor groove binding dye has been used extensively for dsDNA quantification in this study. Figure 4.1 shows the binding of the Hoechst dye into the minor groove of dsDNA. We demonstrate the superior selectivity and sensitivity of this Hoechst dye in the detection of UVC-induced dsDNA damage and DNA base mismatches. Our results identify UVC radiation to be more mutagenic towards ssDNA than dsDNA. This result was further confirmed by melting curve studies using the EG intercalating dye [21], which is more specific in determining the change in the strength of hydrogen bonding upon increasing damage.

4.2 Experimental Section

The oligonucleotide targets and calf thymus DNA were obtained from Integrated DNA Technologies Inc. (Coralville, IA, USA) and Sigma Aldrich (Oakville, ON, Canada), respectively. The Hoechst 33258 dye (H258) (Figure 4.2) was also obtained from Sigma Aldrich (Oakville, ON, Canada). The sequences of the target oligonucleotides used for the mismatch experiment were designed by introducing mismatches at different position of the ssDNA. A clear outline of the different positions where mismatches could be introduced is given in Chart 1 and the ssDNA used for this study are listed in Table 4.1. Oligonucleotides were dissolved in nanopure water from a Barnsted Nanopure (Boston, MA, USA) water system. All samples were kept frozen at - 20^{o}C until

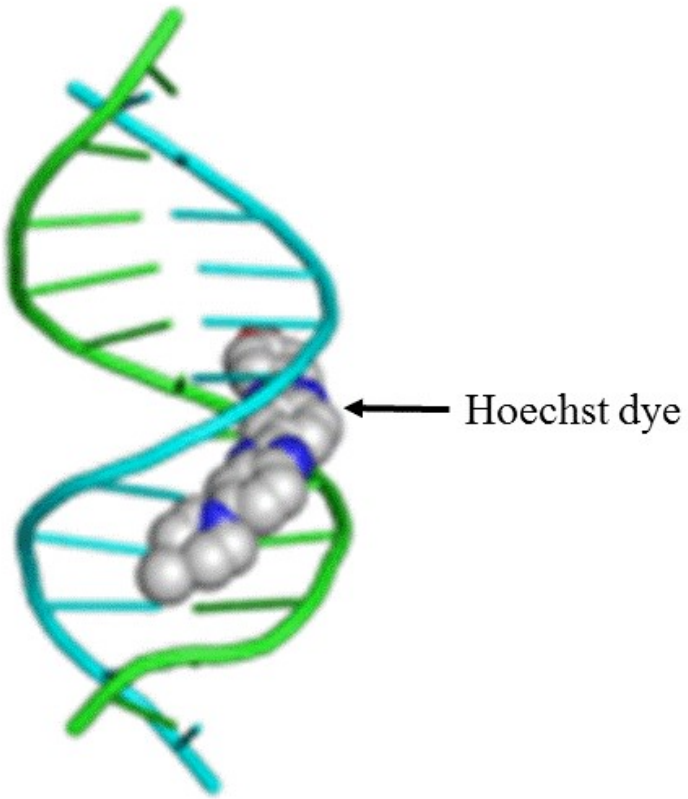

Figure 4.1 Hoechst dye binding into the minor groove of dsDNA. Obtained from http://lightboxkit.com/Assay_DNA.html

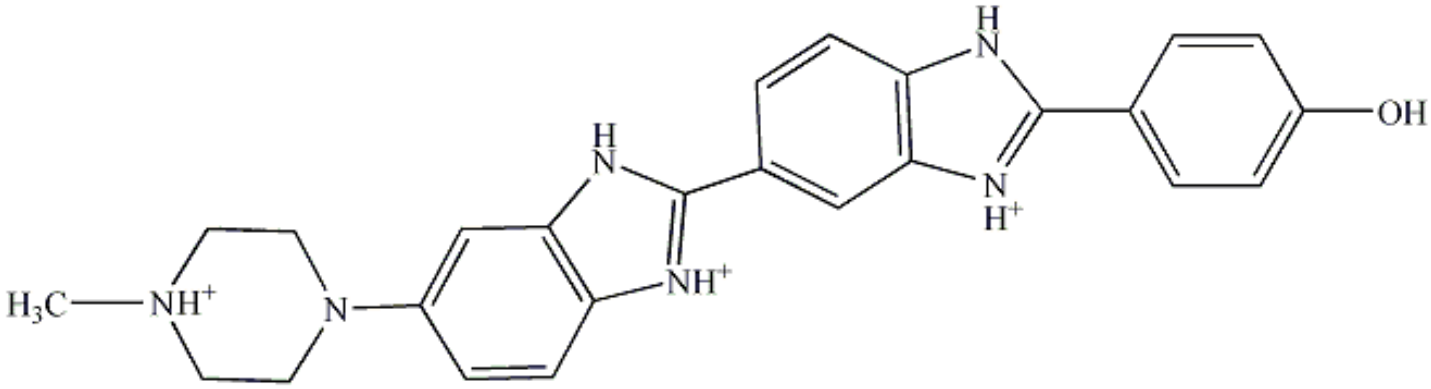

Figure 4.2 Structure of Hoechst 33258 dye

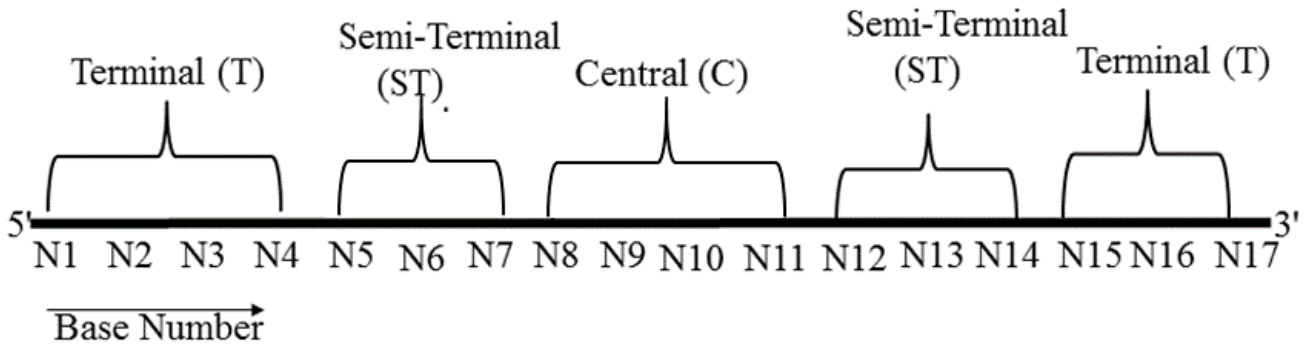

Chart 1: Schematic diagram representing different positions where the mismatch nucleotide could be introduced.

Table 4.1 Oligonucleotides used in this study.

Sequence	Position of Mismatches	Location of Mismatches	Number of Mismatches
5′-AAA AAA AAA AAA AAA AA-3′	0	None	0
5′-**C**AA AAA AAA AAA AAA AA-3′	1	T	1
5′-AAA A**C**A AAA AAA AAA AA-3′	5	ST	1
5′-AAA AAA AA**C** AAA AAA AA-3′	9	C	1
5′-**C**AA AAA AAA AAA AAA A**C**-3′	1,17	TT	2
5′-**C**AA A**C**A AAA AAA AAA AA-3′	1,5	T&ST	2
5′-**C**AA AAA AA**C** AAA AAA AA-3′	1,9	T&C	2
5′-AAA A**C**A AAA AAA AAA A**C**-3′	5,17	ST&T	2
5′-AAA A**C**A AAA AAA A**C**A AA-3′	5,14	ST&ST	2
5′-AAA AAA AA**C** A**C**A AAA AA-3′	8,10	CC	2
5′-**CC**A AAA AAA AAA AAA AA-3′	1,2	TT	2
5′-**CCC** AAA AAA AAA AAA AA-3′	1,2,3	TTT	3
5′-**CCC C**AA AAA AAA AAA AA-3′	1,2,3,4	TTTT	4
5′-AAA A**CC** AAA AAA AAA AA-3′	5,6	ST&ST	2
5′-AAA A**CC C**AA AAA AAA AA-3′	5,6,7	ST&ST&ST	3
5′-AAA A**CC CC**A AAA AAA AA-3′	5,6,7,8	ST&ST&ST&C	4
5′-AAA AAA AA**C C** AA AAA AA-3′	9,10	CC	2
5′-AAA AAA A**CC C**AA AAA AA-3′	8,9,10	CCC	3
5′-AAA AAA A**CC CC** A AAA AA-3′	8,9,10,11	CCCC	4
5′-**CC**A AAA AAA AAA AAA **CC**-3′	1,2,16,17	TTTT	4
5′-AAA A**CC** AAA AA**C C**AA AA-3′	5,6,12,13	ST&ST&ST&ST	4
5′-**CC**A A**CC** AAA AAA AAA AA-3′	1,2,5,6	TT&ST&ST	4

Oligonucleotide sequences were designed to have different positions and/or numbers of mismatches (underlined bases). Columns 2 and 3 represent the position (from the 5′ end) and location of mismatches in the sequences. ‘T’, ‘ST’ and ‘C’ in column 3 denote terminal, semi-terminal and central position, respectively. Column 4 represents the total number of mismatches in the sequences. All the sequences listed above are hybridized with complementary sequence T_{17} to form dsDNA.

needed. Upon thawing, the oligonucleotides are diluted to the required concentration in Tris buffer (10 mM Tris, 1 mM EDTA, 200 mM NaCl, pH ~7.4) for H258 dye and Tris buffer (10 mM Tris, 1 mM EDTA, 10 mM NaCl, pH ~7.4) for EG dye (discussed in Chapter 3.1). For mismatch experiments, all the ssDNA target sequences listed in Table 4.1 were annealed with oligonucleotide sequence T_{17} before use.

UV light from UVC lamps emitting at 254 nm was chosen for the irradiation. The UVC light was turned on for 20 min prior to the experiment to ensure a stabilized light source. The photoreactor was purged continuously with nitrogen to remove oxygen and minimize ozone generation from the lamps. Both ssDNA and dsDNA were subjected to UVC light from lamps with a power density of 75 W m^{-2} at the sample. Similarly, calf thymus DNA was also subjected to UVC light with a power density of 50 W m^{-2} at the sample. Control samples were handled under identical condition but were not exposed to UVC light. After irradiation, aliquots were pipetted into 96-well plates. The fluorescence intensity was studied at a dsDNA:H258 dye concentration ratio of 1:5 and at a dsDNA:EG dye concentration ratio of 1:1.33.

Room-temperature fluorescence intensities were measured using the Safire fluorescence plate reader (Tecan, Mannendorf, Switzerland). Fluorescence emission spectra for the H258 dye were recorded using an excitation wavelength of 360 nm and an emission wavelength of 460 nm and for the EG dye, the excitation wavelength was fixed at 490 nm and emission wavelength at 530 nm.Absorbance measurements were performed on a Hewlett-Packard (Sunnyvale, California) 8452A diode array spectrophotometer

4.3 Result and Discussion

4.3.1 Binding of ds DNA with H258 dye. When the binding of H258 to dsDNA occurs,

a sharp increase in its fluorescence intensity arises (Figure 4.3). However, this strong enhancement of intensity is not observed when H258 binds with ssDNA (data not included). It means that H258 binds more effectively with dsDNA than with ssDNA. It can also be noted that no considerable shift in the emission spectrum of H258 upon binding with ssDNA has been observed, suggesting that the polarity of the environment surrounding the dye is almost unchanged. Previous work has already reported that the H258 dye stability is affected by the polarity of the solvent [28]. Furthermore, there was a very small shift to shorter wavelength of the emission spectrum when H258 binds to dsDNA. This shift could be due to the dye partly penetrating inside the dsDNA along with binding to the surface of dsDNA [28].

This property of the H258 dye ensures that the dye can selectively discriminate between dsDNA and ssDNA. Thus, it could be an effective probe for detecting dsDNA damage. After UV damage of dsDNA, the H258 dye will bind the minor grooves of only undamaged DNA while the damaged DNA breaks up, at least partially, to ssDNA and the fluorescence of H258 dye is quenched as it is released into solution. In this way, the H258 dye produces a detectable signal proportional to the amount of dsDNA remaining after damage. Similarly, this method could also be used to study the effect of introducing mismatches into dsDNA sequences. In order to obtain maximum discrimination between damaged and undamaged dsDNA, we studied the effect of ionic strength and the [H258]/[DNA bp] ratio on the H258 fluorescence signal.

4.3.2 Factors affecting H258 fluorescence. In order to optimize the performance of H258 to discriminate between damaged and undamaged DNA, we studied the effect of Mg^{2+} and Na^{+} ion concentration on the H258 fluorescence intensity of ds T_{17}•A_{17}. Figure 4.4 (A)

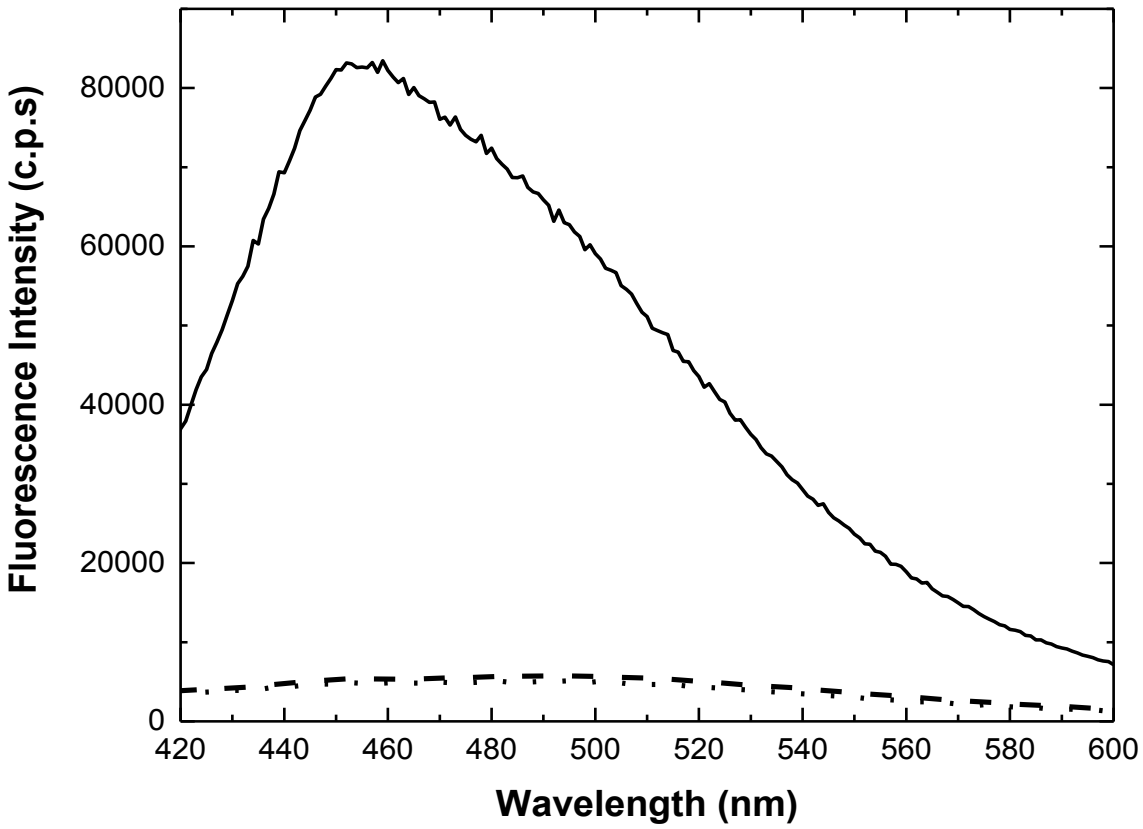

Figure 4.3 The emission spectrum of H258 dye alone (dash line), in the presence of 0.25 μM single-stranded DNA (dotted line) and in the presence of 0.25 μM double-stranded DNA (solid line) in buffered solution (10 mM Tris, 1 mM EDTA, 200 mM NaCl, pH 7.4). The concentration of H258 was 0.20 μM. Excitation was at 360 nm and the spectra were recorded at room temperature. On the y-axis, 'c.p.s' denotes counts per second.

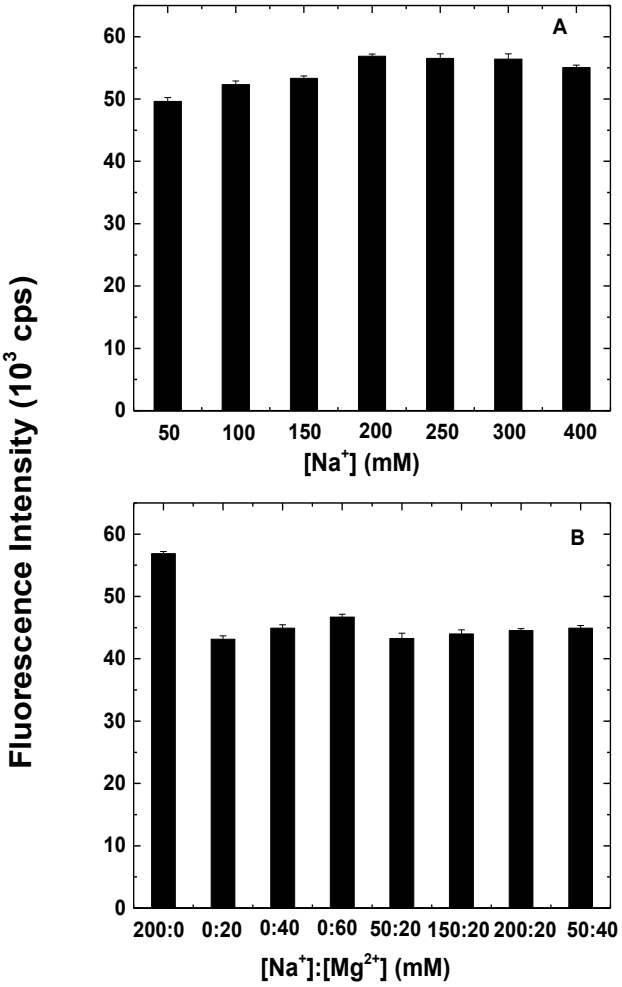

Figure 4.4 The fluorescence intensity of ds T_{17}•A_{17}-H258 as a function of (A) [Na^+] alone and (B) [Na^+]:[Mg^{2+}] ratios in 10 mM Tris with 1 mM EDTA (pH 7.4). The concentration of H258 was 5 μM and ds T_{17}•A_{17} was 1 μM, respectively.

shows the effect of the Na^+ concentration on the fluorescence of H258-dsDNA. The fluorescence of H258 attains a maximum at a Na^+ concentration ($[Na^+]$) of 200 mM and remains constant with further increase in $[Na^+]$. However, after $[Na^+]$ of 300 mM we see a drop in the fluorescence intensity of the H258 dye. Similarly, Figure 4.4 (B) shows the fluorescence intensity of H258 as a function of $[Mg^{2+}]$ alone or both $[Mg^{2+}]$ and $[Na^+]$ simultaneously. The results show that the fluorescence intensity of H258 is quenched in the presence of $[Mg^{2+}]$. Thus, 200 mM NaCl was found to be the optimum concentration to yield the maximum fluorescence intensity for dsDNA-H258. No remarkable change in the fluorescence intensity of H258 was observed upon binding to ssDNA at different $[Mg^{2+}]$ and $[Na^+]$ (data not shown).

To study the optimum [H258]/[DNA bp] ratio, the fluorescence of 1 μM ds T_{17}•A_{17} as a function of increasing concentration of H258 dye was studied (Figure 4.5). Upon addition of H258, the fluorescence of the dye increases significantly and attains a maximum value at a dye concentration of 5 μM. A 3-4 fold enhancement in H258 fluorescence is observed on increasing the concentration of dye from 1 μM to 5 μM. This suggests a binding of ~1 dye per 4 A-T base pair is required to attain the maximum fluorescence intensity of the H258 dye. However, further increases in H258 concentration leads to a rapid drop in fluorescence intensity and the fluorescence intensity continues to decrease with increasing concentration. A 20-25 fold deterioration in H258 fluorescence intensity is observed on increasing the concentration of dye from 5 μM to 40 μM, indicating a different binding mechanism as detailed below. A constant, low fluorescence intensity is observed at a H258 concentration higher than ~40 μM.

It has been proposed that several complexes with distinct stoichiometries between H258 dye and dsDNA helix occur [26]. At low [H258]/[DNA bp] ratios, a strong and "minor groove-

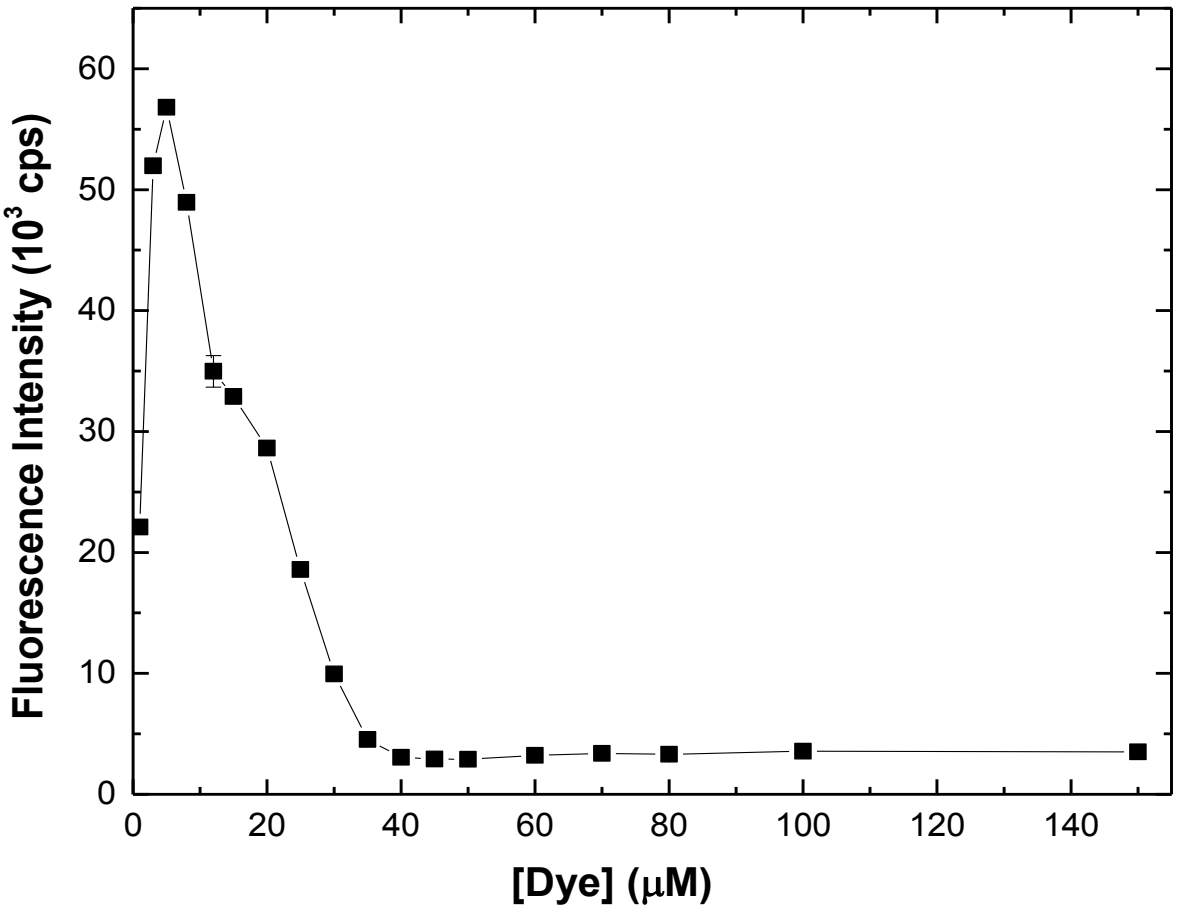

Figure 4.5 H258 dye fluorescence intensity as a function of H258 concentration in the presence of 1 μM $dsT_{17}•A_{17}$ (10 mM Tris, 1 mM EDTA, 200 mM NaCl, pH 7.4). Excitation and emission wavelengths were 360 and 460 nm, respectively. Each data point is the average of four replicate measurements and the error bars correspond to the standard deviation of each measurement. The line is simply drawn to connect the data points. 'c.p.s' denotes counts per second.

specific" binding occurs with an intense increase in fluorescence intensity. This binding requires a specific sequence and is termed as sequence-mediated or specific binding mode. It often requires about 4 A-T base pairs [26] (Figure 4.5, region between 1 μM to5 μM [dye]). However, at [H258]/[DNA bp] ratios = 1:1, a weaker dye-mediated (unspecific) binding mode occurs between the free dye to another dye molecule or to a group of dye molecules or to a dye molecule already bound to dsDNA within the minor groove or to the charged phosphate backbone. Such dye-mediated binding occurs when ~ two dye molecule binds per DNA base pair and results in strong intermolecular quenching. This quenching increases with increasing concentration of dye and we see a sharp decrease in the fluorescence intensity of H258 (Figure 4.5, region between 5 μM to 35 μM [dye]). Further, at higher [H258]/[DNA bp] ratios, the unspecific binding mode reaches its maximum and results in the low, constant fluorescence intensity region (Figure 4.5, region higher than ~40 μM [dye]).

4.3.3 dsDNA mismatch discrimination. To examine the effect of mismatches on the minor groove conformation of dsDNA, a series of mismatched 17-mer double-stranded targets were prepared which varied in the number and position of mismatches. Figure 4.6 shows the decreased fluorescence intensity of the H258-dsDNA complex with different sites of mismatches. In general, H258 binds to the minor groove of a perfectly matched duplex and gives a maximum fluorescence. However, when mismatches are introduced into the dsDNA, we see a drop in fluorescence. This drop in fluorescence can be further related to the change in the minor groove conformation of the dsDNA. Our results show that no specific trend has been followed with increasing the number of mismatches in the given sequences, but that there is a relation between both the position and number of mismatches with the change in fluorescence intensity. If we consider sequences with one mismatch introduced at the terminal, semi-terminal or central positions, a maximum decrease

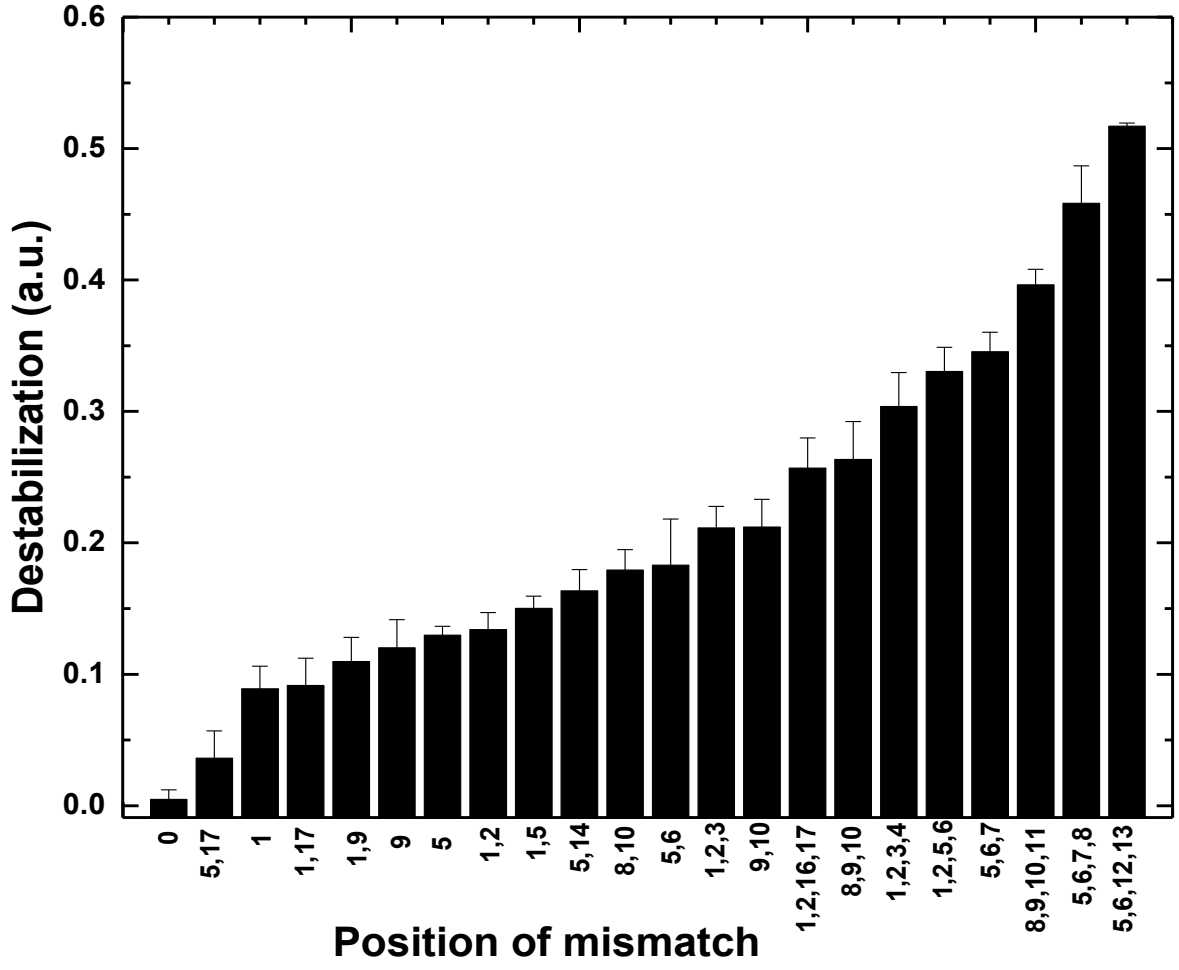

Figure 4.6 Destabilization (1-F) as a function of the number and position of mismatches in dsDNA target. The values on the y-axis are 1-F, where $F = F_i/F_c$, F_i is the fluorescence intensity of H258-dsDNA with mismatches and F_c is the fluorescence intensity of the perfectly complementary H258-dsDNA complex. H258 dye fluorescence intensity is taken in the presence of 1 μM $dsT_{17}•A_{17}$ (10 mM Tris, 1 mM EDTA, 200 mM NaCl, pH 7.4).

in fluorescence intensity, here called destabilization $D= 1-F_i/F_c$, where F_i = fluorescence intensity of H258-dsDNA with mismatches and F_c = fluorescence intensity of the perfectly complementary H258-dsDNA complex, occurs for the semi- terminal and central positions. A trend is observed for sequences with two mismatches. However, for sequences with three and four mismatches a slightly higher destabilization is observed for semi- terminal positions. Here, it is worth mentioning that the destabilization at terminal positions was the minimum for sequences with one, two, three and four mismatches for all sequences in that category. Thus, it could be interpreted that the terminal positions of the dsDNA do not play an important role in deciding the conformation of the minor groove. On the other hand, any mismatch introduced at the semi-terminal positions greatly affects the stability of the minor groove conformation and thus leads to maximum destabilization. These results are expected since dsDNA occurs in a helical form with each turn being 10 nucleotides long. Thus, the sequence with 17 nucleobases will form two turns of a double helix. Mismatches introduced at semi-terminal positions will easily disrupt the helical structure of each turn formed and thus play a greater role in minor groove recognition when compared to other positions.

It is widely accepted that the helical structure of dsDNA depends upon a fine balance between base stacking and base pairing energy. Thus, to further investigate the decreased fluorescence intensity as a function of mismatches, we compared the destabilization with the melting temperatures (T_m) for all the sequences listed in Table 4.1 (Figure 4.7). We found that for most sequences, the destabilization increases with a decrease in the T_m value. This result was expected since the higher the number of mismatches, the greater the destabilization of the double helix and the lower the T_m value. This decrease in T_m is indicative of the weaker hydrogen bonding between Watson-Crick base pairs (A•T and C•G) and resulting disruption of the dsDNA helix conformation

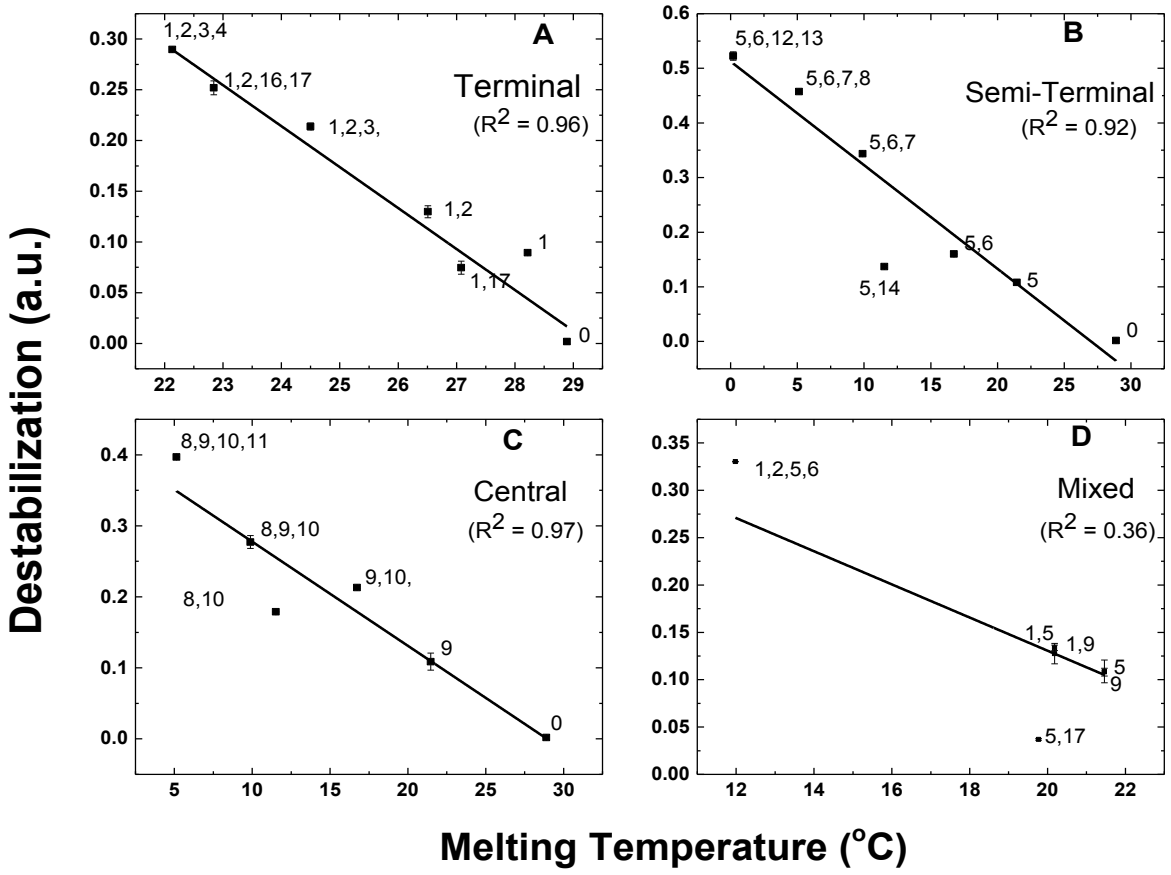

Figure 4.7 Destabilization (1-F) as a function of melting temperature for dsDNA target. The destabilization values on the y-axis are 1-F, where $F = F_i/F_c$, F_i is the fluorescence intensity of H258-dsDNA with mismatches and F_c is the fluorescence intensity of the perfectly complementary H258-dsDNA complex. H258 dye fluorescence intensity is taken in the presence of 1 μM $dsT_{17}•A_{17}$ (10 mM Tris, 1 mM EDTA, 200 mM NaCl, pH 7.4). Melting temperatures were calculated using IDT tool [29].

as mismatches are introduced into the sequences. The T_m values for sequences with one mismatch at any position have the highest melting temperatures compared to all other mismatch sequences. Further we saw that, with increasing numbers of mismatches, the melting temperature decreases and destabilization increases. Also, increase in mismatches will make the dsDNA become more destabilized.

In Figure 4.7 (A) we see that the highest destabilization occurs when the terminal mismatches run in a continuous chain at position 1,2,3,4 rather than the non-continuous positions 1,2,16,17. A similar pattern is observed for 1,2 and 1,17. On the contrary, Figure 4.7 (B) shows that for semi-terminal positions, greater destabilization occurs when the mismatches are introduced at two non-continuous semi-terminal positions 5,6 and 12,13 rather than continuous positions 5,6,7,8. T_m values for these sequences also give a similar trend. As discussed before, it is obvious that since dsDNA of 17 nucleobases can form ~2 turns, the mismatches at positions 5,6 and 12,13 will destabilize both the turns equally thus enforcing the dsDNA to open up. But, when the mismatch is at position 5,6,7,8, only one of the turns undergoes hydrogen bond breaks and the other turn remains intact as dsDNA.

The fluorescence intensity as a function of destabilization and T_m at different mismatch positions gave a similar trend. In Figure 4.7 the scale for the T_m values (x-axis) clearly illustrates that the highest dynamic range for T_m values occurs for sequences with mismatches at semi-terminal positions (~30^{o}C) and lowest at terminal positions (~7^{o}C). Similarly, the scale for destabilization (y-axis) shows that the greatest destabilization occurs for semi-terminal positions (~0.5) and least for terminal positions (~0.3). Another interesting result we found were for the sequence with mismatches at positions 5 and 9 which had the same T_m value and almost the same destabilization values (Figure 4.7 D). A similar trend is observed for sequence with mismatches at

position 1,5 and 1,9. These results confirm that both base pairing and base stacking energy contribute to the disruption of minor groove conformation since the T_m value depends on the strength of hydrogen bonding and destabilization (which depends on fluorescence of H258) depends on the base stacking energy. Any change in the base stacking energy will disrupt the minor groove conformation [30], thus affecting the strength of binding between the H258 minor groove binder and the dsDNA. However, all four sets of graphs in Figure 4.7 have some outliers, for which the T_m values do not agree with the respective linear relationship with destabilization. These contradictory results are difficult to explain with the limited data and are a matter of further investigation.

4.3.4 UVC-induced DNA damage of calf thymus DNA. In order to assess the mutagenic effect of UVC radiation on calf thymus DNA, the fluorescence intensity of H258 was measured as a function of exposure time (Figure 4.8). The maximum UVC exposure time was 420 min. By this time, the fluorescence intensity of H258 has decreased close to the intensity of the H258 dye alone. The damage constants obtained for two independent irradiation experiments of calf thymus DNA with UVC radiation are 77 ± 4.0 and 79 ± 5.0 min, respectively. The value of %RSD for interday precision is 1.8%, which indicates that the damage kinetics of calf thymus DNA detected with H258 dye fluorescence is repeatable. Figure 4.8 illustrates that there is an exponential drop in the fluorescence intensity initially for 60-90 min, but later the H258 fluorescence intensity from calf thymus DNA has completely levelled off at the minimum. The points along the baseline after ~200 min give fluorescence intensity close to the fluorescence intensity of the H258 dye alone, which indicates that the calf thymus DNA is almost completely damaged. Here it is worth mentioning that the result discussed above is obtained based on the fluorescence intensity of H258 which is a minor groove binder. Thus, any damage that disrupts the minor groove conformation would result

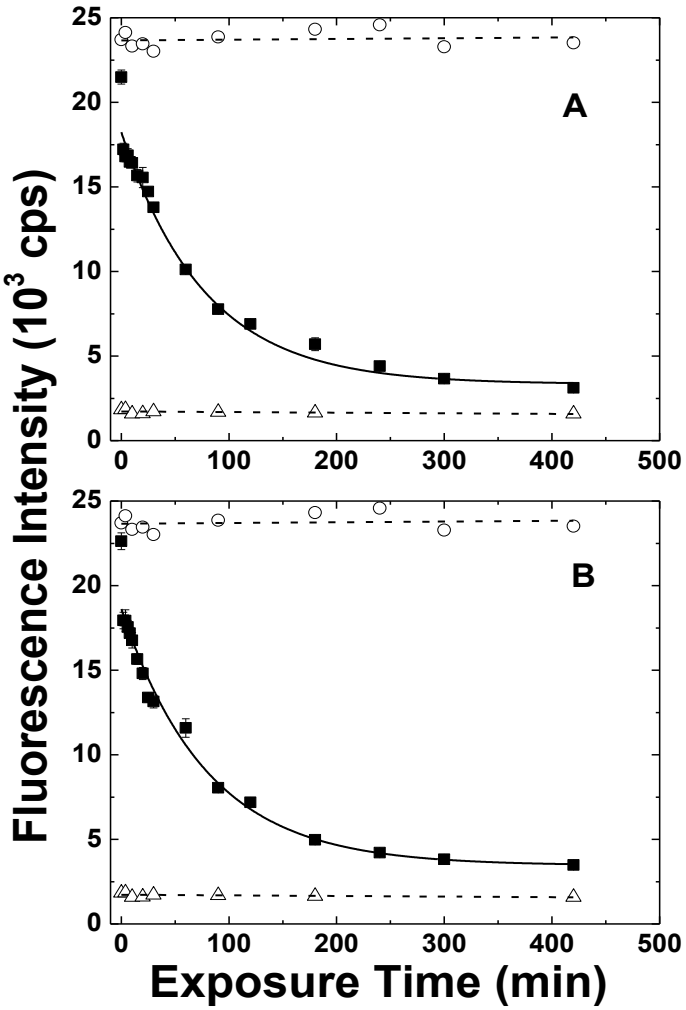
Fluorescence Intensity (10^3 cps)
A
B
Exposure Time (min)
0
5
10
15
20
25
0
100
200
300
400
500

Figure 4.8 Fluorescence intensity at 460 nm as a function of exposure time for calf thymus DNA in a nitrogen atmosphere. Aliquots of the irradiated calf thymus DNA were mixed with H258 (10 mM Tris,1 mM EDTA, 200 mM NaCl, pH 7.4) in a concentration ratio of 1:5 in a 96-well plates. For both the plots open circles represent the fluorescence intensity of control sample, open triangles represents fluorescence intensity of H258 dye alone and filled squares represents the irradiated calf thymus DNA sample. The solid lines through the points are single exponential $I_F = I_o + Ae^{-t/\tau}$ fits. The fluorescence parameters obtained from the fit for calf thymus DNA in (A) are I_o = 3.34 ± 0.20 a.u, A = 14.89 ± 0.37 a.u. and τ_1 = 77.20 ± 3.93 min. The fluorescence parameters obtained from the fit for calf thymus DNA in (B) are I_o = 3.44 ± 0.21 a.u, A = 15.16 ± 0.44 a.u. and τ_1 = 79.15 ± 5.22 min. The control (high fluorescence) and H258 dye alone (low fluorescence) points are fit to a straight line (dash line) with zero slope by eye.

in a drop in fluorescence. With the earlier study discussed in Section 4.3.3, it can be concluded that the drop in fluorescence we noticed for calf thymus DNA depends upon both number as well as the position of damage. However, an earlier Raman study done on calf thymus DNA reveals that DNA was damaged to some extent after 1 h and almost completely damaged after 3 h of a similar dose of UVC discussed in Section 4.3.3, it can be concluded that the drop in fluorescence we noticed for calf radiation [31]. Our results also show a similar trend confirming that the drop in fluorescence intensity of H258 is due to the damage of calf thymus DNA by UVC radiation. No drop in fluorescence intensity of H258 is observed from the unirradiated controls over the long period of exposure time (Figure 4.8).

4.3.5 Comparison of UVC-induced ss- and dsDNA damage detected by H258. Many *in vivo* studies have already shown that ssDNA is more susceptible to DNA damage than dsDNA. In order to determine if this is true at the molecular level in isolated DNA, we analyzed the kinetics of ssDNA and dsDNA with UVC irradiation and H258 fluorescence detection. DNA double helix stability is determined by both base pairing (hydrogen bonding) and base stacking (conformation) energy contributions. In order to facilitate the study of hydrogen bonding and minor groove conformation of ss-and dsDNA during UVC damage we choose to have both EG (hydrogen bonding) and H258 (minor groove conformation) dye together. As discussed in Chapter 3, EG is an intercalating dye which inserts between the stacked dsDNA. The strength of intercalation decreases with breaking up of the hydrogen bonds between the Watson-Crick base pairs leading to the formation of ssDNA. On the contrary, H258 is a minor groove binder and thus any damage that will change the minor groove conformation of the dsDNA will only result in a decrease in fluorescence intensity.

Figure 4.9 shows the UVC-induced damage kinetics of T_{17} ss- and T_{17}•A_{17} dsDNA by recording

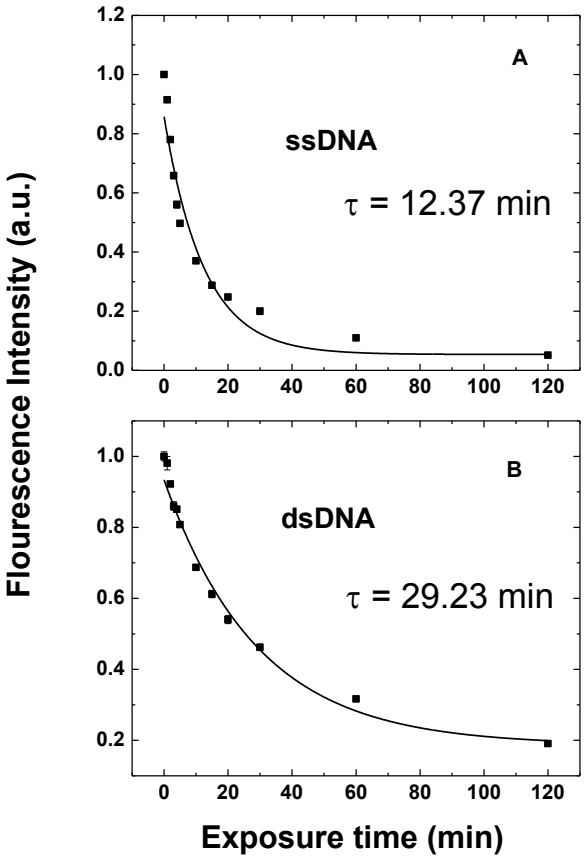

Figure 4.9 Damage curve of 1 μM H258 in Tris buffer (10 mM Tris, 1 mM EDTA, 200 mM NaCl, pH 7.4) with (A) ss dT_{17} hybridized with ss dA_{17} and (B) ds T_{17}•A_{17}. For (A), the hybridization with ss dA_{17} occurred after exposure to UVC light. The curves were obtained by exciting the hybridization mixture at 360 nm and emission recorded at 460 nm. The solid lines through the points are single exponential $I_F = I_o + Ae^{-t/\tau}$ fits. The fluorescence parameters obtained from the fit for ssT_{17} are I_o = 0.05 ± 0.01 a.u, A = 0.80 ± 0.06 a.u. and τ_1 = 12.37 ± 1.44 min. The fluorescence parameters obtained from the fit for dsT_{17}•A_{17}. are I_o = 0.19 ± 0.01 a.u, A = 0.75 ± 0.02 a.u. and τ_1 = 29.23 ± 3.23 min. Here fits to multiple exponentials decreases the goodness of fit.

the fluorescence intensity of H258 as a function of exposure time. Earlier efforts to study the excited-state dynamics in DNA model systems revealed that the excited-state lifetime for dsDNA was a few picoseconds greater than the lifetime of ssDNA [32,33]. This change in lifetime is due to strong base stacking and base pairing in dsDNA. Since the probability of damage increases with an increase in the excited-state lifetime, we expect dsDNA to be more prone to UV-induced damage than ssDNA. However, the damage constant obtained for ssDNA and ds DNA in this study is 12 ± 1.0 and 29 ± 3.0 min, respectively. This result was similar to the results obtained for *in vivo* studies. A clear understanding about this discrepancy between the biological and molecular aspect of DNA damage was put forward by Kohler, et al. [34], who studied the photodimerization kinetics for both ssDNA and dsDNA using femtosecond time-resolved infrared spectroscopy. They suggested that DNA nucleobases must be in the conformation of the transition state to form photoproducts, and that this occurs very infrequently in dsDNA. However, ssDNA is more conformationally flexible and may reach the transition state more often, making it more susceptible to damage. Thus, the more rigid DNA structure, the greater would be the resistance towards photoproduct formation.

Studying the drop in fluorescence intensity of H258 upon increasing UVC exposure time gives the change in the minor groove conformation of ds- and ssDNA. Any change in the minor groove conformation due to increasing damage by UVC radiation will be depicted by a drop in fluorescence since H258 dye binds preferentially to AT-rich region of B-DNA. We also measured the influence of UVC radiation on hydrogen bonding between Watson-Crick bases in ds- and ssDNA. Using the EG dye, which is an intercalating dye. The drop in EG fluorescence upon hydrogen bond breaks can be correlated to the damage of ss- and dsDNA. Thus, for undamaged ds- and ssDNA, the EG dye would perfectly intercalate between the nucleobases and give a

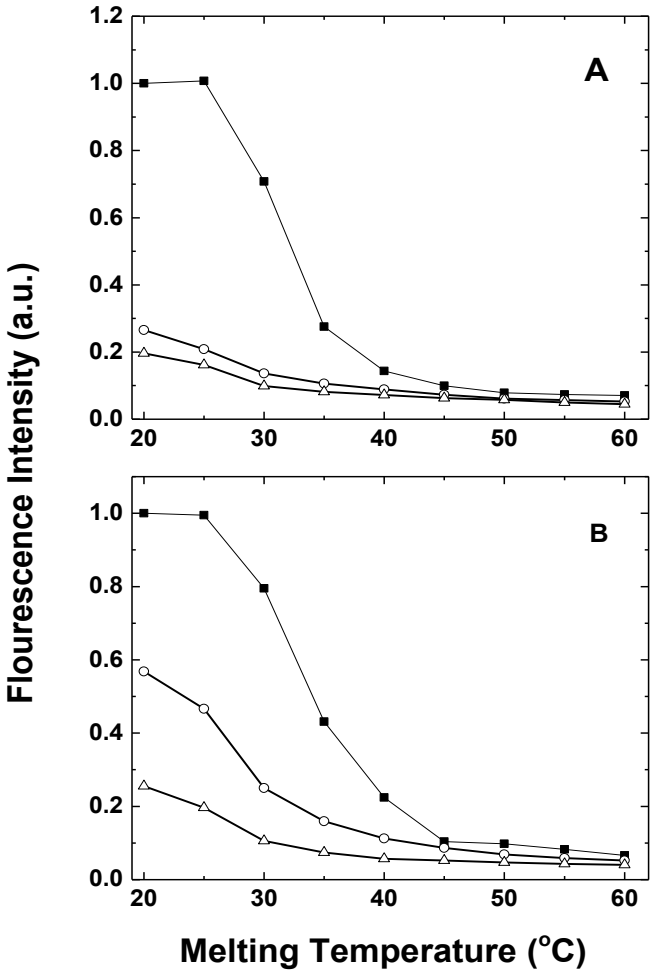

Figure 4.10 Melting curves of (A) 1 μM ss T_{17} hybridized with ssA_{17} (B) 1 μM ds T_{17}•A_{17} after '0' min (filled squares), 10 min (open circles) and 20 min (open triangles) of UVC damage with 1.33 μM of EG in Tris buffer (10 mM Tris, 1 mM EDTA, 10 mM NaCl, pH 7.4). The curves were obtained by exciting the hybridization mixture at 490 nm and emission recorded at 530 nm. The fluorescence intensity has been normalized to the fluorescence intensity at 0 min, 20 °C for each sequence.

maximum fluorescence intensity. But, for damaged DNA, the hydrogen bonds would break, resulting in a higher spacing between the DNA base pairs. With increasing amount of damage the dsDNA will separate into ssDNA which releases the EG dye to solution.

Figure 4.10 shows the melting curves for ss- and dsDNA after exposure to UVC light for 0, 10 and 20 min. For the melting curves of both ss- and dsDNA, we saw an increase in destabilization upon increase in exposure time. This is clearly illustrated by the drop in fluorescence signal at low temperature with increasing exposure time. On comparing the fluorescence intensities between damaged and undamaged ss- and dsDNA, we see a higher decrease in the low-temperature fluorescence intensity for ssDNA after 10 min exposure to UVC radiation, compared to the same curve for dsDNA. The drop in fluorescence for both becomes almost similar on increasing the damage time from 10 to 20 min. Further, if we compare the melting decreases from 35 ^{o}C to 26 ^{o}C upon 10 min damage for ss DNA and 35 ^{o}C to 30 ^{o}C for dsDNA. This decrease in melting temperature can be correlated to the strength of hydrogen bonding. Thus, the greater drop in melting temperature for ssDNA indicates that more hydrogen bonds break for ssDNA than for dsDNA. This result again supports the fact that ssDNA is damaged at a faster rate than dsDNA.

4.4 Conclusion

The fluorescence intensity has been normalized to the fluorescence intensity at 0 min, 20 ^{o}C for each sequence.These results conclusively show that the H258 minor groove binder is a sensitive and inexpensive probe for the analysis for UVC induced damage of ss-, ds- and calf thymus DNA. From our results we found that the regions of ssDNA are much more susceptible to UVC damage than dsDNA, yielding a damage constant that is greater by a factor of two. Thus, it is possible that damage to regions of ssDNA generated during DNA, replication, could contribute to higher numbers of point mutations. Further, we found that the calf thymus DNA, which is ~2000 bp, was

damaged by UVC radiation with a damage constant of 77-79 min. We also studied the effect of mismatches on the stability of dsDNA. Surprisingly we found that stability of the DNA groove conformation is more determined by the position of mismatch than by the number of mismatches. Further studies with different mutagenic agents could reveal their respective hot-spots of damage. Also, in this study we designed a simple, efficient mix-and-read assay for the detection of mismatches in dsDNA and damage in both ss- and dsDNA. This assay along with a potential dsDNA binding probe, H258 could be extended for the *in vitro* study of damage in real nucleic acids.

Reference List

[1] D. Billen, Spontaneous DNA damage and its significance for the" negligible dose" controversy in radiation protection, Radiat. Res. **124** (1990) 242-245.

[2] M.D. Evans, M.S. Cooke, I.D. Podmore, Q. Zheng, K.E. Herbert and J. Lunec, Discrepancies in the measurement of UVC-induced 8-oxo-2′-deoxyguanosine: implications for the analysis of oxidative DNA damage, Biochem. Biophys. Res. Commun. **259** (1999) 374-378.

[3] M.L. Rolfsmeier, M.F. Laughery and C.A. Haseltine, Repair of DNA double-strand breaks following UV damage in three Sulfolobus solfataricus strains, J. Bacteriol. **192** (2010) 4954-4962.

[4] P.J. Rochette and D.E. Brash, Human telomeres are hypersensitive to UV-induced DNA Damage and refractory to repair, PLoS genetics. **6** (2010) e1000926, 1-13.

[5] B. Vogelstein and K.W. Kinzler, Cancer genes and the pathways they control, Nat. Med. **10** (2004) 789-799.

[6] R. Hindges and U. Hubscher, DNA polymerase delta, an essential enzyme for DNA transactions, Biol. Chem. **378** (1997) 345-362.

[7] T. Lindahl, Instability and decay of the primary structure of DNA, Nature. **362** (1993) 709-715.

[8] Y. Yang, J. Sterling, F. Storici, M.A. Resnick and D.A. Gordenin, Hypermutability of damaged single-strand DNA formed at double-strand breaks and uncapped telomeres in yeast Saccharomyces cerevisiae, PLoS genetics. **4** (2008) e1000264, 1-12.v

[9] K. Chan, J.F. Sterling, S.A. Roberts, A.S. Bhagwat, M.A. Resnick and D.A. Gordenin, Base damage within single-strand DNA underlies *in vivo* hypermutability induced by a ubiquitous environmental agent, PLoS genetics. **8** (2012) e1003149, 1-15.

[10] T. Douki, S. Sauvaigo, F. Odin and J. Cadet, Formation of the main UV-induced thymine dimeric lesions within isolated and cellular DNA as measured by high performance liquid chromatography-tandem mass spectrometry, J. Biol. Chem. **275** (2000) 11678-11685.

[11] S.G. Fischer, L.S. Lerman and L.S. Proc, DNA fragments differing by single base-pair substitutions are separated in denaturing gradient gels: correspondence with melting theory, Natl. Acad. Sci. **80** (1983) 1579-1583.

[12] L.C. Riches, A.M. Lynch and N.J. Gooderham, A molecular beacon approach to detecting RAD52 expression in response to DNA damage in human cells, Toxicol. Vitro. **24** (2010) 652-660.

[13] A.F. El-Yazbi and G.R. Loppnow, Locked nucleic acid hairpin detection of UV-induced DNA damage, Can. J. Chem. **89** (2011) 402-408.

[14] S.A. Oladepo and G.R. Loppnow, Self-quenching smart probes as a platform for the detection of sequence-specific UV-induced DNA photodamage, Anal. Bioanal. Chem. **397** (2010) 2949-2957.

[15] A.F. El-Yazbi and G.R. Loppnow, 2-Aminopurine hairpin probes for the detection of ultraviolet-induced DNA damage, Anal. Chim. Acta. **726** (2012) 44-49.

[16] P.E. Nielsen, Targeting double stranded DNA with peptide nucleic acid (PNA), Curr. Med. Chem. **8** (2000) 545-550.

[17] V.V. Demidov, M.V. Yavnilovich and M.D. Frank-Kamenetskii, Kinetic analysis of specificity of duplex DNA targeting by homopyrimidine peptide nucleic acids, Biophys. J. **72** (1997) 2763-2769.

[18] H. Kuhn, V.V. Demidov and M.D. Frank-Kamenetskii, P.E. Nielsen, Kinetic sequence discrimination of cationic bis-PNAs upon targeting of double-stranded DNA, Nucleic Acids Res. **26** (1998) 582-587.

[19] Q. Lu, Z. Zhou, Y. Mei, W. Wei and S. Liu, Detection of DNA damage by thiazole orange fluorescence probe assisted with exonuclease III, Talanta. **116** (2013) 958-963.

[20] T. Sedlackova, G. Repiska, P. Celec, T. Szemes and G. Minarik, Fragmentation of DNA affects the accuracy of the DNA quantitation by the commonly used methods, Biol. Proced. Online. **15** (2013) 1-8

[21] Y. Li, Z. Chu, X. Liu, H. Jing, Y. Liu and D. Hao, A Cost-effective high-resolution melting approach using the EvaGreen dye for DNA polymorphism detection and genotyping in plants, J. Integr. Plant Biol. **52** (2010) 1036-1042.

[22] H. Gudnason, M. Dufva, D.D. Bang and A. Wolff, Comparison of multiple DNA dyes for real-time PCR: effects of dye concentration and sequence composition on DNA amplification and melting temperature**,** Nucleic Acids Res. **35** (2007) e127, 1-8.

[23] H.J. Karlsson, M. Eriksson, E. Perzon, B. Akerman, P. Lincoln, and G. Westman, Groove-binding unsymmetrical cyanine dyes for staining of DNA: syntheses and characterization of the DNA-binding, Nucleic Acids Res. **31** (2003) 6227-6234.

[24] T.G. Deligeorgiev, S. Kaloyanova and J.J. Vaquero, Intercalating cyanine dyes for nucleic acid detection, Recent Pat Mater Sci. **2** (2009) 1-26.

[25] A. Fede, M. Billeter, W. Leupin and K. Wüthrich, Determination of the NMR solution structure of the Hoechst 33258-d $(GTGGAATTCCAC)_2$ complex and comparison with the X-ray crystal structure, Structure. **1** (1993) 177-186.

[26] F.G. Loontiens, P. Regenfuss, A. Zechel, L. Dumortier and R.M. Clegg, Binding characteristics of Hoechst 33258 with calf thymus DNA, poly [d (AT)] and d (CCGGAATTCCGG): multiple stoichiometries and determination of tight binding with a wide spectrum of site affinities, Biochemistry. **29** (1990) 9029-9039.

[27] S.A. Roberts, J. Sterling, C. Thompson, S. Harris, D. Mav, R. Shah, L.J. Klimczak, G.V. Kryukov, E. Malc and P.A. Mieczkowski, Clustered mutations in yeast and in human cancers can arise from damaged long single-strand DNA regions, Mol. Cell. **46** (2012) 424-435.

[28] V. Nikolai, Binding of Hoechst with nucleic acids using fluorescence spectroscopy, J. Biophys. Chem. **2** (2011) 443-447.

[29] R. Owczarzy, A.V. Tataurov, Y. Wu, J.A. Manthey, K.A. McQuisten, H.G. Almabrazi, K.F. Pedersen, Y. Lin, J. Garretson, N.O. McEntaggart, C.A. Sailor, R.B. Dawson and A.S. Peek, IDT SciTools: a suite for analysis and design of nucleic acid oligomers, Nucleic Acids Res. **36** (2008) W163-9.

[30] E.T. Kool, Hydrogen bonding, base stacking and steric effects in DNA replication, Annu.Rev.Biomol.Struct. **30** (2001) 1-22.

[31] Y. Tang and Z. Guo, Influence of ultraviolet radiation on calf thymus DNA studied by Raman spectroscopy, Proc. of SPIE. **5630** (2005) 384-395.

[32] C.T. Middleton, K. de La Harpe, C. Su, Y.K. Law, C.E. Crespo-Hernández and B. Kohler, DNA excited-state dynamics: from single bases to the double helix, Annu. Rev.Phys. Chem. **60** (2009) 217-239.

[33] F. Plasser, A.J. Aquino, H. Lischka and D. Nachtigallová, Electronic excitation processes in single-strand and double-strand DNA: A computational approach, Top. Curr. Chem (2014), Springer Berlin Heidelberg, Germany.

[34] W.J. Schreier, T.E. Schrader, F.O. Koller, P. Gilich, C.E. Crespo-Hernández, V. N. Swaminathan, T. Carell, W. Zinth and B. Kohler, Thymine dimerization in DNA is an ultrafast photoreaction, Science. **315** (2007) 625-629.

Chapter 5
Recognition and Comparison of K-*Ras* and N-*Ras* Mutagenic Hot Spots for Ru *cis*-platin and UV Damage

5.1 Introduction

Mutational activation of the *Ras* family of genes has been found to be one of the most common oncogenic events in cancer [1,2]. The *Ras* family consists of three proto-oncogenes, K-*Ras*, N-*Ras* and H-*Ras* [1,3,4]. Although there is a high degree of similarity among the different *Ras* gene sequences, earlier studies have demonstrated that different tumor types are identified with different *Ras* genes [5]. However, no correlation has been established between an activated *Ras* oncogene and the tumour type present. Apparently, mutation of *Ras* proto-oncogenes is not essential for tumourigeneses but it can still be a contributing factor to human carcinogenesis [6].

Much effort has been made to investigate how mutation leads to activation of the *Ras* genes. Past research studies have shown that mutation at codons 12, 13 and 61 of any three *Ras* genes are capable of activating their oncogenic functions [3,7,8]. Interestingly, it has been found that mutation preferentially occurs at codon 12 of K-*Ras* than at codons 13 or 61 of K-*Ras* or at any condons of N-*Ras* or H-*Ras* [7,9,10]. Furthermore, on investigating the repair mechanism between codon 12 and the other condons, it was observed that there was no substantial difference in their repair rates. These finding raise an important question: what factors determine the oncogenic properties of *Ras* genes? One possibility would be to understand the role of different DNA damage etiological agents and relate them to the mutational hot spots of *Ras* genes.

It is a well-known fact that UV radiation is one of the major cause of skin cancer [11]. Animal model studies [12,13] have shown that UV irradiation can introduce point mutations in the *Ras* proto-oncogenes. This point mutation leads to the production of *Ras* protein with diminished or no

GTPase activity. Loss of GTPase activity shifts the equilibrium between active GTP bound *Ras* protein and inactive GDP bound *Ras* protein to produce more active GTP. This active GTP bound *Ras* protein can now stimulate a diverse spectrum of downstream processes causing unregulated signal transduction and facilitating the development of skin cancer [8,14,15]. The major photoproducts induced in DNA by UV light are the cyclobutane-pyrimidine photodimers (CPDs) and (6-4) pyrimidine-pyrimidinone photoproducts [13,16]. *In vitro* UV irradiation experimental studies have already shown that UV light formed a point mutation at codons 12 and 61 [8] in N-*Ras*. Another site-directed mutagenesis experiment performed by introducing CPDs at predetermined sites showed that the photodimer could induce a point mutation at the modified positions [17]. However, it is equally important to study if the *Ras* genes are activated by the production of CPD in the gene. Recent *in vitro* experiments have shown that proto-oncogene expression in human epidermis increases as a result of UV radiation, leading to a high rate of cell proliferation and differentiation [14,18].

Much evidence now argues that certain anticancer drugs which are used for the treatment of cancer could also lead to DNA damage [19,20]. The most popularly used anticancer drug *cis*-platin exhibited differential inhibition of the p53 tumour suppression gene [21] and increased the rate of apoptosis in K-*Ras*-null murine embryonic stem cells [22]. The mechanism of action by which *cis*-platin and its analogue drugs damages the DNA are by forming intrastrand crosslinking between adjacent guanine bases or adjacent adenine and guanine bases [2,23,24]. It is clear from this mechanism that these anticancer drugs may also cause damage to normal cells along with cancerous cells. Because of this limitation, synthetic chemists are now studying other metallic complexes such as ruthenium (Ru) complexes [25,26]. Ru *cis*-platin is an analogue of *cis*-platin and unlike *cis*-platin, damages DNA when activated with light [27]. Thus, it is used to selectively

target cancerous cells.

Current molecular cancer research has been focused on determining the key steps by which cellular genes become oncogenes, not on the underlying and fundamental chemical damage mechanisms and susceptibility. In this chapter, we investigate the mutational hot spots of chemical damage present in *Ras* genes upon exposure to Ru *cis*-platin and UV damage agents. Detection of damage is accomplished by a simple, sensitive, mix-and-read assay using an EvaGreen (EG) probe in a 96-well microplate. Earlier studies have already proven that, of all the three *Ras* genes (K-, N- and H-*Ras*), K-*Ras* is the most susceptible to mutation and H-*Ras* the least [3,15,28,29]. Thus, in this chapter, we chose to investigate the effect of two etiological agents, UVC radiation and Ru *cis*-platin on the K-*Ras* and N-*Ras* genes.

5.2 Experimental Section

The oligonucleotide targets were obtained from Integrated DNA Technologies Inc. (Coralville, IA, USA) and *cis*-$[Ru(bpy)_2(CH_3CN)_2]Cl_2$ was kindly supplied by Professor Claudia Turro (Ohio State University, Department of Chemistry). The hydrochloric acid was obtained from Anachemia (Montreal, QC, Canada), sodium chloride was obtained from ACP Chemical Inc. (Montreal, Quebec), Tris was obtained from ICN biomedicals (Aurora, OH, USA) and ethylenediaminetetraacetic acid (EDTA) was obtained from BDH Inc. (Toronto, ON, Canada). The complete sequence of K-*Ras* and N-*Ras* genes are listed in Table 5.1 and 5.2, respectively. Based on the number of Gs, Ts and % homology, we have selected a few regions of both the K-*Ras* and N-*Ras* genes for this study. These regions are further subdivided into 12 sequences, with each sequence having a length of 21 nucleobases. The DNA sequences for K-*Ras* and N- *Ras* genes used in this study are listed in Table 5.3. Oligonucleotides were dissolved in nanopure water from a Barnsted Nanopure (Boston, MA, USA) water system. All samples were kept frozen at -20 ^{o}C

Table 5.1 K-*Ras* gene sequence[a].

```
  1   2   3   4   5   6   7   8   9  10  11  12  13  14  15  16  17  18  19  20  21  22  23
ATG ACT GAA TAT AAA CTT GTG GTA GTT GGA GCT GGT GGC GTA GGC AAG AGT GCC TTG ACG ATA CAG CTA
                  10                  20                  30                  40                  50                  60

 24  25  26  27  28  29  30  31  32  33  34  35  36  37  38  39  40  41  42  43  44  45  46
ATT CAG AAT CAT TTT GTG GAC GAA TAT GAT CCA ACA ATA GAG GAT TCC TAC AGG AAG CAA GTA GTA ATT
70                  80                  90                 100                 110                 120                 130

 47  48  49  50  51  52  53  54  55  56  57  58  59  60  61  62  63  64  65  66  67  68  69
GAT GGA GAA ACC TGT CTC TTG GAT ATT CTC GAC ACA GCA GGT CAA GAG GAG TAC AGT GCA ATG AGG GAC
140                 150                 160                 170                 180                 190                 200

 70  71  72  73  74  75  76  77  78  79  80  81  82  83  84  85  86  87  88  89  90  91  92  93
CAG TAC ATG AGG ACT GGG GAG GGC TTT CTT TGT GTA TTT GCC ATA AAT AAT ACT AAA TCA TTT GAA GAT ATT
210                 220                 230                 240                 250                 260                 270

 94  95  96  97  98  99 100 101 102 103 104 105 106 107 108 109 110 111 112 113 114 115 116
CAC CAT TAT AGA GAA CAA ATT AAA AGA GTT AAG GAC TCT GAA GAT GTA CCT ATG GTC CTA GTA GGA AAT
280                 290                 300                 310                 320                 330                 340

117 118 119 120 121 122 123 124 125 126 127 128 129 130 131 132 133 134 135 136 137 138 139
AAA TGT GAT TTG CCT TCT AGA ACA GTA GAC ACA AAA CAG GCT CAG GAC TTA GCA AGA AGT TAT GGA ATT
350                 360                 370                 380                 390                 400                 410

140 141 142 143 144 145 146 147 148 149 150 151 152 153 154 155 156 157 158 159 160 161 162
CCT TTT ATT GAA ACA TCA GCA AAG ACA AGA CAG GGT GTT GAT GAT GCC TTC TAT ACA TTA GTT CGA GAA
420                 430                 440                 450                 460                 470                 480

163 164 165 166 167 168 169 170 171 172 173 174 175 176 177 178 179 180 181 182 183 184 185
ATT CGA AAA CAT AAA GAA AAG ATG AGC AAA GAT GGT AAA AAG AAG AAA AAG AAG TCA AAG ACA AAG TGT
490                 500                 510                 520                 530                 540                 550

186 187 188 189
GTA ATT ATG TAA
560         567
```

[a]The shaded regions are the portion of the gene used in this chapter. The codon number and nucleobase number are represented above and below the sequence line, respectively.

Table 5.2 N-*Ras* gene sequence[a].

```
 1   2   3   4   5   6   7   8   9  10  11  12  13  14  15  16  17  18  19  20  21  22  23
ATG ACT GAG TAC AAA CTG GTG GTG GTT GGA GCA GGT GGT GTT GGG AAA AGC GCA CTG ACA ATC CAG CTA
                10                  20                  30                  40                  50                  60

24  25  26  27  28  29  30  31  32  33  34  35  36  37  38  39  40  41  42  43  44  45  46  47
ATC CAG AAC CAC TTT GTA GAT GAA TAT GAT CCC ACC ATA GAG GAT TCT TAC AGA AAA CAA GTG GTT ATA GAT
70                  80                  90                  100                 110                 120                 130                 140

48  49  50  51  52  53  54  55  56  57  58  59  60  61  62  63  64  65  66  67  68  69  70  71
GGT GAA ACC TGT TTG TTG GAC ATA CTG GAT ACA GCT GGA CAA GAA GAG TAC AGT GCC ATG AGA GAC CAA TAC
            150                 160                 170                 180                 190                 200                 210

72  73  74  75  76  77  78  79  80  81  82  83  84  85  86  87  88  89  90  91  92  93  94  95
ATG AGG ACA GGC GAA GGC TTC CTC TGT GTA TTT GCC ATC AAT AAT AGC AAG TCA TTT GCG GAT ATT AAC CTC
        220                 230                 240                 250                 260                 270                 280

96  97  98  99 100 101 102 103 104 105 106 107 108 109 110 111 112 113 114 115 116 117 118 119
TAC AGG GAG CAG ATT AAG CGA GTA AAA GAC TCG GAT GAT GTA CCT ATG GTG CTA GTG GGA AAC AAG TGT GAT
    290                 300                 310                 320                 330                 340                 350

120 121 122 123 124 125 126 127 128 129 130 131 132 133 134 135 136 137 138 139 140 141 142 143
TTG CCA ACA AGG ACA GTT GAT ACA AAA CAA GCC CAC GAA CTG GCC AAG AGT TAC GGG ATT CCA TTC ATT GAA
360                 370                 380                 390                 400                 410                 420

144 145 146 147 148 149 150 151 152 153 154 155 156 157 158 159 160 161 162 163 164 165 166 167
ACC TCA GCC AAG ACC AGA CAG GGT GTT GAA GAT GCT TTT TAC ACA CTG GTA AGA GAA ATA CGC CAG TAC CGA
430                 440                 450                 460                 470                 480                 490                 500

168 169 170 171 172 173 174 175 176 177 178 179 180 181 182 183 184 185 186 187 188 189 190
ATG AAA AAA CTC AAC AGC AGT GAT GAT GGG ACT CAG GGT TGT ATG GGA TTG CCA TGT GTG GTG ATG TAA
        510                 520                 530                 540                 550                 560                 570
```

[a]The shaded regions are the portion of the gene used in this chapter. The codon number and nucleobase number are represented above and below the sequence line, respectively

Table 5.3 K-*Ras* and N-*Ras* sequences used in this study.

Sequence Name	K-*Ras* sequence	N-*Ras* sequence	% Homology
$S_{7\text{-}13}$	5'-GTG GTA GTT GGA GCT GGT GGC-3' 19 39	5'-GTG GTG GTT GGA GCA GGT GGT-3' 19 39	86
$S_{31\text{-}37}$	5'-GAA TAT GAT CCA ACA ATA GAG-3' 91 111	5'-GAA TAT GAT CCC ACC ATA GAG-3' 91 111	90
$S_{37\text{-}43}$	5'-GAG GAT TCC TAC AGG AAG CAA-3' 109 129	5'-GAG GAT TCT TAC AGA AAA CAA-3' 109 129	90
$S_{55\text{-}61}$	5'-ATT CTC GAC ACA GCA GGT CAA-3' 163 183	5'-ATA CTG GAT ACA GCT GGA CAA-3' 163 183	76
$S_{61\text{-}67}$	5'-CAA GAG GAG TAC AGT GCA ATG-3 181 201	5'-CAA GAA GAG TAC AGT GCC ATG-3' 181 201	90
$S_{67\text{-}73}$	5'-ATG AGG GAC CAG TAC ATG AGG-3 199 219	5'-ATG AGA GAC CAA TAC ATG AGG-3 199 219	90
$S_{73\text{-}79}$	5'-AGG ACT GGG GAG GGC TTT CTT-3 217 237	5'-AGG ACA GGC GAA GGC TTC CTC-3' 217 237	76
$S_{85\text{-}91}$	5'-AAT AAT ACT AAA TCA TTT GAA-3' 253 273	5'-AAT AAT AGC AAG TCA TTT GCG-3 253 273	76
$S_{97\text{-}103}$	5'-AGA GAA CAA ATT AAA AGA GTT-3' 289 309	5'-AGG GAG CAG ATT AAG CGA GTA-3' 289 309	71
$S_{109\text{-}115}$	5'-GTA CCT ATG GTC CTA GTA GGA-3' 325 345	5'-GTA CCT ATG GTG CTA GTG GGA-3' 325 345	90
$S_{139\text{-}145}$	5'-ATT CCT TTT ATT GAA ACA TCA-3' 415 435	5'-ATT CCA TTC ATT GAA ACC TCA-3' 415 435	86
$S_{145\text{-}151}$	5'-TCA GCA AAG ACA AGA CAG GGT-3 433 453	5'-TCA GCC AAG ACC AGA CAG GGT-3' 433 453	90

Oligonucleotide sequences were designed from the selected regions of K-*Ras* and N-*Ras* genes. The numbers in the subscript of column 1 denote the start and end codon numbers. The subscript numbers in column 2 and 3 denote the start and end nucloebase numbers. All the sequences listed above were annealed with their complementary sequences to form their respective dsDNA sequence.

until needed. Upon thawing, the oligonucleotides are diluted to the required concentration in Tris buffer (10 mM Tris, 1 mM EDTA, 10 mM NaCl, pH ~7.4).

5.2.1 DNA damage induced by *cis*-[Ru(bpy)$_2$(CH$_3$CN)$_2$]Cl$_2$. 25 μM aqueous *cis*-[Ru(bpy)$_2$(CH$_3$CN)$_2$]Cl$_2$ was irradiated in a UV-transparent 1 cm path length cuvette for 10 min in a Luzchem (Ottawa, Ontario) DEV photoreactor chamber with UVA lamps emitting in the wavelength range of 320-400 nm. Absorbance spectra were taken on a Hewlett-Packard 8452A diode array spectrophotometer (Sunnyvale, CA) before and after irradiation. The formation of the peak at 490 nm confirms the photolysis of the Ru complex into the *cis*-[Ru(bpy)$_2$(H$_2$O)]$_2$Cl$_2$ active form (Figure 3.2).

For DNA damage experiments, dsDNA solutions of all the target (Table 5.3) oligonucleotides and the activated Ru complex in a fixed concentration ratio of 1:6 were constantly stirred on a magnetic stirrer. Aliquots from each solution were pipetted out after reaction times of 0 and 72 hr. These samples were further diluted with Tris buffer to give a final concentration of 1 μM dsDNA in each well of the 96-well microplate (Corning Special Optics, NY, USA) along with 1.33 μM EG dye.

5.2.2 DNA damage induced by UV radiation. For DNA damage experiments, 147 μL of 1.36 μM nitrogen-purged dsDNA samples of all target sequences mentioned in Table 5.3 were placed in a 96-well plate. UV light from UVC lamps emitting at 254 nm was chosen for the irradiation. The UVC light was turned on for 20 min prior to the experiment to ensure a stabilized light source. The photoreactor was purged continuously with nitrogen to remove oxygen and minimize ozone generation from the lamp. Finally, the 96-well microplate was placed inside the Luzchem (Ottawa, ON, Canada) DEV photoreactor. Each well of the 96-well microplate was exposed to UVC light continuously for 2 hr. Control samples were handled under identical condition, but were not

exposed to UVC light and kept in the dark. After irradiation, the 96-well microplates were removed from the photoreactor and EG dye was added to each well. The final concentrations of the dsDNA and EG dye were made to a fixed ratio of 1:1.33.

5.2.3 Fluorescence measurements. Room-temperature fluorescence intensities for dsDNA solutions from both the activated Ru complex and UVC-induced damage were measured using a Safire fluorescence plate reader (Tecan, Mannendorf, Switzerland) after the addition of EG dye followed by incubation at 37 ^{o}C for 20 min in the dark. Fluorescence emission spectra were recorded using an excitation wavelength of 490 nm and an emission wavelength of 530 nm. Here, it is worth mentioning that the fluorescence spectra of the Ru complex alone or the dsDNA alone gave a minimum or zero background at the 530 nm emission wavelength (Figure A6).

5.3 Results and Discussion

5.3.1 K-*Ras* and N-*Ras* damage by activated *cis*-[Ru(bpy)$_2$(CH$_3$CN)$_2$]Cl$_2$. To examine whether the Ru complex induces damage in the K-*Ras* and N-*Ras* genes, we treated the different sequences of *Ras* gene with the activated form of the Ru complex (*cis*-[Ru(bpy)$_2$(H$_2$O)$_2$]Cl$_2$) and detected the resulting damage. Tables 5.4 and 5.5 show the damage for the twelve different dsDNA sequences of the K-*Ras* and N-*Ras* proto-oncogenes. All the sequences show damage from the Ru complex confirming that the activated form of this anticancer drug is efficient in damaging both *Ras* genes.

To understand the relationship between damage and the number and type of different nucleobase pairs present, we first plotted correlation diagrams for all possible nucleobases and nucleobase pairs. Figure 5.1 and 5.2 shows the most significant correlation diagrams with a positive and negative slopes for the different nucleobases for both K-*Ras* and N-*Ras* genes. All other correlation diagrams with a lower R^2 value for both K-*Ras* and N-*Ras*

Table 5.4 Damage susceptibility of K-*Ras* sequences damaged by activated Ru complex.

Seq. No.	K-Ras	Damage Susceptibility	G	GG	GA
$S_{7\text{-}13}$	GTG GTA GTT GGA GCT GGT GGC	0.61±0.02	13	4	3
$S_{73\text{-}79}$	CAC CAT CAA CCT CGA CCA CCG AGG ACT GGG GAG GGC TTT CTT	0.57±0.02	12	6	6
$S_{67\text{-}73}$	TCC TGA CCC CTC CCG AAA GAA ATG AGG GAC CAG TAC ATG AGG	0.59±0.02	11	4	4
$S_{145\text{-}151}$	TAC TCC CTG GTC ATG TAC TCC TCA GCA AAG ACA AGA CAG GGT	0.85 ±0.00	10	2	5
$S_{109\text{-}115}$	AGT CGT TTC TGT TCT GTC CCA GTA CCT ATG GTC CTA GTA GGA	0.73±0.01	10	4	6
$S_{61\text{-}67}$	CAT GGA TAC CAG GAT CAT CCT CAA GAG GAG TAC AGT GCA ATG	0.73±0.01	10	1	4
$S_{37\text{-}43}$	GTT CTC CTC ATG TCA CGT TAC GAG GAT TCC TAC AGG AAG CAA	0.49±0.02	10	3	7
$S_{55\text{-}61}$	CTC CTA AGG ATG TCC TTC GTT ATT CTC GAC ACA GCA GGT CAA	0.45±0.02	10	1	2
$S_{31\text{-}37}$	TAA GAG CTG TGT CGT CCA GTT GAA TAT GAT CCA ACA ATA GAG	0.35±0.02	7	1	5
$S_{139\text{-}145}$	CTT ATA CTA GGT TGT TAT CTC ATT CCT TTT ATT GAA ACA TCA	0.48±0.02	5	1	4
$S_{97\text{-}103}$	TAA GGA AAA TAA CTT TGT AGT AGA GAA CAA ATT AAA AGA GTT	0.20±0.02	5	0	4
$S_{85\text{-}91}$	TCT CTT GTT TAA TTT TCT CAA AAT AAT ACT AAA TCA TTT GAA TTA TTA TGA TTT AGT AAA CTT	0.03±0.02	3	0	3

This table is ordered by the number of Gs in the K-*Ras* sequences. Column 2 represents the dsDNA sequence for each of the K-*Ras* gene used in this study. Column 3 denotes the damage susceptibility (1-F), where $F = F_i/F_c$, F_i is the fluorescence intensity of EG-dsDNA upon damage and F_c is the fluorescence intensity of the control sample. Columns 4, 5 and 6 denotes the number of Gs, (-GG-) and (-GA-) nucleobases or nucleobase pairs, respectively.

Table 5.5 Damage susceptibility of N-*Ras* sequences damaged by activated Ru complex.

Seq. No.	N-Ras	Damage Susceptibility	G	GG	GA
$S_{73\text{-}79}$	AGG ACA GGC GAA GGC TTC CTC	0.50±0.02	13	4	8
$S_{7\text{-}13}$	TCC TGT CCG CTT CCG AAG GAG GTG GTG GTT GGA GCA GGT GGT	0.47±0.03	13	5	2
$S_{145\text{-}151}$	CAC CAC CAA CCT CGT CCA CCA TCA GCC AAG ACC AGA C*A*G GGT	0.74±0.02	12	4	5
$S_{109\text{-}115}$	AGT CGG TTC TGG TCT GTC CCA GTA CCT ATG GTG CTA GTG GGA	0.54±0.02	11	4	4
$S_{61\text{-}67}$	CAT GGA TAC CAC GAT CAC CCT CAA GAA GAG TAC AGT GCC ATG	0.78±0.01	10	1	4
$S_{97\text{-}103}$	GTT CTT CTC ATG TCA CGG TAC AGG GAG CAG ATT AAG CGA GTA	0.31±0.01	10	2	5
$S_{67\text{-}73}$	TCC CTC GTC TAA TTC GCT CAT ATG AGA GAC CAA TAC ATG AGG	0.59±0.03	9	2	4
$S_{55\text{-}61}$	TAC TCT CTG GTT ATG TAC TCC ATA CTG GAT ACA GCT GGA CAA	0.49±0.02	9	2	5
$S_{31\text{-}37}$	TAT GAC CTA TGT CGA CCT GTT GAA TAT GAT CCC ACC ATA GAG	0.28±0.01	9	3	5
$S_{37\text{-}43}$	CTT ATA CTA GGG TGG TAT CTC GAG GAT TCT TAC AGA AAA CAA	0.43±0.01	7	1	4
$S_{139\text{-}145}$	CTC CTA AGA ATG TCT TTT GTT ATT CCA TTC ATT GAA ACC TCA	0.42±0.01	7	2	4
$S_{85\text{-}91}$	TAA GGT AAG TAA CTT TGG AGT AAT AAT AGC AAG TCA TTT GCG TTA TTA TCG TTC AGT AAA CGC	0.15±0.03	7	0	3

This table is ordered by the number of Gs in the N-*Ras* sequences. Column 2 represents the dsDNA sequence for each of the N-*Ras* gene used in this study. Column 3 denotes the damage susceptibility (1-F), where $F = F_i/F_c$, F_i is the fluorescence intensity of EG-dsDNA and F_c is the fluorescence intensity of the control sample. Columns 4, 5 and 6 denotes the number of Gs, (-GG-) and (-GA-) nucleobases or nucleobase pairs, respectively.

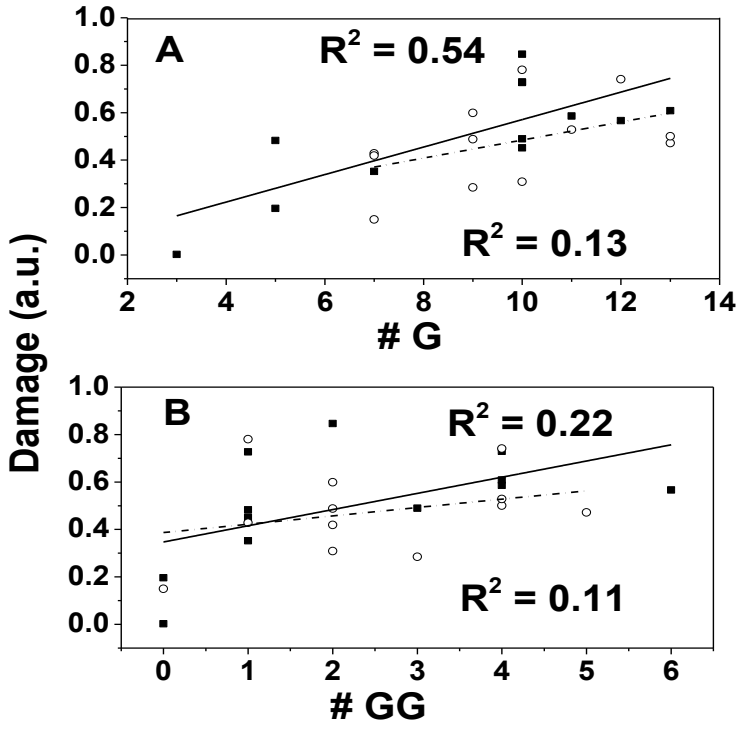

Figure 5.1 Ru complex damage susceptibility (1-F) as a function of number of G and GG sites. The damage susceptibility on the y-axis is 1-F, where $F = F_i/F_c$, F_i is the fluorescence intensity of EG-dsDNA upon Ru damage and F_c is the fluorescence intensity of the control sample. EG dye fluorescence intensities at 530 nm are measured in the presence of 1 μM dsDNA (10 mM Tris, 1 mM EDTA, 10 mM NaCl, pH 7.4) For all the plots, the filled squares represent the damage of K-*Ras* sequences and the open circles represent the damage of N-*Ras* sequences. The solid lines through the filled square points are linear fits for the K-*Ras* sequences with their respective R^2 values indicated in the upper portion of each plot. The dashed lines through the open circle points are linear fits for the N-*Ras* sequences with their R^2 value indicated in the lower portion of each plot. Here $R^2$is the linear regression coefficient and R^2 =1 represents a perfect line.

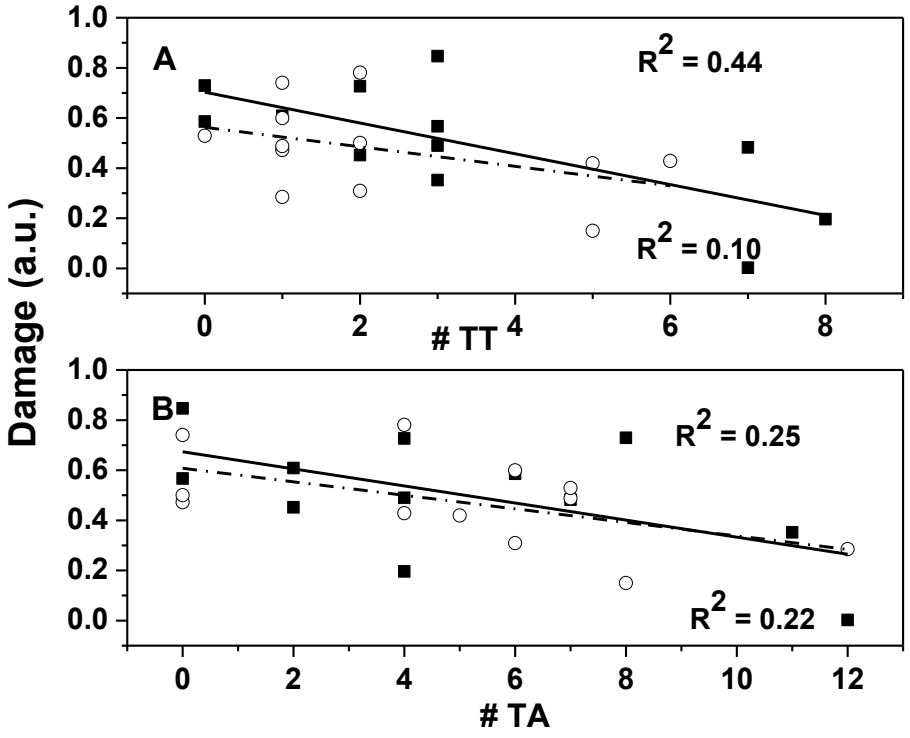

Figure 5.2 Ru complex damage susceptibility (1-F) as a function of number of TT and TA sites. The damage susceptibility on the y-axis is 1-F, where $F = F_i/F_c$, F_i is the fluorescence intensity of EG-dsDNA upon Ru damage and F_c is the fluorescence intensity of the control sample. EG dye fluorescence intensities at 530 nm are measured in the presence of 1 μM dsDNA (10 mM Tris, 1 mM EDTA, 10 mM NaCl, pH 7.4) For all the plots, the filled squares represent the damage of K-*Ras* sequences and the open circles represent the damage of N-*Ras* sequences. The solid lines through the filled square points are linear fits for the K-*Ras* sequences with their respective R^2 values indicated in the upper portion of each plot. The dashed lines through the empty circle points are linear fits for the N-*Ras* sequences with their R^2 value indicated in the lower portion of each plot.

sequences are given in Figure A 9. The R^2 values in Figure 5.1 illustrates a moderately good correlation of Ru damage with increasing number of Gs for both K-*Ras* and N-*Ras* sequences. However, the correlation is better for the K-*Ras* sequences than the N-*Ras* sequences. It is worth mentioning that we also obtained moderately significant R^2 values for TT and TA nucleobase pairs, but with negative slopes (Figure 5.2). This clearly states that the Ru complex damage susceptibility decreases with increasing number of TT and TA sites for both K-*Ras* and N-*Ras* sequences.

Examining the K-*Ras* sequences in more detail, the sequences $S_{7\text{-}13}$, $S_{73\text{-}79}$, $S_{67\text{-}73}$, $S_{145\text{-}151}$, $S_{109\text{-}115}$ and $S_{61\text{-}67}$ with 10-13 Gs give a high damage susceptibility greater than or equal to 60 % whereas sequences $S_{31\text{-}37}$, $S_{139\text{-}145}$, $S_{97\text{-}103}$ and $S_{85\text{-}91}$ with 3-7 Gs give a low damage susceptibility less than or equal to 50 %. Surprising results were obtained for sequences $S_{37\text{-}43}$ and $S_{55\text{-}61}$ with 10 Gs, which show a damage less than or equal to 50 %. These results indicate that the number of Gs present in the sequence plays a major role in determining Ru complex damage susceptibility, but other factors may be at play. We actually thought that the Ru damage occurs due to the mono- and diadduct formation (Chapter 3). Thus, GC, GT and GA sites with a smaller correlation coefficient (Figure A8), also have a minor effect on the damage susceptibility of the activated Ru complex. However, Figure 5.2 describes that TT and TA sites show some protection and this effect tends to be dominant in the above mentioned sequences. Thus the damage we see is the net effect of all the different nucleobases and nucleobase pairs present. As a result we see a weak correlation of different nucleobases and nucleobase pairs with their damage susceptibility.

In our previous work, described in Chapter 3.3, we investigated the preferential binding sites of the *cis*-$[Ru(bpy)_2(CH_3CN)_2]^{2+}$ complex with synthetic ssDNA. Our results show that there is a strong correlation between diadduct formation and the number of GG and GA sites,

although we observed that the activated Ru complex prefers to bind to GG sites more than GA sites. Also, there is a possibility of monoadduct formation to Gs, the rate of which is affected by the identity of neighbouring nucleobases. Previous results described in Chapter 3 showed that neighbouring thymine greatly increases the monoadduct formation of G when compared to neighbouring cytosine and adenine. Results in this study also show a similar trend. Sequences $S_{145\text{-}151}$, and $S_{61\text{-}67}$ with 10 Gs and the highest damage susceptibility had neighbouring thymines at most of the G sites. However, sequence $S_{37\text{-}43}$ with 10 Gs shows a lower value of damage susceptibility. Here most of the Gs have neighbouring cytosines or adenines.

Activated Ru complex-induced dsDNA damage experiments were also performed on the N-*Ras* sequences. Our data (Figure 5.1) suggest that for N-*Ras* sequences, there is not a simple relationship between damage susceptibility and the number of Gs. Rather, the correlation plot (Figure 5.1) shows that the presence of Gs is not the primary factor determining the rate of activated Ru complex-induced dsDNA damage. Other factors include position, number and the type of damage site present. Therefore, isolating one factor and correlating the damage to it leads to lower R^2 values.

On analyzing the results obtained for both K-*Ras* and N-*Ras* sequences, we found that another factor determining the damage susceptibility of activated Ru complex-induced dsDNA damage is the identity of the nucleobases neighbouring to the GG sites. Our results show a higher rate of GG-Ru diadduct formation in the presence of adenines next to the GG sites, but a lower GG-Ru diadduct formation in the presence of neighbouring thymines. Sequences $S_{61\text{-}67}$, $S_{139\text{-}145}$ of K-*Ras* and $S_{37\text{-}43}$ of N-*Ras* have adenines next to GG sites. These sequences with only one GG sites give a higher damage susceptibility than other sequences with same number of Gs but higher number

of GG sites. Similarly $S_{7\text{-}13}$ for K-*Ras* and $S_{109\text{-}115}$ and $S_{7\text{-}13}$ for N-*Ras* with 4-5 GG sites shows a lower damage susceptibility than other sequences with a low number of GG sites. All these latter sequences were found to have thymines adjacent to the GG sites. Thus, thymines which seemed to increase G-Ru monoadduct formation (as described in Chapter 3), surprisingly found to decreases GG-Ru diadduct formation. It is important to note here that, to best of our knowledge, no such sequence dependent study of activated Ru complex-induced dsDNA damage has been done previously. Thus, a further, more detailed study to understand the neighbouring nucleobase effect on the rate of GG-Ru diadduct formation is required to explain these results.

5.3.2 K-*Ras* and N-*Ras* damage by UVC radiation. Both K-*Ras* and N-*Ras* genes were examined to study the effect of UVC radiation. Similar to activated Ru complex-induced dsDNA damage, all sequences for both *Ras* genes exhibit damage in response to UVC radiation. The results of UVC-induced damage are listed in Table 5.6 for K-*Ras* and Table 5.7 for N-*Ras*, respectively.

Similar to the activated Ru complex-induced dsDNA damage study, we plotted the correlation diagram for all possible dinucleotide sites to understand the relationship between UVC damage and the number of different nucleobases and nucleobases pairs. Only the most significant correlation diagrams for the different nucleobases and nucleobases pairs for both K-*Ras* and N-*Ras* sequences are shown in Figure 5.3 while all other correlation diagrams are given in Figure A 10.

From the correlation diagrams it can be clearly seen that the damage shows a linear correlation with increasing numbers of TT sites. Again, similar to the activated Ru complex-induced dsDNA damage study, UVC-induced dsDNA damage also gave a better R^2 value for the K-*Ras* sequences than the N-*Ras* sequences. The results in Tables 5.6 and Figure 5.3 show a decrease in damage susceptibilities with decreasing number of TT sites in K-*Ras* sequences. Sequences $S_{73\text{-}79}$, $S_{37\text{-}43}$,

Table 5.6 UVC-induced DNA damage susceptibility of K-*Ras* sequences.

Seq. No.	K-*Ras*	Damage Susceptibility	TT	CC	CT
$S_{97\text{-}103}$	AGA GAA CAA ATT AAA AGA GTT	0.88±0.02	8	0	4
$S_{139\text{-}145}$	TCT CTT GTT TAA TTT TCT CAA ATT CCT TTT ATT GAA ACA TCA	0.81±0.01	7	1	7
$S_{85\text{-}91}$	TAA GGA AAA TAA CTT TGT AGT AAT AAT ACT AAA TCA TTT GAA	0.78±0.02	7	0	12
$S_{73\text{-}79}$	TTA TTA TGA TTT AGT AAA CTT AGG ACT GGG GAG GGC TTT CTT	0.53±0.01	3	6	0
$S_{37\text{-}43}$	TCC TGA CCC CTC CCG AAA GAA GAG GAT TCC TAC AGG AAG CAA	0.41±0.01	3	3	4
$S_{145\text{-}151}$	CTC CTA AGG ATG TCC TTC GTT TCA GCA AAG ACA AGA CAG GGT	0.29 ±0.04	3	2	0
$S_{31\text{-}37}$	AGT CGT TTC TGT TCT GTC CCA GAA TAT GAT CCA ACA ATA GAG	0.26±0.01	3	1	11
$S_{61\text{-}67}$	CTT ATA CTA GGT TGT TAT CTC CAA GAG GAG TAC AGT GCA ATG	0.22±0.01	2	1	4
$S_{55\text{-}61}$	GTT CTC CTC ATG TCA CGT TAC ATT CTC GAC ACA GCA GGT CAA	0.20±0.01	2	1	2
$S_{7\text{-}13}$	TAA GAG CTG TGT CGT CCA GTT GTG GTA GTT GGA GCT GGT GGC	0.21±0.03	1	4	2
$S_{67\text{-}73}$	CAC CAT CAA CCT CGA CCA CCG ATG AGG GAC CAG TAC ATG AGG	0.25±0.01	0	4	6
$S_{109\text{-}115}$	TAC TCC CTG GTC ATG TAC TCC GTA CCT ATG GTC CTA GTA GGA CAT GGA TAC CAG GAT CAT CCT	0.12±0.03	0	4	8

This table is ordered by the number of TT's in the K-*Ras* sequences. Column 2 represent the dsDNA sequence for each of the K-*Ras* gene used in this study. Column 3 denote the damage susceptibility (1-F), where $F = F_i/F_c$, F_i is the fluorescence intensity of EG-dsDNA upon damage and F_c is the fluorescence intensity of the control sample. Columns 4, 5 and 6 denotes the number of (-TT-), (-CC-) and (-CT-) nucleobase pairs, respectively.

Table 5.7 UVC-induced DNA damage susceptibility of N-*Ras* sequences.

Seq. No.	N-Ras	Damage Susceptibility	TT	CC	CT
$S_{37\text{-}43}$	GAG GAT TCT TAC AGA AAA CAA	0.66±0.02	6	1	7
$S_{139\text{-}145}$	CTC CTA AGA ATG TCT TTT GTT ATT CCA TTC ATT GAA ACC TCA	0.75±0.01	5	2	5
$S_{85\text{-}91}$	TAA GGT AAG TAA CTT TGG AGT AAT AAT AGC AAG TCA TTT GCG	0.44±0.06	5	0	3
$S_{97\text{-}103}$	TTA TTA TCG TTC AGT AAA CGC AGG GAG CAG ATT AAG CGA GTA	0.44±0.01	2	4	8
$S_{73\text{-}79}$	TCC CTC GTC TAA TTC GCT CAT AGG ACA GGC GAA GGC TTC CTC	0.36±0.02	2	2	6
$S_{61\text{-}67}$	TCC TGT CCG CTT CCG AAG GAG CAA GAA GAG TAC AGT GCC ATG	0.16±0.03	2	1	6
$S_{31\text{-}37}$	GTT CTT CTC ATG TCA CGG TAC GAA TAT GAT CCC ACC ATA GAG	0.27±0.02	1	3	6
$S_{55\text{-}61}$	CTT ATA CTA GGG TGG TAT CTC ATA CTG GAT ACA GCT GGA CAA	0.26±0.02	1	2	7
$S_{7\text{-}13}$	TAT GAC CTA TGT CGA CCT GTT GTG GTG GTT GGA GCA GGT GGT	0.26±0.00	1	5	3
$S_{67\text{-}73}$	CAC CAC CAA CCT CGT CCA CCA ATG AGA GAC CAA TAC ATG AGG	0.49±0.02	1	2	7
$S_{145\text{-}151}$	TAC TCT CTG GTT ATG TAC TCC TCA GCC AAG ACC AGA C*A*G GGT	0.11±0.02	1	4	0
$S_{109\text{-}115}$	AGT CGG TTC TGG TCT GTC CCA GTA CCT ATG GTG CTA GTG GGA CAT GGA TAC CAC GAT CAC CCT	0.11±0.02	0	4	4

This table above is ordered by the number of TT's in the N-*Ras* sequences. Column 2 represent the dsDNA sequence for each of the N-*Ras* gene used in this study. Column 3 denote the damage susceptibility (1-F), where $F = F_i/F_c$, F_i is the fluorescence intensity of EG-dsDNA upon damage and F_c is the fluorescence intensity of the control sample. Columns 4, 5 and 6 denotes the number of (-TT-), (-CC-) and (-CT-) nucleobase pairs, respectively.

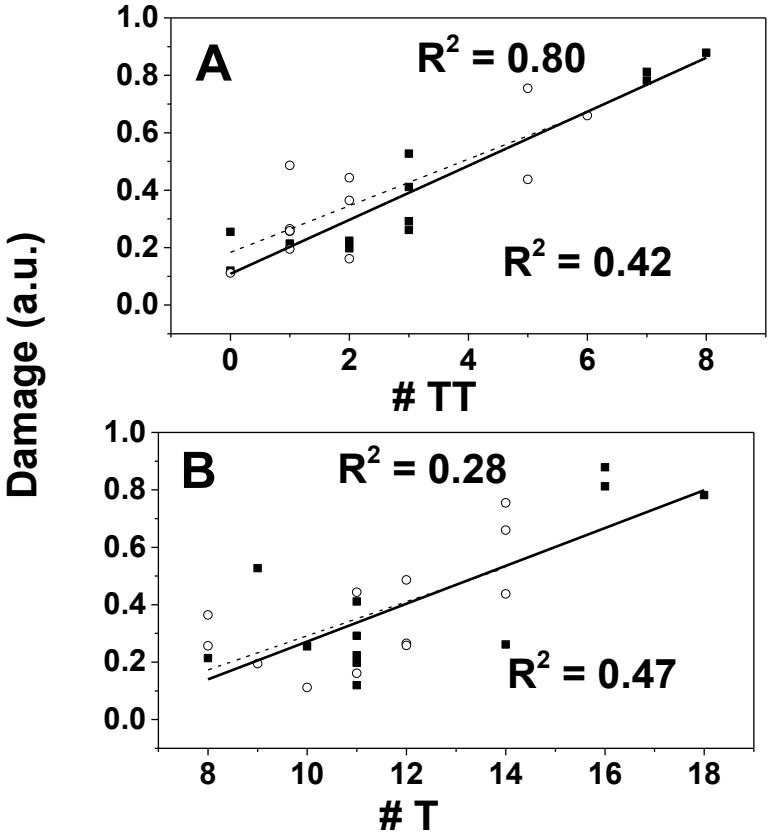

Figure 5.3 UVC damage susceptibility (1-F) as a function of number of TT and T sites. The damage susceptibility on the y-axis is 1-F, where $F = F_i/F_c$, F_i is the fluorescence intensity of EG-dsDNA upon UVC damage and F_c is the fluorescence intensity of the control sample. EG dye fluorescence intensities at 530 nm are measured in the presence of 1 μM dsDNA (10 mM Tris, 1 mM EDTA, 10 mM NaCl, pH 7.4) For all the plots, the filled squares represent the damage of K-*Ras* sequences and the open circles represent the damage of N-*Ras* sequences. The solid lines through the filled square points are linear fits for the K-*Ras* sequences with their respective R^2 values indicated in the upper portion of each plot. The dashed lines through the open circle points are linear fits for the N-*Ras* sequences with their R^2 value indicated in the lower portion of each plot.

$S_{145\text{-}151}$ and $S_{31\text{-}37}$ with 3 TT sites, have damage susceptibilities ranging between 20-50 %. On analyzing these sequences we found that the presence of a neighbouring guanine to the TT sites lowers the damage susceptibility of UVC- induced dsDNA damage. Our next approach was to investigate the effect of neighbouring nucleobases on T<>T photodimer formation. Several previous studies have shown that for UVC-induced dsDNA damage, the T<>T photodimer yield is the highest compared to any other bipyrimidine lesion [30,30-32]. Sarasin, et al. [32] and Kohler, et al. [34], in sequence-dependent studies on T<>T photodimer rates, have established that in tetrads of the type XTTY, the rate of dimer formation is higher for TTTG, TTTC, TTTA, TTTT, ATTC and ATTA, and lower for GTTA, ATTT, GTTC, GTTT and CTTC. This result shows that all the tetrads with neighbouring Gs to the TT site lower the rate of T<>T photodimer formation.

Having established that the damage of K-*Ras* sequences by UVC irradiation is probably related to TT sites, we now similarly analyze the N-*Ras* gene sequences (Table 5.7). Here, we also see a decrease in damage susceptibility with decreasing number of TT sites. However, we see a few more noteworthy exceptions than in K-*Ras*. These will be discussed in detail.

Sequences $S_{139\text{-}145}$ and $S_{85\text{-}91}$, both with 5 TT sites, gives a lower damage susceptibility for sequences $S_{85\text{-}91}$ than for sequence $S_{139\text{-}145}$. Similarly for sequences $S_{97\text{-}103}$, $S_{73\text{-}79}$ and $S_{61\text{-}67}$, which each have 2 TT sites, sequence $S_{61\text{-}67}$ gives a lower damage susceptibility than the other two sequences. Using the discussion above, we observe a larger drop in the damage susceptibility with the presence of G next to TT site for both the $S_{85\text{-}91}$ and $S_{61\text{-}67}$ sequences. This result is also consistent if we compare $S_{85\text{-}91}$ of both K-*Ras* and N-*Ras* sequences. These sequences differ only in the neighboring nucleobase at 1 TT site out of the 3 TT sites present, excluding terminal TT sites with the least effect on damage susceptibility (see Chapter 4) The neighbouring adenine in K-*Ras* sequence $S_{85\text{-}91}$ is replaced by a neighbouring guanine in the analogous N-*Ras* sequence.

This change drops the damage susceptibility by a value of 1.8. Thus, it is reasonable to say that the quenching effect of a neighbouring nucleobase plays a vital role in the T<>T photodimer formation rate [33].

These results for UVC-induced DNA damage in K-*Ras* and N-*Ras* sequences establishes an excellent agreement between damage and the effect of neighbouring guanine nucleobase on T<>T photodimer formation rate, as seen in previous studies [32, 34]. A potential discrepancy in this model of damage susceptibility is observed for sequences $S_{67\text{-}73}$ for K-*Ras* and $S_{109\text{-}115}$ for both the K-*Ras* and N-*Ras* sequences. All these sequences have no TT sites yet show damage between 10 -25 %. This could be due to the fact that UVC radiation damages other bipyrimidine sites, such as TC, CT and CC. Photodimer formation with all possible bipyrimidine sites in the presence of UVC radiation is reported to occur in the order TT>TC>CT>CC [32] Thus in the absence of the possibility of forming a T<>T photodimer, there is a probability of forming other bipyrimidine photoproducts which may be reflected in the damage susceptibility reported here. However, it is the number of TT sites that dominates the damage susceptibility when they are present.

5.3.3 Comparative study of activated Ru complex- and UVC-induced DNA damage for K-*Ras* and N-*Ras* genes. Several biological studies performed on different tumour types have confirmed K-*Ras* to be more prone to mutation then N-*Ras* genes [28]. The COSMIC (Catalog of Somatic Mutations in Cancer) dataset confirms that 22% of K-*Ras* genes are mutated in comparison to 8 % of N-*Ras* genes in all the tumours analyzed [3]. Most of the correlation plots discussed in this chapter also show K-*Ras* sequences to be more correlated to damage susceptibility than N-Ras sequences. To get a better insight into these results and relate them to the biological tumour results we compared the activated Ru complex and UVC-induced dsDNA damage susceptibility for both K-*Ras* and N-*Ras* sequences (Figure 5.4). Consistent with the biological

tumour results, our data, gives larger damage susceptibility (~85-88%) for K-*Ras* sequences than N-*Ras* (~75-78%) for both types of damages.

We analyzed the sequences $S_{7\text{-}13}$, $S_{55\text{-}61}$ and $S_{61\text{-}67}$, which consists of biologically active 12, 13 and 61 codons, respectively. These codons are composed of 1-2 guanine nucleobases, which makes them a good candidate to undergo oxidative DNA damage [34]. Our experiments which were done in anaerobic conditions, show that these sequences are more prone to activated Ru complex-induced dsDNA damage than UVC-induced damage. This is expected, since both codons 12 and 13 of K-*Ras* and N-*Ras* sequences have one GG site. On the contrary, codon 61 contains a TT site that is expected to be more susceptible to UVC-induced DNA than activated Ru complex-induced damage. However, it may be less susceptible to this type of damage, due to the presence of a neighbouring guanine (see above). In contrast, neighbouring thymines to G sites increase the possibility of monoadduct formation for activated Ru complex-induced dsDNA damage (see above and chapter 3). In order to understand the role of this mutagen on the biologically active codons of *Ras* genes in detail, further studies are required by designing sequences with and without these codons.

Another interesting result is that sequences $S_{61\text{-}67}$ and $S_{109\text{-}115}$ with a higher activated Ru complex-induced dsDNA damage susceptibility for K-*Ras* and N-*Ras* genes shows minimum damage susceptibility for UVC radiation. This result is obvious since GC and AT content is mutually exclusive in DNA. Our results show that the activated Ru complex forms adduct with Gs and UVC radiation forms a photoproduct with TTs in all the sequences. Thus considering the mutual exclusivity of GC and AT base pairs for DNA, these results are expected.

Further, we also studied the damage susceptibility for Ru and UVC-induced DNA damage as a

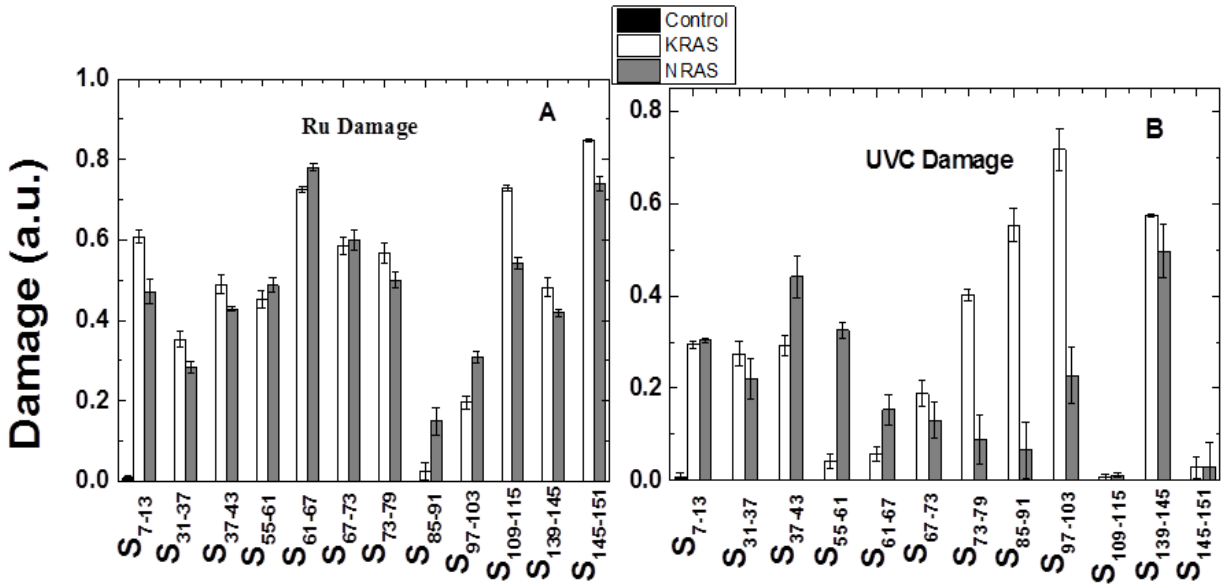

Figure 5.4 Comparison of the damage susceptibility to (A) activated Ru complex and (B) UVC radiation obtained for all the K-*Ras* and N-*Ras* sequences in Table 5.2 and 5.3, respectively. The values on the y-axis are (1-F), where $F = F_i/F_c$, F_i is the fluorescence intensity of the EG-dsDNA complex upon damage and F_c is the fluorescence intensity of the control sample. Aliquots of (A) activated Ru complex-induced dsDNA damage and (B) UVC irradiated samples were mixed with EG (10 mM Tris, 1 mM EDTA, 10 mM NaCl, pH 7.4) in a concentration ratio of 1:1.33 in 96-well plates. For both the plots, the white bars represent the damage susceptibility of the K-*Ras* sequences and the grey bars represents the damage susceptibility of the N-*Ras* sequences.

function of % homology between K-*Ras* and N-*Ras* sequences (Figure A11 and A12). From the plots, it can be seen that no strong correlation could be established between the observed damage susceptibility for both Ru and UVC damage and % homology. This result could be expected due to the seeming importance of neighbouring nucleobases at damage sites, as discussed above.

5.4 Conclusions.

The damage susceptibility of different K-*Ras* and N-*Ras* sequences upon activated Ru complex-induced and UVC-induced dsDNA damage were studied and compared. Results shows a higher extent of damage for K-*Ras* sequences than N-*Ras* sequences. This result is in excellent agreement with past studies which has shown that K-*Ras* genes are more mutated in tumours than other *Ras* genes. The results discussed in this chapter are also in agreement with previous sequence-dependence studies of UV-induced DNA damage. We've expanded on the work in those studies to measure the sequence-dependence of activated Ru complex-induced damage. It should be noted that to study the damage, we have designed a rapid mix-and-read assay using EvaGreen dye as a fluorescent probe. Although in the current study we mainly focus on a few sequences of the K-*Ras* and N-*Ras* genes, one promising future direction will be development of the method described in this work for measurement of damage in various other oncogenes with different mutagenic agents. This will help us to increase our understanding of the mutagenic character of chemical damage mechanisms.

Reference List

[1] Y. Jin, Y. Shima, M. Furu, T. Aoyama, T. Nakamata, T. Nakayama, T. Nakamura and J. Toguchida, Absence of oncogenic mutations of RAS family genes in soft tissue sarcomas of 100 Japanese patients, Anticancer Res. **30** (2010) 245-251.

[2] G.J. Peters, A.M. Bergman, V.W. Ruiz van Haperen, G. Veerman, C.M. Kuiper and B.J. Braakhuis, Interaction between cisplatin and gemcitabine in vitro and in vivo, Semin. Oncol. **22** (1995) 72-79.

[3] I.A. Prior, P.D. Lewis and C. Mattos, A comprehensive survey of Ras mutations in cancer, Cancer Res. **72** (2012) 2457-2467.

[4] B. Bailleul, K. Brown, M. Ramsden, R.J. Akhurst, F. Fee and A. Balmain, Chemical induction of oncogene mutations and growth factor activity in mouse skin carcinogenesis, Environ. Health Perspect. **81** (1989) 23-27.

[5] M.D. To, R. Rosario, P.M. Westcott, K.L. Banta and A. Balmain, Interactions between wild-type and mutant Ras genes in lung and skin carcinogenesis, Oncogene. **32** (2012) 4028-4033.

[6] A. Fernández-Medarde and E. Santos, Ras in cancer and developmental diseases, Genes & cancer. **2** (2011) 344-358.

[7] Z. Feng, W. Hu, J.X. Chen, A. Pao, H. Li, W. Rom, M.C. Hung and M.S. Tang, Preferential DNA damage and poor repair determine ras gene mutational hotspot in human cancer, J. Natl. Cancer Inst. **94** (2002) 1527-1536.

[8] W.E. Pierceall, M.L. Kripke and H.N. Ananthaswamy, N-ras mutation in ultraviolet radiation-induced murine skin cancers, Cancer Res. **52** (1992) 3946-3951.

[9] S.L. Graziano, G.P. Gamble, N.B. Newman, L.Z. Abbott, M. Rooney, S. Mookherjee, M.L. Lamb, L.J. Kohman and B.J. Poiesz, Prognostic significance of K-ras codon 12 mutations in patients with resected stage I and II non-small-cell lung cancer, J. Clin. Oncol. **17** (1999) 668-675.

[10] R.J. Slebos, R.H. Hruban, O. Dalesio, W.J. Mooi, G.J. Offerhaus and S. Rodenhuis, Relationship between K-ras oncogene activation and smoking in adenocarcinoma of the human lung, J. Natl. Cancer Inst. **83** (1991) 1024-1027.

[11] A.G. Glass and R.N. Hoover, The emerging epidemic of melanoma and squamous cell skin cancer, JAMA. **262** (1989) 2097-2100.

[12] F. Su, A. Viros, C. Milagre, K. Trunzer, G. Bollag, O. Spleiss, J.S. Reis-Filho, X. Kong, R.C. Koya and K.T. Flaherty, RAS mutations in cutaneous squamous-cell carcinomas in patients treated with BRAF inhibitors, N. Engl. J. Med. **366** (2012) 207-215.

[13] H. Kamiya, N. Murata, T. Murata, S. Iwai, A. Matsukage, C. Masutani, F. Hanaoka and E. Ohtsuka, Cyclobutane thymine dimers in a ras proto-oncogene hot spot activate the gene by point mutation, Nucleic Acids Res. **21** (1993) 2355-2361.

[14] P.K. Roddey, M. Garmyn, H. Park, J. Bhawan and B.A. Gilchrest, Ultraviolet irradiation induces c-fos but not c-Ha-ras proto-oncogene expression in human epidermis, J. Invest. Dermatol. **102** (1994) 296-299.

[15] A.T. Baines, D. Xu and C.J. Der, Inhibition of Ras for cancer treatment: the search continues, Future medicinal chemistry. **3** (2011) 1787-1808.

[16] T. Climent, I. González-Ramírez, R. González-Luque, M. Merchán, L and Serrano-Andrés, Cyclobutane Pyrimidine Photodimerization of DNA/RNA Nucleobases in the Triplet State, J. PhysChem. Lett. **1** (2010) 2072-2076.

[17] S.K. Banerjee, A. Borden, R.B. Christensen, J.E. LeClerc and C.W. Lawrence, SOS-dependent replication past a single trans-syn T-T cyclobutane dimer gives a different mutation spectrum and increased error rate compared with replication past this lesion in uninduced cells, J. Bacteriol. **172** (1990) 2105-2112.

[18] M. Brenner, S.G. Coelho, J.Z. Beer, S.A. Miller, R. Wolber, C. Smuda and V.J. Hearing, Long-lasting molecular changes in human skin after repetitive in situ UV irradiation, J. Invest. Dermatol. **129** (2008) 1002-1011.

[19] L.J. Bradley, K.J. Yarema, S.J. Lippard and J.M. Essigmann, Mutagenicity and genotoxicity of the major DNA adduct of the antitumor drug cis-diamminedichloroplatinum (II), Biochemistry **32** (1993) 982-988.

[20] V. Cepeda, M.A. Fuertes, J. Castilla, C. Alonso, C. Quevedo and J.M. Pérez, Biochemical mechanisms of cisplatin cytotoxicity, Anti-Cancer Agents in Medicinal Chemistry (Formerly Current Medicinal Chemistry-Anti-Cancer Agents). **7** (2007) 3-18.

[21] S. Fan, M.L. Smith, D.J. Rivet 2nd, D. Duba, Q. Zhan, K.W. Kohn, A.J. Fornace Jr and P.M. O'Connor, Disruption of p53 function sensitizes breast cancer MCF-7 cells to cisplatin and pentoxifylline, Cancer Res. **55** (1995) 1649-1654.

[22] D.G. Brooks, R.M. James and C.E. Patek, J. Williamson and M.J. Arends, Mutant K-ras enhances apoptosis in embryonic stem cells in combination with DNA damage and is associated with increased levels of p19(ARF), Oncogene. **20** (2001) 2144-2152.

[23] M. Baik, R.A. Friesner and S.J. Lippard, Theoretical study of cisplatin binding to purine bases: why does cisplatin prefer guanine over adenine? J. Am. Chem. Soc. **125** (2003) 14082-14092.

[24] M. Crul, R. Van Waardenburg, J. Beijnen and J. Schellens, DNA-based drug interactions of cis platin, Cancer Treat. Rev. **28** (2002) 291-303.

[25] M.J. Clarke, Ruthenium metallopharmaceuticals, Coord. Chem. Rev. 236 (2003) 209-233.

[26] F. Schmitt, P. Govindaswamy, G. Süss-Fink, W.H. Ang, P.J. Dyson, L. Juillerat-Jeanneret and B. Therrien, Ruthenium porphyrin compounds for photodynamic therapy of cancer, J. Med. Chem. **51** (2008) 1811-1816.

[27] T.N. Singh and C. Turro, Photoinitiated DNA binding by cis-$[Ru\ (bpy)_2\ (NH3)_2]_2$, Inorg. Chem. **43** (2004) 7260-7262.

[28] L. Johnson, K. Mercer, D. Greenbaum, R.T. Bronson, D. Crowley, D.A. Tuveson and T. Jacks, Somatic activation of the K-ras oncogene causes early onset lung cancer in mice, Nature. **410** (2001) 1111-1116.

[29] S. Schubbert, M. Zenker, S.L. Rowe, S. Böll, C. Klein, G. Bollag, I. van der Burgt, L. Musante, V. Kalscheuer and L. Wehner, Germline KRAS mutations cause Noonan syndrome, Nat. Genet. **38** (2006) 331-336.

[30] K.W. Zheng, Z. Chen, Y.H. Hao and Z. Tan, Molecular crowding creates an essential environment for the formation of stable G-quadruplexes in long double-stranded DNA, Nucleic Acids Res. **38** (2010) 327-338.

[31] A.M. Fleming and C.J. Burrows, G-Quadruplex Folds of the Human Telomere Sequence Alter the Site Reactivity and Reaction Pathway of Guanine Oxidation Compared to Duplex DNA, Chem. Res. Toxicol. **26** (2013) 593-607.

[32] F. Bourre, G. Renault and P.C. Seawell, A. Sarasin, Distribution of ultraviolet-induced lesions in Simian Virus 40 DNA, Biochimie. **67** (1985) 293-299.

[33] T. Douki, Low ionic strength reduces cytosine photoreactivity in UVC-irradiated isolated DNA, Photochem. Photobiol. Sci. **5** (2006) 1045-1051.

[34] Y.K. Law, R.A. Forties, X. Liu, M.G. Poirier, and B. Kohler, Sequence-dependent thymine dimer formation and photoreversal rates in double-stranded DNA, Photochem. Photobiol. Sci. **12** (2013) 1431-1439.

Chapter 6
Conclusion and Future Work

6.1 Overall Summary

The work presented in this thesis involves the development of a multiplex method for DNA damage studies coupled with various probes. The method was used to investigate damage induced by UV and chemical damaging agents on multiple sequences of single-stranded DNA (ssDNA) and double-stranded DNA (dsDNA) simultaneously. The importance of the study is that it provides significant insight into the chemical damage mechanism of both ss and dsDNA.

Hybridization assays with fluorescence probes serve as a simple and sensitive method for DNA damage studies. Previous work from our group [1,2] indicates that the amount of DNA damage present in solution can be measured by this hybridization technique using various fluorescent probes. However, a major limitation of this work was the use of the cuvette method to measure damage [3-5] in a single sample. Detection of DNA damaged by cuvette method typically requires large quantities of samples and multiple iterations of screening, which makes the assay laborious for multiple sample assay. To transcend this shortcoming we took advantage of a 96-well microplate platform to study DNA damage. This platform is ideal for performing studies on multiple DNA samples or multiple repetitions on the same sample simultaneously while using very small amounts. However, achievement of high sensitivity with precision and accuracy was one of the major challenges in extending the hybridization assay on multiple samples. In Chapter 2, we mainly focused on reproducing DNA damage experiments done by cuvette method, replacing cuvettes with 96-well microplates followed by the quantification of damage using Smart Probes (SPs). Here we designed an assay for UVC-induced DNA damage of four ssDNA target simultaneously for different exposure time on a 96-well microplate coupled with a novel

automated sample mover. Our results show that the oligonucleotide damage constants obtained with this method are reproducible and similar to those obtained in the cuvettes. The results also show that the damage kinetics upon irradiation with UVC light is sensitive to different types of photoproducts formed in the four sequences used. Thus detecting DNA damage in a 96-well microplate and quantifying the damage with SPs is a simple fast mix-and-read technique for multiplexed sequence-specific DNA damage detection.

Another pitfall of the work done in our group was the use of expensive fluorescent probes to quantitate DNA damage. These probes include MBs [3,4], SPs [5], 2APs [6] and chMBs [7], which have superior selectivity and sensitivity to detect damage, but they are limited because of their high cost and complexity in designing them for multiple samples. The work discussed in Chapter 2 couldn't overcome this limitation since it was done using SPs that were designed complementary for each sequence under study. Therefore, our next challenge was to design multiplex assays for DNA damage detection with inexpensive probes.

In Chapter 3, we focus on studying the damage of multiple samples with intercalating dyes such as EvaGreen (EG). Here we developed an assay for detecting DNA damage in multiple sequences in a 96-well microplate platform using fluorescence of EG dye. In this work, we studied the factors affecting the selectivity of EG-dsDNA to detect Ru-induced DNA damage. Results show that a low ionic strength and low target concentration improves the performance of the EG intercalating dye in detecting Ru-induced DNA damage. Our results also show that the EG probe could quantify ssDNA damage induced by the Ru complex. This result was confirmed by melting curves and matrix-assisted laser desorption/ionization time-of-flight mass spectrometry (MALDI-TOF-MS). These advantages allow 96-well microplate method coupled with fluorescence intensity of EG our method of choice for detection and quantification of DNA damage in multiple samples. Thus, in

this chapter we developed a simple, sensitive, cost-effective, mix-and-read assay for detecting ssDNA damage. Detecting damage on multiple sequences of dsDNA was important to get a better insight of their damage kinetics and relate them to the hot spots of DNA damage.

In Chapter 4, we examine UVC-induced damage in both ss- and dsDNA. Here we studied the damage with another intercalating dye, Hoechst 33258 (H258). This dye is a minor groove binder and has high selectivity towards dsDNA when compared to ssDNA. The dye gives maximum fluorescence with undamaged dsDNA and minimum fluorescence with damaged dsDNA. Thus, the higher the damage rate, the lower the fluorescence intensity will be. We used our previous experience in working with multiple samples to study the effect of mismatches on 22 different sequences simultaneously. Our results show that both the number and position of mismatches determine the stability of dsDNA. To have a better understanding of the kinetics of dsDNA damage, we further studied UVC-induced DNA damage of dsDNA and compared it to that of ssDNA. The kinetics show ssDNA to be more mutagenic towards UVC irradiation than dsDNA. This breakthrough result supports the biological studies [8,9] that show ssDNA to be more vulnerable to damage than dsDNA in the cell. Thus, our results provide a chemical basis for the difference in damage susceptibility for ss and dsDNA. We further extended our work by studying UVC-induced DNA damage of calf thymus DNA. This was to test the selectivity of our dye in detecting damage in naturally occurring sequences with ~ 2000 bp. A high precision between the damage constant obtained for two independent irradiation experiments indicate the reproducibility of the method. The results obtained provided valuable input in understanding the damage kinetics of UVC-induced damage.

To get a better insight into DNA damage and mutagenesis, it is important to study the effect of different mutagenic agents on human genomic sequences. In Chapter 5, we investigated the effect

of a Ru complex and UVC irradiation on few of the *Ras* proto-oncogene sequences. It has been well established [10] that mutations in K-*Ras* and N-*Ras* proto-oncogenes can convert them into active oncogenes. The current molecular cancer research [11,12] has been focused on determining the key steps by which cellular genes become oncogenes. Here in this work, we focus on the underlying and fundamental chemical damage mechanism and mutational hot spots of damage of K-*Ras* and N-*Ras* genes upon exposure to a Ru *cis*-platin analog and UV damaging agent. Detection of damage is accomplished by a simple, sensitive, inexpensive, mix-and-read assay using an EG probe in a 96-well microplate. Our results show that although there is a high degree of similarity among K-*Ras* and N-*Ras* genes, they show different responses to particular damaging agent. We discuss the effect of the Ru complex and UVC radiation on various codons of K-*Ras* and N-*Ras* genes, and potential reasons that may lead to a differential pattern of damage. Our results show that the rate of Ru complex damage is determined by the number of Gs and the rate of UVC damage is determined by the number of Ts present in the sequences. Further, our results found K-*Ras* sequences to be more mutagenic than N-*Ras* sequences. Thus, this chapter illustrates the application of our multiplex method and elaborates the initial steps required to develop the library of hot spots of damage.

Early detection and measurement of the amount of DNA damage helps in understanding the distribution of mutational hot spots in the human genome and may inform future treatments for cancer. This led to the focus of current research in the development of high throughput screening assays (HTS) for testing the effect of different mutagens on ss and dsDNA. Simple, rapid and highly reproducible microplate-based methods have been extensively used for drug discovery and genotoxicity testing [13]. These methods emphasize the advantage of high-throughput screening of various chemicals and drugs for their potential toxicology effects. Many *in vivo* [14] and *in vitro*

[15] HTS have been developed during recent years for screening chemical libraries against potential cancer genes in parallel. Single cell gel electrophoresis (the comet assay) is one of the current HTS method used for detecting DNA damage in multiple cells simultaneously [16]. Due to its simplicity and ease of use, this method is gaining popularity. Various simplifications and modifications has been done in past years to increase the sensitivity, versatility and high-throughput of the method [17] including the use of platform coupled with 96-well microplates to accomplish effective cell loading, increased reproducibility and ability to perform analysis on 96 samples simultaneously [18]. However, the wider acceptance of comet assay is limited due to the use of laborious, time-consuming and potentially biased image processing softwares [19] for sample analysis. The use of different software's affects the reproducibility of comet assay method from lab to lab.

The 96-well microplate method combined with fluorescence detection of DNA damage by hybridization method discussed in this thesis serves as a simple, fast, inexpensive and sensitive method for damage studies. Unlike the multiplex comet assay, this method uses neither laborious software for data analysis nor any chemical such as sodium hydroxide for DNA unwinding and denaturation processes which can induce additional DNA damage. Our method incorporates most of the elements required for HTS assays. The sample preparation is done in a 96-well microplate without any centrifugation, separation or washing steps. The fluorescence dye used in our work, proved to be quit reproducible well-to-well, pate-to-plate and day-to-day. Other major highlights of this assay are its simplicity, low volume of sample, shorter analysis time and homogenous mix-and-read mode of detection. Although, the reagent dilution for our work was manually done, the current progress in HTS assays has developed robots to specifically handle microplates. The use of robot for sampling and dilution will reduce the time and increase the reproducibility of our

assay. However, one downside of this method is that the assays are performed on isolated DNA samples. Therefore, to make our method a suitable screening assay for genotoxicity testing it is important to extend this method from isolated DNA to cellular DNA.

6.2 Future Work

As discussed in the preceding section the work presented in this thesis develops a multiplex method to detect DNA damage in synthetic ss and dsDNA samples. However, to expand our contribution to cancer research, it is important to perform these experiments at a cellular level. The success of any new technique is determined by its cost, simplicity and sensitivity. Thus, to extend our method as a diagnostic tool it is also important to develop an assay or platform that is less expensive, easily available and eco-friendly

6.2.1 *In vitro* assay for detecting DNA damage in individual cell.

Detection of DNA damage at the cellular level warrants high significance in the field of genotoxicity/environmental testing and diagnostic of genetic disorder [20]. There are many *in vitro* and *in vivo* assays for the intracellular detection of DNA damage. The commonly used assays are the bacterial Ames test [21-24], mammalian chromosome aberration test [24,25] and comet assay [20,26,27]. The Ames test and mammalian chromosome aberration test are the most commonly used method to test if a chemical is a mutagen. They are simple *in vitro* assays. However, the Ames test is limited in use since it is done on a bacterial cell which obviously differs from mammalian cells. Thus, a chemical recognized as a carcinogen by the Ames test may or may not be a potential carcinogen in higher organisms. The mammalian chromosome aberration test can give a negative result if the cells are not analyzed at an appropriate time after exposure. In order to overcome these limitations, the comet assay has been used as a powerful tool for the assessment of mutagenicity gel electrophoresis, and its advantages and disadvantages were described above.

Thus, extending our method of DNA damage detection in single cell will open ways for fast screening assays. Single cell electrophoresis assay (comet assay) has been successfully used for studying damage in individual cells [28]. Similarly, we plan to perform damage studies inside the cell by extracting the DNA and quantitating the damage by fluorescence measurements of intercalating dyes. Further estimating the amount of DNA damage after regular interval of time will help us in understanding the role of repair enzymes in determining the damage rate of DNA and the general difference between *in vitro* and *in situ* rates of DNA damage.

Also, all these methods use harsh chemicals such as sodium hydroxide and sodium dodecyl sulfate for isolation of DNA from cells [28]. This isolation step introduces many experimental artifacts which may lead to additional DNA damage and affect the sensitivity of the assay. To overcome this limitation we plan to damage the DNA inside the cell and quantitate the damage by staining the cell with cell-permeable intercalating dyes such as H258 and PicoGreen. These *in situ* studies will help to move a step further into cancer research.

6.2.2 Different diagnostic platform for DNA damage studies.

The need for simple, rapid and high-throughput screening assays has driven the development of solid-phase assays for the analysis of DNA, RNA and protein targets [29,30]. The use of a paper-based assay [31] is one such method. This method is growing interest as a low-cost and portable diagnostic tool with simple readout instrumentation for screening assays. Paper-based platforms have now been successfully used for biological assays, including cell assays. This technique overcomes the high cost of microplates and is easy to use. Recently, paper-based platforms immobilized with quantum dots (QDs) [32] were used for single nucleotide polymorphism (SNP) detection using a hybridization assay. In this study, the quantum dots were attached to the surface of paper modified with an imidazole group. Disulfide modified

oligonucleotide sequences would bind to the QDs. The SNP was detected by adding the complementary oligonucleotide sequence with Cy3 dye at one of the oligonucleotide termini. In the absence of DNA, the QDs gave a green color. However, with increasing amount of DNA, the Cy3 increasingly quenches the QDs fluorescence yielding a yellow fluorescence. This change in green to yellow fluorescence was used to detect the SNP.

This same idea could be used in the future to replace the well plate by the paper based microplates for DNA damage detection. The paper surface could be chemically modified with an epoxide group. Covalent coupling of amino-modified DNA strands to the modified paper would take place in a single step. These strands can then be subjected to UV light or other damage agents. Quantification of damage can be done by adding the complementary strands with a fluorescent probe at one end. In the absence of damage, hybridization will occur resulting in maximum fluorescence. However, in the presence of damage, the complementary strands will be washed away, giving minimum fluorescence. This method could be further made inexpensive by the use of complementary strands without any fluorescent dye attached but designed with two regions (Figure 6.1), region 1 with exact complementary bases to the target strand (variable region) and region 2 with a small chain of non-complementary nucleobases (constant region). Here the fluorescent probe is attached to the oligonucleotide chain designed complementary to the constant region. Thus, by designing different sequences with same constant regions, we can use a single fluorescent probe for studying damage in multiple sequences.

Further advancement of paper-based techniques have resulted in a novel Teflon-impregnated paper [33] that introduces specific zones of patterned arrays allowing assays to be performed similar to the microplates. This technique has already been used successfully to study cell responses to different peptides. Performing our DNA hybridization experiments coupled with

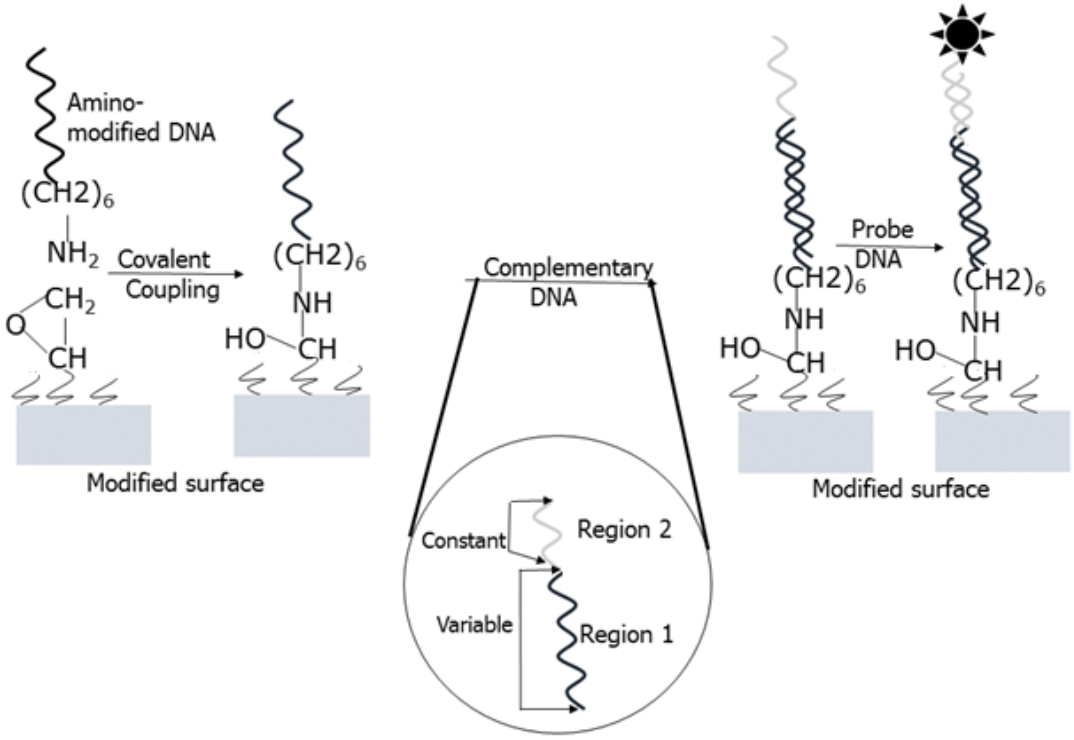

Figure 6.1 Schematic representation of a paper-based assay with a single probe for DNA damage detection. The complementary DNA has two regions, region 1 designed complementary to the target DNA and region 2 designed complementary to the single probe sequence. Region 1 varies with different targets but region 2 is constant for multiple sequences. This design allows for the use of a single fluorescently-labelled probe, typically the most expensive elements in a fluorescent hybridization assay.

Another approach is the use of DNA microarrays in which DNA is immobilized on a solid support in a very small area [29]. The solid support could be glass, plastic or silicon. However, the microarray experiments are limited by issues of reproducibility, due to non-uniform spots and lack of information about the number of binding sites on the slides. To overcome this limitation we can bind the DNA to the well plates by modifying the DNA and the well plate surface. One example is the reaction of modified DNA containing a primary amine group at one end to the well plate that has been modified with a covalently-linked N-oxysuccinimide (NOS) group [34,35]. Use of plates with such modification has an added advantage that it do not requires activation with UV light or other coupling agents. Thus, binding the DNA to the 96-well microplates would be a better way to obtain accurate and precise results since each well of the well plate represents an individual spot. The shapes of the spots is uniform and have a fixed number of binding sites, as reported by the plate providers. The use of an internal standard would also help us to evaluate the binding sites. Hence, this method will provide reproducible spots with same number of binding sites and will increase the precision of the method. Unlike microarray, the data analysis of the well plate experiments does not require any complicated software. Previous work with this type of modified well plates gave reproducible results for DNA-protein interaction studies via a kinase assay [36]. Our goal is to design a multiplex mix-and-read assay on these modified microplates by linking the amine-modified DNA to the well plate and then subjecting them to different damage agents. The quantification of damage can further be done by our hybridization technique coupled with measuring the fluorescence intensity of the intercalating dyes. This assay will serve as an intermediate step between solid-phase and solution-phase DNA studies.

The development of *in-vitro* assays in the 96-well microplates and further extending them to high-density 384 and 1584 multi-well microplates would extend the application of our mix-and

read-assays in measuring hot spots of DNA damage. As discussed in Chapter 5 of this thesis, we have successfully used our method to study the effect of different damaging agents on a few sequences of *Ras* genes. We anticipate that similar research along with *in vitro* assays performed on various other oncogenes and with high-density multi-well microplates, will help us to construct a library of hot spots of DNA damage.

Reference List

[1] A.F. El-Yazbi and G.R. Loppnow, Locked nucleic acid hairpin detection of UV-induced DNA damage, Canadian Journal of Chemistry. **89** (2011) 402-408.

[2] S.A. Oladepo and G.R. Loppnow, The effect of tryptophan on UV-induced DNA Photodamage, Photochem. Photobiol. **86** (2010) 844-851.

[3] S. Yarasi, C. McConachie and G.R. Loppnow, Molecular beacon probes of photodamage in thymine and uracil oligonucleotides. Photochem. Photobiol. **81** (2005) 467-473.

[4] Z.J. Shire and G.R. Loppnow, Molecular beacon probes for the detection of cisplatin-induced DNA damage, Anal. Bioanal. Chem. **88** (2012) 1-6.

[5] S.A. Oladepo and G.R. Loppnow, Self-quenching smart probes as a platform for the detection of sequence-specific UV-induced DNA photodamage, Anal. Bioanal. Chem. **397** (2010) 2949-2957.

[6] A.F. El-Yazbi and G.R. Loppnow, 2-Aminopurine hairpin probes for the detection of ultraviolet-induced DNA damage, Anal. Chim. Acta. **726** (2012) 44-49.

[7] A.F. El-Yazbi and G.R. Loppnow, Chimeric RNA–DNA Molecular Beacons for Quantification of Nucleic Acids, Single Nucleotide Polymophisms, and Nucleic Acid Damage, Anal. Chem. Acta. **85** (2013) 4321-4327.

[8] K. Chan, J.F. Sterling, S.A. Roberts, A.S. Bhagwat, M.A. Resnick and D.A. Gordenin, Base damage within single-strand DNA underlies in vivo hypermutability induced by a ubiquitous environmental agent, PLoS genetics. **8** (2012) e1003149.

[9] S.A. Roberts, J. Sterling, C. Thompson, S. Harris, D. Mav, R. Shah, L.J. Klimczak, G.V. Kryukov, E. Malc and P.A. Mieczkowski, Clustered mutations in yeast and in human cancers can arise from damaged long single-strand DNA regions, Mol. Cell. **46** (2012) 424-435.

[10] A.T. Baines, D. Xu and C.J. Der, Inhibition of Ras for cancer treatment: the search continues, Future Med. Chem. **3** (2011) 1787-1808.

[11] D.G. Brooks, R.M. James, C.E. Patek, J. Williamson and M.J. Arends, Mutant K-ras enhances apoptosis in embryonic stem cells in combination with DNA damage and is associated with increased levels of p19(ARF), Oncogene. **20** (2001) 2144-2152.

[12] Z. Feng, W. Hu, J.X. Chen, A. Pao, H. Li, W. Rom, M.C. Hung and M.S. Tang, Preferential DNA damage and poor repair determine ras gene mutational hotspot in human cancer, J. Natl. Cancer Inst. **94** (2002) 1527-1536.

[13] P.H. Johnson, R.P. Walker, S.W. Jones and K. Stephens, Multiplex gene expression analysis for high-throughput drug discovery: screening and analysis of compounds affecting genes overexpressed in cancer cells, Mol.Cancer.Ther. **1** (2002) 1293-1304.

[14] D. Ribble, N. B. Goldstein, D.A. Norris and Y.G. Shellman, A simple technique for quantifying apotosis in 96-well plates. Bio.Med Central **5** (2005) 12.

[15] J.R. Ridpath, S. Takeda, J.A. Swenberg and J. Nakamura, Convenient, multi-well plate-based DNA damage response analysis using DT40 mutants is applicable to high-throughput genotoxicity assay with characterization of modes of action, Envior. Mol. Muta.. **52** (2011) 153-160

[16] D.K. Wood, D.M. Weingeist, S.N. Bhatia, B.P. Engelward, Single cell trapping and DNA damage analysis using microwell arrays. Proc. Natl. Acad. Sci. **107** (2010) 10008-10013.

[17] G. Brunborg, P. Jackson, S. Shaposhnikov, H. Dahl, A. Azqueta, A.R. Collins and K.B. Gutzkow, High throughput sample processing and automated scoring, Front. Gent. **5** (2014) 373-

[18] J. Ge, S. Prasongtanakij, D.K. Wood, D. M. Weingeist, J. Fessler, P. Navasummrit, M. Ruchirawat and B.P.Engelward, CometChip: A high-throughput 96-well platform for measuring DNA damage in microarrayed human cell, J. Vis. Exp. **92** (2014)

[19] M. Karbaschi and M.S. Cooke, Novel method for the high-throughput processing of slides for the comet assay. Sci. Rep. **4** (2014) 1-6.

[20] S. Nandhakumar, S. Parasuraman, M.M. Shanmugam, K.R. Rao, P. Chand and B.V. Bhat, Evaluation of DNA damage using single-cell gel electrophoresis (Comet Assay), J. Pharmacol. Pharmacother. **2** (2011) 107-111.

[21] A. Hakura, S. Suzuki and T. Satoh, Improvement of the Ames test using human liver S9 preparation, J. Pharmacol. Toxicol. Methods, **46** (2001), 169-172.

[22] J. McCann, E. Choi, E. Yamasaki and B.N. Ames, Detection of carcinogens as mutagens in the Salmonella/microsome test: assay of 300 chemicals, Proc. Natl. Acad. Sci. U. S. A. **72** (1975) 5135-5139.

[23] K. Mortelmans and E. Zeiger, The Ames *Salmonella/microsome* mutagenicity assay, Mutat. Res-Fund Mol. M. **455** (2000) 29-60.

[24] M.F. Wu, F.C. Peng, Y.L. Chen, C.S. Lee, Y.Y. Yang, M.Y. Yeh, C.M. Liu, J.B. Chang, R.S. Wu, C.C. Yu, H.F. Lu and J.G. Chung, Evaluation of genotoxicity of Antrodia cinnamomea in the Ames test and the in vitro chromosomal aberration test, In Vivo. **25** (2011) 419-423.

[25] S. Galloway, E. Lorge, M.J. Aardema, D. Eastmond, M. Fellows, R. Heflich, D. Kirkland, D.D. Levy, A.M. Lynch and D. Marzin, Workshop summary: Top concentration for in vitro mammalian cell genotoxicity assays; and report from working group on toxicity measures and

top concentration for in vitro cytogenetics assays (chromosome aberrations and micronucleus), Matat. Res-Gen Tox.En. **723** (2011) 77-83.

[26] A. Dhawan, M. Bajpayee and D. Parmar, Comet assay: a reliable tool for the assessment of DNA damage in different models, Cell Biol. Toxicol. **25** (2009) 5-32.

[27] G. Speit and A. Rothfuss, The comet assay: a sensitive genotoxicity test for the detection of DNA damage and repair, Methods Mol.Biol. **314,** (2006) 275-286.

[28] P. Grigaravicius, A. Rapp and K.O. Greulich, A direct view by immunofluorescent comet assay (IFCA) of DNA damage induced by nicking and cutting enzymes, ionizing (137)Cs radiation, UV-A laser microbeam irradiation and the radiomimetic drug bleomycin, Mutagenesis. **24** (2009) 191-197.

[29] D.A. Khodakov and A.V. Ellis, Recent developments in nucleic acid identification using solid-phase enzymatic assays, Microchimica Acta. **181** (2014) 1-14.

[30] H. Tian, L. Cao, Y. Tan, S. Williams, L. Chen, T. Matray, A. Chenna, S. Moore, V. Hernandez, V. Xiao, M. Tang and S. Singh, Multiplex mRNA assay using electrophoretic tags for high-throughput gene expression analysis, Nucleic Acids Res. **32** (2004) e126.

[31] Y. Chen and Z. Kuo, C. Cheng, Paper–a potential platform in pharmaceutical development, Trends Biotechnol. **33** (2015) 4-9.

[32] M.O. Noor and U.J. Krull, Camera-Based Ratiometric Fluorescence Transduction of Nucleic Acid Hybridization with Reagentless Signal Amplification on a Paper-Based Platform Using Immobilized Quantum Dots as Donors, Anal. Chem. **86** (2014) 10331-10339.

[33] F. Deiss, W.L. Matochko, N. Govindasamy, E.Y. Lin and R. Derda, Flow-Through Synthesis on Teflon-Patterned Paper To Produce Peptide Arrays for Cell-Based Assays, Angew. Chem. Int. Ed. **53** (2014) 6374-6377.

[34] B. Liu, Y. Qin, J. Wang and Y. Wang, Detection and comparison of protein–DNA interactions using DNA–BIND plate and horseradish peroxidase-based colorimetric assay, Anal. Biochem. **412** (2011) 111-113.

[35] A.Y. Mercedes-Camacho and F.A. Etzkorn, Enzyme-linked enzyme-binding assay for Pin1 WW domain ligands, Anal. Biochem. **402** (2010) 77-82.

[36] P. Renard, I. Ernest, A. Houbion, M. Art, H. Le Calvez, M. Raes and J. Remacle, Development of a sensitive multi-well colorimetric assay for active NFkappaB, Nucleic Acids Res. **29** (2001) e21.

Appendix

(Supplementary Information)

Table A1. Fluorescence intensity of blank sample.

Fluorescence Intensity (x 10^5 cps)
4.7
4.6
4.8
4.8
4.6
4.7
4.6
4.6
4.7
4.7
4.6
4.8
4.8
4.6
4.7
4.5
4.7
4.6
Avg ± SD 4.7 ± 0.07

Fluorescence intensity for 0.18 μM SP_{dT17} in buffer. 'Avg' is average and 'SD' is standard deviation. These values were used for calculating the LOD and LOQ.

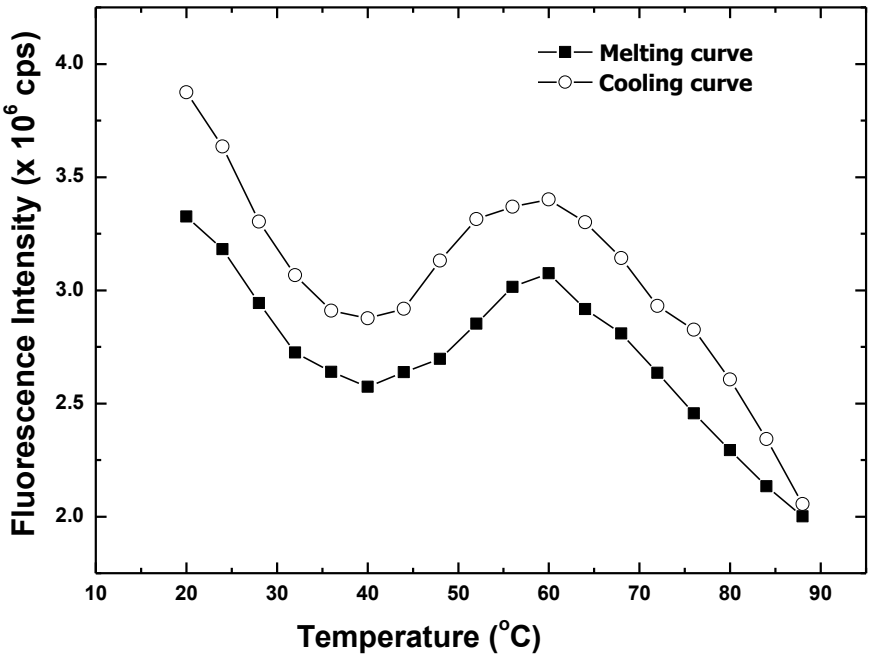

Figure A1. Melting (filled squares) and cooling curve (open circles) of 0.18 μM SP_{TarC} alone. The melting curve was generated at a heating rate of 1 ºC/min, in 4 ºC increments and with a 5 min holding time after each increment. The cooling curve was performed with all the above conditions, except -4 ºC increments were used.

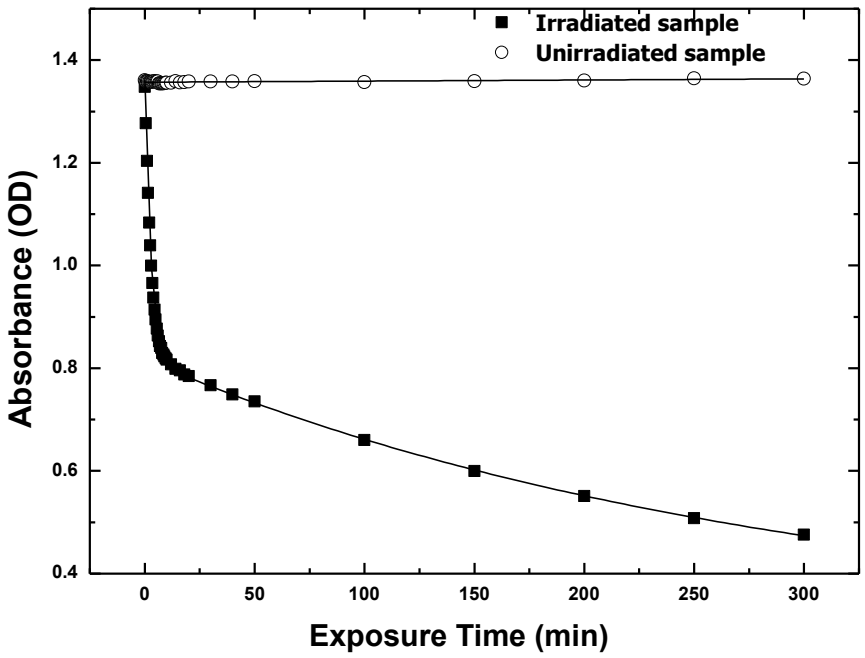

Figure A2. Absorbance at 260 nm as a function of UVC exposure time for a 10 μM dT_{17} irradiated sample (filled squares) and 10 μM unirradiated dT_{17} control (open circles). The solid line through the filled squares is fit to a double exponential function, $A = A_0 + C_1 e^{-t/\tau_1} + C_2 e^{-t/\tau_2}$. The absorbance parameter obtained from the fit are C_1 = 0.81 OD, C_2 = 0.53 OD, A_0= 0.29 OD, τ_1 = 2.79 ± 0.04 min, τ_2 = 288.46 ± 41.43 min. The solid line through the open circles is fit to a straight line of zero slope by eye.

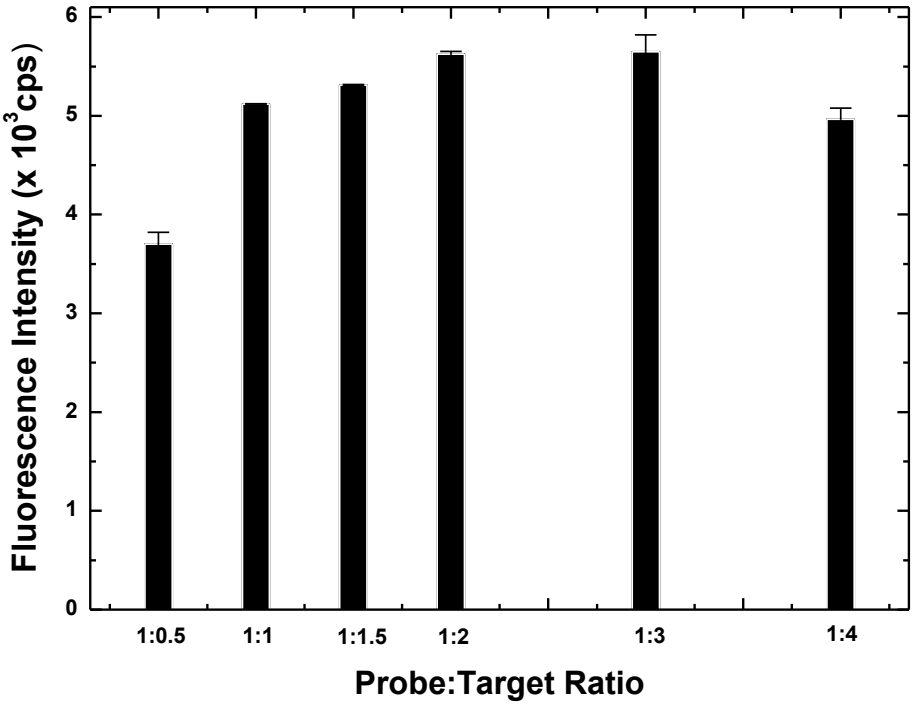

Figure A3. Fluorescence intensities for different ratios of SP_{TarC} :TarC. Different ratios are obtained by keeping the concentration of SP constant at 0.18 μM and varying the concentration of target.

-

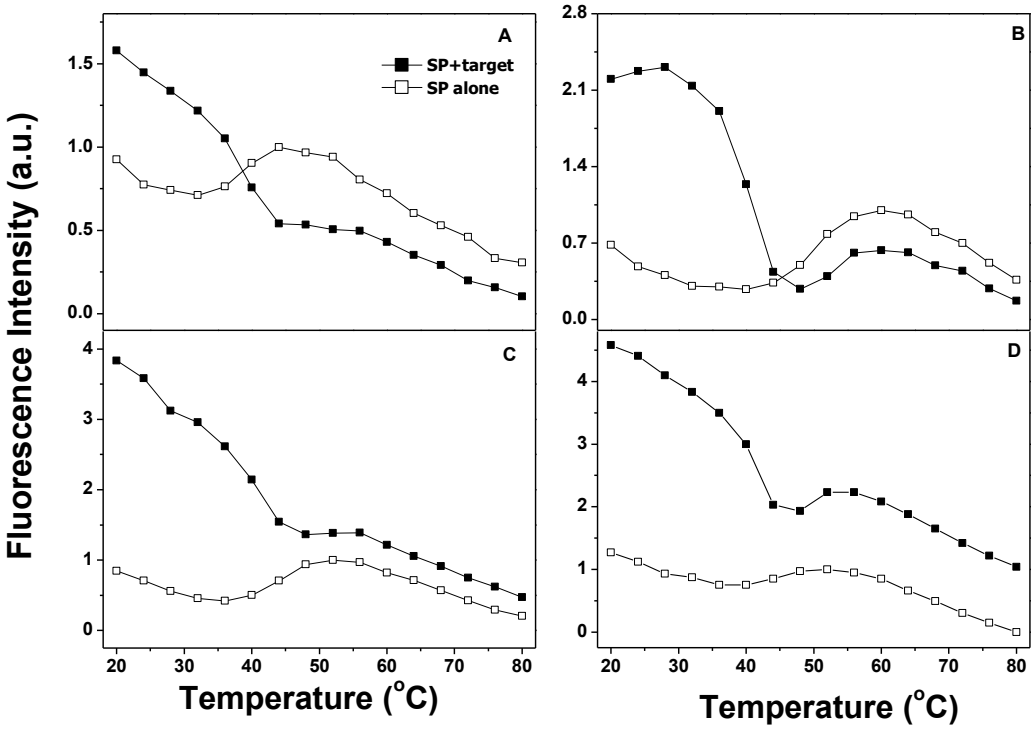

Figure A4. Melting curves of 0.18 μM SP alone (open circles) and 0.18 μM SP in the presence of a 3-fold excess of perfectly complementary oligonucleotide target sequence (filled squares) in 10mM Tris and 1mM EDTA with varying Na^+ and Mg^{2+} concentrations. The melting curves use (A) 1 mM $MgCl_2$, (B) 3 mM $MgCl_2$, (C) 3 mM $MgCl_2$ and 20 mM NaCl and (D) 5 mM $MgCl_2$ and 20 mM NaCl. Fluorescence curves have each been scaled to SP alone.

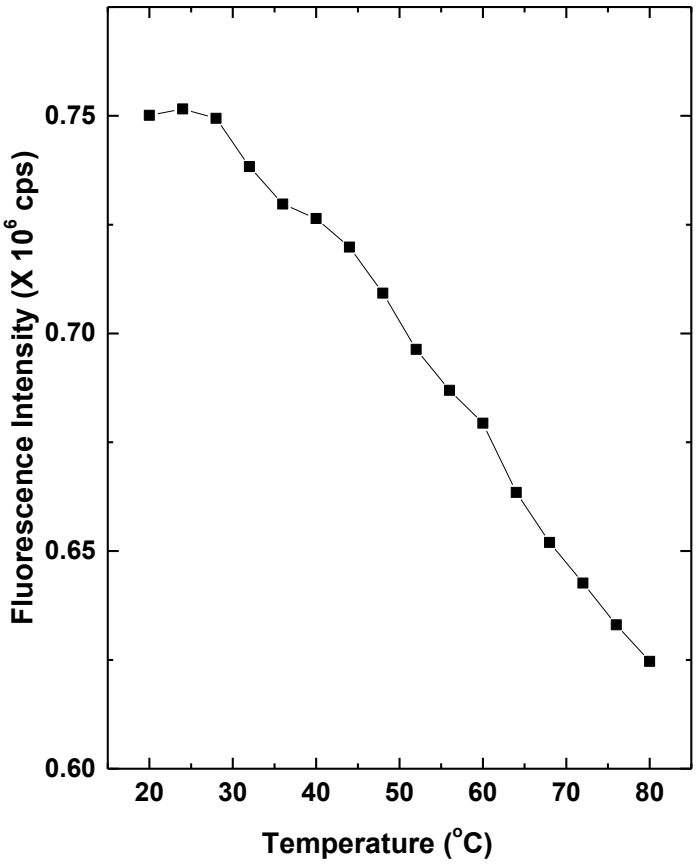

Figure A5. Plot of temperature-dependent fluorescence of 2μM FAM dye in 5 mM $MgCl_2$, 20 mM NaCl, 10mM Tris and 1mM EDTA, pH 7.4.

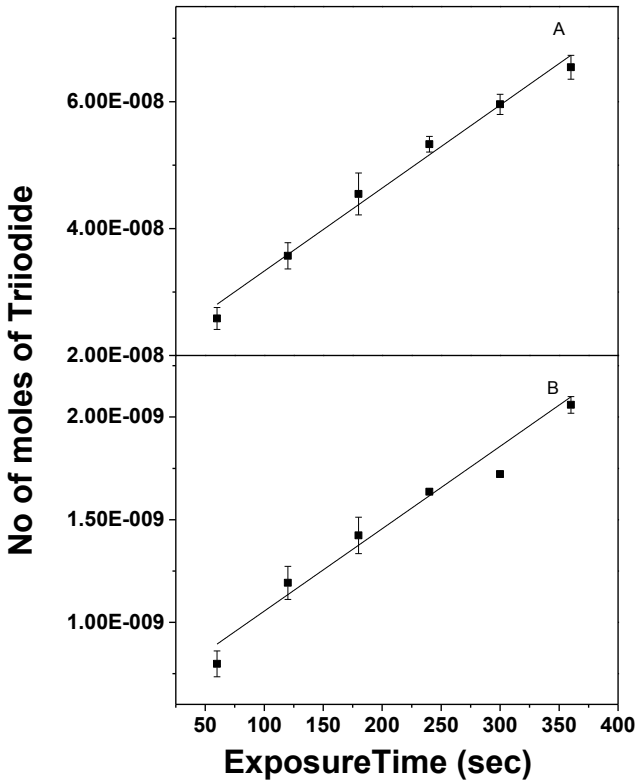

Figure A6. Moles of triiodide formed as a function of exposure time for (A) Cuvette method and (B) Well plate method. The solid line through the points are linear fit with slope of the calibration curve for cuvette method = 1.31 x 10^{-10} mol.s^{1}and well plate method = 4.01 x 10^{-12} mol.s^{-1} respectively.

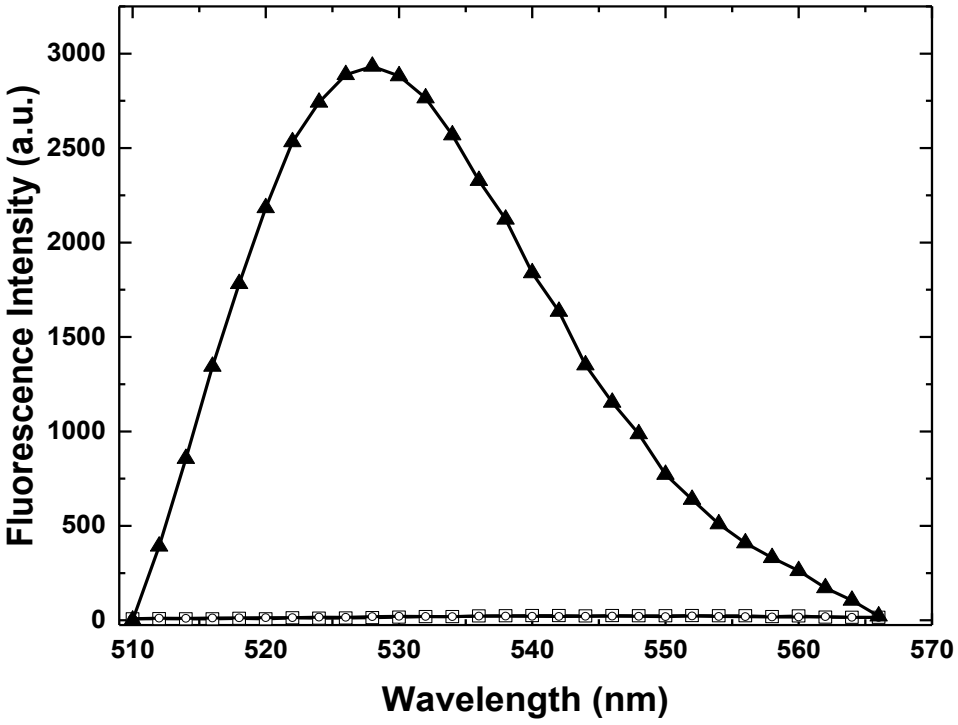

Figure A7. The emission spectra of EG-ds T_{17} DNA complex (closed triangles), ds T_{17} alone (open circles) and activated Ru complex irradiated for 10 min (open squares). The emission scan was recorded at excitation wavelength of 490 nm at room temperature.

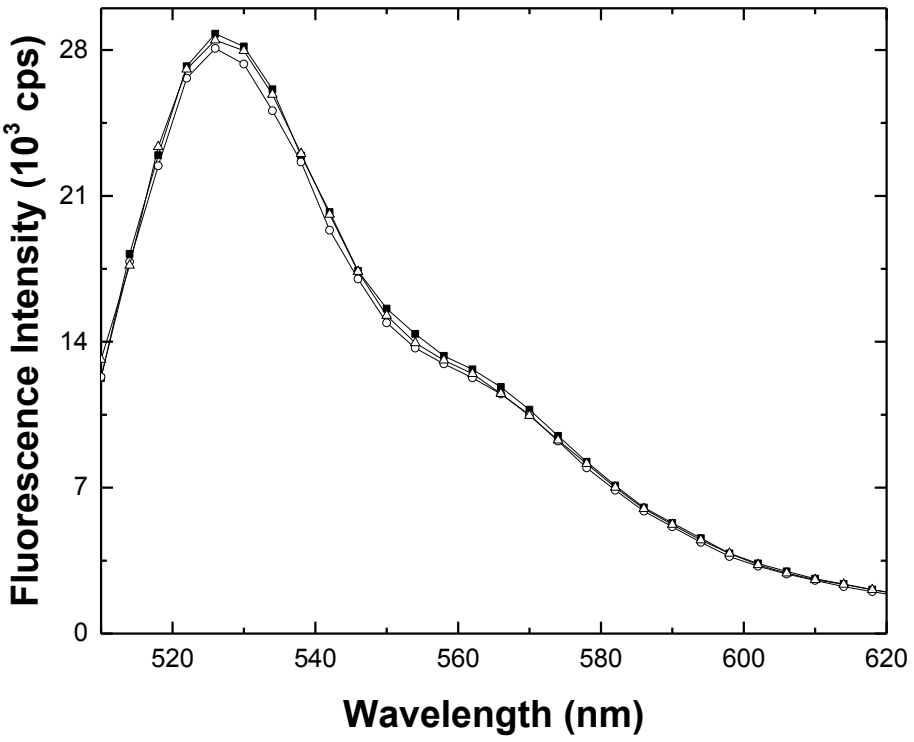

Figure A8 Emission scans for 1.33 μM EG excited at 490 nm in the presence of dsDNA alone (open circles), ssDNA-Ru complex damaged for 0 min and then hybridized with the complementary target (open triangles) and dsDNA in presence of activated Ru complex kept in the dark for 48 hr (closed triangles).

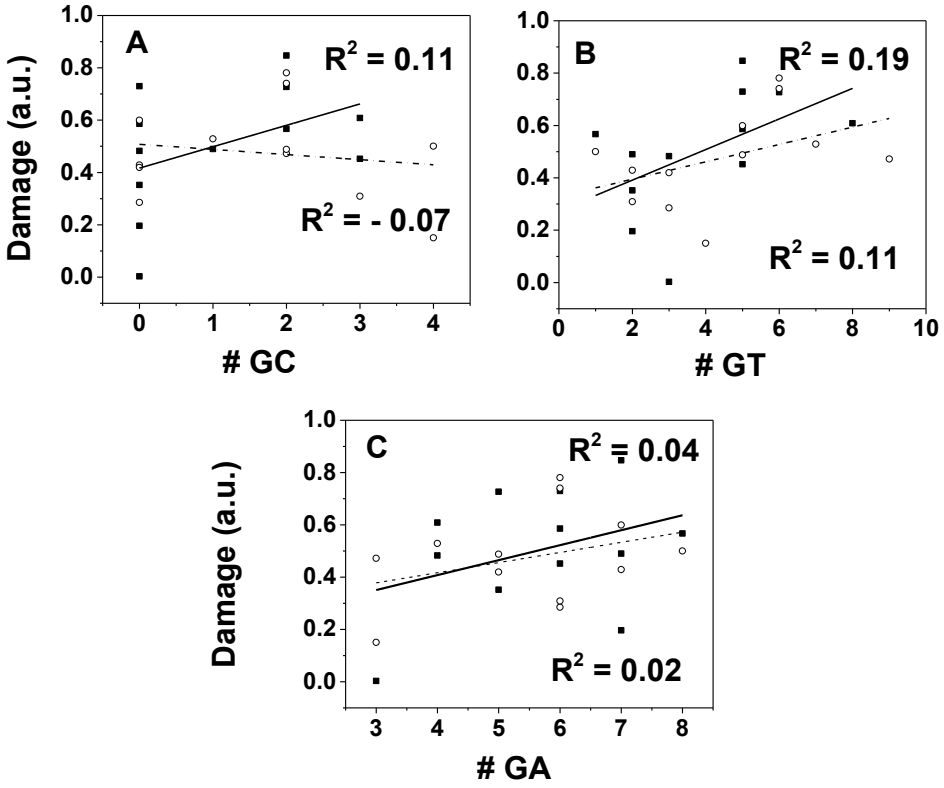

Figure A9. Activated Ru complex-induced damage susceptibility (1-F) as a function of number of GC, GT and GA sites. The damage susceptibility on the y-axis are 1-F, where $F = F_i/F_c$, F_i is the fluorescence intensity of EG-dsDNA upon Ru damage and F_c is the fluorescence intensity of the control sample. EG dye fluorescence intensity at 530 nm is measured in the presence of 1 μM dsDNA (10 mM Tris, 1 mM EDTA, 10 mM NaCl, pH 7.4) For all the plots, the filled squares represent the damage of K-*Ras* sequences and the open circles represent the damage of N-*Ras* sequences. The solid lines through the filled square points are linear fits for the K-*Ras* sequences with their respective R^2 values indicated in the upper portion of each plot. The dash line through the empty circle points are linear fits for the N-*Ras* sequences with their R^2 value indicated in the lower portion of each plot.

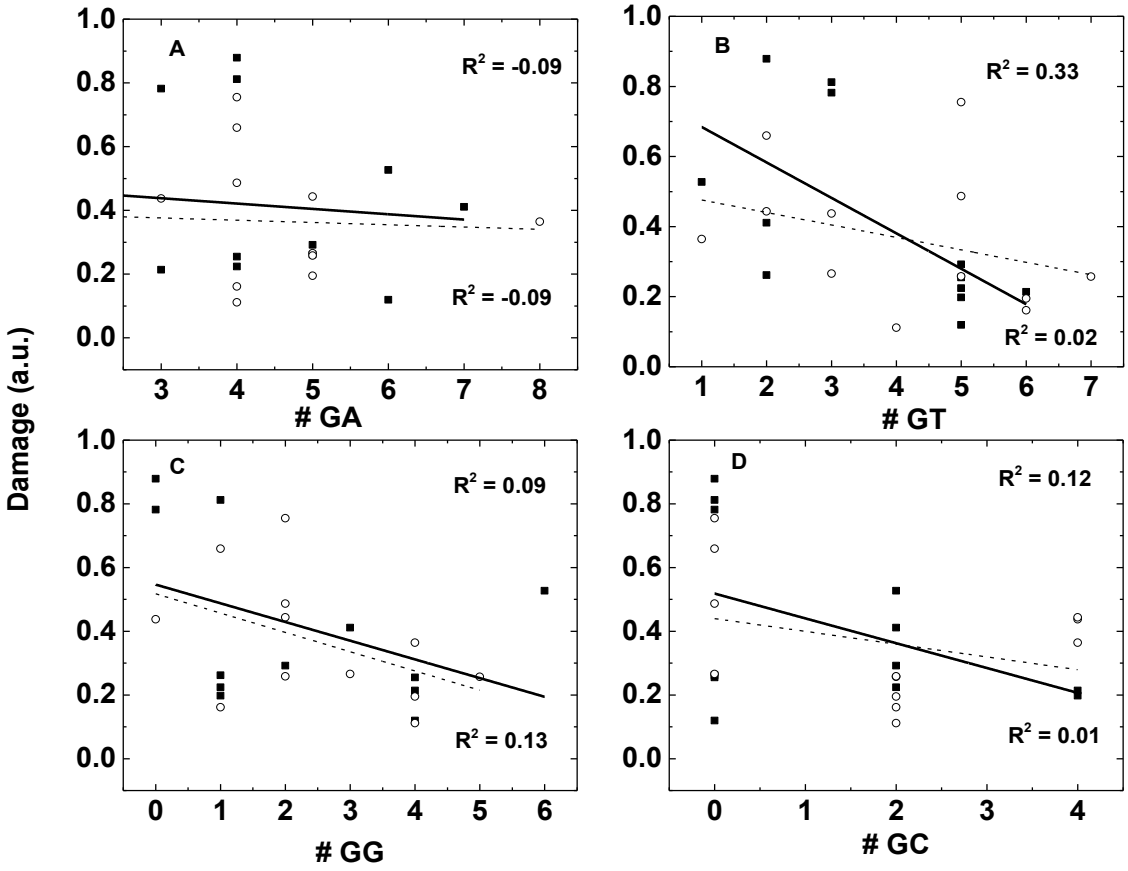

Figure A10. UVC-induced damage susceptibility (1-F) as a function of number of GA, GT, GG and GC sites. The damage susceptibility on the y-axis are 1-F, where $F = F_i/F_c$, F_i is the fluorescence intensity of EG-dsDNA upon UVC damage and F_c is the fluorescence intensity of the control sample. EG dye fluorescence intensity at 530 nm is measured in the presence of 1 μM dsDNA (10 mM Tris, 1 mM EDTA, 10 mM NaCl, pH 7.4) For all the plots, the filled squares represent the damage of K-*Ras* sequences and the open circles represent the damage of N-*Ras* sequences. The solid lines through the filled square points are linear fits for the K-*Ras* sequences with their respective R^2 values indicated in the upper portion of each plot. The dash line through the empty circle points are linear fits for the N-*Ras* sequences with their R^2 value indicated in the lower portion of each plot.

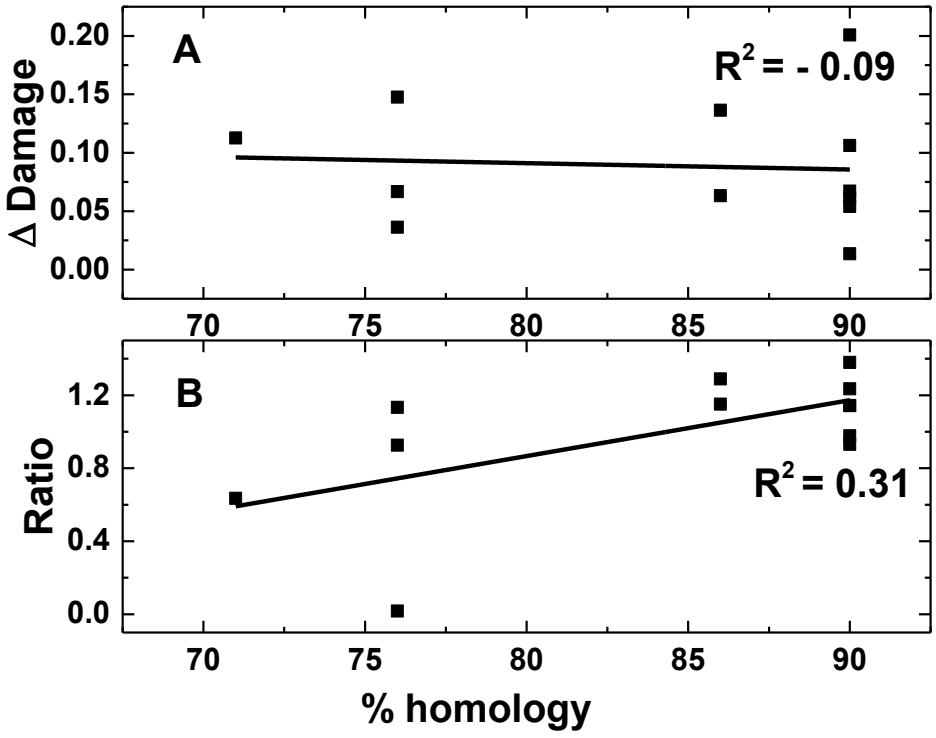

Figure A11. Δ Damage between damage susceptibility of K-*Ras* and N-*Ras* sequences (A) and ratio between damage susceptibility of K-*Ras* and N-*Ras* sequences (B) as a function of % homology between K-*Ras* and N-*Ras* sequences for Ru-induced DNA damage. The damage susceptibility is 1-F, where $F = F_i/F_c$, F_i is the fluorescence intensity of EG-dsDNA upon damage and F_c is the fluorescence intensity of the control sample. EG dye fluorescence intensity is measure at 530 nm in the presence of 1 μM dsDNA (10 mM Tris, 1mM EDTA, 10 mM NaCl, pH 7.4). The solid lines through the filled square points are linear fit with their R^2 values indicated for each plot.

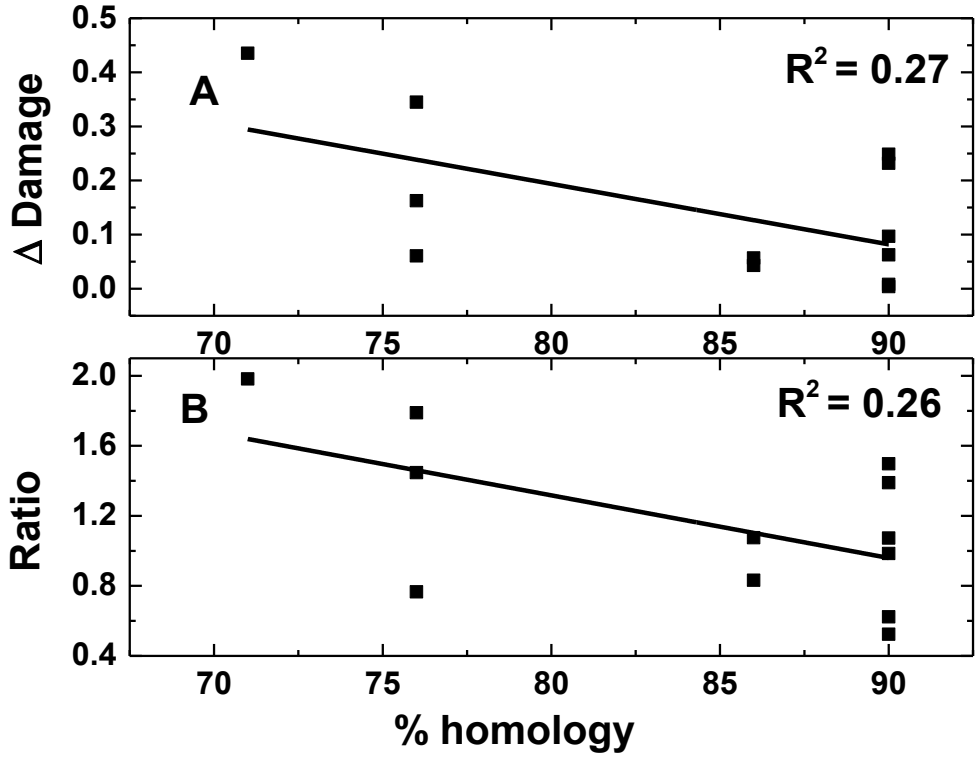

Figure A12. Δ Damage between damage susceptibility of K-*Ras* and N-*Ras* sequences (A) and ratio between damage susceptibility of K-*Ras* and N-*Ras* sequences (B) as a function of % homology between K-*Ras* and N-*Ras* sequences for UVC-induced DNA damage. The damage susceptibility is 1-F, where $F = F_i/F_c$, F_i is the fluorescence intensity of EG-dsDNA upon damage and F_c is the fluorescence intensity of the control sample. EG dye fluorescence intensity is measure at 530 nm in the presence of 1 μM dsDNA (10 mM Tris, 1mM EDTA, 10 mM NaCl, pH 7.4). The solid lines through the filled square points are linear fit with their R^2 values indicated for each plot.

Bibliography

[1] C.F.A. Bryce and D. Pacini, The Biochemical Society, (1998) pp 6-14, Holbrooks press, UK.

[2] J.M. Berg, J.T. Tymoczko and L. Stryer, Biochemistry, (2002) pp 117-128 Macmillan press, NY.

[3] J.D. Watson and F.H. Crick, Molecular structure of nucleic acids, Nature. **171** (1953) 737-738.

[4] T. Lindahl, Instability and decay of the primary structure of DNA, Nature. **362** (1993) 709-715.

[5] M.S. Cooke, M.D. Evans, M. Dizdaroglu and J. Lunec, Oxidative DNA damage: mechanisms, mutation and disease, FASEB J. **17** (2003) 1195-1214.

[6] S.P. Jackson and J. Bartek, The DNA-damage response in human biology and disease, Nature. **461** (2009) 1071-1078.

[7] B.N. Ames and L.S. Gold, Endogenous mutagens and the causes of aging and cancer, Mutat. Res-Fund Mol M. **250** (1991) 3-16.

[8] A.I. Haza and P. Morales, Spanish honeys protect against food mutagen-induced DNA damage, J. Sci. Food Agric. **93** (2013) 2995-3000.

[9] L.J. Marnett and J.P. Plastaras, Endogenous DNA damage and mutation, Trends Genet.**17** (2001) 214-221.

[10] H.A. Yousef, A. Afify, H.M. Hasan and A.A. Meguid, DNA damage in hemocytes of Schistocerca gregaria (Orthoptera: Acrididae) exposed to contaminated food with cadmium and lead, Nat. Sci. **2** (2010) 292.

[11] J.H. Hoeijmakers, DNA damage, aging and cancer, N. Engl. J. Med. **361** (2009) 1475-1485.

[12] M. Peak, J. Peak, M. Moehring and R. Webs, Ultraviolet action spectra for DNA dimer induction, lethality, and mutagenesis in Escherichia coli with emphasis on the UVB region, Photochem. Photobiol. **40** (1984) 613-620.

[13] R.P. Rastogi, Richa, A. Kumar, M.B Tyagi and R.P. Sinha, Molecular mechanisms of ultraviolet radiation-induced DNA damage and repair, J. Nucleic Acids. **2010** (2010) 592980-593012.

[14] R.P. Sinha and D. Häder, UV-induced DNA damage and repair: a review, Photochem. Photobiol. Sci. **1** (2002) 225-236.

[15] M. Ichihashi, M. Ueda, A. Budiyanto, T. Bito, M. Oka, M. Fukunaga, K. Tsuru and T. Horikawa, UV-induced skin damage, Toxicology. **189** (2003) 21-39.

[16] L. Francesco and W. Horspool, CRC handbook of Organic Photochemistry and Photobiology, (2003) pp.140.1-140.8. CRC Press, USA.

[17] J.L. Ravanat, T. Douki and J. Cadet, Direct and indirect effects of UV radiation on DNA and its components, J. Photochem. Photobiol. B. **63** (2001) 88-102.

[18] A.G. Zavala, R.T. Morris, J.J. Wyrick and M.J. Smerdon, High-resolution characterization of CPD hotspot formation in human, Nucleic Acid Res. **42** (2014) 893-905.

[19] Y.K. Law, J. Azadi, C.E. Crespo-Hernández, E. Olmon and B. Kohler, Predicting thymine dimerization yields from molecular dynamics simulations, Biophys. J. **94** (2008) 3590-3600.

[20] S.I. Tsilimigaki, N. Messini-Nikolaki, M. Kanariou and S.M. Piperakis, A study on the effects of seasonal solar radiation on exposed populations, Mutagenesis. **18** (2003) 139-143.

[21] K. Lin and A.Wang, UV mutagenesis in Escherichia coli K-12: Cell survival and mutation frequency of the chromosomal genes lacZ, rpoB, ompF, and ampA, J. Exp. Microbiol. Immunol. **1** (2001) 32-46.

[22] D.L. Mitchell, J. Jen and J.E. Cleaver, Sequence specificity of cyclobutane pyrimidine dimers in DNA treated with solar (ultraviolet B) radiation, Nucleic Acids Res. **20** (1992) 225-229.

[23] J. Li, Z. Liu, C. Tan, X. Guo, L. Wang, A. Sancar and D. Zhong, Dynamics and mechanism of repair of ultraviolet-induced (6-4) photoproduct by photolyase, Nature. **466** (2010) 887-890.

[24] G.P. Pfeifer, Formation and processing of UV photoproducts: effects of DNA sequence and chromatin environment, Photochem. Photobiol. **65** (1997) 270-283.

[25] P.J. Rochette, N. Bastien, T. Todo and R. Drouin, Pyrimidine (6–4) pyrimidone photoproduct mapping after sublethal UVC doses: nucleotide resolution using terminal transferase-dependent PCR, Photochem. Photobiol. **82** (2006) 1370-1376.

[26] A. Besaratinia, S.I. Kim and G.P. Pfeifer, Rapid repair of UVA-induced oxidized purines and persistence of UVB-induced dipyrimidine lesions determine the mutagenicity of sunlight in mouse cells, FASEB J. **22** (2008) 2379-2392.

[27] S. Kumar, P.C. Joshi, N.D. Sharma, S.N. Bose, R. Jeremy, H. Davies, N. Takeda and J.A. McCloskey, Adenine photodimerization in deoxyadenylate sequences: elucidation of the mechanism through structural studies of a major d(ApA) photoproduct, Nucleic Acids Res. **19** (1991) 2841-2847.

[28] F.P. Gasparro and J.R. Fresco, Ultraviolet-induced 8,8-adenine dehydrodimers in oligo- and polynucleotides, Nucleic Acids Res. **14** (1986) 4239-4251.

[29] R.O. Rahn, Search for an adenine photoproduct in DNA, Nucleic Acids Res. **3** (1976) 879-890.

[30] J. Cadet, S. Courdavault, J. Ravanat and T. Douki, UVB and UVA radiation-mediated damage to isolated and cellular DNA, Pure Appl. Chem. **77** (2005) 947-961.

[31] T. Douki, D. Perdiz, P. Grof, Z. Kuluncsics, E. Moustacchi, J. Cadet and E. Sage, Oxidation of guanine in cellular DNA by solar UV radiation: biological role, Photochem. Photobiol. **70** (1999) 184-190.

[32] J. Cadet, E. Sage and T. Douki, Ultraviolet radiation-mediated damage to cellular DNA, Mutat. Res-Fund Mol M. **571** (2005) 3-17.

[33] L.H. Swift and R.M. Golsteyn, Genotoxic anti-cancer agents and their relationship to DNA damage, mitosis and checkpoint adaptation in proliferating cancer cells, Int. J. Mol. Sci. **15** (2014) 3403-3431.

[34] I. Casorelli, C. Bossa and M. Bignami, DNA damage and repair in human cancer: molecular mechanisms and contribution to therapy-related leukemias, Int. J. Environ. Res. Public Health. **9** (2012) 2636-2657.

[35] M.C. Poirier, Chemical-induced DNA damage and human cancer risk, Nat. Rev. Cancer. **4** (2004) 630-637.

[36] C.S. Allardyce and P.J. Dyson, Ruthenium in medicine: current clinical uses and future prospects, Platin. Met. Rev. **45** (2001) 62-69

[37] M. Groessl, Y.O. Tsybin, C.G. Hartinger, B.K. Keppler and P.J. Dyson, Ruthenium versus platinum: interactions of anticancer metallodrugs with duplex oligonucleotides characterized by electrospray ionization mass spectrometry, J. Biol. Inorg. Chem. **15** (2010) 677-688.

[38] S. Page and R. Wheeler, Ruthenium compounds as anticancer agents, Educ. Chem. **49** (2012) 26-29.

[39] B. Peña, R. Barhoumi, R.C. Burghardt, C. Turro and K.R. Dunbar, Confocal fluorescence microscopy studies of a fluorophore-labeled dirhodium compound: visualizing metal–metal bonded molecules in lung cancer (A549) Cells, J. Am. Chem. Soc. **136** (2014) 7861-7864.

[40] M. Zec, T. Srdic-Rajic, A. Konic-Ristic, T. Todorovic, K. Andjelkovic, I. Filipovic-Ljeskovic and S. Radulovic, Anti-metastatic and anti-angiogenic properties of potential new anti-cancer drugs based on metal complexes of selenosemicarbazones, Anti-Cancer Agents in Med. Chem.**12** (2012) 1071-1080.

[41] S. Chattopadhyay, S. Chakraborty, D. Laha, R. Baral, P. Pramanik and S. Roy, Surface-modified cobalt oxide nanoparticles: new opportunities for anti-cancer drug development, Cancer Nanotechnology. **3** (2012) 13-23.

[42] A.S. Abu-Surrah and M. Kettunen, Platinum group antitumor chemistry: design and development of new anticancer drugs complementary to cisplatin, Curr. Med. Chem. **13** (2006) 1337-1357.

[43] Y. Esaka, S. Inagaki and M. Goto, Separation procedures capable of revealing DNA adducts, J. Chrom. B. **797** (2003) 321-329.

[44] R. Singh and P.B. Farmer, Liquid chromatography-electrospray ionization-mass spectrometry: the future of DNA adduct detection, Carcinogenesis. **27** (2006) 178-196.

[45] T. Douki and J. Cadet, Individual determination of the yield of the main UV-induced dimeric pyrimidine photoproducts in DNA suggests a high mutagenicity of CC photolesions, Biochemistry. **40** (2001) 2495-2501.

[46] D.P. Wasalathanthri, S. Malla, I. Bist, C.K. Tang, R.C. Faria and J.F. Rusling, High-throughput metabolic genotoxicity screening with a fluidic microwell chip and electrochemiluminescence, Lab Chip. **13** (2013) 4554-4562.

[47] V.A. Bespalov, A. Conconi, X. Zhang, D. Fahy and M.J. Smerdon, Improved method for measuring the ensemble average of strand breaks in genomic DNA, Environ. Mol. Mutagen. **38** (2001) 166-174.

[48] D.B. Yarosh, S. Boumakis, A.B. Brown, M.T. Canning, J.W. Galvin, D.M. Both, E. Kraus, A. O. Connor and D.A. Brown, Measurement of UVB-induced DNA damage and its consequences in models of immunosuppression, Methods. **28** (2002) 55-62.

[49] J. Komura and A.D. Riggs, Terminal transferase-dependent PCR: a versatile and sensitive method for in vivo footprinting and detection of DNA adducts, Nucleic Acids Res. **26** (1998) 1807-1811.

[50] J.A. Sikorsky, D.A. Primerano, T.W. Fenger and J. Denvir, Effect of DNA damage on PCR amplification efficiency with the relative threshold cycle method, Biochem. Biophys. Res. Commun. **323** (2004) 823-830.

[51] K.A. Grimaldi, C.J. McGurk, P.J. McHugh and J.A. Hartley, PCR-based methods for detecting DNA damage and its repair at the sub-gene and single nucleotide levels in cells, Mol. Biotechnol. **20** (2002) 181-196.

[52] H. Waller, E. Friess and J. Kiefer, On the immunological detection of X-ray induced DNA damage, Radiat. Environ. Biophys. **19** (1981) 259-264.

[53] J. Peccia and M. Hernandez, Rapid immunoassays for detection of UV-induced cyclobutane pyrimidine dimers in whole bacterial cells, Appl. Environ. Microbiol. **68** (2002) 2542-2549.

[54] M.C. Poirier, S.H. Yuspa, I.B. Weinstein and S. Blobstein, Detection of carcinogen–DNA adducts by radioimmunoassay, Nature **270** (1977) 186-188.

[55] M.C. Poirier, The use of carcinogen-DNA adduct antisera for quantitation and localization of genomic damage in animal models and the human population, Environ. Mutagen. **6** (1984) 879-887.

[56] M. Karbaschi, N.J. Brady, M.D. Evans and M.S. Cooke, DNA repair protocols, (2012) 163-175, Springer, Humuna Press, NJ.

[57] S. Kumari, R.P. Rastogi, K.L. Singh, S.P. Singh and R.P. Sinha, DNA damage: detection strategies, EXCLI J. **7** (2008) 44-62.

[58] A.A. Wani, S.M. D.Ambrosio and N.K. Alvi, Quantification of pyrimidine of pyrimidine dimers by immunoslot blot following sublethal UV-Irradiation of human cells, Photochem. Photobiol. **46** (1987) 477-482.

[59] N.P. Singh, M.T. McCoy, R.R. Tice and E.L. Schneider, A simple technique for quantitation of low levels of DNA damage in individual cells, Exp. Cell Res. **175** (1988) 184-191.

[60] D. Anderson, T.W. Yu and D.B. McGregor, Comet assay responses as indicators of carcinogen exposure, Mutagenesis. **13** (1998) 539-555.

[61] D.W. Fairbairn, P.L. Olive and K.L. O'Neill, The comet assay: a comprehensive review, Mut. Res-Rev Gen. Toxicol. **339** (1995) 37-59.

[62] P. Moller, L.E. Knudsen, S. Loft and H. Wallin, The comet assay as a rapid test in biomonitoring occupational exposure to DNA-damaging agents and effect of confounding factors, Cancer Epidemiol. Biomarkers Prev. **9** (2000) 1005-1015.

[63] M. Lemay and K.A. Wood, Detection of DNA damage and identification of UV-induced photoproducts using the CometAssay™ kit, BioTechniques. **27** (1999) 846-851.

[64] L. Marrot, J. Belaidi, F. Lejeune, J. Meunier, D. Asselineau and F. Bernerd, Photostability of sunscreen products influences the efficiency of protection with regard to UV-induced genotoxic or photoageing-related endpoints, Br. J. Dermatol. **151** (2004) 1234-1244.

[65] A. Azqueta, J. Slyskova, S. Langie, I. Gaivão and A.R. Collins, Comet assay to measure DNA repair: approach and applications, Front. Genet. **5** (2014) 1-19.

[66] M. Glei and W. Schlörmann, Functional analysis of DNA and chromatin, (2014) pp 39-48, Springer,Humuna Press, NJ.

[67] G. Speit and A. Rothfuss, DNA repair protocols, 2012, pp. 79-90, Springer, Humuna Press, NJ.

[68] A. Maksimenko, A.A. Ishchenko, G. Sanz, J. Laval, R.H. Elder and M.K. Saparbaev, A molecular beacon assay for measuring base excision repair activities, Biochem. Biophys. Res. Commun. **319** (2004) 240-246.

[69] W. Tan, K. Wang and T.J. Drake, Molecular beacons, Curr. Opin. Chem. Biol. **8** (2004) 547-553.

[70] L.C. Riches, A.M. Lynch and N.J. Gooderham, A molecular beacon approach to detecting RAD52 expression in response to DNA damage in human cells, Toxicology in Vitro. **24** (2010) 652-660.

[71] Z.J. Shire and G.R. Loppnow, Molecular beacon probes for the detection of cisplatin-induced DNA damage, Anal. Bioanal. Chem. **88** (2012) 1-6.

[72] S. Tyagi and F.R. Kramer, Molecular beacons: probes that fluoresce upon hybridization, Nat. Biotechnol. **14** (1996) 303-308.

[73] X.H. Peng, Z.H. Cao, J.T. Xia, G.W. Carlson, M.M. Lewis, W.C. Wood and L. Yang, Real-time detection of gene expression in cancer cells using molecular beacon imaging: new strategies for cancer research, Cancer Res. **65** (2005) 1909-1917.

[74] Y.L. Jiang, C.A. McGoldrick, D. Yin, J. Zhao, V. Patel, M.F. Brannon, J.W. Lightner, K. Krishnan and W.L. Stone, A specific molecular beacon probe for the detection of human prostate cancer cells, Bioorg. Med. Chem. Lett. **22** (2012) 3632-3638.

[75] D. Klein, Quantification using real-time PCR technology: applications and limitations, Trends Mol. Med. **8** (2002) 257-260.

[76] S.A. Oladepo and G.R. Loppnow, Self-quenching smart probes as a platform for the detection of sequence-specific UV-induced DNA photodamage, Anal. Bioanal. Chem. **397** (2010) 2949-2957.

[77] K.T. Kim, R.N. Veedu, Y.J. Seo and B.H. Kim, Quencher-free molecular beacons as probes for oligonucleotides containing CAG repeat sequences, Chem. Commun. **50** (2014) 1561-1563.

[78] N. Kim, S and Jinks-Robertson, Transcription as a source of genome instability, Nature Rev. Genet. **13** (2012) 204-214.

[79] J.P. Knemeyer, N. Marme and M. Sauer, Probes for detection of specific DNA sequences at the single-molecule level, Anal. Chem. **72** (2000) 3717-3724.

[80] A.F. El-Yazbi and G.R. Loppnow, 2-Aminopurine hairpin probes for the detection of ultraviolet-induced DNA damage, Anal. Chim. Acta. **726** (2012) 44-49.

[81] S. Chakravarty, W. Lai, K. Moncivais, X. Wang, C. Lin, Z.J. Zhang and R.T. Chen, Photonic crystal microarray nanoplatform for high throughput detection of biomolecules, **8034** (2011)m 1-6.

[82] R. Wang, A. Biales, D. Bencic, D. Lattier, M. Kostich, D. Villeneuve, G.T. Ankley, J. Lazorchak and G.Toth, DNA microarray application in ecotoxicology: experimental design,

microarray scanning, and factors affecting transcriptional profiles in a small fish species, Environ. Toxicol. Chem. **27** (2008) 652-663.

[83] H. Wei, P.F. Kuan, S. Tian, C. Yang, J. Nie, S. Sengupta, V. Ruotti, G.A. Jonsdottir, S. Keles, J.A. Thomson and R. Stewart, A study of the relationships between oligonucleotide properties and hybridization signal intensities from NimbleGen microarray datasets, Nucleic Acids Res. **36** (2008) 2926-2938.

[84] A. Sassolas, B.D. Leca-Bouvier and L.J. Blum, DNA biosensors and microarrays, Chem. Rev. **108** (2008) 109-139.

[85] O. Brandt and J.D. Hoheisel, Peptide nucleic acids on microarrays and other biosensors, Trends Biotechnol. **22** (2004) 617-622.

[86] O. Brandt, J. Feldner, A. Stephan, M. Schroder, M. Schnolzer, H.F. Arlinghaus, J.D. Hoheisel and A. Jacob, PNA microarrays for hybridisation of unlabelled DNA samples, Nucleic Acids Res. **31** (2003) 119.

[87] J. Powell, M. Bennett, R. Waters and S. Reed, A novel global genome method to measure and map DNA damage: application for chemotherapy treatment stratification, The Lancet. **383** (2014) 46-49.

[88] J. Yoo and A. Aksimentiev, In situ structure and dynamics of DNA origami determined through molecular dynamics simulations, PNAS. **110** (2013) 20099-20104.

[89] L. Marrot and J. R. Meunier, Skin DNA photodamage and its biological consequences. J. Am. Acad. Dermatol. **58,** (2008) S139-S148.

[90] A. J. Varghese and S. Y. Wang, Thymine-thymine adduct as a photoproduct of thymine. Science. **160**, (1968) 186-187.

[91] P. Schuchert, M. Langsford, E. Kaslin and J. Kohli, A specific DNA sequence is required for high frequency of recombination in the *ade6* gene of fission yeast. EMBO J. **10**, (1991) 2157-2163.

[92] W.P. Wahls and M. K. Davidson, DNA sequence-mediated, evolutionarily rapid redistribution of meiotic recombination hotspots. Genetics. **189**, (2011) 685-694.

[93] N. Galtier, D. Enard, Y. Radondy, E. Bazin and K. Belkhir, Mutation hot spots in mammalian mitochondrial DNA. Genome Res. **16**, (2006) 215-222.

[94] I. B. Rogozin and Y. I. Pavlov, Theoretical analysis of mutation hotspots and their DNA sequence context specificity. Mutat. Res. **544**, (2003) 65-85.

[95] E. Hodis, I. R. Watson, G. V. Kryukov, S. Arold, M. Imielinski, J. Theurillat, E. Nickerson, D. Auclair, L. Li, C. Place, D. DiCara, A. H. Ramos, Lawrence, M. S. K. Cibulskis, A.

Sivachenko, D. Voet, G. Saksena, N. Stransky, R. C. Onofrio, W. Winckler, K. Ardlie, N. Wagle, J. Wargo, K. Chong, D. L. Morton, K. S. Hale, G. Chen, M. Noble, M. Meyerson, J. E. Ladbury, M. A. Davies, J. E. Gershenwald, S. N. Wagner, D. S. B. Hoon, D. Schadendorf, E. S. Lander, S. B. Gabriel, G. Getz, L. A. Garraway and L. A. Chin, Landscape of driver mutation in melanoma. Cell. **150**, (2012) 251-263.

[96] L.E. Smith, M.F. Denissenko, W.P. Bennett, H. Li, S. Amin, M.S. Tang and G.P. Pfeifer, Targeting of lung cancer mutational hotspots by polycyclic aromatic hydrocarbans. J. Natl.Cancer Inst. **92**, (2000) 803-811.

[97] M.F. Denissenko, J.X. Chen, M.S.Tang and G.P. Pfeifer, Cytosine methylation determines hot spots of DNA damage in the human P53 gene. Proc. Natl. Acad. Sci. **94**, (1997) 3893-3898.

[98] A. Kumar, M.B. Tyagi and P.N. Jha, Evidences showing ultraviolet-B radiation-induced damage of DNA in cyanobacteria and its detection by PCR assay. Biochem. Biophys. Res. Commun. **318**, (2004) 1025-1030.

[99] T. Douki, S. Sauvaigo, F. Odin and J. Cadet, Formation of the main UV-induced thymine dimeric lesions within isolated and cellular DNA as measured by high performance liquid chromatography-tandem mass spectrometry. J. Biol. Chem. **275**, (2000) 11678-11685.

[100] S. Mouret, C. Baudouin, M. Charveron, A. Favier, J. Cadet and T. Douki, Cyclobutane pyrimidine dimers are predominant DNA lesions in whole human skin exposed to UVA radiation. Proc. Natl. Acad. Sci. **103**, (2006) 13765-13770.

[101] S. Frelon, T. Douki and J. Cadet, Radical oxidation of the adenine moiety of nucleoside and DNA: 2-hydroxy-2'-deoxyadenosine is a minor decomposition product. Free Radic. Res. **36**, (2002) 499-508.

[102] M. Dizdaroglu, The use of capillary gas chromatography-mass spectrometry for identification of radiation-induced DNA base damage and DNA base-amino acid cross-links. J. Chromatogr. A. **295**, (1984) 103-121.

[103] T.A. Slieman and W.L. Nicholson, Artificial and solar UV radiation induces strand breaks and cyclobutane pyrimidine dimers in Bacillus subtilis spore DNA. Appl. Environ. Microbiol. **66**, (2000) 199-205.

[104] M. Weinfeld and K.J.M. Soderlind, Phosphorus-32-postlabeling detection of radiation-induced DNA damage: identification and estimation of thymine glycols and phosphoglycolate termini. Biochemistry. **30**, (1991) 1091-1097.

[105] A.G. Kriste, B.S. Martincigh and L. F. Salter, A sensitive immunoassay technique for thymine dimer quantitation in UV-irradiated DNA. J. Photochem. Photobiol. A. **93**, (1996) 185-192.

[106] S. Yarasi, C. McConachie and G. R. Loppnow, Molecular beacon probes of photodamage in thymine and uracil oligonucleotides. Photochem. Photobiol. **81**, (2005) 467-473.

[107] A. Maksimenko, A.A. Ishchenko, G. Sanz, J. Laval, R.H. Elder and M.K. Saparbaev, A molecular beacon assay for measuring base excision repair activities. Biochem. Biophys. Res. Commun. **319**, (2004) 240-246.

[108] N.E. Broude, Stem-loop oligonucleotides: a robust tool for molecular biology and biotechnology. Trends Biotechnol. **20**, (2002) 249-256.

[109] A. Misra, P. Kumar and K. Gupta, Design and synthesis of hairpin probe for specific mis-match discrimination. Nucleic Acids Symp. Ser. **51**, (2007) 311-312.

[110] A. Tsourkas, M.A. Behlke and G. Bao, Structure–function relationships of shared-stem and conventional molecular beacons. Nucleic Acids Res. **30**, (2002) 4208-4215.

[111] A. Tsourkas, M.A. Behlke, S.D. Rose and G. Bao, Hybridization kinetics and thermodynamics of molecular beacons. Nucleic Acids Res. **31**, (2003) 1319-1330.

[112] A.F. El-Yazbi and G.R. Loppnow, Locked nucleic acid hairpin detection of UV-induced DNA damage. Can. J. Chem. **89**, (2011) 402-408.

[113] S.A. Oladepo and G.R. Loppnow, The Effect of Tryptophan on UV-induced DNA Photodamage. Photochem. Photobiol. **86**, (2010) 844-851.

[114] K. Stohr, B. Hafner, O. Nolte, J. Wolfrum, M. Sauer and D.P. Herten, Species-specific identification of mycobacterial 16S rRNA PCR amplicons using smart probes. Anal. Chem. **77**, (2005) 7195-7203.

[115] T. Maruyama, T. Shinohara, T. Hosogi, H. Ichinose, N. Kamiya and M. Goto, Masking oligonucleotides improve sensitivity of mutation detection based on guanine quenching. Anal. Biochem. **354**, (2006) 8-14.

[116] J.P. Knemeyer, M. Sauer and N. Marme, Probes for detection of specific DNA sequences at the single-molecule level. Anal. Chem. **72**, (2000) 3717-3724.

[117] O.R. Rahn, Potassium iodide as a chemical actinometer for 254 nm radiation: use of iodate as an electron scavenger. Photochem. Photobiol. **66**, (1997) 450-455.

[118] A.F. El-Yazbi and G.R. Loppnow, 2-amino purine hairpin probes for the detection of UV-Induced DNA damage. Anal. Chim. Acta. **726**, (2012) 44-49.

[119] X. Zhang, B. S. Rosenstein, Y. Wang, M. Lebwohl, D.M. Mitchell and H. Wei, Induction of 8-Oxo-7, 8-Dihydro-2'-Deoxyguanosine by Ultraviolet Radiation in Calf Thymus DNA and HeLa Cells. Photochem. Photobiol. **65**, (1997) 119-124.

[120] C.A. Smith and J. Taylor, Preparation and characterization of a set of deoxyoligonucleotide 49-mers containing site-specific cis-syn, trans-syn-I, 96-40, and dewar photoproducts of thymidyly (3′-5′)-thymidine. J. Biol. Chem. **15**, (1993) 11143-11151.

[121] S.A. Oladepo and G.R. Loppnow, Initial excited-state structural dynamics of 9-methyladenine from UV resonance raman spectroscopy. J. Phys. Chem. *B*. **115**, (2011) 6149-6156.

[122]Y. Kurosaki, H. Abe, H. Morioka, J. Hirayama, K. Ikebuchi, N. Kamo, O. Nikaido, H. Azuma and H. Ikeda, Pyrimidine dimer formation and oxidative damage in M13 bacteriophage inactivation by Ultraviolet C irradiation. Photochem. Photobiol. **78**, (2003) 349-354.

[123] L.M. Kundu, U. Linne, M. Marahiel and T. Carell, RNA is more UV resistant than DNA: The formation of UV-induced DNA lesions is strongly sequence and conformation dependent. Chem. Eur. J. **10**, (2004) 5697-5705.

[124] O.R. Rahn, I. M. Stefan, R.J. Bolton, E. Goren, S.P. Shaw and R.K. Lykke, Quantum yeild of the iodide-iodate chemical actinometer: dependence on wavelength and concentration. Photochem. Photobiol. (2003) **78**, 146-152.

[125] L. Kelland, The resurgence of platinum-based cancer chemotherapy, Nat. Rev. Cancer. **7** (2007) 573-584.

[126] R.N. Garner, L.E. Joyce and C. Turro, Effect of electronic structure on the photoinduced ligand exchange of Ru (II) polypyridine complexes, Inorg. Chem. **50** (2011) 4384-4391.

[127] R.B. Sears, L. Joyce, M. Ojaimi, J. Gallucci, R. Thummel and C. Turro, Photoinduced ligand exchange and DNA binding of *cis*-[Ru (phpy)(phen)$(CH_3CN)_2]^+$ with long wavelength visible light, J. Inorg. Biochem. **121** (2012) 77-87.

[128] S. Page and R. Wheeler, Ruthenium compounds as anticancer agents, Educ. Chem. **49** (2012) 26-29.

[129] V. Brabec and O. Nováková, DNA binding mode of ruthenium complexes and relationship to tumor cell toxicity, Drug Resist. Updates. **9** (2006) 111-122.

[130] C.S. Allardyce and P.J. Dyson, Ruthenium in medicine: current clinical uses and future prospects, Platin. Met. Rev. **45** (2001) 62-69.

[131] S. Fruhauf and W.J. Zeller, New platinum, titanium, and ruthenium complexes with different patterns of DNA damage in rat ovarian tumor cells, Cancer Res. **51** (1991) 2943-2948.

[132] S. Kapitza, M.A. Jakupec, M. Uhl, B.K. Keppler and B. Marian, The heterocyclic ruthenium (III) complex KP1019 (FFC14A) causes DNA damage and oxidative stress in colorectal tumor cells, Cancer Lett. **226** (2005) 115-121.

[133] J.M. Kelly, A.B. Tossi, D.J. McConnell and C. OhUigin, A study of the interactions of some polypyridylruthenium (II) complexes with DNA using fluorescence spectroscopy, topoisomerisation and thermal denaturation, Nucleic Acids Res. **13** (1985) 6017-6034.

[134] M. Groessl, Y.O. Tsybin, C.G. Hartinger, B.K. Keppler and P.J. Dyson, Ruthenium versus platinum: interactions of anticancer metallodrugs with duplex oligonucleotides characterized by electrospray ionization mass spectrometry, J. Biol. Inorg. Chem. **15** (2010) 677-688.

[135] Y. Liu, N. Wang, W. Mei, F. Chen, L. He, L. Jian, R. Wang and F. Wu, Photoinduced cleavage and DNA-binding of the ruthenium (II) polypyridyl complex [Ru $(phen)_2$ (ipbd)]$(ClO_4)_2$, Transit. Met. Chem. **32** (2007) 332-337.

[136] F. Sang and J. Ren, Capillary electrophoresis of double-stranded DNA fragments using a new fluorescence intercalating dye EvaGreen, J. Sep. Sci. **29** (2006) 1275-1280.

[137] R.M. Santella, Immunological methods for detection of carcinogen-DNA damage in humans, Cancer Epidemiol. Biomarkers Prev. **8** (1999) 733-739.

[138] S.G. Nair and G.R. Loppnow, Multiplexed, UVC-induced, sequence-dependent DNA damage detection, Photochem. Photobiol. **89** (2013) 884-890.

[139] G. Cosa, K. Focsaneanu, J. McLean, J. McNamee and J. Scaiano, Photophysical properties of fluorescent DNA-dyes bound to single-and double-stranded DNA in aqueous buffered solution, Photochem. Photobiol. **73** (2001) 585-599.

[140] J. Olmsted J and D.R. Kearns, Mechanism of ethidium bromide fluorescence enhancement on binding to nucleic acids, Biochem. **16** (1977) 3647-3654.

[141] S.J. Ahn, J. Costa and J.R. Emanuel, PicoGreen quantitation of DNA: effective evaluation of samples pre- or post-PCR, Nucleic Acids Res. **24** (1996) 2623-2625.

[142] T.G. Deligeorgiev, S. Kaloyanova and J.J. Vaquero, Intercalating cyanine dyes for nucleic acid detection, Recent Pat Mater Sci. **2** (2009) 1-26.

[143] X. Yan, W.K. Grace, T.M. Yoshida, R.C. Habbersett, N. Velappan, J.H. Jett, R.A. Keller and B.L. Marrone, Characteristics of different nucleic acid staining dyes for DNA fragment sizing by flow cytometry, Anal. Chem. **71** (1999) 5470-5480.

[144] Y. Li, Z. Chu, X. Liu, H. Jing, Y. Liu and D. Hao, A Cost-effective high-resolution melting approach using the EvaGreen dye for DNA polymorphism detection and genotyping in plants, J. Integr. Plant Biol. **52** (2010) 1036-1042.

[145] P. Zhang, Y. Liu, M. Alsarakibi, J. Li, T. Liu, Y. Li and G. Li, Application of HRM assays with EvaGreen dye for genotyping Giardia duodenalis zoonotic assemblages, Parasitol. Res. **111** (2012) 2157-2163.

[146] W. Wang, K. Chen and C. Xu, DNA quantification using EvaGreen and a real-time PCR instrument, Anal. Biochem. **356** (2006) 303-305.

[147] T.N. Singh and C. Turro, Photoinitiated DNA binding by *cis*-$[Ru(bpy)_2(NH_3)_2]_2$, Inorg. Chem. **43** (2004) 7260-7262.

[148] M. Safdar, Y. Junejo, K. Arman and M. Abasiyanik, Rapid bovine and Caprine species identification in ruminant feeds by duplex real-time PCR melting curve analysis using EvaGreen fluorescence dye, Mol. Biotechnol. **56** (2014) 770-776.

[149] A. Robertazzi and J.A. Platts, Hydrogen bonding and covalent effects in binding of cisplatin to purine bases: ab initio and atoms in molecules studies, Inorg. Chem. **44** (2005) 267-274.

[150] M. Boudvillain, R. Dalbies, C. Aussourd and M. Leng, Intrastrand cross-links are not formed in the reaction between transplatin and native DNA: relation with the clinical inefficiency of transplatin, Nucleic Acids Res. **23** (1995) 2381-2388.

[151] S. Ramachandran, B.R. Temple, S.G. Chaney and N.V. Dokholyan, Structural basis for the sequence-dependent effects of platinum-DNA adducts, Nucleic Acids Res. **37** (2009) 2434-2448.

[152] D. Billen, Spontaneous DNA damage and its significance for the" negligible dose" controversy in radiation protection, Radiat. Res. **124** (1990) 242-245.

[153] M.D. Evans, M.S. Cooke, I.D. Podmore, Q. Zheng, K.E. Herbert and J. Lunec, Discrepancies in the measurement of UVC-induced 8-oxo-2′-deoxyguanosine: implications for the analysis of oxidative DNA damage, Biochem. Biophys. Res. Commun. **259** (1999) 374-378.

[154] M.L. Rolfsmeier, M.F. Laughery and C.A. Haseltine, Repair of DNA double-strand breaks following UV damage in three Sulfolobus solfataricus strains, J. Bacteriol. **192** (2010) 4954-4962.

[155] P.J. Rochette and D.E. Brash, Human telomeres are hypersensitive to UV-induced DNA Damage and refractory to repair, PLoS genetics. **6** (2010) e1000926, 1-13.

[156] B. Vogelstein and K.W. Kinzler, Cancer genes and the pathways they control, Nat. Med. **10** (2004) 789-799.

[157] R. Hindges and U. Hubscher, DNA polymerase delta, an essential enzyme for DNA transactions, Biol. Chem. **378** (1997) 345-362.

[158] Y. Yang, J. Sterling, F. Storici, M.A. Resnick and D.A. Gordenin, Hypermutability of damaged single-strand DNA formed at double-strand breaks and uncapped telomeres in yeast Saccharomyces cerevisiae, PLoS genetics. **4** (2008) e1000264, 1-12.v

[159] K. Chan, J.F. Sterling, S.A. Roberts, A.S. Bhagwat, M.A. Resnick and D.A. Gordenin, Base damage within single-strand DNA underlies *in vivo* hypermutability induced by a ubiquitous environmental agent, PLoS genetics. **8** (2012) e1003149, 1-15.

[160] S.G. Fischer, L.S. Lerman and L.S. Proc, DNA fragments differing by single base-pair substitutions are separated in denaturing gradient gels: correspondence with melting theory, Natl. Acad. Sci. **80** (1983) 1579-1583.

[161] P.E. Nielsen, Targeting double stranded DNA with peptide nucleic acid (PNA), Curr. Med. Chem. **8** (2000) 545-550.

[162] V.V. Demidov, M.V. Yavnilovich and M.D. Frank-Kamenetskii, Kinetic analysis of specificity of duplex DNA targeting by homopyrimidine peptide nucleic acids, Biophys. J. **72** (1997) 2763-2769.

[163] H. Kuhn, V.V. Demidov and M.D. Frank-Kamenetskii, P.E. Nielsen, Kinetic sequence discrimination of cationic bis-PNAs upon targeting of double-stranded DNA, Nucleic Acids Res. **26** (1998) 582-587.

[164] Q. Lu, Z. Zhou, Y. Mei, W. Wei and S. Liu, Detection of DNA damage by thiazole orange fluorescence probe assisted with exonuclease III, Talanta. **116** (2013) 958-963.

[165] T. Sedlackova, G. Repiska, P. Celec, T. Szemes and G. Minarik, Fragmentation of DNA affects the accuracy of the DNA quantitation by the commonly used methods, Biol. Proced. Online. **15** (2013) 1-8

[166] H. Gudnason, M. Dufva, D.D. Bang and A. Wolff, Comparison of multiple DNA dyes for real-time PCR: effects of dye concentration and sequence composition on DNA amplification and melting temperature**,** Nucleic Acids Res. **35** (2007) e127, 1-8.

[167] H.J. Karlsson, M. Eriksson, E. Perzon, B. Akerman, P. Lincoln, and G. Westman, Groove-binding unsymmetrical cyanine dyes for staining of DNA: syntheses and characterization of the DNA-binding, Nucleic Acids Res. **31** (2003) 6227-6234.

[168] A. Fede, M. Billeter, W. Leupin and K. Wüthrich, Determination of the NMR solution structure of the Hoechst 33258-d $(GTGGAATTCCAC)_2$ complex and comparison with the X-ray crystal structure, Structure. **1** (1993) 177-186.

[169] F.G. Loontiens, P. Regenfuss, A. Zechel, L. Dumortier and R.M. Clegg, Binding characteristics of Hoechst 33258 with calf thymus DNA, poly [d (AT)] and d (CCGGAATTCCGG): multiple stoichiometries and determination of tight binding with a wide spectrum of site affinities, Biochemistry. **29** (1990) 9029-9039.

[170] S.A. Roberts, J. Sterling, C. Thompson, S. Harris, D. Mav, R. Shah, L.J. Klimczak, G.V. Kryukov, E. Malc and P.A. Mieczkowski, Clustered mutations in yeast and in human cancers can arise from damaged long single-strand DNA regions, Mol. Cell. **46** (2012) 424-435.

[171] V. Nikolai, Binding of Hoechst with nucleic acids using fluorescence spectroscopy, J. Biophys. Chem. **2** (2011) 443-447.

[172] R. Owczarzy, A.V. Tataurov, Y. Wu, J.A. Manthey, K.A. McQuisten, H.G. Almabrazi, K.F. Pedersen, Y. Lin, J. Garretson, N.O. McEntaggart, C.A. Sailor, R.B. Dawson and A.S. Peek, IDT SciTools: a suite for analysis and design of nucleic acid oligomers, Nucleic Acids Res. **36** (2008) W163-9.

[173] E.T. Kool, Hydrogen bonding, base stacking and steric effects in DNA replication, Annu.Rev.Biomol.Struct. **30** (2001) 1-22.

[174] Y. Tang and Z. Guo, Influence of ultraviolet radiation on calf thymus DNA studied by Raman spectroscopy, Proc. of SPIE. **5630** (2005) 384-395.

[175] C.T. Middleton, K. de La Harpe, C. Su, Y.K. Law, C.E. Crespo-Hernández and B. Kohler, DNA excited-state dynamics: from single bases to the double helix, Annu. Rev.Phys. Chem. **60** (2009) 217-239.

[176] F. Plasser, A.J. Aquino, H. Lischka and D. Nachtigallová, Electronic excitation processes in single-strand and double-strand DNA: A computational approach, Top. Curr. Chem (2014), Springer Berlin Heidelberg, Germany.

[177] W.J. Schreier, T.E. Schrader, F.O. Koller, P. Gilich, C.E. Crespo-Hernández, V. N. Swaminathan, T. Carell, W. Zinth and B. Kohler, Thymine dimerization in DNA is an ultrafast photoreaction, Science. **315** (2007) 625-629.

[178] Y. Jin, Y. Shima, M. Furu, T. Aoyama, T. Nakamata, T. Nakayama, T. Nakamura and J. Toguchida, Absence of oncogenic mutations of RAS family genes in soft tissue sarcomas of 100 Japanese patients, Anticancer Res. **30** (2010) 245-251.

[179] G.J. Peters, A.M. Bergman, V.W. Ruiz van Haperen, G. Veerman, C.M. Kuiper and B.J. Braakhuis, Interaction between cisplatin and gemcitabine in vitro and in vivo, Semin. Oncol. **22** (1995) 72-79.

[180] I.A. Prior, P.D. Lewis and C. Mattos, A comprehensive survey of Ras mutations in cancer, Cancer Res. **72** (2012) 2457-2467.

[181] B. Bailleul, K. Brown, M. Ramsden, R.J. Akhurst, F. Fee and A. Balmain, Chemical induction of oncogene mutations and growth factor activity in mouse skin carcinogenesis, Environ. Health Perspect. **81** (1989) 23-27.

[182] M.D. To, R. Rosario, P.M. Westcott, K.L. Banta and A. Balmain, Interactions between wild-type and mutant Ras genes in lung and skin carcinogenesis, Oncogene. **32** (2012) 4028-4033.

[183] A. Fernández-Medarde and E. Santos, Ras in cancer and developmental diseases, Genes & cancer. **2** (2011) 344-358.

[184] Z. Feng, W. Hu, J.X. Chen, A. Pao, H. Li, W. Rom, M.C. Hung and M.S. Tang, Preferential DNA damage and poor repair determine ras gene mutational hotspot in human cancer, J. Natl. Cancer Inst. **94** (2002) 1527-1536.

[185] W.E. Pierceall, M.L. Kripke and H.N. Ananthaswamy, N-ras mutation in ultraviolet radiation-induced murine skin cancers, Cancer Res. **52** (1992) 3946-3951.

[186] S.L. Graziano, G.P. Gamble, N.B. Newman, L.Z. Abbott, M. Rooney, S. Mookherjee, M.L. Lamb, L.J. Kohman and B.J. Poiesz, Prognostic significance of K-ras codon 12 mutations in patients with resected stage I and II non-small-cell lung cancer, J. Clin. Oncol. **17** (1999) 668-675.

[187] R.J. Slebos, R.H. Hruban, O. Dalesio, W.J. Mooi, G.J. Offerhaus and S. Rodenhuis, Relationship between K-ras oncogene activation and smoking in adenocarcinoma of the human lung, J. Natl. Cancer Inst. **83** (1991) 1024-1027.

[188] A.G. Glass and R.N. Hoover, The emerging epidemic of melanoma and squamous cell skin cancer, JAMA. **262** (1989) 2097-2100.

[189] F. Su, A. Viros, C. Milagre, K. Trunzer, G. Bollag, O. Spleiss, J.S. Reis-Filho, X. Kong, R.C. Koya and K.T. Flaherty, RAS mutations in cutaneous squamous-cell carcinomas in patients treated with BRAF inhibitors, N. Engl. J. Med. **366** (2012) 207-215.

[190] H. Kamiya, N. Murata, T. Murata, S. Iwai, A. Matsukage, C. Masutani, F. Hanaoka and E. Ohtsuka, Cyclobutane thymine dimers in a ras proto-oncogene hot spot activate the gene by point mutation, Nucleic Acids Res. **21** (1993) 2355-2361.

[191] P.K. Roddey, M. Garmyn, H. Park, J. Bhawan and B.A. Gilchrest, Ultraviolet irradiation induces c-fos but not c-Ha-ras proto-oncogene expression in human epidermis, J. Invest. Dermatol. **102** (1994) 296-299.

[192] A.T. Baines, D. Xu and C.J. Der, Inhibition of Ras for cancer treatment: the search continues, Future medicinal chemistry. **3** (2011) 1787-1808.

[193] T. Climent, I. González-Ramírez, R. González-Luque, M. Merchán, L and Serrano-Andrés, Cyclobutane Pyrimidine Photodimerization of DNA/RNA Nucleobases in the Triplet State, J. PhysChem. Lett. **1** (2010) 2072-2076.

[194] S.K. Banerjee, A. Borden, R.B. Christensen, J.E. LeClerc and C.W. Lawrence, SOS-dependent replication past a single trans-syn T-T cyclobutane dimer gives a different mutation spectrum and increased error rate compared with replication past this lesion in uninduced cells, J. Bacteriol. **172** (1990) 2105-2112.

[195] M. Brenner, S.G. Coelho, J.Z. Beer, S.A. Miller, R. Wolber, C. Smuda and V.J. Hearing, Long-lasting molecular changes in human skin after repetitive in situ UV irradiation, J. Invest. Dermatol. **129** (2008) 1002-1011.

[196] L.J. Bradley, K.J. Yarema, S.J. Lippard and J.M. Essigmann, Mutagenicity and genotoxicity of the major DNA adduct of the antitumor drug cis-diamminedichloroplatinum (II), Biochemistry **32** (1993) 982-988.

[197] V. Cepeda, M.A. Fuertes, J. Castilla, C. Alonso, C. Quevedo and J.M. Pérez, Biochemical mechanisms of cisplatin cytotoxicity, Anti-Cancer Agents in Medicinal Chemistry (Formerly Current Medicinal Chemistry-Anti-Cancer Agents). **7** (2007) 3-18.

[198] S. Fan, M.L. Smith, D.J. Rivet 2nd, D. Duba, Q. Zhan, K.W. Kohn, A.J. Fornace Jr and P.M. O'Connor, Disruption of p53 function sensitizes breast cancer MCF-7 cells to cisplatin and pentoxifylline, Cancer Res. **55** (1995) 1649-1654.

[199] D.G. Brooks, R.M. James and C.E. Patek, J. Williamson and M.J. Arends, Mutant K-ras enhances apoptosis in embryonic stem cells in combination with DNA damage and is associated with increased levels of p19(ARF), Oncogene. **20** (2001) 2144-2152.

[200] M. Baik, R.A. Friesner and S.J. Lippard, Theoretical study of cisplatin binding to purine bases: why does cisplatin prefer guanine over adenine? J. Am. Chem. Soc. **125** (2003) 14082-14092.

[201] M. Crul, R. Van Waardenburg, J. Beijnen and J. Schellens, DNA-based drug interactions of cis platin, Cancer Treat. Rev. **28** (2002) 291-303.

[202] M.J. Clarke, Ruthenium metallopharmaceuticals, Coord. Chem. Rev. 236 (2003) 209-233.

[203] F. Schmitt, P. Govindaswamy, G. Süss-Fink, W.H. Ang, P.J. Dyson, L. Juillerat-Jeanneret and B. Therrien, Ruthenium porphyrin compounds for photodynamic therapy of cancer, J. Med. Chem. **51** (2008) 1811-1816.

[204] L. Johnson, K. Mercer, D. Greenbaum, R.T. Bronson, D. Crowley, D.A. Tuveson and T. Jacks, Somatic activation of the K-ras oncogene causes early onset lung cancer in mice, Nature. **410** (2001) 1111-1116.

[205] S. Schubbert, M. Zenker, S.L. Rowe, S. Böll, C. Klein, G. Bollag, I. van der Burgt, L. Musante, V. Kalscheuer and L. Wehner, Germline KRAS mutations cause Noonan syndrome, Nat. Genet. **38** (2006) 331-336.

[206] K.W. Zheng, Z. Chen, Y.H. Hao and Z. Tan, Molecular crowding creates an essential environment for the formation of stable G-quadruplexes in long double-stranded DNA, Nucleic Acids Res. **38** (2010) 327-338.

[207] A.M. Fleming and C.J. Burrows, G-Quadruplex Folds of the Human Telomere Sequence Alter the Site Reactivity and Reaction Pathway of Guanine Oxidation Compared to Duplex DNA, Chem. Res. Toxicol. **26** (2013) 593-607.

[208] F. Bourre, G. Renault and P.C. Seawell, A. Sarasin, Distribution of ultraviolet-induced lesions in Simian Virus 40 DNA, Biochimie. **67** (1985) 293-299.

[209] T. Douki, Low ionic strength reduces cytosine photoreactivity in UVC-irradiated isolated DNA, Photochem. Photobiol. Sci. **5** (2006) 1045-1051.

[210] Y.K. Law, R.A. Forties, X. Liu, M.G. Poirier, and B. Kohler, Sequence-dependent thymine dimer formation and photoreversal rates in double-stranded DNA, Photochem. Photobiol. Sci. **12** (2013) 1431-1439.

[211] D.G. Brooks, R.M. James, C.E. Patek, J. Williamson and M.J. Arends, Mutant K-ras enhances apoptosis in embryonic stem cells in combination with DNA damage and is associated with increased levels of p19(ARF), Oncogene. **20** (2001) 2144-2152.

[212] Z. Feng, W. Hu, J.X. Chen, A. Pao, H. Li, W. Rom, M.C. Hung and M.S. Tang, Preferential DNA damage and poor repair determine ras gene mutational hotspot in human cancer, J. Natl. Cancer Inst. **94** (2002) 1527-1536.

[213] P.H. Johnson, R.P. Walker, S.W. Jones and K. Stephens, Multiplex gene expression analysis for high-throughput drug discovery: screening and analysis of compounds affecting genes overexpressed in cancer cells, Mol.Cancer.Ther. **1** (2002) 1293-1304.

[214] D. Ribble, N. B. Goldstein, D.A. Norris and Y.G. Shellman, A simple technique for quantifying apotosis in 96-well plates. Bio.Med Central **5** (2005) 12.

[215] J.R. Ridpath, S. Takeda, J.A. Swenberg and J. Nakamura, Convenient, multi-well plate-based DNA damage response analysis using DT40 mutants is applicable to high-throughput genotoxicity assay with characterization of modes of action, Envior. Mol. Muta.. **52** (2011) 153-160

[216] D.K. Wood, D.M. Weingeist, S.N. Bhatia, B.P. Engelward, Single cell trapping and DNA damage analysis using microwell arrays. Proc. Natl. Acad. Sci. **107** (2010) 10008-10013.

[217] G. Brunborg, P. Jackson, S. Shaposhnikov, H. Dahl, A. Azqueta, A.R. Collins and K.B. Gutzkow, High throughput sample processing and automated scoring, Front. Gent. **5** (2014) 373-

[218] J. Ge, S. Prasongtanakij, D.K. Wood, D. M. Weingeist, J. Fessler, P. Navasummrit, M. Ruchirawat and B.P.Engelward, CometChip: A high-throughput 96-well platform for measuring DNA damage in microarrayed human cell, J. Vis. Exp. **92** (2014)

[219] M. Karbaschi and M.S. Cooke, Novel method for the high-throughput processing of slides for the comet assay. Sci. Rep. **4** (2014) 1-6.

[220] S. Nandhakumar, S. Parasuraman, M.M. Shanmugam, K.R. Rao, P. Chand and B.V. Bhat, Evaluation of DNA damage using single-cell gel electrophoresis (Comet Assay), J. Pharmacol. Pharmacother. **2** (2011) 107-111.

[221] A. Hakura, S. Suzuki and T. Satoh, Improvement of the Ames test using human liver S9 preparation, J. Pharmacol. Toxicol. Methods, **46** (2001), 169-172.

[222] J. McCann, E. Choi, E. Yamasaki and B.N. Ames, Detection of carcinogens as mutagens in the Salmonella/microsome test: assay of 300 chemicals, Proc. Natl. Acad. Sci. U. S. A. **72** (1975) 5135-5139.

[223] K. Mortelmans and E. Zeiger, The Ames *Salmonella/microsome* mutagenicity assay, Mutat. Res-Fund Mol. M. **455** (2000) 29-60.

[224] M.F. Wu, F.C. Peng, Y.L. Chen, C.S. Lee, Y.Y. Yang, M.Y. Yeh, C.M. Liu, J.B. Chang, R.S. Wu, C.C. Yu, H.F. Lu and J.G. Chung, Evaluation of genotoxicity of Antrodia cinnamomea in the Ames test and the in vitro chromosomal aberration test, In Vivo. **25** (2011) 419-423.

[225] S. Galloway, E. Lorge, M.J. Aardema, D. Eastmond, M. Fellows, R. Heflich, D. Kirkland, D.D. Levy, A.M. Lynch and D. Marzin, Workshop summary: Top concentration for in vitro mammalian cell genotoxicity assays; and report from working group on toxicity measures and top concentration for in vitro cytogenetics assays (chromosome aberrations and micronucleus), Matat. Res-Gen Tox.En. **723** (2011) 77-83.

[226] A. Dhawan, M. Bajpayee and D. Parmar, Comet assay: a reliable tool for the assessment of DNA damage in different models, Cell Biol. Toxicol. **25** (2009) 5-32.

[227] G. Speit and A. Rothfuss, The comet assay: a sensitive genotoxicity test for the detection of DNA damage and repair, Methods Mol.Biol. **314,** (2006) 275-286.

[228] P. Grigaravicius, A. Rapp and K.O. Greulich, A direct view by immunofluorescent comet assay (IFCA) of DNA damage induced by nicking and cutting enzymes, ionizing (137)Cs radiation, UV-A laser microbeam irradiation and the radiomimetic drug bleomycin, Mutagenesis. **24** (2009) 191-197.

[229] D.A. Khodakov and A.V. Ellis, Recent developments in nucleic acid identification using solid-phase enzymatic assays, Microchimica Acta. **181** (2014) 1-14.

[230] H. Tian, L. Cao, Y. Tan, S. Williams, L. Chen, T. Matray, A. Chenna, S. Moore, V. Hernandez, V. Xiao, M. Tang and S. Singh, Multiplex mRNA assay using electrophoretic tags for high-throughput gene expression analysis, Nucleic Acids Res. **32** (2004) e126.

[231] Y. Chen and Z. Kuo, C. Cheng, Paper–a potential platform in pharmaceutical development, Trends Biotechnol. **33** (2015) 4-9.

[232] M.O. Noor and U.J. Krull, Camera-Based Ratiometric Fluorescence Transduction of Nucleic Acid Hybridization with Reagentless Signal Amplification on a Paper-Based Platform Using Immobilized Quantum Dots as Donors, Anal. Chem. **86** (2014) 10331-10339.

[233] F. Deiss, W.L. Matochko, N. Govindasamy, E.Y. Lin and R. Derda, Flow-Through Synthesis on Teflon-Patterned Paper To Produce Peptide Arrays for Cell-Based Assays, Angew. Chem. Int. Ed. **53** (2014) 6374-6377.

[234] B. Liu, Y. Qin, J. Wang and Y. Wang, Detection and comparison of protein–DNA interactions using DNA–BIND plate and horseradish peroxidase-based colorimetric assay, Anal. Biochem. **412** (2011) 111-113.

[235] A.Y. Mercedes-Camacho and F.A. Etzkorn, Enzyme-linked enzyme-binding assay for Pin1 WW domain ligands, Anal. Biochem. **402** (2010) 77-82.

[236] P. Renard, I. Ernest, A. Houbion, M. Art, H. Le Calvez, M. Raes and J. Remacle, Development of a sensitive multi-well colorimetric assay for active NFkappaB, Nucleic Acids Res. **29** (2001) e21.